Design, Synthesis and Evaluation of Donepezil-Rasagiline Based Compounds as Multipotent Inhibitors for the Treatment of Alzheimer's Disease

A Thesis submitted to the Central University of Punjab

For the award of

Doctor of Philosophy

In

Pharmaceutical Sciences

By

Bhupinder Kumar

Research Supervisor: Dr. Vinod Kumar

Research Co-supervisor: Dr. Jyoti Parkash

Department of Pharmaceutical Sciences and Natural Products

School of Basic and Applied Sciences

Central University of Punjab, Bathinda

August, 2019

DECLARATION

I declare that the thesis entitled “Design, Synthesis and Evaluation of Donepezil-Rasagiline Based Compounds as Multipotent Inhibitors for the Treatment of Alzheimer’s Disease” has been prepared by me under the guidance of Dr. Vinod Kumar, Assistant Professor, Department of Pharmaceutical Sciences and Natural Products; and Dr. Jyoti Parkash, Assistant Professor, Department of Animal Sciences, School of Basic and Applied Sciences, Central University of Punjab, Bathinda. No part of this thesis has formed the basis for the award of any degree or fellowship previously**.**

Bhupinder Kumar
Department of Pharmaceutical Sciences and Natural Products,
School of Basic and Applied Sciences,
Central University of Punjab,
Bathinda – 151001

Date:

CERTIFICATE

We certify that Mr. Bhupinder Kumar has prepared his thesis entitled “Design, Synthesis and Evaluation of Donepezil-Rasagiline Based Compounds as Multipotent Inhibitors for the Treatment of Alzheimer’s Disease” for the award of Ph. D (Pharmaceutical Sciences) degree of the Central University of Punjab, under our guidance. He has carried out this work at the Department of Pharmaceutical Sciences and Natural Products and Department of Animal Sciences, School of Basic and Applied Sciences, Central University of Punjab, Bathinda.

Supervisor
Dr. Vinod Kumar
Assistant Professor
Department of Pharmaceutical Sciences and Natural Products

Co-supervisor
Dr. Jyoti Parkash
Assistant Professor
Department of Animal Sciences

School of Basic and Applied Sciences,
Central University of Punjab, Bathinda-151001

Date:

ABSTRACT

"Design, Synthesis and Evaluation of Donepezil-Rasagiline Based Compounds as Multipotent Inhibitors for the Treatment of Alzheimer's Disease"

Name of student : Bhupinder Kumar

Registration Number : 15phdphm02

Degree for which submitted : Ph. D (Pharmaceutical Sciences)

Supervisor : Dr. Vinod Kumar

Co-supervisor : Dr. Jyoti Parkash

Department : Pharmaceutical Sciences and Natural Products

School of Studies : Basic and Applied Sciences

Key words: Alzheimer's disease, MAO inhibitors, Diphenylpyrimidine, Acetylcholinesterase inhibitors, Dual inhibitors, Neuroprotective agents

Alzheimer's disease (AD) is multifactorial in nature and different enzymes including MAO, AChE, and amyloid beta are implicated in its pathogenesis. The pathomechanism of AD is complex in nature and single target drugs proved to be ineffective for the treatment of the disease. With an aim of developing dual/multipotent inhibitors, 4,6-diphenylpyrimidines were optionally substituted with propargyl group and an ethyl chain containing a cyclic or acyclic tertiary nitrogen atom (piperidine/morpholine/pyrrolidine/N,N-dimethyl) as potential pharmacophores for MAO and AChE enzymes. Compound **VB1** was found to be the most potent MAO-A (IC_{50} value of 18.34 ± 0.38 nM) inhibitor and **VB8** was found to be the most potent AChE (IC_{50} value of 9.54 ± 0.07 nM) inhibitor. Compound **VB3** was another promising compound in series-I with IC_{50} values of 28.33 ± 3.22 nM and 18.92 ± 0.29 nM against MAO-A and AChE, respectively and displayed very high selectivity index (103) for AChE over BuChE. These compounds were found to be reversible inhibitors of MAO and AChE enzymes and non-toxic to the human neuroblastoma SH-SY5Y cells. Based on structure-activity relationship analysis of the first series of compounds, second series of the compounds were designed by fixing the position of piperidine/morpholine ethyl chain at the para position of one of the phenyl rings. In the second series, compound **VP15**

was found to be a multi-potent inhibitor of MAO-B and AChE with IC_{50} values of 0.37 ± 0.03 μM and 0.04 ± 0.003 μM, respectively. **VP15** was found to be selective for MAO-B with selectivity index of 270 over MAO-A. It also displayed SI of 625 for AChE over BuChE. **VP15** was found to be irreversible inhibitor of MAO-B. In the third series of target compounds, both the phenyl rings of diphenylpyrimidines were substituted with *O*-propargyl groups. Different derivatives have been synthesized with *O*-propargyl groups substituted at ortho, meta and para positions of the phenyl rings. In the third series of compounds, **AVB1** and **AVB4** were found to be the most potent inhibitors of AChE and MAO-B with IC_{50} values of 1.35 ±0.03 μM and 1.49 ± 0.09 μM, respectively. In the reversible inhibition studies, the lead compounds were found to be reversible inhibitors of MAO-B and AChE enzymes. In the ROS protection inhibition studies, **AVB1** and **AVB4** displayed good activity in SH-SY5Y cells and **AVB1** reduced the ROS levels up to 30% at 5 μM. This series of compounds were also found to be non-toxic to the SH-SY5Y cells in the cytotoxicity studies. Thus, from the present study it can be concluded that 4,6-diphenylpyrimidine derivatives can act as potential lead for the development of effective drug candidates for the treatment of AD. Compound **VB3** and **VP15** were found to be the most potent dual inhibitors of MAO and AChE.

(Bhupinder Kumar) **(Dr. Jyoti Parkash)** **(Dr. Vinod Kumar)**

Dedicated

To

My

Beloved

Grandfather

Acknowledgments

First of all, I would also like to express my thanks to **Prof. (Dr.) R. K. Kohli**, Vice Chancellor, Central University of Punjab, Bathinda for providing necessary facilities for carrying out research work.

I would also like to express my sincere thanks to **Prof. (Dr.) P. Ramarao**, Dean, Academic Affairs, Central University of Punjab, Bathinda for his direction, valuable suggestions and listening my queries.

I would like to express my deepest gratitude to **Dr. Vinod Kumar** my research supervisor, my guide, my mentor for his support and valuable guidance throughout my research work. I consider myself lucky as I got chance to work under his guidance. I owe a lot of gratitude to him for always being there for me and I feel privileged to be associated with a person like him during my life.

I would also like to express my thanks to **Dr. Jyoti Parkash** Assistant Professor, Department of Animal Sciences, Central University of Punjab, Bathinda whose help and suggestions, especially for the biological part of the project helped to match up my project. Special thanks to Mr. **Vikash Prashar (Bakwas Par-asar)** for helping me in biological studies and support in whole time.

I would also like to thank **Dr. Raj Kumar**, Associate Professor, **Dr. Vikas Jaitak**, **Dr. Pradeep Kumar**, Assistant Professor, Department of Pharmaceutical Sciences and Natural Products for their help and support throughout the dissertation.

I would like to especially acknowledge **Dr. Rakesh Kumar**, for his valuable help and advices in my research work. It was my pleasure to work with him.

I am very much thankful to my friends **Samreet**, **Vijay (Chotu)**, **Amit (Buda)**, **Ashish Dwivedi**, **Sourav (Nona)**, **Gaurav Joshi**, **Kamal, Manav, Sukha (Gappi)**… my **seniors,** my **juniors, the list is endless…thanks to one and all** for enduring my endless talks, supporting throughout this research periods, helping to overcome setbacks, focusing on research, completing the project and loving me at my best and at my worst.

I would like to extend my thanks to **Mr. Rajesh Tiwari, Harman** and **Mr. Preeti Prabhat** for providing facilities for research work.

I am highly obliged to my parents **Mr. Ravinder Kumar**, **Mrs. Kanta Rani** who gave all their best for my education & never raised an eyebrow when I claimed my thesis would be finished 'in the next two weeks' for nearly a year, and my sister **Rajinder Pal Mittal** for her love and support. This all could not have been possible without their continuous support, strength, love, inspiration throughout all these years.

(Bhupinder Kumar)

TABLE OF CONTENTS

LIST OF TABLES

LIST OF FIGURES

LIST OF APPENDICES

LIST OF ABBREVATIONS

S. No.	Full Form	Abbreviation
1.	Acetyl cholinesterase	AChE
2.	Alzheimer’s disease	AD
3.	Amyloid precursor protein	APP
4.	Blood brain barrier	BBB
5.	Bovine serum albumin	BSA
6.	Brain derived neurotropic factor	BDNF
7	Dichloromethane	DCM
8.	Dimethyl formamide	DMF
9.	Dimethyl sulfoxide	DMSO
10.	Dopamine	DA
11.	Dulbecco's modified Eagle's medium	DMEM
12.	Fetal bovine serum	FBS
13.	Flavin Adenine Dinucleotide	FAD
14.	Gas chromatography-Mass spectrometry	GC-MS

15.	Glial cell line derived neurotropic factor	GDNF
16.	Glyceraldehydes-3-phosphate	GADPH
17.	5-Hydroxytryptamine	5-HT
18.	Monoamine oxidase	MAO
19.	Nerve Growth Factor	NGF
20.	Norepinephrine	NA
21.	Nuclear magnetic resonance	NMR
22.	Parkinson’s disease	PD
23.	Protein data bank	PDB
24.	Reactive oxygen species	ROS
25.	Round bottom flask	RBF
26.	Selectivity index	SI
37.	Structure activity relationship	SAR
28.	Superoxide dismutase	SOD
29.	Thin layer chromatography	TLC
30.	Tyrosine	Tyr

Chapter- 1
Introduction

Alzheimer's disease (AD) is a multifactorial neurological disorder characterized by progressive memory loss, dementia and other cognitive impairments (Goedert Michel and Spillantini, 2006). It is estimated that one in every three senior persons dies with AD and one in ten persons over 65 years of age has AD (Alzheimer's, 2017). According to Alzheimer's association, in recent years deaths due to stroke, heart disease, and HIV decreased 21%, 14%, and 54%, respectively, whereas deaths due to AD are increased by 89% (Alzheimer's, 2017). According to world health organization (WHO), it is estimated that population effected from AD will reach to 95 million by 2050 (Więckowska *et al.*, 2018). AD stands out fourth leading cause of death among the neurodegenerative diseases and is the most common cause of acquired dementia in the elderly population. There are two forms of AD; first form is a familial one in which multiple family members are affected by AD and second form is a sporadic one in which one or a few members of a family develop AD.

Symptoms and characteristics of AD shows similarities with various other defined neurodegenerative disorders such as Parkinson's disease and other type of dementias. Thus, in most of the cases it becomes difficult to recognize that it is a foreseeable part of normal ageing or a discrete disease developed from other risk factors (Masters *et al.*, 2015). The main problem associated with AD and dementia is loss of neurons in the brain region which are involved with the memory, language and problem solving but in case of AD additional symptoms of declining body functions like walking and eating can be seen due to the damage occurred to the neurons in other parts or whole of the brain. AD is ultimately a fatal disease and the person affected with it requires 24h care in their final stages (Alzheimer's, 2013).

The exact molecular pathogenesis of AD is not clear however, in most of the cases the disease state is linked with the degeneration of neurons and glial cells or inclined metabolism of signaling neurotransmitters. Various biochemical and histopathological studies indicate that over expressed monoamine oxidase (MAO) enzyme, low acetylcholine levels, amyloid-β (Aβ) deposits (Kung, 2012), hyperphosphorylated tau-protein aggregation and oxidative stress play crucial roles in the pathophysiology of the disease. Depressive symptoms occur in patients suffering with AD and these may be associated with the decreased serotonergic and noradrenergic transmission in the limbic system (Cummings *et al.*, 1995; Garcia-

Alloza *et al.*, 2005). Hyper activation of MAO enzyme has been observed in patients suffering with AD that decreases the concentration of dopaminergic and serotoninergic neurotransmitters. Some clinical trials have shown that deprenyl, a potential MAO-B inhibitor, alleviate the symptoms of AD (Müller *et al.*, 2000; Sano *et al.*, 1997). Acetylcholine is an important enzyme in the regulation of learning and memory processes. It is hydrolyzed by acetylcholinesterase and cholinesterase inhibitors enhance the level of acetylcholine. Thus cholinergic system have been explored as an important target for the treatment of AD. Currently, donepezil (Sugimoto *et al.*, 2000), galantamine (Marco-Contelles *et al.*, 2006), and rivastigmine (Anand and Singh, 2013) are FDA (Food and Drug Administration US) approved drugs that improve AD symptoms by inhibiting AChE (Anand and Singh, 2013; Gura, 2008; Racchi *et al.*, 2004b). Apart from the beneficial palliative properties of AChE inhibitors in AD (Munoz-Torrero, 2008), cholinergic drugs have shown little efficacy to prevent the progression of the disease. Consequently, there is no efficient drug to cure, stop or even slow the progression of the disease; therefore, effective therapeutics are sought for the permanent treatment of AD (Small and Greenfield, 2015; Yiannopoulou and Papageorgiou, 2013).

The pathogenesis of AD is complex and targeting single pathway may not be an effective strategy for the complete treatment of the disease. Multi-targeted ligands design strategy involves the incorporation of two or more distinct pharmacophores of different drugs in the single structure to develop hybrid molecules (Oliveira Pedrosa *et al.*, 2017; Oset-Gasque and Marco-Contelles, 2018). Hence, the multitargeting ligands which can simultaneously inhibit MAO and AChE enzymes are being developed as drugs for the management/treatment of AD. From the literature search, we noted that the propargyl moiety play an important role in providing neuronal and mitochondrial protective properties (Bolea *et al.*, 2011; Weinreb *et al.*, 2010). Similarly, piperidine motif of donepezil is reported to inhibit cholinesterases along with inhibition of Aβ aggregation (Hughes *et al.*, 2016). The chain length between the propargyl and piperidine moieties is reported to control the dual interaction of these moieties with both catalytic active site and peripheral anionic site of the enzyme (Samadi *et al.*, 2011). Based on this background, number of multitargeting ligands have been reported as potential therapeutic agents for the treatment of AD (Agis-Torres *et al.*, 2014). Recently, ASS234 is developed as a multitargeting ligand from the juxtaposition of pharmacophores of donepezil and

PF9601N (Fig. 1.1) (Marco-Contelles *et al.*, 2016). This compound was found to be effective against multiple targets like AChE, MAO and β-amyloid and also displayed antioxidant and neuroprotective potential. Although many newly developed MAO and AChE inhibitors are under different phases of clinical trials, but till date none of these could reach to clinical use because of the number of adverse effects.

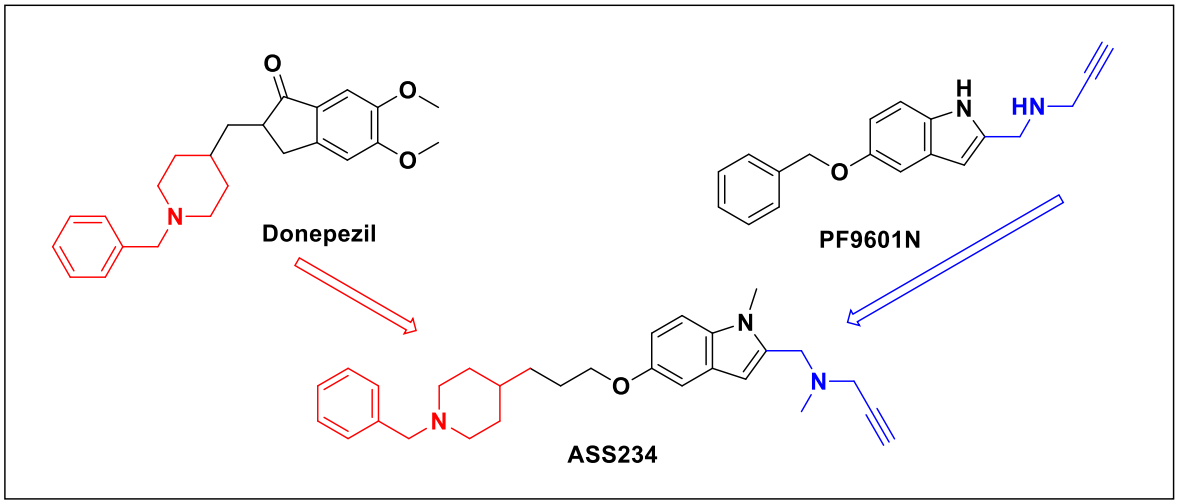

Fig. 1.1 Designing strategy for ASS234 through hybridization of pharmacophores of donepezil and PF9601N

Thus, with the aim of developing dual/multipotent inhibitors, in the present research work, three different series of 4,6-diphenylpyrimidine derivatives have been designed, synthesized and evaluated as dual inhibitors of MAO and AChE enzymes. The 4,6-diphenylpyrimidine scaffold was optionally substituted with a propargyl group and a piperidine/morpholine/pyrrolidine/N,N-dimethyl moieties as potential pharmacophores for MAO and AChE enzymes. The synthesized compounds were evaluated for their antialzheimer's activities *via* determining their inhibitory potential against AChE (Amplex® Red assay kit, Invitrogen), BuChE (Ellman method) and MAO (Amplex® Red MAO assay kit, Invitrogen) enzymes using different enzyme inhibition assays. Most active compounds obtained from the series were evaluated for their neuroprotective potential (using 6-hydroxydopamine as neurotoxin) and cytotoxicity against SH-SY5Y cells using MTT assay. Compounds were also evaluated for their reversible/irreversible properties using dilution method and mode of inhibition using kinetic studies. In addition, compounds were also evaluated for their intracellular ROS production inhibition potential using 2´,7´-dichlorofluorescein diacetate compound and free radical scavenging properties using DPPH assay. Molecular docking and molecular dynamic simulation studies were used to identify

the probable binding mode and their stability at the binding site of MAO and AChE enzymes.

Chapter- 2
Review of literature

2.1 Alzheimer's disease (AD)

Alzheimer's disease (AD) is an irreversible age-related neurological disorder characterized by progressive mental deterioration associated with degeneration of brain regions involved in superior cognitive functions like memory, language skills, judgments, and reasoning. Some important clinical features of AD are behavior alterations such as apathy, agitation, progressive memory loss, and psychosis. In 1906, a German renowned physician Dr. Alois Alzheimer for the first time recognized brain cell abnormalities through an autopsy performed on the brain of a woman, who had died after years of suffering memory problems, confusion, and difficulty in understanding questions (Alzheimer, 1907). In his studies, Dr. Alois found dense deposits outside and around nerve cells, and presence of twisted bands of fibers inside the nerve cells. After this observation, it took about 70 years to recognize this disease as a basis of dementia and a major cause of death.

2.2 Pathogenesis of Alzheimer's disease and therapeutic targets

In the past decades, various hypothesis for the pathogenesis of AD have been proposed which includes cholinergic hypothesis (Bartus *et al.*, 1982; Talesa, 2001), monoamine oxidase hypothesis (Avramovich-Tirosh *et al.*, 2007; Tariot *et al.*, 1987), amyloid cascade hypothesis (Hardy, 2006; Hardy and Selkoe, 2002), oxidative stress hypothesis (Lin and Beal, 2006), tau protein hypothesis (Goedert *et al.*, 1989) and so on (Fig. 2.1).

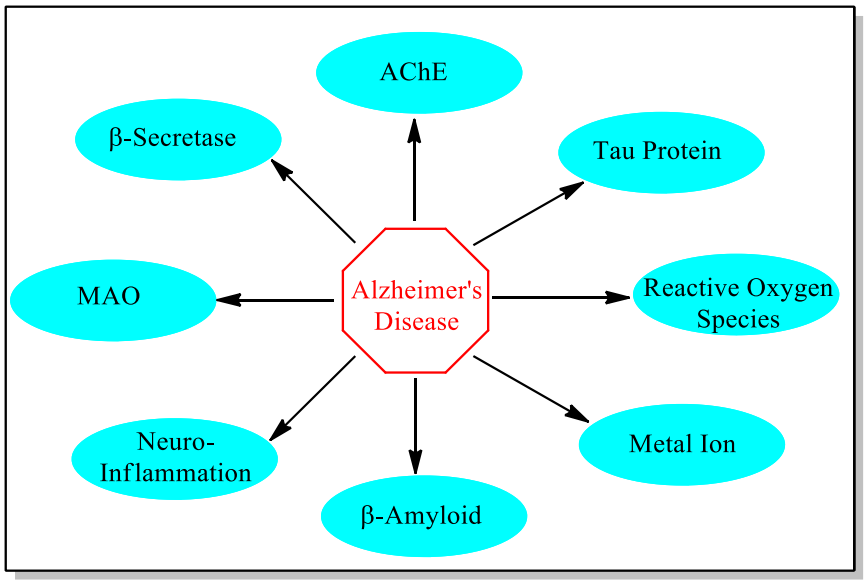

Fig. 2.1 Various targets for the treatment of Alzheimer's disease

2.2.1 Cholinergic hypothesis

Cholinergic hypothesis of AD was presented over 35 years ago and is one of the most studied pathogenesis of AD (Francis *et al.*, 1999). According to cholinergic hypothesis AD is a neurodegenerative disease of the CNS which is linked to the decreased level of acetylcholine (ACh, a crucial cholinergic neurotransmitter) in hippocampal and cortical regions of the brain (Selkoe, 2001; Vitale *et al.*, 2018). Cholinergic neurotransmission plays important role in the control of cerebral blood flow, cortical activity, sleep-wake cycle, and many other cognitive functions of the body. This neurotransmitter (Ach) is synthesized from choline and Acetyl CoA in the presence of enzyme choline acetyltransferase within parasympathetic nerve terminals and transferred to synaptic vesicles through vesicular acetylcholine transporter (VAChT). Depolarization of the presynaptic cholinergic neurons due to the entry of Ca^{2+} through voltage-dependent Ca^{2+} channels results in the release of ACh from nerves fibers to synapse. This released ACh binds to the nicotinic ACh receptors (ligand gated ion channels) or muscarinic ACh receptors (G-protein coupled receptors) leading to the initiation of various neuronal processes (Soreq and Seidman, 2001). After its signal transduction, ACh is hydrolyzed by the cholinesterases (ChE) into choline and acetic acid and choline reuptake occurs through cholinergic neurons (Fig. 2.2). This acetylcholinesterase mediated catalysis of ACh is an essential process in the cholinergic neurotransmission (Klafki *et al.*, 2006).

When ChEs are upregulated, these hydrolyses and inactivates ACh which lead to the decreased concentration of this neurotransmitter at the synapse. It also leads to reduced expression of choline acetyltransferase (ChAT) which is responsible for the ACh synthesis. ACh neurotransmitter mediated signaling is vital for CNS functions and its sudden obstruction is fatal. The gradual loss of ACh neurotransmission in brain leads to AD (Wright *et al.*, 1993) and multiple system atrophy (Polinsky *et al.*, 1989). The active site of human AChE is a narrow cavity shaped and is composed of catalytic anionic site (CAS) and peripheral anionic site (PAS). CAS composed of Trp84, Tyr130, Phe330, and Phe331 residues, whereas PAS consists of five amino acids-Tyr70, Asp72, Tyr121, Trp279, and Tyr334 (Cheung *et al.*, 2012). In catalytic site near anionic site, the quaternary ammonium group of ACh binds through cation−π interactions. From the crystal structure analysis, it has been found that the

quaternary ammonia binding site of AChE is uncharged and contains number of hydrophobic aromatic residues (Harel *et al.*, 1993; Nolte *et al.*, 1980). PAS in AChE plays crucial role in the binding of ACh to AChE and it leads to the accelerated hydrolysis of ACh (Szegletes *et al.*, 1999).

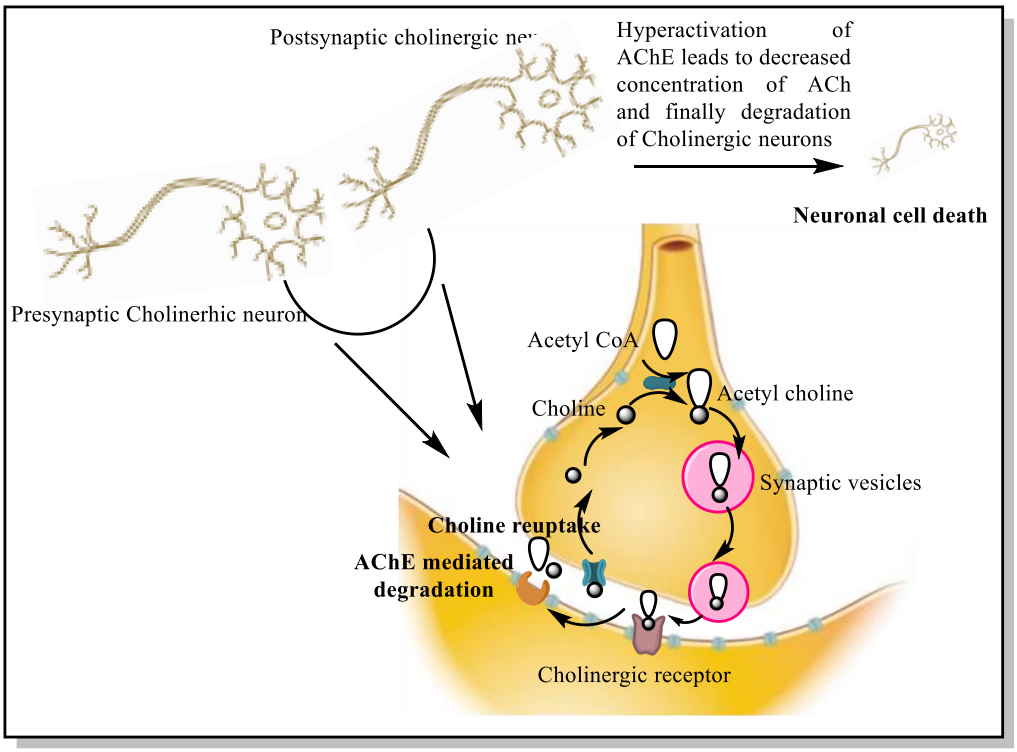

Fig. 2.2 Cholinergic neurotransmission in brain.

Another ChE i.e. butyrylcholinesterase (BuChE, EC 3.1.1.8) can also hydrolyze ACh but less specifically as compared to AChE and may play a role in the cholinergic transmission. In comparison to AChE (300 Å), the size of the active binding site of BuChE is large (500 Å). BuChE also lacks the PAS which is present in AChE and contribute toward its hydrolysis activity (Savini *et al.*, 2003; Saxena *et al.*, 1997). AChE is expressed in cholinergic neurons and neuromuscular junctions where its primary function is the rapid breakdown of the neurotransmitter ACh released during cholinergic neurotransmission (Mohamed and Rao, 2011). Thus, the patients suffering with AD were found to have low levels of cholinergic neurons causing decreased concentration of acetylcholine (ACh) in the brain which in turn affects the learning and memory functions (Jakob-Roetne and Jacobsen, 2009). Based on the cholinergic hypothesis, one possible approach to treat AD is to restore the level of

acetylcholine by inhibiting AChE. Inhibitors of AChE prevent the hydrolysis of acetylcholine and thus increases its concentration in the synaptic cleft. Donepezil (Sugimoto *et al.*, 2000), galantamine (Marco-Contelles *et al.*, 2006), tacrine and rivastigmine (Anand and Singh, 2013) are FDA (Food and Drug Administration US) approved drugs that improve AD symptoms by inhibiting AChE.

2.2.2 Monoamine oxidase (MAO) hypothesis

The etiology of AD is mainly linked with the cholinergic neurotransmission however, recently number of studies have revealed that MAOs are associated with number of psychiatric and neurological disorders, like depression, Parkinson's disease (PD) and Alzheimer's disease (AD) (Binda *et al.*, 2002; Kumar *et al.*, 2016; Youdim *et al.*, 2006). Monoamine oxidases (MAO-A and MAO-B), belong to a family of flavin-adenine dinucleotide (FAD) dependent enzymes which are responsible for catalyzing the oxidative deamination of various xenobiotic and endogenous neurotransmitters and modulate their concentration in the brain and peripheral tissues (Kumar *et al.*, 2015; Shih and Thompson, 1999). MAO-A selective inhibitors have potential to be developed as drugs for the treatment of depression and anxiety disorders (Du *et al.*, 2004; Fuller, 1978), whereas MAO-B selective inhibitors are effective in several neurological disorders such as PD, AD, Huntington chorea and

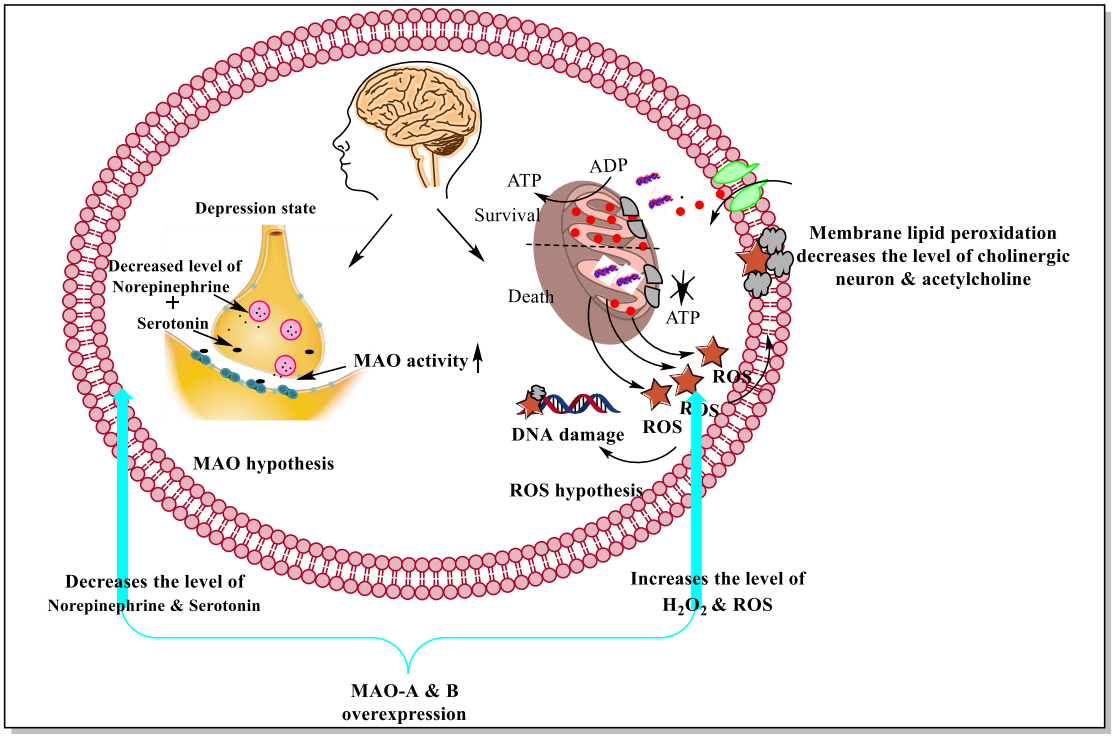

Fig. 2.3 Monoamine oxidase hypothesis for AD and its linkage to ROS hypothesis

amyotrophic lateral sclerosis (Yamada and Yasuhara, 2004). MAO is directly related to the advanced brain functions by regulating the levels of monoamine neurotransmitters. Due to hyperactivity of MAO reported in AD patients, MAO hypothesis is emerging as effective strategy to combat AD. MAO generates hydrogen peroxide and hydroxyl free radicals that play a vital role in the progression of AD (Fig. 2.3 and Fig. 2.4).The presence of oxidative stress, and MAO-B hyperactivity in gliosis increases the levels of H_2O_2 and oxidative free radicals (Christen, 2000). In the preclinical studies, it has been found that MAO-B inhibition can cause cognitive improvement.

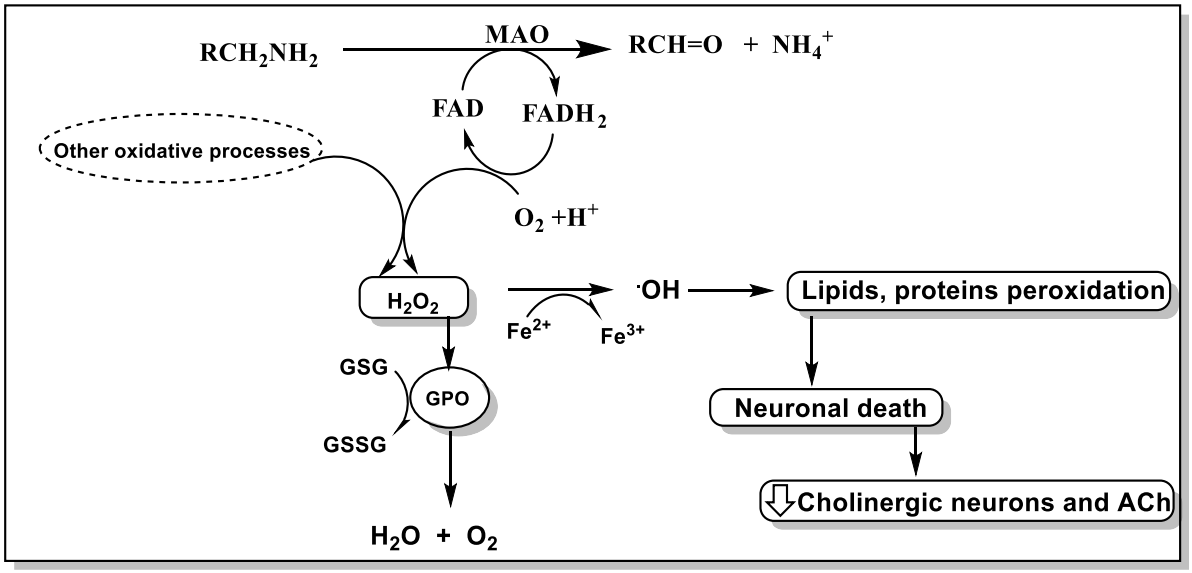

Fig. 2.4 General flow chart for the progression of Alzheimer's disease. The hyper-activity of MAO in the brain increases the concentration of hydrogen peroxide and reactive oxygen species (ROS). This causes degradation of the cholinergic neurons and low levels of acetylcholine affects learning and memory functions of the brain.

MAO generates hydrogen peroxide and hydroxyl free radicals that play a vital role in the progression of AD (Youdim *et al.*, 2006). The neurotoxic aldehyde and hydroxyl free radical generated during MAO catalyzed metabolism of monoamine neurotransmitters are responsible for the neural damage and death. Significant reduction in serotoninergic and noradrenergic transmission might explain the relatively high incidence of depression found in AD patients. Activated MAO increases the expression of β- and γ-secretase and increases Aβ generation from APP also (Cai, 2014). The inhibition of MAO enzyme halts the catalytic cycle and decreases the production of hydroxyl free radicals (Youdim *et al.*, 2006). In addition,

recent reports on the neuroprotective and neurorescue potential (Bar-Am *et al.*, 2007; Naoi and Maruyama, 2009) of MAO inhibitors have generated enormous interests for exploring their role in the aetiology of AD.

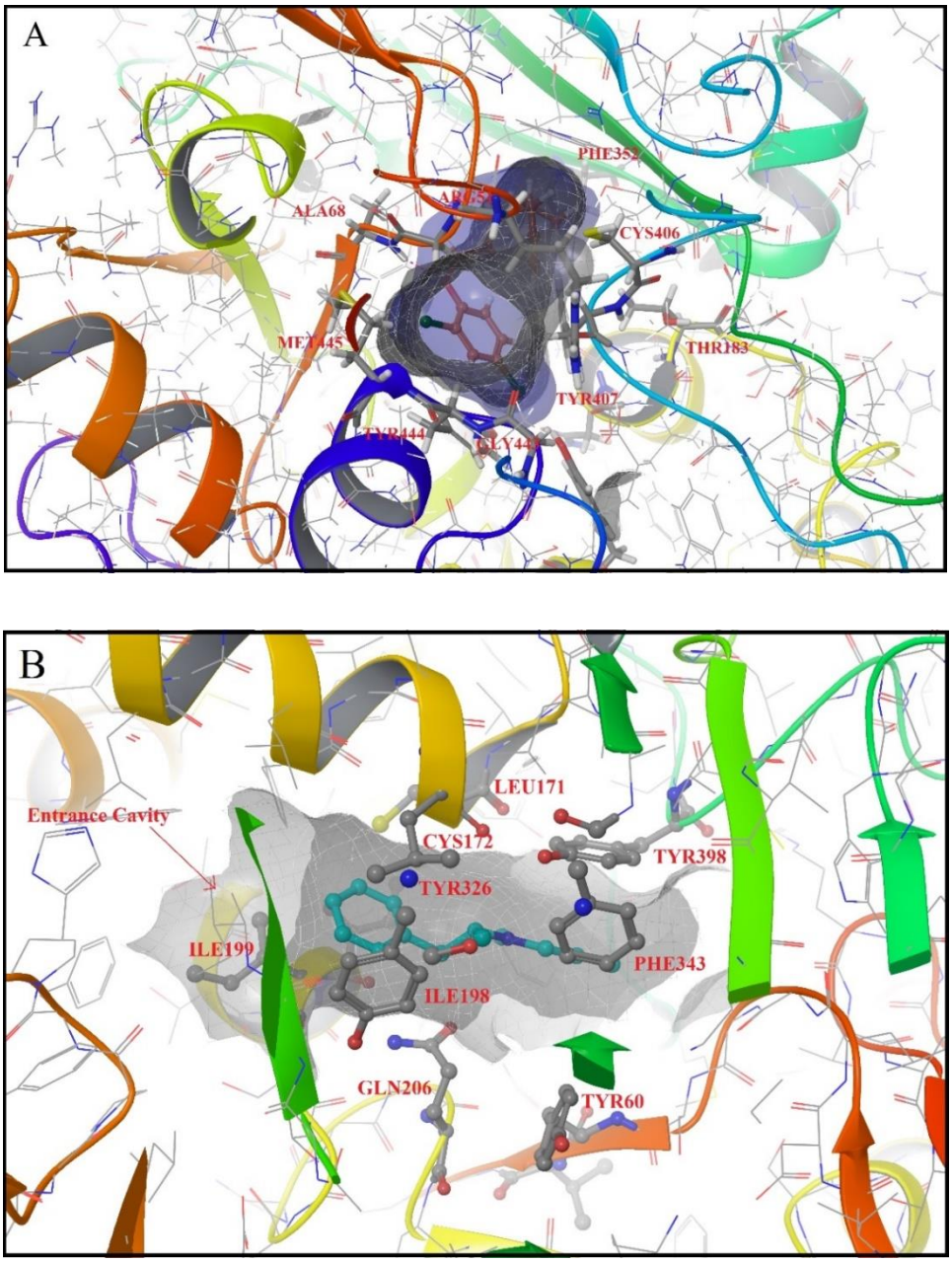

Fig. 2.5 A) The co-crystallized structure of clorgyline with human MAO-A PDB ID (2Z5X). The figure shows ligand interactions at the active site of MAO-A isoform with various amino acids; **B**) The co-crystallized structure of human deprenyl with MAO-B (dimeric) PDB ID (2BYB). In the figure entrance cavity of the MAO-B isoform is shown along with the ligand's interactions with various amino acids at the active site cavity.

The dual inhibitors targeting MAO-B and acetylcholinesterases can play an important role in the management/treatment of AD (Bortolato *et al.*, 2008). Since last few years, there is a surge in the number of research articles published on the synthesis and screening of multi-targeting hybrids as potential drug candidates for the treatment of AD which inhibit AChE and MAO along with other pathways.

X-ray crystal structures of human MAO-B and human MAO-A were reported in year 2002 and 2005 respectively (Binda *et al.*, 2002; De Colibus *et al.*, 2005). Crystallographic studies of the enzyme showed that human MAO-B and rat MAO-A crystallizes as dimer (Binda *et al.*, 2007) while human MAO-A crystalizes as monomeric unit (Fig. 2.5). However, it has been observed that most of the membrane proteins are dimeric in the membrane form (Sachs and Engelman, 2006). Andres *et al*. through modeling studies and species-dependent genetic analysis concluded that the monomeric structure of human MAO-A could be due to Glu151Lys mutation near the dimer interface (Andres *et al.*, 2004). The EPR data showed that rat and human MAO-A and MAO-B enzymes are dimeric in the membrane bound forms however human MAO-A crystalizes as monomer while MAO-B crystalizes as dimer (Binda *et al.*, 2011). The volume of human MAO-A and MAO-B cavities are ~400 $Å^3$ and ~ 700 $Å^3$ respectively. The MAO-B cavity is divided into two separate spaces, the active site cavity for substrate binding (~400 $Å^3$) and the entrance cavity (~300 $Å^3$) (Milczek *et al.*, 2011). Ile199 and Tyr326 side chains separate the two cavities in MAO-B isoform.

Mutagenesis experiments on human MAO-B, Ile199Phe showed that bulky Phe side chain hampers conformational flexibility, reduces the space of the entrance cavity and interferes with the binding of MAO-B selective inhibitors (Hubálek *et al.*, 2005). Thus, Ile199 serves as a structural determinant for substrate and inhibitor recognition. Similarly, Tyr326 exhibit its conformational changes on the inhibitor binding to human MAO-B isoform. A single Ile199Ala mutation to the MAO-B permanently open the gate and double mutations Ile199Ala-Tyr326Ala exhibit inhibitor binding properties similar to those of MAO-A than to MAO-B. This shows that the bipartite cavity structure in the MAO-B plays an important role in substrate and inhibitor recognition to distinguish its specificities from those of MAO-A. The entrance cavity may act as an allosteric binding site for the MAO-B selective inhibitors and potentiation of ligand binding to the entrance cavity of MAO-B by the

ligand occupancy in the substrate cavity opens up possibilities for the design of highly specific MAO-B inhibitors that specifically target the entrance cavity space (Bonivento *et al.*, 2010). This information would be helpful in designing selective inhibitors for MAO-A and MAO-B isoforms (Milczek *et al.*, 2011).

2.2.3 Amyloid cascade hypothesis

The amyloid cascade hypothesis postulates that neurodegeneration in AD is caused by abnormal accumulation of amyloid β plaques in various areas of the brain (Zhang *et al.*, 2011). This progressive accumulation of amyloid β-protein (Aβ) leads to the multifaceted cascade that includes neuronal inflammation, microgliosis, synaptic alterations which ultimately leads to the neuronal dysfunction and loss, and causes impaired memory and cognitive functions. In general, Aβ accumulation is the result of chronic imbalance in the production of Aβ versus its clearance. This imbalance causes increased levels of Aβ in brain than its normal state and its accumulation in the form of plaques around neurons. These plaques are toxic to the neurons and also causes various other cellular changes which ultimately leads to the disease state.

In number of cases with early-onset familial AD, where the genetic mutations in the amyloid precursor protein (APP) PS1 and PS2 genes has been observed, an increase in the production of $A\beta_{1-42}$ is observed through *in vitro* (in cultured cells) and *in vivo (*in transgenic mice and in patients) studies (Haass *et al.*, 1995; Scheuner *et al.*, 1996) via cleavage of APP. APP with size ranging from 695 to 770 amino acids, is an integral membrane protein with a single membrane-spanning domain, a large extracellular glycosylated N-terminus and a shorter cytoplasmic C-terminus. The most abundant form of APP is produced by neurons in the brain of the size of 695 amino acids. It lacks the kunitz-type protease inhibitor sequence in its ectodomain as compared to other APP present in different parts of the body (Hardy, 1997; Mattson, 1997). There are three different secretase enzymes involved in the cleavage of APP at three different cleavage sites i.e. α-, β- and γ-secretase sites (Selkoe and Schenk, 2003).

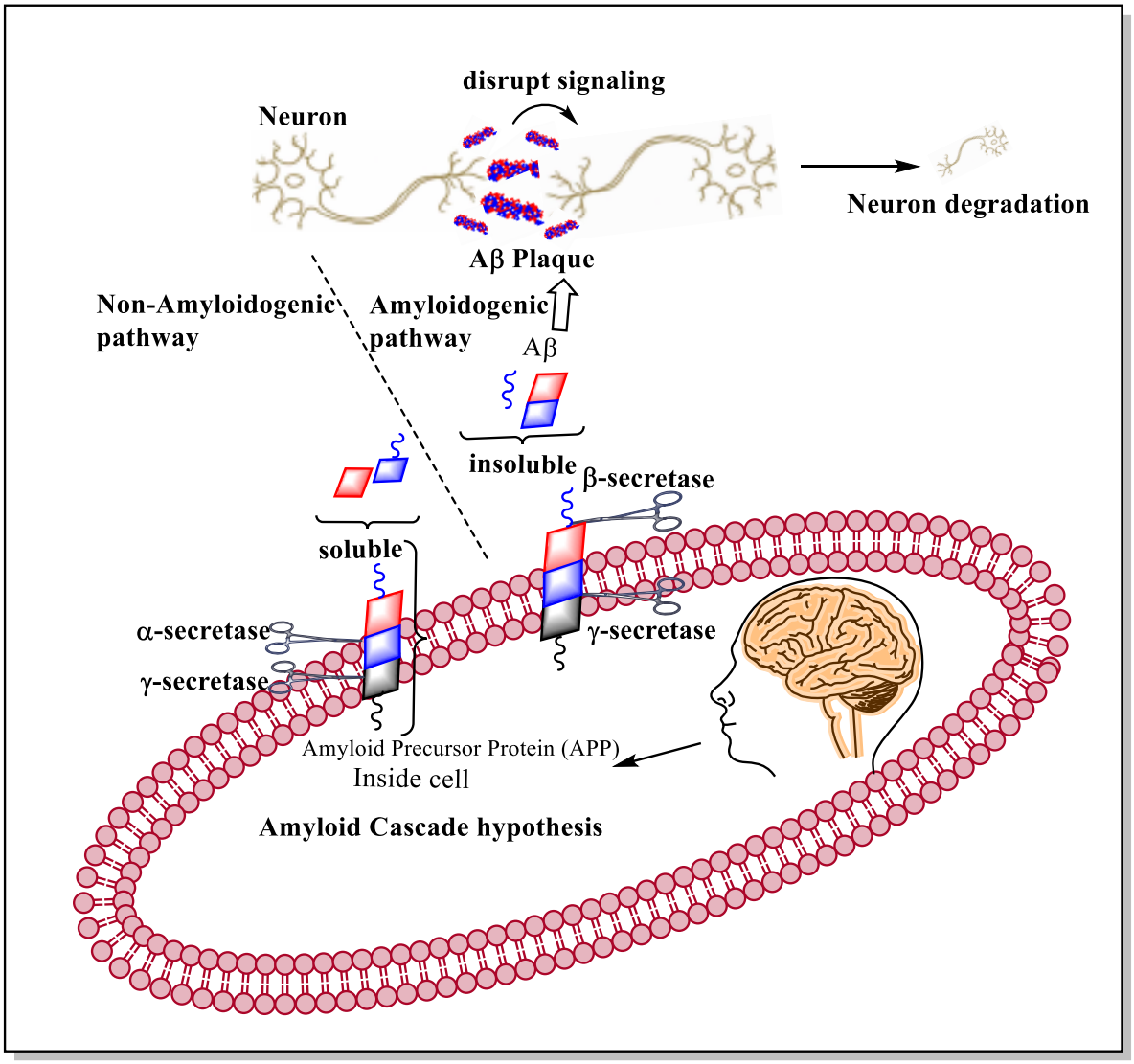

Fig. 2.6 Amyloid Cascade hypothesis of Alzheimer's disease

In non-amyloidogenic pathway α-secretase acts on APP, followed by a γ-secretase forming a harmless and highly soluble peptide but in amyloidogenic pathway, there is a breakdown of APP by β-secretase followed by γ-secretase which results in the formation of chemically insoluble Aβ plaque (Fig. 2.6). The Aβ senile plaques are composed of Aβ peptides, which consist of 39–43 amino acid residues but oligomers consisting of the 42 amino acid Aβ derivative ($A\beta_{42}$) are believed to be critical as these are insoluble and highly hydrophobic (Kumar *et al.*, 2016). Apolipoproteins E (APOE) and various other ligands such as heparin sulfates also interact with Aβ and affect its production, deposition, and clearance in sporadic Alzheimer's disease. These increase the polymerization of Aβ monomers to form senile plaques. According to the Amyloid Cascade Hypothesis, this accumulation of plaques acts

as a pathological trigger for a cascade that includes neuritic injury, formation of neurofibrillary tangles (NFTs) via tau protein, neuronal dysfunction and cell death. Aβ interacts with plasma membrane and impairs its integrity. It is also transported into the cell and crosses mitochondrial membranes which may affect the mitochondrial membrane potential. These can cause mitochondrial dysfunction, overproduction of reactive oxygen species and initiation of apoptosis (Hardy and Selkoe, 2002). Although various *in vitro* and *in vivo* studies reported the neurotoxicity of Aβ peptide (Mucke and Selkoe, 2012), but approximately 30% of normal aged humans also have same amount of Aβ plaque as much in AD affected brain. The major difference is the presence of tau phosphorylation in cases of AD (Van Duinen *et al.*, 1987).

In many studies it has been observed that AChE interacts with Amyloid β (Aβ) through hydrophobic pocket close to the peripheral anionic site (PAS), thus promoting Aβ aggregate formation (Inestrosa *et al.*, 1996; Reyes *et al.*, 1997). Production of Aβs in the brain result in amyloid plaques. Human and mouse recombinant AChE enzymes were reported to accelerate amyloid formation, which produces few amyloid-like fibrils (Inestrosa *et al.*, 1996). Reyes *et al.* reported the inhibition of amyloid formation triggered by AChE by monoclonal antibody 25B1 (Reyes *et al.*, 1997). These reports created a new interest in AChE inhibitors with Aβ inhibition potential.

2.2.4 Other pathways associated with AD

Apart from the above mentioned pathophysiologies behind the progression of AD, various other factors have been linked with the development of AD. Excess activation of N-methyl-D-aspartate (NAMDA) type glutamate receptors cause excessive Ca^{2+} influx and hyperactivation of glutamate, which leads to the production of excessive free radicals and causes neuronal cell death (Lipton, 2005). GSK-3β is a kinase enzyme responsible for the phosphorylation of tau proteins. Overactivation of GSK-3β leads to the hyperphosphorylation of tau proteins and causes deposition of neurofibrillary tangles (NFT) around neurons. These toxic NFTs leads to the neurodegeneration and ultimately to AD (Hooper *et al.*, 2008). Along with these factors, colocalization of metal ions such as Cu, Fe, and Zn in senile plaques is reported in AD patients. Although, these metals ions are important

for biological processes in CNS system like signal transmission, catalysis, stabilization of protein's structure, and metabolism but, dyshomeostasis and miscompartmentalization of these metal ions can lead to the production of ROS, metal ion induced Aβ aggregation and NFT formation which ultimately leads to AD (Zheng and Monnot, 2012). Various members of phosphodiesterase (PDE) family have also been linked to AD (Bollen and Prickaerts, 2012; Pérez-Torres and Mengod, 2003). Different studies have reported the increased expression of PDE4, PDE7, and PDE8 in the AD-affected brain (Pérez-Torres, Silvia *et al.*, 2003). Glutaminyl cyclase, a catalytic enzyme responsible for the pGlu modification of Aβ has also attracted the attention as a potential therapeutic target for AD due to its Aβ-mediated toxicity and upregulation in areas of the brain affected by AD (Morawski *et al.*, 2014; Schilling *et al.*, 2008). Its overexpression is found to cause various behavioral discrepancies (Saido *et al.*, 1995). Peroxisome proliferator activator receptor γ (PPAR-γ) is also reported as an important factor behind AD (Kitamura *et al.*, 1999). Sastre *et al.* suggested that PPAR-γ ligands may downregulate BACE1 transcription and NSAIDs can regulate BACE1 promoter activity (Sastre *et al.*, 2003; Sastre *et al.*, 2005). Camacho *et al.* reported that PPAR-γ does not affect any of secretases but its ligands may fasten the Aβ clearing mechanism (Camacho *et al.*, 2004). d'Abramo *et al.* suggested that PPAR-γ overexpression can lead to reduced Aβ secretion and APP downregulation does not involve ant pathway of secretase (d'Abramo *et al.*, 2005). In addition, many other pathological pathways like phospholipase A2 (PLA2s) (Sanchez-Mejia *et al.*, 2008), cyclophilin D (CypD) (Du *et al.*, 2008), GD3 synthase (Bernardo *et al.*, 2009), plasminogen activator (Melchor *et al.*, 2003), dickkopf1 (DKK1) (Caricasole *et al.*, 2004), calpain (Saito *et al.*, 1993), and histone deacetylases (HDACs) (Kilgore *et al.*, 2010), have been identified that are expected to play significant role in the development of AD.

2.3 Multifactorial nature of AD

The exact molecular pathogenesis of AD is unclear however, deficiency of ACh in AD brain, degeneration of neurons and glial cells or inclined metabolism of signaling neurotransmitters and various biochemical and histopathological studies have been reported to describe the best possible pathogenesis of AD (Gauthier, 2002). It has been found that variation in the biological cholinergic system effects the metabolism

of APP, amyloid-β (Aβ) production and its deposition in the brain (Pákáski and Kálmán, 2008). Depressive symptoms reported in the AD patients are linked with the degradation of various monoamine neurotransmitters in the brain. Overactivation of MAO-B is also reported in the brain of AD patients (Riederer *et al.*, 2004).

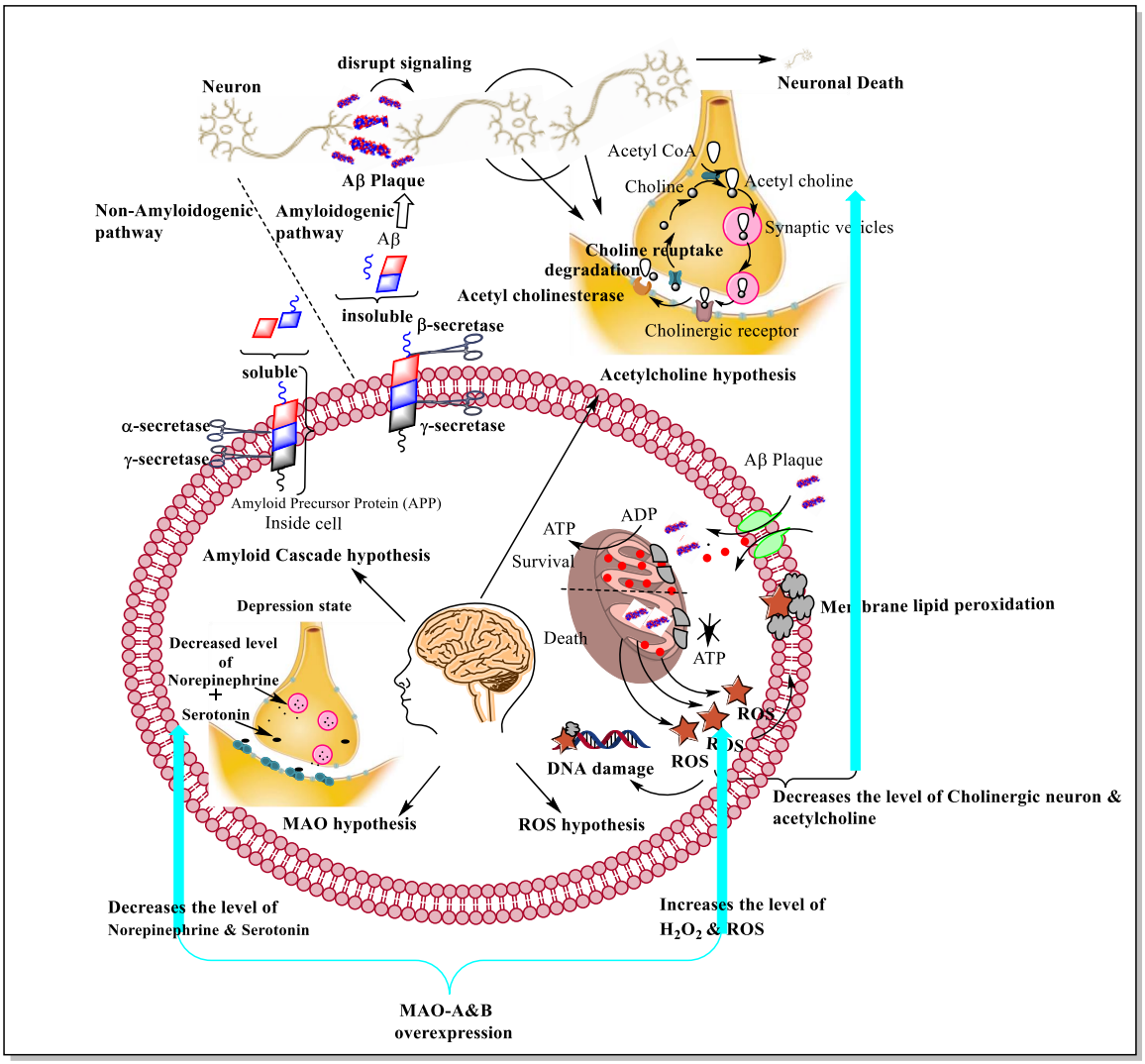

Fig. 2.7 Multifactorial nature of AD and crosslinking of various biological dysfunctions with each other in the progression of AD

The behavioral changes observed in the AD patients are linked with the alterations in serotoninergic and dopaminergic neuronal systems. In addition, oxidative stress plays crucial role in the pathophysiology of AD. MAO mediated metabolism of monoaminergic neurons can generate neurotoxic products like aldehydes, hydrogen peroxide and further increases the concentration of reactive oxygen species. Ultimately it leads to the neuronal membrane damage, membrane lipid

peroxidation and neuronal cell death. Different cellular pathways that have potential to develop AD are represented in Fig. 2.7.

2.4 Current therapies for AD

Currently cholinestrase inhibitors donepezil (Sugimoto *et al.*, 2000), galantamine (Marco-Contelles *et al.*, 2006), tacrine, rivastigmine (Anand and Singh, 2013) and NAMDA receptor antagonist memantine (Fig. 2.8) are the only Food and Drug Administration (US-FDA) approved drugs that improve AD symptoms. These drugs inhibit the acetylcholinestrase enzyme and improve the concentration of acetylcholine in synaptic cleft. Acetylcholine is the neurotransmitter mainly involved in hippocampus and cortex region of the brain for memory. But these drugs do not reverse the damage caused to brain by AD and provide only symptomatic relief. These drugs merely slow the progression of AD, but proved ineffective for the permanent treatment of AD.

2.4.1 Tacrine

Tacrine, 9-amino-1,2,3,4-tetrahydroacridine (Brand name: Cognex), was the first drug to get US FDA approval in 1993 for the symptomatic relief from AD. It is reversible AChE inhibitor with long duration of action. It binds close to the CAS in the enzyme. Tacrine also effect the muscarinic (Ml, M2) and nicotinic receptors (Tsopelas and Marin, 2001). In 1986, tacrine receiving patients showed significant improvement in cognitive performance (Summers *et al.*, 1986). These encouraging results led to the muticenter study from 1990-1994. In 1991, beneficial effect of tacrine over placebo has been reported in the mini mental state examination (MMSE) score (Eagger *et al.*, 1991). However, dose-dependent rise in levels of serum alanine aminotransferase was observed in high population of tacrine treated patients. But this increased serum level was found to be reversible and return to normal level on withdrawal of tacrine treatment. In double blind placebo controlled multicenter six-week trial, in the Mini-Mental State Examination tacrine showed favorable results, but the differences as compared to control studies were very small and statistically non-significant (Davis *et al.*, 1992). A 30-week randomized, double-blind trial for high dose of tacrine was carried out to evaluate the efficacy and safety of high dose of tacrine (Knapp *et al.*, 1994). In this study, dose-related improvements were observed on objective performance-based tests and measures of quality of

life. But due to asymptomatic liver transaminase elevations (28%) and gastrointestinal complaints (16%) some of the patients withdrawn from this trial. Although, these effects were found to be reversible and most of the patients restarted tacrine treatment, but careful monitoring of ALT level was required in patients receiving tacrine. In 2003, this drug was retrieved from US market due to safety issues and its hepatotoxicity reports.

2.4.2 Donepezil

Donepezil (Brand name: Aricept), with a *N*-benzylpiperidine and an indanone moiety in its structure, is a mixed type AChE inhibitor and was second drug to get US FDA approval in 1996 for the treatment of AD (Simoes *et al.*, 2014). The history of development of donepezil starts from 1983, when Sugimoto and co-workers at Eisai Co. started a new research project to develop new tacrine derivatives to eliminate the hepatotoxic effects of tacrine and limitations of oral bioavailability and pharmacokinetic profile of rivastigmine. Although, they failed to develop a non-toxic derivative of tacrine, but a novel *N*-benzylpiperazine derivative screened for arterial sclerosis has attracted their attention. Even though this ligand showed low potency against AChE, however it has been used as a potent lead for the further developments. More than 700 derivatives of this scaffold had been synthesized and it was observed that replacing *N*-benzylpiperazine with *N*-benzylpiperidine moiety resulted in the dramatic increase in potency for AChE inhibition (Sugimoto *et al.*, 1992; Sugimoto *et al.*, 1990). Replacement of amide bond with cyclic amide led to 1-benzyl-4-(2-isoindolin-2-ylethyl)piperidine, which acted as a prototype in the development of new AChE derivatives. Further structural modifications on the indanone moiety led to donepezil, 1-benzyl-4-[5,6-dimethoxy-(1-indanone)-2-yl]-methylpiperidine hydrochloride which showed most potent inhibitory activity against AChE with an IC_{50} of 5.7 nM (Sugimoto *et al.*, 1995; Sugimoto *et al.*, 2000). Donepezil was found to be 1250-folds more selective for AChE as compared to butyrylcholinesterase, more selective than physostigmine and tacrine (Sugimoto *et al.*, 1995). In *in vivo* studies on mice donepoezil showed longer duration of action and significantly increased the ACh level in mice, brain at a dose of 5 mg/kg (v.o.) and does not showed any significant toxicity in short term trials. In double blind placebo-controlled phase II and III trials, donepezil improved memory, speaking skills and other cognitive functions of participated volunteers without showing

hepatotoxicity (Viegas *et al.*, 2011). In 1996 US FDA approved the use of donepezil for the treatment of moderate to severe AD. There is increased risk of GIT bleeding in case of peptic ulcers or use of NSAIDs along with donepezil (http://labeling.pfizer.com/ShowLabeling.aspx?id=510).

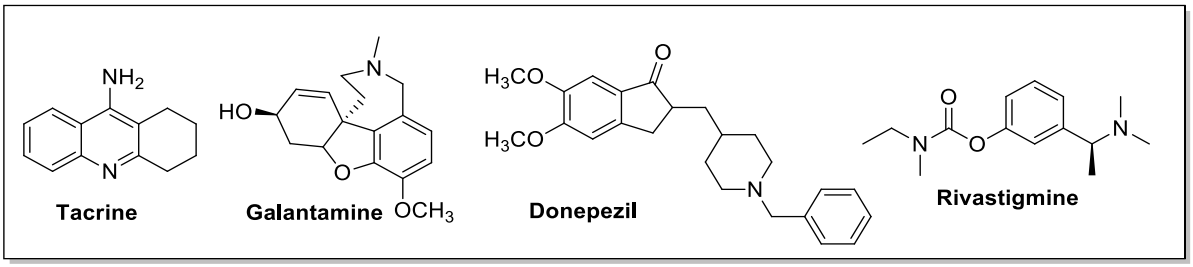

Fig. 2.8 FDA approved drugs for Alzheimer's disease

2.4.3 Galantamine

Galantamine (Brand name: Reminyl®), a tertiary alkaloid, is another acetylcholinestrase inhibitor used for the treatment of AD. The chemical name of galantamine is (4a*S*, 6*R*, 8a*S*)-4a,5,9,10,11,12-hexahydro-3-methoxy-11-methyl-6*H*-benzofuro[3a,3, 2-*ef*][2]benzazepin-6-ol hydrobromide. Galantamine is not only a reversible and competitive inhibitor of AChE but it also modulates the nicotinic acetylcholine receptors (nAChRs) (Albuquerque *et al.*, 2001). Decrease in the expression and activity of nAChRs plays significant role in the reduction in central cholinergic neurotransmission in patients suffering with AD. Thus, this property of galantamine to modulate nAChRs becomes utterly important feature in the treatment of AD. First report on isolation of galantamine from the bulbs of the Caucasian snowdrops, *Galanthus woronowi* was published in 1952 (Proskurnina and Yakovleva, 1952) and subsequently it was isolated from the bulbs of the common snowdrop, *Galanthus nivalis* and several *Amaryllidaceae* plants (Sramek *et al.*, 2000). Till 1980, the use of galantamine was limited to Bulgaria, Italy, France and Germany. Its high price (US$40,000/kg) and unavailability of industrially acceptable synthetic process halted its development to become first AChE inhibitor for treatment of AD. During this period, the tacrine was developed as first drug for the treatment of AD. In 1998, concise scalable synthesis of galantamine was reported allowing batch sizes in the range of 100 kg which made it industrially acceptable (Czollner *et al.*, 1998). After some clinical trials in 2000, galantamine

was approved for the treatment of AD in USA and other European countries. Galantamine is rapidly absorbed on oral administration with 80-100% bioavailability, but plasma protein binding is very low (approximately 18%), and have short plasma half-life (approximately 7 h) (Bickel *et al.*, 1991).

2.4.4 Rivastigmine

Rivastigmine (SDZ ENA 713, Brand name: Exelon), (+) (S)-*N*-ethyl-3-[(1-dimethyl-amino) ethyl], is a second-generation pseudo reversible AChE inhibitor and was approved for the treatment of moderate to severe AD in 2000. It was structurally different from earlier approved two AChE inhibitors (Birks *et al.*, 2015). The presence of carbamate moiety of rivastigmine facilitates its binding to the catalytic triad of AChE. As compared to acetate moiety of ACh it remains bounded at site for longer time and prevents the hydrolysis of ACh. It makes the enzyme inactive for much longer time until rivastigmine get out of circulation. The other significant feature of rivastigmine is that it is not metabolized or inactivated by hepatic cytochrome P450 enzyme in first pass metabolism (Onor *et al.*, 2007). Rivastigmine was found to have more selectivity for the hippocampus and cortex (rather than the striatum and pons/medulla) regions in the brain as compared to other AChE inhibitors. Thus, it increases the AChE inhibition in the hippocampus and cortex regions, which are the most affected areas of brain by Alzheimer's disease. The major side effects reported in rivastigmine treated patients were nausea, vomiting, dizziness and fatigue. Thus, dose calculations were important features to get maximal beneficial effects of rivastigmine (Brufani *et al.*, 1997). Now transdermal patches were developed for rivastigmine for treatment of AD. These transdermal patches were found to be as effective as orally administered rivastigmine. The chances of GIT cholinergic adverse effects were reduced by three time on use of transdermal patches of rivastigmine (Winblad, B *et al.*, 2007).

2.5 Problems with current therapies for AD

Alzheimer's pharmacotherapy is based on maintaining the optimum levels of neurotransmitters like acetylcholine (ACh), dopamine, serotonin, norepinephrine and others. Among these, acetylcholine is metabolized by cholinesterases while monoamine oxidase enzymes metabolise dopamine, serotonin, norepinephrine

neurotransmitters and low levels of these neurotransmitters are linked with the progression of AD (Hroudová *et al.*, 2016).

At present, there are four FDA-approved drugs (Tacrine, donepezil, galantamine and rivastigmine) (Gura, 2008; Racchi *et al.*, 2004a) that improve AD symptoms by inhibiting AChE and thereby raising ACh concentration in the synapsis. Current pharmacotherapy for AD provides only symptomatic relief by targeting cognitive revival. Apart from the beneficial palliative properties of AChE inhibitors in AD (Munoz-Torrero, 2008), cholinergic drugs have shown little efficacy to prevent the progression of the disease. Tacrine was withdrawn from the market due to incidence of hepatocellular injuries in patients receiving this drug. Low plasma binding and short half-life of galantamine are major concerns with this drug, which minimize its use in treatment of AD. Similarly, various side effects of rivastigmine like nausea, vomiting, dizziness and fatigue observed in rivastigmine treated patients, declined its use in the treatment of AD. Further, the involvement of multiple factors, such as reduced acetylcholine (ACh) level, over expressed MAO, amyloid-β (Aβ) and tau protein aggregation, excessive metal ions (e.g., Cu^{2+}, Zn^{2+}, Fe^{3+}) and oxidative stress made the current therapies ineffective against AD (Barnham *et al.*, 2004; Brown and Kozlowski, 2004; Mattson, 2004). Thus, due to the involvement of multiple pathways in the progression of AD, these single targeting acetylcholinesterase inhibitors failed to cure the disease. Consequently, there is no efficient drug to cure, stop or even slow the progression of the disease or progressive neurodegeneration. Therefore, effective therapeutics are sought for the permanent treatment of AD.

2.6 Why multi-target-directed ligands (MTDLs)

The biochemical complexity of the neurodegenerative diseases proves that targeting single pathophysiological process among the number of the altered ones is a challenging goal and it would likely result in insufficient effectiveness to prevent, retard, stop or reverse the disease conditions. Indeed, many new drugs showing a single–target mechanism are also in the clinical trials for these multi-factorial diseases although their therapeutic efficacy is limited to an essentially palliative and/or symptomatic relief (Hughes *et al.*, 2016). To overcome the problems related to such drugs, different pharmacological approaches can be used. For example,

when a single medicine is not sufficient to effectively treat a disease, a multiple-medication therapy (MMT) also referred as a “cocktail” or “combination therapy” can be used. Usually, combination therapy involves two or three different drugs with different pharmacological mechanisms. But the disadvantage of this approach is for patients with compliance problems (Cavalli *et al.*, 2008). Different solubilities and pharmacokinetic profile of the combined drugs can modify the bloodstream uptake of these drugs, which can reduce level of drug below required or can enhance to toxic level. Another disadvantage of this approach is different pharmacodynamic properties of the drugs. In addition to these problems, the regulatory requirements are more complex when the agents are used in combination because safety profile of each drug would have to be demonstrated before clinical trials. Thus, drug discovery process can be further delayed due to regulatory or IP issues if the drugs involved in combination therapy are being developed by different companies. Another approach is the use of a multiple-compound medication (MCM) also referred as “single-pill drug combination”, which involves the incorporation of different drugs into the single formulation in order to improve patient compliance and simplify dosing regimens. But the problems with multiple single-drug entities are different bioavailability, pharmacokinetics, and metabolism (Morphy and Rankovic, 2005). Thus finally, a third strategy is now emerging on the basis of the assumption that a single compound may be able to hit multiple targets which is termed as “multi-target-directed ligand” (MTDL).

Undoubtedly, a single drug that targets multiple biological targets would have intrinsic advantages over MMT or MCM. A multi-target-directed drug can recognize different targets involved in the pathological events of a disease. Thus, such a multi-target-directed medication could be more promising approach for treating multifactorial diseases like Alzheimer’s disease. With development of MTDL, therapeutic treatment would be significantly simplified in relation to combination therapy and further the risk of possible drug-drug interactions can be avoided. Thus, these all considerations are important in new drug development for the treatment of multifactorial neurological diseases. Therefore, there are strong indications for the development of compounds or drugs which are able to hit multiple targets i.e. “multi-target-directed ligands” (MTDLs).

2.7 Recent developments in MTDLs for the treatment of AD

Regardless of great efforts and investment in research against AD, no drug could be developed in the last decade for its treatment. Various research groups put substantial efforts in this field to find novel lead for treatment of AD but still no successful preventive cure or therapy is available. However, in last decade researchers put their attention to explore new therapeutic targets along with targeting multiple targets through single drug.

Currently, strategy of targeting AChE and MAO simultaneously for the treatment of AD gained attention of the researchers. This is due to the direct involvement of both enzymes in the progression of AD. Firstly, the memory impairment is mainly associated with the loss of cholinergic transmission in the temporal lobe and other cortical brain regions. The overexpression of AChE causes the excessive hydrolysis of ACh and reduces its level below normal required for neuronal signaling. Along with memory impairment, it also decreases the intellectual ability and causes severe alterations in behavior (Coyle *et al.*, 1983). Similarly, overexpression of monoamine oxidase (MAO) activity is also observed in AD patients, which causes the increased metabolism of dopamine, serotonin and results in higher levels of H_2O_2 and oxidative free radicals (Saura *et al.*, 1994). Thus, both the enzymes, AChE (which degrades synoptically released acetylcholine) and MAO (which degrades catecholamine neurotransmitters like dopamine, serotonin, adrenaline etc.), became most important targets for the treatment of AD. In last few years, numbers of publications are reported on the development of various multitargeting compounds for the treatment of AD.

Samadi *et al.* reported synthesis, biological screening and docking studies of two different series of compounds which simultaneously inhibit MAO as well as acetylcholinesterase (AChE) and butyrylcholinesterase (BuChE) (Samadi *et al.*, 2011). The screening of compounds led to the identification of a lead that can act as multi-potent drug exhibiting high and selective AChE inhibitory activity (IC_{50} = 37 ± 4 nM) and moderate, but selective MAO-A inhibition activity (IC_{50} = 41 ± 7 μM). Molecular modeling studies of the most active compound confirmed its dual AChE inhibition activity, binding simultaneously at the catalytic active site and at the peripheric anionic site. The compound **1** (Fig. 2.9) was reported as the most active

and selective dual AChE inhibitor, displaying a moderate and selective MAO-A inhibition activity. Compound **1** was proposed as a multi-potent lead that could be developed as a drug that simultaneously binds to two pharmacological targets and could play a role in the treatment of AD. Bolea *et al.* synthesized a series of compounds using a hybrid molecular approach by combining the benzylpiperidine scaffold of the donepezil (AChE inhibitor) and indolylpropargylamino part of the MAO inhibitor *N*-[(5-benzyloxy-1-methyl-1*H*-indol-2-yl)methyl]-*N*-methylprop-2-yn-1-amine (Bolea *et al.*, 2011).

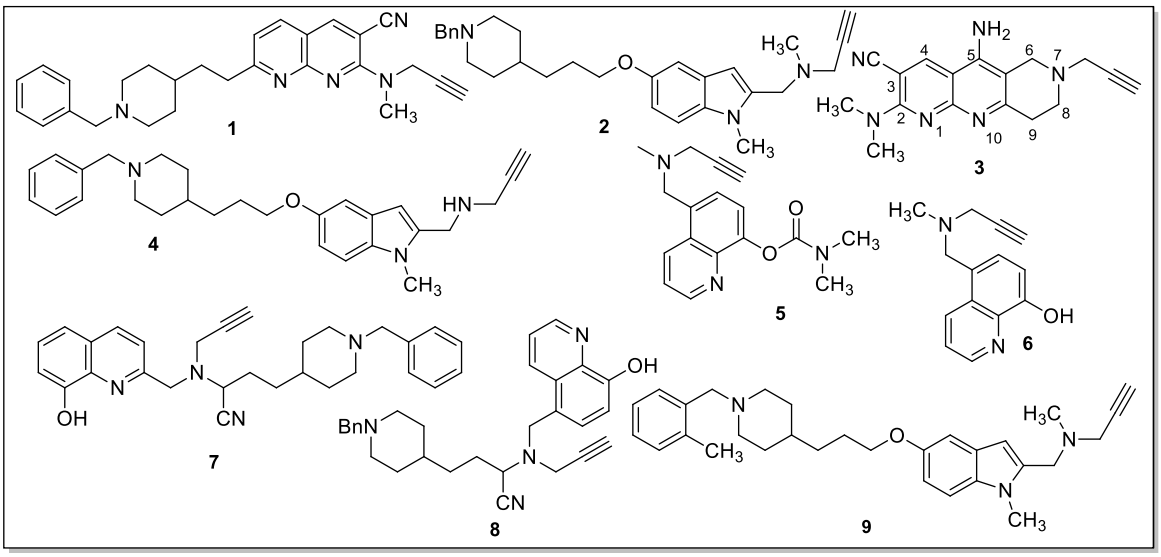

Fig. 2.9 Propargylamine derivatives as multi-receptor inhibitors for AD

The two parts of the hybrid molecule were linked through an oligomethylene linker. Molecular docking and kinetic studies showed that the most promising hybrid **2** (Fig. 2.9) was the inhibitor of both MAO-A (IC_{50} = 5.2 ± 1.1 nM) and MAO-B (IC_{50} = 43 ± 8 nM) isoforms and it also exhibited potency towards AChE and BuChE. The same research group (Samadi *et al.*, 2012) designed heterocyclic substituted alkyl and cycloalkylpropargylamines as multi-targeting agents that simultaneously bind to the monoamine oxidases as well as cholinesterases. Indole derivatives reported in the series I type of compounds were well known MAO inhibitors and were investigated for their capacity to inhibit AChE and BuChE. In the series I, *N*-[(5-(benzyloxy)-1*H*-indol-2-yl)methyl]-*N*-methylbut-2-yn-1-amine has been found to be multi-potent compound that could selectively inhibit MAO-B (IC_{50} = 31 ± 2 nM) and eqBuChE (IC_{50} = 7 ± 1 μM) enzymes. The molecular modeling studies of this compound showed that high MAO-B inhibitory activity might be due to the presence of methyl

propargyl group in the proximity of N5 of FAD in MAO-B. The series II compounds, i.e., 5-amino-7-(prop-2-yn-1-yl)-6,7,8,9-tetrahydropyrido[2,3-b][1,6]naphthyridines were reported as weak MAO inhibitors, but displayed selective AChE inhibitory activity. 5-Amino-7-(2-propyn-1-yl)-2-(1-pyrrolidinyl)-6,7,8,9-tetrahydropyrido[2,3-b]-1,6-naphthyridine-3-carbonitrile (**3**) (Fig. 2.9) exhibited a multi-potent pharmacological profile simultaneously binding to BuChE and MAO-B and it was proposed as a lead for the design of novel and potent multi-targeting cholinesterase and MAO inhibitors. Bautista-Aguilera *et al.* further designed and synthesized a series of donepezil-indolyl based amines, amides and carboxylic acid derivatives derived from *N*-((5-(3-(1-benzylpiperidin-4-yl)propoxy)-1-methyl-1*H*-indol-2-yl)methyl)-*N*-methylprop-2-yn-1-amine (**2**) (Bautista-Aguilera *et al.*, 2014). These were found to be multipotent inhibitors, targeting cholinesterase and MAO enzymes. The amines were more potent ChE inhibitors than the corresponding amides and carboxylic acids, showing a clear selectivity for EeChE inhibition The most potent inhibitor obtained in the series, i.e. [N-((5-(3-(1- benzylpiperidin-4-yl)propoxy)-1-methyl-1H-indol-2-yl)methyl)prop-2-yn-1-amine] (**4**) (Fig. 2.9) showed multi-receptor affinity profile for MAO-A (IC_{50} = 5.5 ± 1.4 nM), MAO-B (IC_{50} = 150 ± 31 nM), EeAChE (IC_{50} = 190 ± 10 nM) and eqBuChE (IC_{50} = 830 ± 160 nM). Compound **4** displayed good drug-like characteristics and ADMET properties and it can be developed as a drug candidate for the prevention and treatment of AD. Zheng *et al*. designed site**-**activated chelators targeting both AChE and MAO. The most active compound (**5**) had only little affinity for metal (Fe, Cu, and Zn) ions (Zheng *et al.*, 2010). The interesting characteristic of this compound is that the iron chelation capacity becomes activated after inhibition of AChE to release the active chelators M30 (**6**) (Fig. 2.9). Compound **5** showed high potency, *in vitro*, against MAO-A with an IC_{50} value of 7.0 ± 0.7 nM and weak inhibition of MAO-B. It displayed lower cytotoxicity and more lipophilicity than its activated brain permeable chelator **6**. The compound **6** was able to modulate amyloid precursor protein regulation and β-amyloid reduction, suppress oxidative stress, and passivate excess metal ions (Fe, Cu, and Zn), which showed that chelators have potential to treat the underlying cause of AD.

A number of donepezil derivatives (Wu *et al.*, 2015) were designed, synthesized and found to be potent metal chelators that target different enzyme systems related to

AD (ChEs and MAO-A). Compound **7** exhibited excellent ChEs and a selective MAO-A inhibition potency (vs MAO-B) along with the strong complexing affinities for zinc and copper ions (involved in the progression of AD). Compound **7** has shown significant MAO-A, human recombinant (*hr*) AChE and *hr*BuChE inhibitory activities with IC_{50} values of 10.1 ± 1.1 μM, 0.029 ± 0.003 μM and 0.039 ± 0.003 μM respectively. Compound **7** as a donepezil-hydroxyquinoline hybrid was found to be a lead with the disease modifying anti-Alzheimer's drugs (DMAAD) profile. Wang *et al.* synthesized and evaluated multi target directed donepezil, propargylamine and 8-hydroxyquinoline hybrids for the treatment of Alzheimer's disease (Wang *et al.*, 2014). The most active derivative obtained in the series was racemic α-aminotrile 4-(1-benzylpiperidin-4-yl)-2-(((8-hydroxyquinolin-5-yl)methyl)(prop-2-yn-1-yl)amino)butanenitrile (**8**) (Fig. 2.9) exhibiting affinity to MAO-A (IC_{50} = 6.2 ± 0.7 μM), MAO-B (IC_{50} = 10.2 ± 0.9 μM), AChE (IC_{50}= 1.8 ± 0.1 μM) and BuChE (IC_{50} = 1.6 ± 0.2 μM). In the docking studies compound **8** was found to be interacting simultaneously with the catalytic and peripheral site of eeAChE. Most of the compounds showed good ADMET profile and brain penetration capacity for the CNS activity. In the passive avoidance task, compound **8** significantly decreased scopolamine-induced learning deficits when tested on the mice with experimentally induced amnesia. Nineteen donepezil-indolyl hybrids (Bautista-Aguilera *et al.*, 2014) were designed, synthesized and evaluated as multifunctional agents binding to the MAO and ChE enzymes. Compound **9** was the most potent inhibitor in the series exhibiting irreversible hMAO-A inhibition activity with an IC_{50} value of 6.3 ± 0.4 nM and was nine times more potent than the reference drug clorgyline and 29-fold more selectivie towards MAO-A over MAO-B. Compound **9** also showed hAChE and hBuChE inhibition potential with IC_{50} values of 2.8 ± 0.1 μM and 4.9 ± 0.2 μM respectively. Molecular docking studies with **9** showed that *ortho* methyl group improved the ligand recognition and increased the ligand-enzyme hydrophobic interaction in the hBuChE and π−π stacking in hMAO-A, hMAO-B, and hAChE enzyme. Virtual ADMET analysis of compound **9** showed good drug like characteristics with better brain penetration ability as compared to the standard drug selelgiline.

Jiang *et al.* designed and synthesized novel GSK-3β/AChE dual-target inhibitors. Among these hybrids, compound **10** (Fig. 2.10) was found to be the most promising

inhibitor of both hAChE (IC_{50} = 6.5 nM) and hGSK-3β kinase activity (IC_{50} = 66 nM). It also showed good inhibitory effect on β-amyloid self-aggregation (inhibitory rate = 46%) at 20 μM concentration. Compound **10** also inhibited hyperphosphorylation of tau protein in mouse neuroblastoma N2a-Tau cells (Jiang *et al.*, 2018). These compounds were also found safe toward hepatotoxicity. Thus, this concurrent inhibition of the two crucial AD targets, glycogen synthase kinase-3β (GSK-3β) and human acetylcholinesterase (hAChE), represented an important breakthrough in the quest for treatment of AD. Czarnecka *et al.* designed and synthesized novel series of conjugated 9-amino-1,2,3,4-tetrahydroacridine and 5,6-dichloronicotinic acid moieties with different linkers. In multifunctional biological evaluation studies, compound **11** (Fig. 2.10) was found to be the most promising AChE inhibitor with IC_{50} value of 1.02 nM with mixed type of inhibition. Compound **11** also Inhibited the Aβ aggregation upto 46.63% and 19.41% at 50 μM and 5 μM concentrations, respectively and no cytotoxicity was observed for the mentioned concentrations (Czarnecka *et al.*, 2018). Xu *et al.* designed and synthesized another series of novel propargylamine-modified pyrimidinylthiourea derivatives as dual inhibitors of ChEs and MAOs with other functions against AD. Compound **12** (Fig. 2.10) was found to be the most potent dual inhibitor of AChE (IC_{50} = 0.032 ± 0.007 μM) and MAO-B (IC_{50} = 2.117 ± 0.061 μM). Compound **12** also displayed the improved *in vitro* blood-brain barrier (BBB) permeability, antioxidant ability, and good copper chelating property. From *in vivo* studies, hydrochloride salt of compound **12** was found to inhibit the cerebral AChE/MAO-B activities and alleviate scopolamine-induced cognitive impairment in mice (Xu *et al.*, 2018). Sang *et al.* designed and synthesized a novel series of ferulic acid derivatives as multitarget-directed ligands (MTDLs) for the treatment of AD. Compound **13** (Fig. 2.10) was found to be the most potent BuChE inhibitor with IC_{50} value of 8.9 nM, along with potent MAO-A and MAO-B inhibition with IC_{50} values of 6.3μM and 8.6μM, respectively. Compound **13** also inhibited (53.9%) and disaggregated (43.8%) the self-induced Aβ aggregation along with potential antioxidant activity (ORAC = 0.52 eq) and neuroprotective effect against Aβ1-42-mediated neurotoxicity in the SH-SY5Y cells (Sang *et al.*, 2018). Denya *et al.* designed and synthesized indole derivatives as multifunctional agents against AD. From the series, compound **14** (Fig. 2.10) was found to be the most potent multifunctional agent (hMAO-A IC_{50} = 4.31 μM, hMAO-B IC_{50} = 2.62 μM, eeAChE IC_{50} = 3.70 μM, eqBuChE IC_{50} = 2.82 μM) and displayed better potency

than ladostigil. It also showed potent neuroprotective properties at 1 μM concentration against MPP+ treated SH-SY5Y neural cells (Denya *et al.*, 2018). Hu *et al.* designed and synthesized a novel series of dual-targeting AChE/PDE9A inhibitors bearing N-benzylpiperidine and pyrazolo[3,4-d]pyrimidinone moieties. Amongst the different compounds in the series, compound **15** was found to be the most balanced dual AChE/PDE9A inhibitor with IC_{50} values of 0.048 μM and 0.530 μM against AChE and PDE9A, respectively. Further, this compound possesses good blood-brain barrier (BBB) permeability and low neurotoxicity. In *in vivo* studies **15** was found to improve cognitive and spatial memory in $A\beta_{25-35}$-induced cognitive deficit mice in the Morris water-maze test (Hu *et al.*, 2018).

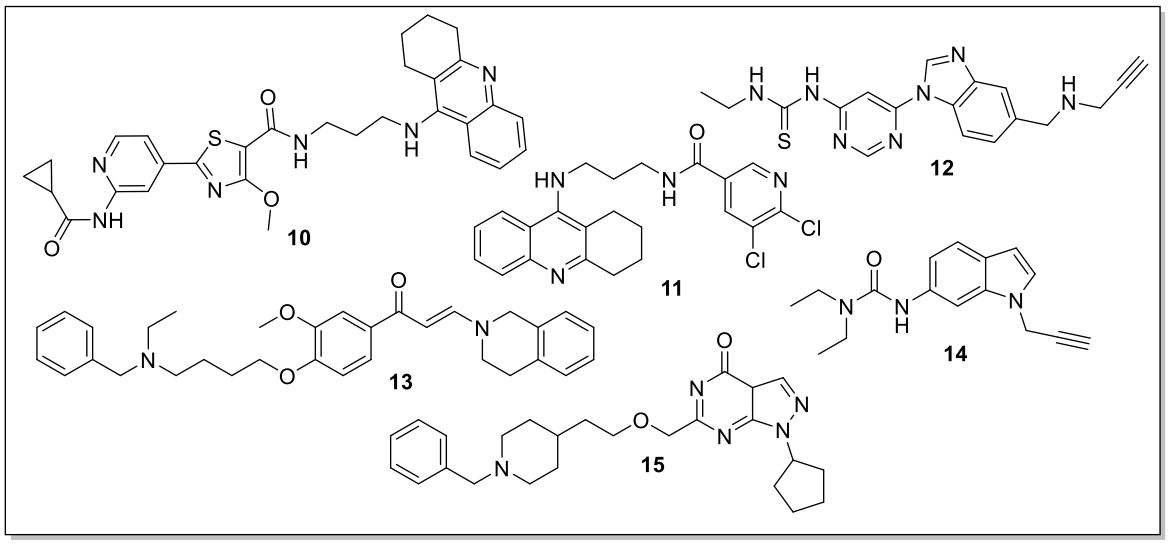

Fig. 2.10 Various multi targeting compounds reported for the treatment of AD

Many of the promising lead compounds are undergoing toxicological studies and are in various stages of clinical developments. Safinamide **(16)**, a reversible MAO-B selective inhibitor, has completed Phase III trials for the treatment of PD. Safinamide was found to be an effective inhibitor of dopamine uptake and a modulator of glutamate release (Stocchi *et al.*, 2006). Varinel Inc., a US based pharmaceutical company, is developing VAR-10200 and VAR-10300 as dual iron chelating and MAO-B selective inhibitors for the treatment of neurodegenerative disorders (Thomson Reuters Pharma, update of Feb. 24, 2012 and May 15, 2012) (Zheng *et al.*, 2005). Ladostigil (TV-3326) **(17)** is being developed by Avraham Pharmaceutical as dual MAO and acetylcholinesterase inhibitor. This compound is under phase II clinical trials in Europe (Thomson Reuters Pharma, update of May

18, 2012). Orizon Genomics is developing OG-45 as a dual inhibitor of MAO-B and lysine specific demethylase-I (Thomson Reuters Pharma, update of April 16, 2012). Similarly, Roche is developing RG1577 (RO-4602522; EVT-302), as a lead compound for the treatment of AD. This orally active compound is reversible and selective inhibitor of MAO-B isoform and is under phase II clinical trials (Thomson Reuters Pharma, update of August 8, 2012). Rasagiline **(18)** with clinicalTrials.gov identifier no NCT02359552 is under phase II clinical trial from Feburary 2015 for the treatment of AD. The aim of the study is to evaluate the effect of the drug in patients suffering from moderate AD. Rasagiline (Azilect) with clinicalTrials.gov identifier no NCT02068625 is under phase IV of clinical studies from February 2014 to investigate its effects in patients suffering from macula off retinal detachment. Currently, CX157 (3-fluoro-7-(2,2,2-trifluoroethoxy)phenoxathiin-10,10-dioxide), a selective MAO-A inhibitor, is under clinical development for the treatment of major depressive disorders (Burch *et al.*, 2014).

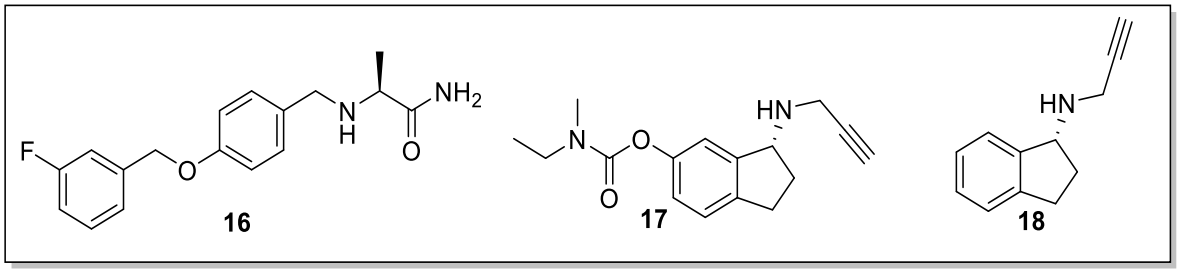

Fig. 2.11 Multi-targeting compounds under clinical trials for the treatment of AD

2.8 Concluding remarks from review of literature

AD is reported to originate through multiple pathogenic factors and targeting single pathway may not be an effective strategy for the complete treatment of the disease. Single-site-targeting' drugs like donepezil, galantamine and rivastigmine have failed to render sufficient neuroprotective and/or neurorestorative activity. Multitarget based drug discovery is the alternative approach in which a single compound can bind to multiple targets so as to manage multiple symptoms. Hence, the dual or multi targeting ligands which can simultaneously inhibit cholinesterases, MAO, Amyloid β, metal chelation etc. are being developed as drugs for the management of AD. Although many newly developed dual or multi targeting inhibitors are under different phases of clinical trials but none of these still reached to clinical use because of the number of adverse effects or low BBB permeability.

Chapter- 3
Rationale and Objectives

3.1 Hypothesis

Most of the human diseases such as cancer, diabetes, heart disease, arthritis and neurodegenerative diseases involve multiple pathogenetic factors. Therefore, more and more efforts are devoted in the quest for new therapeutics aiming at multiple targets (Keith *et al.,* 2005). Although the etiology of AD is not clear, multiple factors including reduced acetylcholine (ACh) levels and overexpressed MAO enzyme have been implicated in the pathogenesis of the disease.

Currently, the only approved therapy for AD is based on a reduction of the cognitive deficits by enhancing cholinergic transmission through inhibition of acetylcholinesterase (AChE). These anti-AChE agents include tacrine, galanthamine, donepezil, and rivastigmine (Fig. 3.1), which have been shown to induce a modest improvement in the memory and cognitive functions, but do not appear to prevent or slow the progressive neurodegeneration. Current pharmacotherapy for AD provides only symptomatic relief by targeting cognitive revival.

Similarly, selegiline (Fig. 3.2), a MAO inhibitor, has been reported to retard the deterioration of cognitive functions and provides relief from the symptoms of AD (Thomas, 2000)**.**

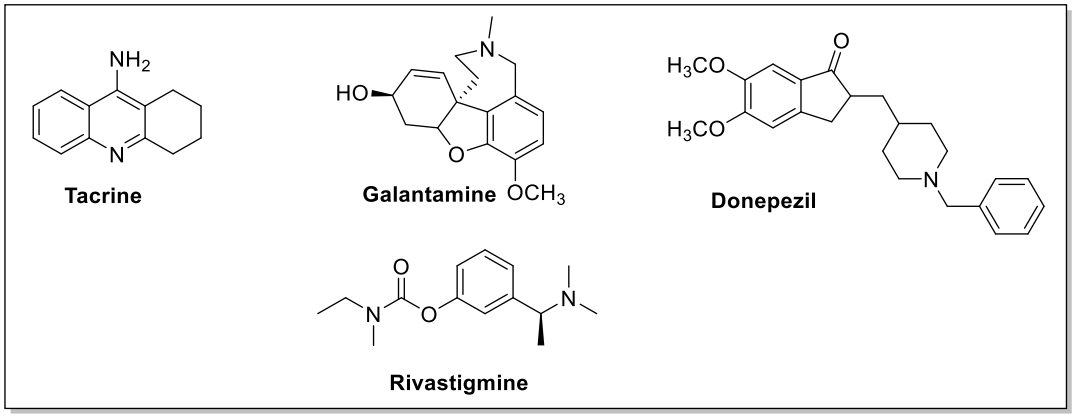

Fig. 3.1 FDA Approved Drugs for the treatment of Alzheimer's disease

In the current research work, we got interested in the identification of a ligand that can be equipotent to both AChE and MAO enzymes and therefore may be developed as a drug candidate for the treatment of AD and other neurodegenerative diseases. The X-ray crystal structure of the active site of both the enzymes is available and it is planned to design target compounds that can best fit in the

cavities. Thus, with the help of docking and SAR studies we tend to know various requirements of the active sites so as to develop potent drug candidate for the treatment of AD.

3.2 Rationale

Acknowledging the multi-factorial character of Alzheimer's disease imply that targeting any single receptor or enzymatic system site will not result in the successful treatment or retardation of this disease progression and as such, many 'single-site-targeting' drugs have failed to render sufficient neuroprotective activity. Now, it is widely accepted that a more effective therapy would result from the use of multi-target directed ligands (MTDLs) that have ability to intrude to the multiple pathological events underlying the etiology of neuronal disorders (Bolea *et al.*, 2013)**.** This multi-targeted ligand design strategy involves the incorporation of two or more distinct pharmacophores of different drugs in the single structure to develop hybrid molecules. In these hybrid molecules, each pharmacophore of the hybrid drug should essentially retain the ability to interact with its specific site(s) on the target to produce the consequent pharmacological response as produced in the parent molecule. The approach of dually inhibiting AChE and MAO enzymatic systems may find significant application in the treatment of AD.

Donepezil is a second generation reversible, noncompetitive, acetylcholinesterase inhibitor with longer half-life and greater specificity for brain tissue (Samanta *et al.*, 2006). Efficacy of donepezil for long-term use has been studied in three one-year trials (Mohs *et al.*, 2001; Winblad *et al.*, 2001). Donepezil was found well tolerated in most of the clinical studies and side effects were mostly dose related, mild and gastrointestinal in nature (Burns *et al.*, 1999). The most commonly reported adverse effects with the use of donepezil are gastrointestinal complaints such as nausea, diarrhea and vomiting, and central nervous system conditions including dizziness, headache, and insomnia. Although in some cases, donepezil developed restless legs, mumbling and stuttering (Amouyal-Barkate *et al.*, 2000), purpuric rash (Bryant *et al.*, 1998) and urinary incontinence (Hashimoto *et al.*, 2000). Rasagiline [N-propargyl-l(R)-aminoindan] mesylate is a second generation propargylamine derivative that inhibits brain MAO-B irreversibly and approved by US FDA as monotherapy and adjunctive therapy for the management of PD (Chen *et al.*, 2007). SAR studies provide evidence that the propargyl moiety (propargylamine) of

rasagiline promotes neuronal survival via neuroprotective/neurorescue pathways (Weinreb *et al.*, 2009). Based on these results ladostigil (Fig. 3.2) was designed by merging the neuroprotective propargyl moiety of rasagiline to the carbamate moiety of AChE inhibitor rivastigmine. The resulting molecule was a novel cholinesterase and selective MAO inhibitor in brain with no inhibition of peripheral MAO (Weinstock *et al.*, 2003). Another derivative of rasagiline, M-30 (Fig. 3.2) was developed by combining the propargyl moiety of rasagiline to the skeleton of VK- 28 (Fig. 3.2), a brain permeable neuroprotective iron chelator (Avramovich-Tirosh *et al.*, 2007; Zheng *et al.*, 2005). Preclinical experiments showed that both compounds have anti AD activities.

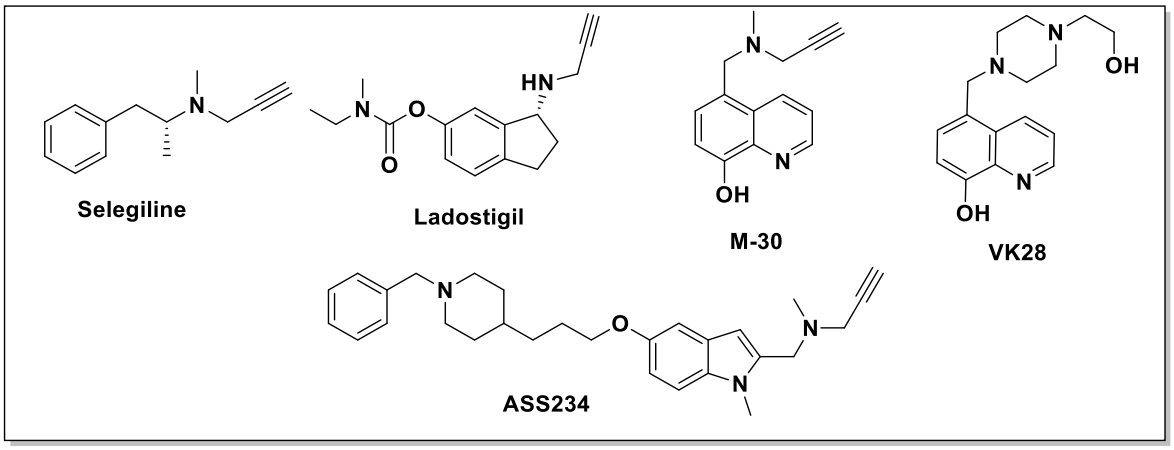

Fig. 3.2 Some propargylamine derivatives reported as neuroprotective agents

The propargylamine moiety is known to play an important role in providing the neuronal and mitochondrial protective properties (Weinreb *et al.*, 2010; Youdim *et al.*, 2005) along with other pharmacological activities like antiapoptotic (Sterling *et al.*, 2002; Yogev-Falach *et al.*, 2006) and amyloid-β (Aβ) aggregation inhibition (Bar-Am *et al.*, 2010). Recently, number of potent MAO inhibitors having propargylamine moiety incorporated in the scaffolds have been reported by various research groups (Fig. 3.3). The propargylamine moiety present in these molecules is reported to form covalent bond with FAD co-factor of MAO enzyme and result in the irreversible inhibition of the enzyme. These features of the propargylamine moiety have led to its incorporation into many drug-like compounds designed for the neuroprotection and afford molecules with broader therapeutic profiles to potentially meet the

curative needs of the multifactorial AD. Thus, propargyl group was selected as pharmacophore-I for the current studies.

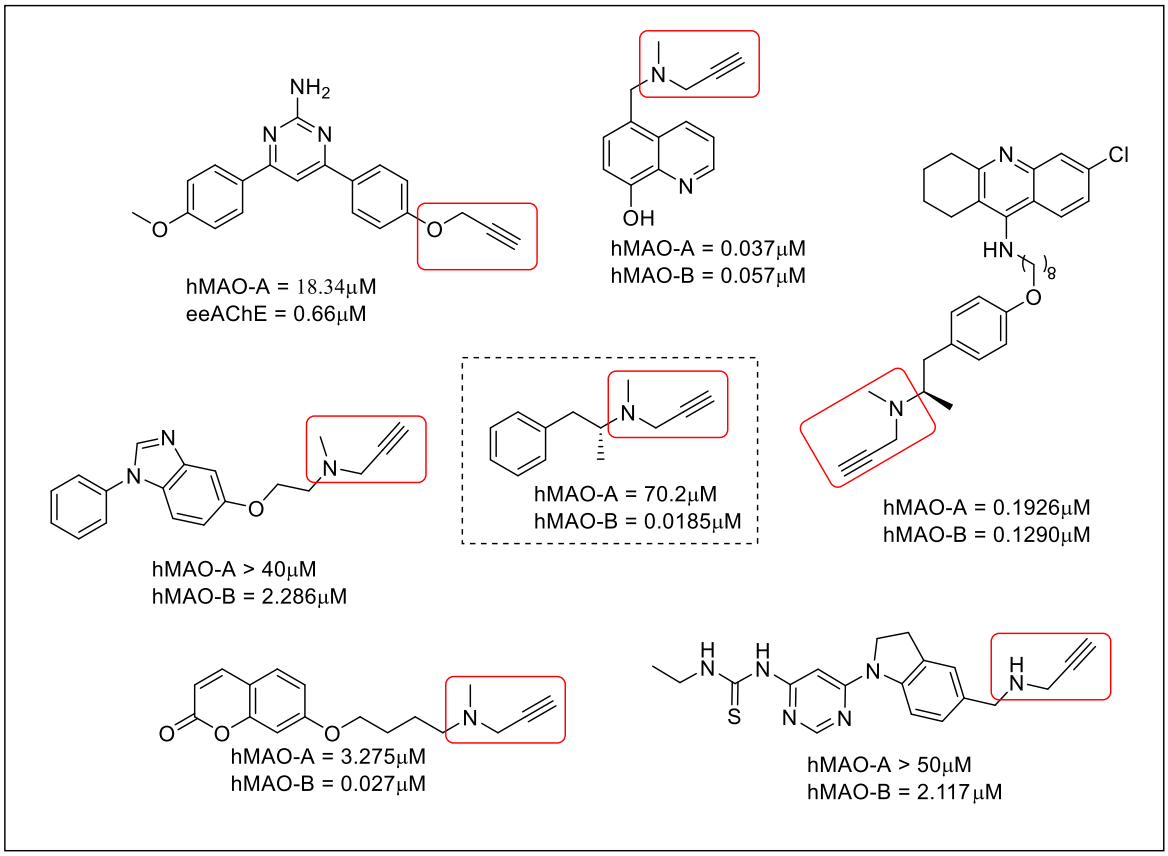

Fig. 3.3 MAO inhibitors reported with neuroprotective properties having propargylamine group as important pharmacophore in the structure.

Benzylpiperidine motif of donepezil is reported to inhibit cholinesterases along with inhibition of Aβ aggregation (Hughes *et al.*, 2016). Hybrid compound ASS234 (Fig. 3.2) designed by incorporating the juxtaposition of donepezil and propargylamine motif of PF9601N, showed inhibition of hAChE (IC_{50} = 0.81± 0.06 μM), hBuChE (IC_{50} = 1.82± 0.14 μM) along with inhibition of MAO isoforms in nanomolar range (MAO-A IC_{50} = 5.44± 1.74 nM, MAO-B IC_{50} = 177 ± 25 nM) (Hughes *et al.*, 2016). The reference compounds donepezil was ineffective against MAO enzyme while PF9601N was ineffective against ChEs. From extensive literature search, it was clear that most of the FDA approved drugs for the treatment of AD (Rivastigmine, donepezil and galantamine) and other reported multitarget AChE inhibitors, contain a tertiary nitrogen present in the open chain or cyclic ring (Fig. 3.4). This tertiary nitrogen atom is expected to interact with the catalytic active site (CAS) or peripheral anionic site (PAS) of AChE. Thus, it was decided to incorporate a tertiary nitrogen

atom in the form of cyclic (morpholine/piperidine/pyrrolidine etc.) or acyclic chain as pharmacophore-II attached to a heterocyclic moiety through appropriate chain length. Recently various phenyl-/benzhydrylpiperazine derivatives (Kumar *et al.*, 2018) have been reported from our laboratory as selective ligands for MAO-A and MAO-B isoforms. Similarly, a number of pyrimidine bridged biaryls (Kumar *et al.*, 2018) have been synthesized and screened from our laboratory for their MAO inhibition potential. Most of these compounds were found to be reversible and selective inhibitors of MAO-B isoform. Taking leads from these studies we got interested in the design and synthesis of dual acting ligands that are equipotent to both MAO and AChE enzymes for the treatment of AD.

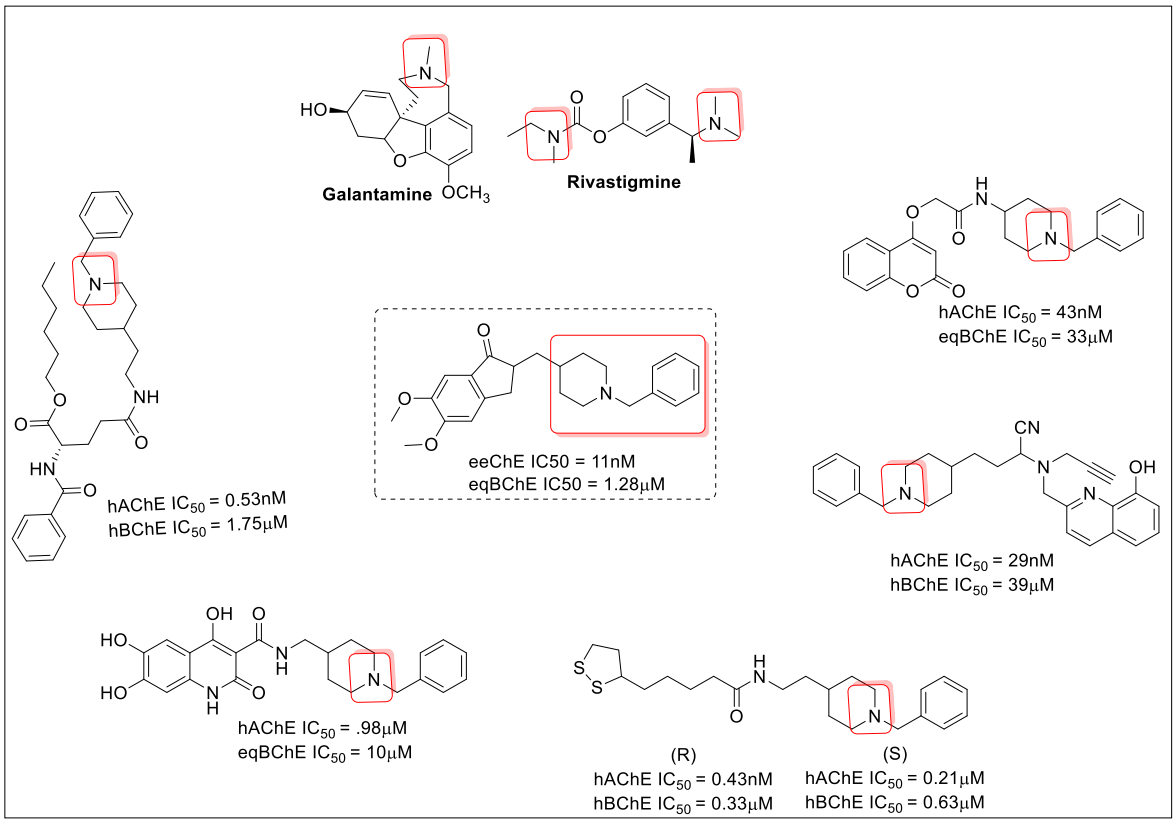

Fig. 3.4 AChE and various other multi-target inhibitors with tertiary nitrogen atom reported for the treatment of AD.

In the current research work we have designed, synthesized and screened a number of heterocyclic ligands as potential multi-targeted ligands (Fig. 3.5) by incorporating propargyl moiety (MAO inhibitor, neuroprotective) as pharmacophore I, and a cyclic or acyclic moiety with tertiary nitrogen as pharmacophore II (potential acetylcholinesrase inhibitor) attached with a heterocyclic moiety. The chain length

between the propargyl group and tertiary nitrogen atom is reported to control the dual interaction of these moieties with both the catalytic active site (CAS) and peripheral anionic site (PAS) of AChE enzyme (Samadi *et al.*, 2011).

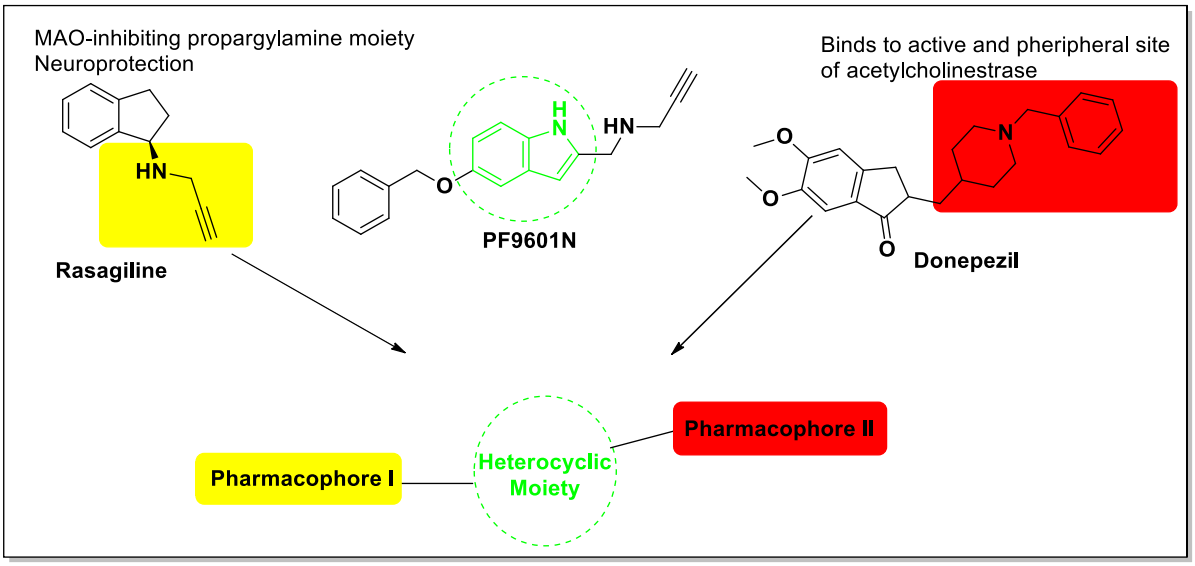

Fig. 3.5 Design of proposed multi-target ligands based on incorporation of different pharmacophores in single structure

3.3 Objectives to be achieved

- Docking studies of the proposed ligands with the cholinesterase and MAO enzymes
- Synthesis of the lead compounds obtained through molecular modeling studies
- Screening of synthesized compounds as MAO and cholinesterase inhibitors
- Structure-activity relationship studies for lead optimization

Chapter- 4
Material and Methods

4.1 Materials and Instruments used

4.1.1 General

1. The reagents for synthesis were purchased from Sigma-Aldrich, Loba-Chemie Pvt. Ltd., S.D. Fine Chemicals, Avra synthesis and used without further purification.
2. Thin layer chromatography was done on glass silica plates with silica gel G as the adsorbent. Ethyl acetate: Petroleum ether (1:1), (2:3) and Methanol: Chloroform (0.5% methanol in chloroform with 2-3 drops of ammonium hydroxide) mixtures were used as solvent system. Spots were visualized under UV light and iodine chamber.
3. Compounds were purified using flash chromatography (Biotage)/column chromatography (Unless otherwise stated). Chromatography was conducted using high-purity grade silica gel, pore size 60 - 120 mesh particle size, 35 - 75 µm particle size, to obtain the pure product.
4. Infrared spectra of compounds were recorded on Bruker IR spectrophotometer.
5. Mass spectra were recorded on GC-MS (ESI), Central Instruments laboratory (CIL), Central University of Punjab, Bathinda.
6. The ^{1}H and ^{13}C NMR of the compounds were recorded on Bruker Advance II instrument at 400 MHz frequency, in $CDCl_3$, DMSO and TMS (δ=0) as internal standard at IIT Ropar, and Guru Jambheshwar University of Science and Technology, Hisar.
7. HRMS of the compounds were recorded on UPLC-G2-XS QTOF Mass Spectrometer at IIT Ropar.
8. Dulbecco's Modified Eagle's Medium (DMEM), antibiotic solutions, phosphate buffer saline (PBS) and fetal bovine serum (FBS), used in cell culturing were purchased from Gibco.
9. Extra pure DMSO (Dimethyl sulfoxide) was purchased from HiMedia.
10. Amplex Red Monoamine oxidase kits and Amplex red acetylcholinesterase assay kits were purchased from Molecular Probes (Invitrogen), Life technologies, India and Sigma-Aldrich, India.
11. Butyrylcholinesterase, butyrylthiocholine iodide, DTNB, acetylthiocholine iodide and phosphate buffer were purchased from Sigma-Aldrich, India.

4.1.2 Instruments

Instruments Used	Company	Purpose
Rotavapour	IImvac	Drying fractions
UV-VIS spectrophotometer	Shimadzu	Absorption studies
CO_2 Incubator	Galaxy, New Brunswick	Incubation
Centrifuge 5430 R	Eppendorf, Germany	Centrifugation
Laminar air flow	Klen Airflow	For aseptic condition
Microplate Reader	Biotek	Fluorescence studies
Inverted microscope	Magnus, Olympus	Visualization of the cells

4.1.3 Cell lines

1**.** For *in vitro* studies, SH-SY5Y cells were used. SH-SY5Y cells are subcloned (SK-N-SH -> SH-SY -> SH-SY5 -> SH-SY5Y) thrice from original bone marrow biopsy derived line called SK-N-SH. The original cell line called SK-N-SH was subcloned and isolated from the bone marrow biopsy, taken from 4 year old female with neuroblastoma (ATTC product data for SH-SY5Y cells, catalog CRL-2266). SH-SY5Y cells are adrenergic in phenotype. In addition, these cells also express dopaminergic markers and, due to this, this cell line have been used as a model to study neurogenesis, and other characteristics of brain cells.

4.2 Designing of heterocyclic compounds for targeting MAO and AChE

4.2.1 Library generation and screening

A library of designed compounds with different heterocyclic moieties containing pharmacophore or its mimicking substituents was generated using ChemBio Draw Ultra-12 and saved in sdf (standard data format). The core heterocyclic moieties such as pyrimidine, diphenylpyrimidine, indole, pyridine, quinazoline, benzimidazole substituted with various tertiary nitrogen atom containing chains like benzylpiperidine, benzylpiperazine, morpholine-, piperidine-, *N, N*-dimethyl-, and pyrrolidine- ethyl chain as pharmacophore I and propargyl group attached to oxygen or nitrogen atom as pharmacophores II. Compounds were screened using docking and ADMET studies and were selected for further screening. The filtering criteria followed for screening included docking score, molecular weight, QPlog (octanol/water ratio), hydrogen bond donor atoms, hydrogen bond acceptor atoms, percentage oral absorption, QPlogBBB (blood brain barrier permeability).

4.2.2 Docking of designed compounds with MAO and AChE

The two-dimensional (2D) structures of ligands was constructed using the ChemBio Draw Ultra-12 and saved in sdf (standard data format). These 2D structures were converted to three-dimensional (3D) structure using Ligprep module of Maestro 11.1 software. This module adds hydrogens and eliminates any discrepancies in bond angles and length. The X-ray crystal structures of AChE (PDB ID: 1EVE), MAO-A (PDB ID: 2BXR) and MAO-B (PDB ID: 2BYB) were imported from protein data bank (www.rscb.org). Proteins were prepared using "protein preparation wizard" application of Schrödinger suite 2017. In protein preparation hydrogens were added, water molecules were removed (which are not part of active site), missing side chains were added and bond lengths and angles were corrected. Energy was minimized using OPLS2005 force field. Grids were generated for each protein around co-crystallized ligands using glide grid module. Ligand docking was performed using Glide module of Maestro 11.1. For each compound, the top-score docking poses were chosen for final ligand-target interaction analysis employing XP interaction visualizer of Maestro 11.1 software. Docking poses were considered for determining and comparing the binding score and mode of different heterocyclic moieties containing pharmacophore or mimicking substituents attached to it (Fig. 3.5). Docking scores were determined considering several factors such as hydrogen bonds, hydrophobic interactions, Van der Waal interactions, charged polar interactions, rotatable bonds etc.

4.3 Synthetic methods

4.3.1 General protocol for the synthesis of Series-I (Scheme-I)

4.3.1.1 General procedure for the synthesis of 1 and 2

To hydroxy substituted acetophenone (0.5 g) or benzaldehydes (0.5 g), morpholine or piperidine ethylchloride (1.2 eq) was added in the presence of potassium carbonate as base (2.4 eq) and acetone (30 ml) as solvent. The reaction mixture was refluxed for 12 h at 60˚C. The progress of reaction was monitored via TLC. After completion of the reaction, excess of solvent was evaporated from the mixture using vacuum rotary evaporator, water (10 mL) was added and aqueous phase was extracted with ethyl acetate (10 mL × 3), and washed with brine, dried over

anhydrous Na_2SO_4 and the organic solvent was concentrated under vacuum using rotary evaporator.

Scheme-1: Reaction scheme for the synthesis of target molecules

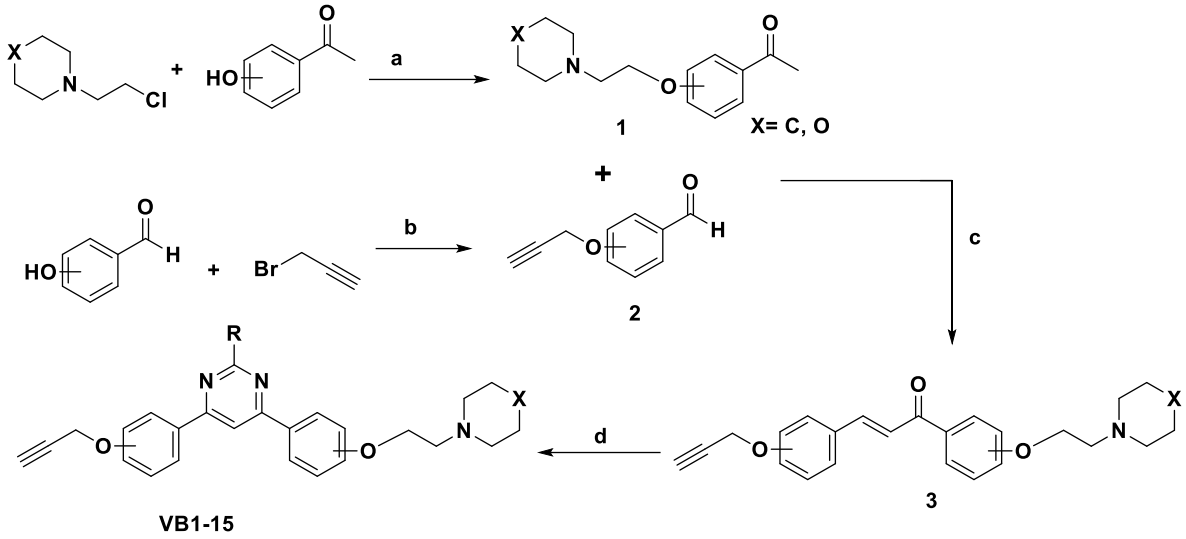

Reagents and conditions: a) K_2CO_3, KI, acetone, reflux, 6 h; **b)** K_2CO_3, acetone, reflux, 6 h; **c)** CH_3OH, 10% NaOH aq., rt, stirring, 3 h; and **d)** Na_2CO_3, CH_3CN, amidine/guanidine/benzamidine, reflux, 24h

4.3.1.2 General procedure for the synthesis of 3

To a mixture of 1 (1 eq) and 2 (1 eq) in methanol (20 ml), aqueous sodium hydroxide (20%) was added slowly with continuous stirring. The reaction mixture was stirred for 3 h at room temperature. The completion of reaction was monitored via TLC. After completion of reaction, excess of solvent was evaporated from the mixture using rotary evaporator. Chilled water was poured into the reaction mixture and precipitates of **3** were filtered and dried.

4.3.1.3 General procedure for the synthesis of VB1-VB15

To a mixture of 3 (500 mg), and amidine (1.2 eq), anhydrous sodium carbonate (2.4 eq) was added in acetonitrile (5 mL) as solvent. The reaction mixture was refluxed for 24 h at 85˚C. The progress of the reaction was monitored via TLC. After completion of the reaction, excess of solvent was evaporated under vacuum using rotary evaporator, water (10 mL) was added aqueous phase was extracted with ethyl acetate (3 × 10 mL), washed with brine, dried over anhydrous Na_2SO_4, and the organic solvent was concentrated under vacuum using rotary evaporator and

purified via column chromatography (EtOAc:Pet ether). The final products were characterized by NMR spectroscopy and HRMS.

4.3.1.4 Spectral analysis

4-(4-(2-morpholinoethoxy)phenyl)-6-(4-(prop-2-yn-1-yloxy)phenyl)pyrimidin-2-amine (**VB1**):

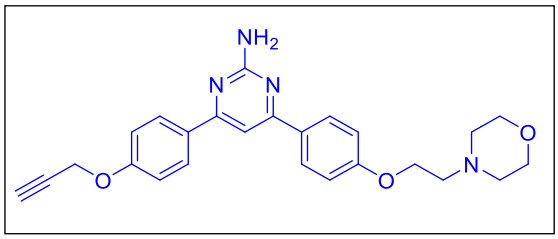

Yield 59%, ^{1}H NMR ($CDCl_3$, 400 MH_Z, δ with TMS=0): 8.05-8.00 (4H, m), 7.35 (1H, s), 7.07 (2H, d, *J*= 8Hz), 6.99 (2H, d, *J*= 8Hz), 5.16 (2H, s), 4.76 (2H, d, *J*= 2.4Hz), 4.18 (2H, t, *J*= 4Hz), 3.75 (4H, t, *J*= 4Hz), 2.83 (2H, t, *J*= 4Hz), 2.60 (4H, t, *J*= 4Hz), 2.55 (1H, t, *J*= 2.4Hz), ^{13}C NMR **(**$CDCl_3$, 100 MH_Z, δ with TMS=0**)** δ: 165.40, 165.28, 163.49, 160.71, 159.41, 131.13, 130.36, 128.36, 128.58, 115.00, 114.70, 102.86, 78.19, 75.89, 66.93, 65.89, 57.58, 55.85, 54.13 **HRMS**: for $C_{25}H_{26}N_4O_3$, calculated $[M+H]^+$: 431.2083; observed $[M+H]^+$: 431.2060

4-(2-(4-(2-phenyl-6-(4-(prop-2-yn-1-yloxy)phenyl)pyrimidin-4-yl)phenoxy)ethyl)morpholine (**VB2**):

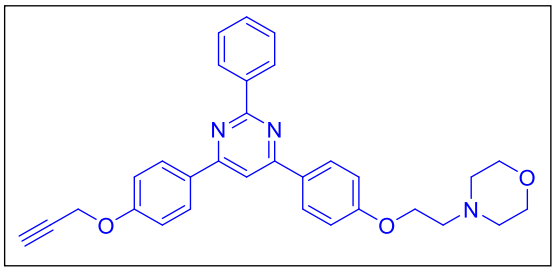

Yield 63%, ^{1}H NMR ($CDCl_3$, 400 MH_Z, δ with TMS=0): 8.68 (2H, d, *J*= 8Hz), 8.24 (4H, t, *J*= 8Hz), 7.86 (1H, s), 7.53-7.49 (3H, m), 7.12 (2H, d, *J*= 8Hz), 7.04 (2H, d, *J*= 8Hz), 4.77 (2H, d, *J*= 2.4Hz), 4.19 (2H, t, *J*= 4Hz), 3.75 (4H, t, *J*= 4Hz), 2.84 (2H, t, *J*= 4Hz), 2.60 (4H, t, *J*= 4Hz), 2.56 (1H, t, *J*= 2.4Hz), ^{13}C NMR **(**$CDCl_3$, 100 MH_Z, δ with TMS=0**)** δ: 164.01, 163.89, 161.02, 159.73, 138.40, 130.59, 130.28, 128.83,

128.48, 115.20, 114.89, 108.75, 78.19, 75.89, 66.99, 65.93, 57.66, 55.95, 54.20 **HRMS**: for $C_{31}H_{29}N_3O_3$, calculated $[M+H]^+$: 492.2287; observed $[M+H]^+$: 492.2271

4-(2-(4-(2-methyl-6-(4-(prop-2-yn-1-yloxy)phenyl)pyrimidin-4-yl)phenoxy)ethyl)morpholine (**VB3**):

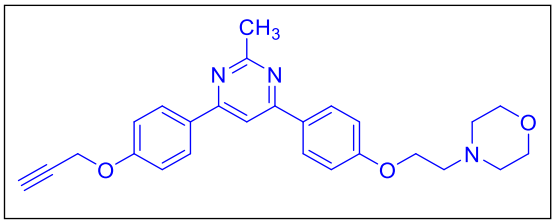

Yield 58%, ^{1}H NMR ($CDCl_3$, 400 MHz, δ with TMS=0): 8.11-8.07 (4H, m), 7.76 (1H, s), 7.10 (2H, d, *J*= 8Hz), 7.02 (2H, d, *J*= 8Hz), 4.77 (2H, d, *J*= 2.4Hz), 4.19 (2H, t, *J*= 4Hz), 3.75 (4H, t, *J*= 4Hz), 2.84 (2H, t, *J*= 4Hz), 2.81 (3H, s), 2.61 (2H, t, *J*= 4Hz), 2.56 (1H, t, *J*= 2.4Hz), **(**$CDCl_3$, 100 MHz, δ with TMS=0**)** δ: 168.32, 164.07, 163.96, 160.85, 159.55, 130.94, 130.17, 128.72, 115.18, 114.87, 108.49, 78.13, 75.93, 66.91, 65.90, 57.57, 55.87, 54.13, 26.53 **HRMS**: for $C_{26}H_{27}N_3O_3$, calculated $[M+H]^+$: 430.2131; observed $[M+H]^+$: 430.2079

2-phenyl-4-(4-(2-(piperidin-1-yl)ethoxy)phenyl)-6-(4-(prop-2-yn-1-yloxy)phenyl)pyrimidine (**VB4**):

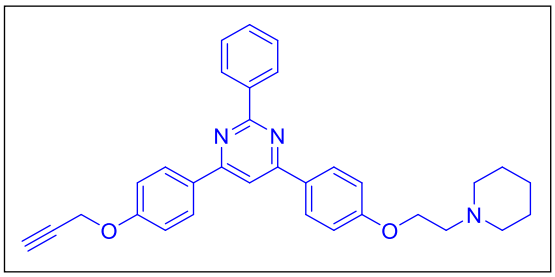

Yield 61%, ^{1}H NMR ($CDCl_3$, 400 MHz, δ with TMS=0): 8.69 (2H, dd, J_1= 8Hz, J_2= 4Hz), 8.23 (4H, t, *J*= 8Hz), 7.84 (1H, s), 7.52-7.42 (3H, m) 7.11 (2H, d, *J*= 8Hz), 7.03 (2H, d, *J*= 8Hz), 4.76 (2H, d, *J*= 2.4Hz), 4.19 (2H, t, *J*= 4Hz), 2.82 (2H, t, *J*= 4Hz), 2.57-2.55 (5H, m), 1.66-1.60 (4H,m) 1.46 (2H, brs), **(**$CDCl_3$, 100 MHz, δ with TMS=0**)** δ: 164.26, 164.04, 163.82, 161.12, 159.70, 138.43, 131.04, 130.56, 130.11, 128.80, 128.71, 128.48, 115.18, 114.89, 108.71, 78.26, 76.04, 66.02, 57.83, 55.94, 55.14, 29.81, 25.88, 24.19 **HRMS**: for $C_{32}H_{31}N_3O_2$, calculated $[M+H]^+$: 490.2495; observed $[M+H]^+$: 490.2470

2-methyl-4-(4-(2-(piperidin-1-yl)ethoxy)phenyl)-6-(4-(prop-2-yn-1-yloxy)phenyl)pyrimidine (**VB5**):

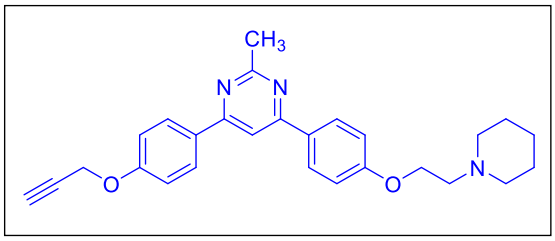

Yield 67%,^{1}H NMR ($CDCl_3$, 400 MH_Z, δ with TMS=0): 8.07 (4H, t, *J*= 8Hz), 7.74 (1H, s), 7.08 (2H, d, *J*= 8Hz), 7.00 (2H, d, *J*= 8Hz), 4.75 (2H, d, *J*= 4Hz), 4.17 (2H, t, *J*= 4Hz), 2.82-2.79 (5H, m), 2.53 (4H, b), 1.61 (4H, b), 1.44 (2H, b), 1.23 (1H, b), **(**$CDCl_3$, 100 MH_Z, δ with TMS=0**)** δ: 168.35, 164.18, 163.98, 161.03, 159.59, 131.01, 130.79, 130.35, 130.11, 130.06, 129.47, 128.77, 115.33, 115.23, 114.95, 108.53, 78.21, 76.01, 66.07, 57.85, 55.92, 55.13, 29.79, 25.89, 24.17, **HRMS**: for $C_{27}H_{29}N_3O_2$, calculated $[M+H]^+$: 428.2338; observed $[M+H]^+$: 428.2293

4-(2-(4-(2-phenyl-6-(3-(prop-2-yn-1-yloxy)phenyl)pyrimidin-4-yl)phenoxy)ethyl)morpholine (**VB6**):

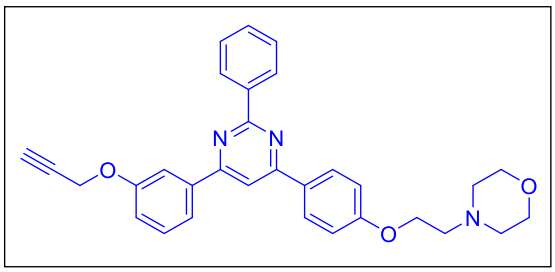

Yield 62%,^{1}H NMR ($CDCl_3$, 400 MH_Z, δ with TMS=0): 8.70 (2H, dd, J_1= 8Hz, J_2= 4Hz), 8.25 (2H, d, *J*= 8Hz), 7.97 (1H,s), 7.91 (1H,s), 7.86 , (1H, d, *J*= 8Hz), 7.54-7.56 (4H, m), 7.15 (1H, dd, J_1= 8Hz, J_2= 4Hz), 7.06 (2H, d, *J*= 8Hz), 4.82 (2H, d, *J*= 4Hz), 4.20 (2H, t, *J*= 4Hz), 3.76 (4H, t, *J*= 4Hz), 2.85 (2H, t, *J*= 4Hz), 2.60 (5H, m), **(**$CDCl_3$, 100 MH_Z, δ with TMS=0**)** δ: 164.37, 164.27, 164.06, 161.13, 158.17, 139.32, 138.25, 130.70, 130.10, 130.01, 128.88, 128.51, 120.50, 117.11, 114.93, 113.99, 109.61, 78.50, 75.94, 67.01, 65.98, 57.65, 56.13, 54.21, **HRMS**: for $C_{31}H_{29}N_3O_3$, calculated $[M+H]^+$: 492.2287; observed $[M+H]^+$: 492.2256

4-(4-(2-morpholinoethoxy)phenyl)-6-(3-(prop-2-yn-1-yloxy)phenyl)pyrimidin-2-amine (**VB7**):

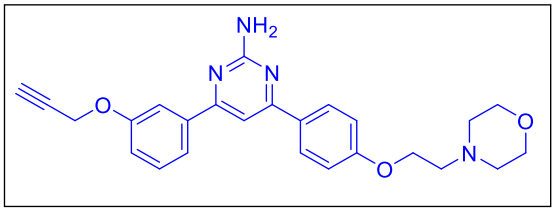

Yield 59%,^{1}H NMR ($CDCl_3$, 400 MH_Z, δ with TMS=0): 8.00 (2H, d, *J*= 8Hz), 7.90 (1H, dd, J_1= 8Hz, J_2= 4Hz), 7.65 (1H, m), 7.39 (1H, t, *J*= 8Hz), 7.36 (1H, s), 7.08 (1H, dd, J_1= 8Hz, J_2= 4Hz), 6.98 (2H, d, *J*= 8Hz), 6.90 (1H, t, *J*= 8Hz), 5.22 (2H, s), 4.77 (2H, d, *J*= 4Hz), 4.16 (4H, t, *J*= 4Hz), 3.73 (2H, t, *J*= 4Hz), 2.82 (4H, t, *J*= 4Hz), 2.53 (2H, brs), **(**$CDCl_3$, 100 MH_Z, δ with TMS=0**)** δ: 165.71, 163.56, 160.86, 158.01, 139.49, 130.69, 129.89, 128.70, 120.44, 117.08, 114.79, 114.48, 114.29, 113.53, 103.73, 78.49, 75.82, 66.97, 65.93, 57.63, 56.04, 54.18, **HRMS**: for $C_{25}H_{26}N_4O_3$, calculated $[M+H]^+$: 431.2083; observed $[M+H]^+$: 431.2060

4-(2-(4-(2-methyl-6-(3-(prop-2-yn-1-yloxy)phenyl)pyrimidin-4-yl)phenoxy)ethyl)morpholine (**VB8**):

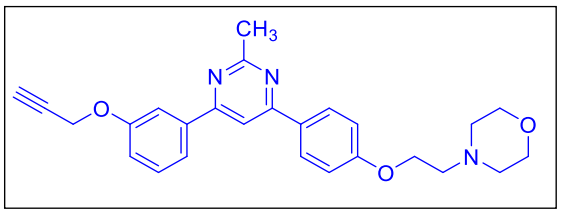

Yield 59%,^{1}H NMR ($CDCl_3$, 400 MH_Z, δ with TMS=0): 8.08 (2H, d, *J*= 8Hz), 7.78 (1H, m), 7.72-7.69 (2H, m), 7.43 (1H, t, *J*= 8Hz), 7.10 (1H, d, *J*= 8Hz), 7.01 (2H, t, *J*= 8Hz), 4.78 (2H, d, *J*= 4Hz), 4.18 (2H, t, *J*= 4Hz), 3.74 (4H, t, *J*= 4Hz), 2.83 (2H, t, *J*= 4Hz), 2.83 (3H, s), 2.59 (4H, t, *J*= 4Hz), 2.54 (1H, t, *J*= 4Hz), **(**$CDCl_3$, 100 MH_Z, δ with TMS=0**)** δ: 168.50, 164.37, 164.29, 161.01, 158.14, 139.31, 131.03, 130.07, 128.83, 120.56, 117.13, 114.97, 113.77, 109.45, 78.44, 75.84, 66.98, 65.97, 57.64, 56.08, 54.20, 29.79, **HRMS**: for $C_{26}H_{27}N_3O_3$, calculated $[M+H]^+$: 430.2131; observed $[M+H]^+$: 430.2086

4-(4-(2-morpholinoethoxy)phenyl)-6-(2-(prop-2-yn-1-yloxy)phenyl)pyrimidin-2-amine (**VB9**):

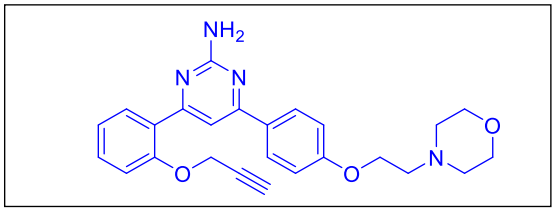

Yield 55%,^{1}H NMR ($CDCl_3$, 400 MH_Z, δ with TMS=0): 8.00 (2H, d, *J*= 8Hz), 7.85 (1H, dd, J_1= 8Hz, J_2= 4Hz), 7.60 (1H, m), 7.40 (1H, dd, J_1= 8Hz, J_2= 4Hz), 7.12 (2H, t, *J*= 8Hz), 6.97 (2H, d, *J*= 8Hz), 5.12 (2H, s), 4.75 (2H, d, *J*= 4Hz), 4.16 (2H, t, *J*= 4Hz), 3.73 (4H, t, *J*= 4Hz), 2.82 (2H, t, *J*= 4Hz), 2.59 (4H, brs), 2.52 (1H, t, *J*= 4Hz), **(**$CDCl_3$, 100 MH_Z, δ with TMS=0**)** δ: 164.69, 164.30, 163.39, 160.70, 155.69, 130.94, 128.81, 122.22, 114.70, 114.16, 113.54, 109.19, 108.56, 78.53, 75.92, 66.99, 65.92, 57.66, 56.69, 54.18, **HRMS**: for $C_{25}H_{26}N_4O_3$, calculated $[M+H]^+$: 431.2083; observed $[M+H]^+$: 431.2036

4-(2-(4-(2-phenyl-6-(2-(prop-2-yn-1-yloxy)phenyl)pyrimidin-4-yl)phenoxy)ethyl)morpholine (**VB10**):

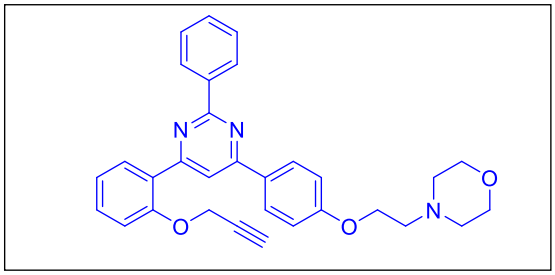

Yield 63%,^{1}H NMR ($CDCl_3$, 400 MH_Z, δ with TMS=0): 8.67 (1H, dd, J_1= 8Hz, J_2= 4Hz), 8.27 (1H, s), 8.26 (2H, d, *J*= 8Hz), 7.53-7.44 (4H, m), 7.21 (1H, t, *J*= 8Hz), 7.13 (1H, d, *J*= 8Hz), 7.04 (2H, d, *J*= 8Hz), 4.80 (2H, d, *J*= 4Hz), 4.19 (2H, t, *J*= 4Hz), 3.75 (4H, t, *J*= 4Hz), 2.84 (2H, t, *J*= 4Hz), 2.60 (4H, brs), 2.56 (1H, t, *J*= 4Hz), **(**$CDCl_3$, 100 MH_Z, δ with TMS=0**)** δ: 164.19, 163.29, 162.79, 160.97, 156.23, 138.60, 131.59, 131.33, 130.56, 130.40, 128.97, 128.44, 128.41, 126.56, 122.35, 114.86, 114.72, 113.53, 78.50, 76.00, 67.02, 66.05, 57.68, 56.82, 54.22, **HRMS**: for $C_{31}H_{29}N_3O_3$, calculated $[M+H]^+$: 492.2287; observed $[M+H]^+$: 492.2256

4-(2-(3-(2-phenyl-6-(4-(prop-2-yn-1-yloxy)phenyl)pyrimidin-4-yl)phenoxy)ethyl)morpholine (**VB11**):

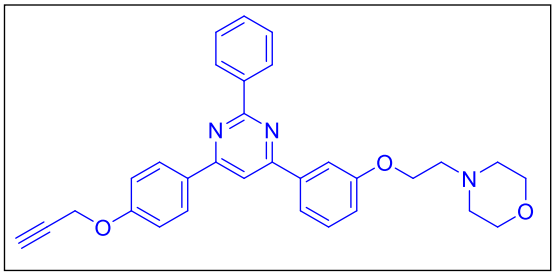

Yield 62%,^{1}H NMR ($CDCl_3$, 400 MH_Z, δ with TMS=0): 8.68 (2H, dd, J_1= 8Hz, J_2= 4Hz), 8.26 (2H, dd, J_1= 8Hz, J_2= 4Hz), 7.90 (1H, d, J= 8Hz), 7.85 (1H, s), 7.81 (1H, d, J= 8Hz), 7.54-7.50 (3H, m), 7.44 (1H, d, J= 8Hz), 7.13 (2H, dd, J_1= 8Hz, J_2= 4Hz), 7.01 (1H, dd, J_1= 8Hz, J_2= 4Hz), 4.78 (2H, d, J= 4Hz), 4.26 (2H, t, J= 4Hz), 3.77 (4H, t, J= 4Hz), 2.90 (2H, t, J= 4Hz), 2.67 (4H, brs), 2.56 (1H, t, J= 4Hz), **(**$CDCl_3$, 100 MH_Z, δ with TMS=0**)** δ: 166.67, 163.80, 161.95, 160.94, 147.89, 138.06, 130.75, 129.60, 128.88, 128.62, 128.42, 119.49, 116.86, 114.91, 114.58, 112.04, 110.66, 80.96, 76.80, 71.58, 66.75, 65.72, 57.56, 54.09, **HRMS**: for $C_{31}H_{29}N_3O_3$, calculated $[M+H]^+$: 492.2287; observed $[M+H]^+$: 492.2256

4-(3-(2-morpholinoethoxy)phenyl)-6-(4-(prop-2-yn-1-yloxy)phenyl)pyrimidin-2-amine (**VB12**):

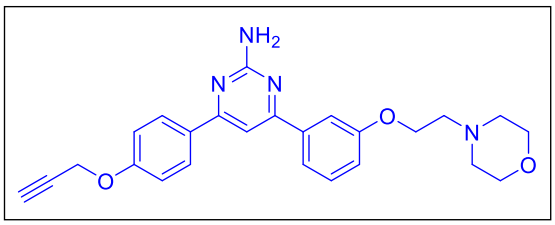

Yield 72%, ^{1}H NMR ($CDCl_3$, 400 MH_Z, δ with TMS=0): 8.01 (2H, d, J= 8Hz), 7.60 (1H, s), 7.57 (1H, d, J= 8Hz), 7.36 (2H, t, J= 8Hz), 7.04 (2H, d, J= 12Hz), 7.00 (1H, d, J= 8Hz), 5.35 (2H, s), 4.73 (2H, d, J= 2.4Hz), 4.18 (2H, t, J= 4Hz), 3.73 (4H, t, J= 4Hz), 2.82 (2H, t, J= 4Hz), 2.59 (4H, t, J= 4Hz), 2.54 (1H, t, J= 4Hz), **(**$CDCl_3$, 100 MH_Z, δ with TMS=0**)** δ: 165.71, 163.56, 160.86, 158.01, 139.49, 130.69, 129.89, 128.70, 120.44, 117.08, 114.79, 114.48, 114.29, 113.53, 103.73, 78.49, 75.82, 66.97, 65.93, 57.63, 56.04, 54.18, **HRMS**: for $C_{25}H_{26}N_4O_3$, calculated $[M+H]^+$: 431.2083; observed $[M+H]^+$: 431.2018

4-(2-(3-(2-methyl-6-(4-(prop-2-yn-1-yloxy)phenyl)pyrimidin-4-yl)phenoxy)ethyl)morpholine (**VB13**):

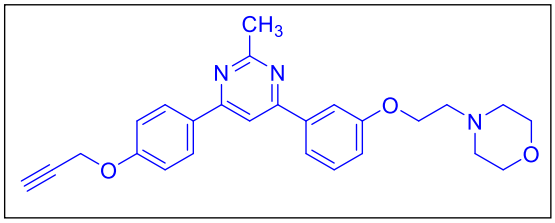

Yield 54%, ^{1}H NMR ($CDCl_3$, 400 MHz, δ with TMS=0): 8.09 (2H, d, *J*= 8Hz), 7.78 (1H, s), 7.64 (1H, d, *J*= 8Hz), 7.51-7.47 (1H, m), 7.38 (1H, t, *J*= 8Hz), 7.07 (2H, d, *J*= 12Hz), 7.02 (1H, dd, J_1= 8Hz, J_2= 4Hz), 4.74 (2H, d, *J*= 4Hz), 4.28 (2H, t, *J*= 4Hz), 4.19 (2H, t, *J*= 4Hz), 3.72 (4H, t, *J*= 4Hz), 2.81 (3H, s), 2.59 (4H, t, *J*= 4Hz), 2.54 (1H, t, *J*= 2.4Hz), **(**$CDCl_3$, 100 MHz, δ with TMS=0**)** δ: 168.47, 164.44, 164.25, 159.72, 159.33, 139.14, 131.02, 130.02, 128.91, 128.83, 118.83, 116.96, 115.27, 113.29, 109.49, 78.18, 76.07, 66.98, 65.88, 65.66, 57.75, 55.92, 54.17, **HRMS**: for $C_{26}H_{27}N_3O_3$, calculated $[M+H]^+$: 430.2131; observed $[M+H]^+$: 430.2101

2-phenyl-4-(4-(2-(piperidin-1-yl)ethoxy)phenyl)-6-(3-(prop-2-yn-1-yloxy)phenyl)pyrimidine (**VB14**):

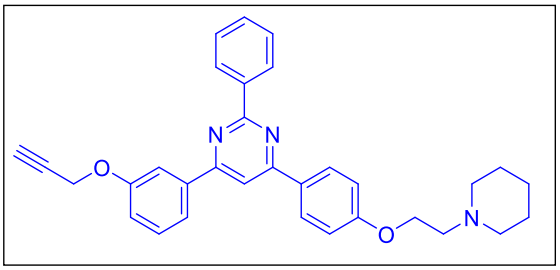

Yield 53%, ^{1}H NMR ($CDCl_3$, 400 MHz, δ with TMS=0): 8.70 (2H, dd, J_1= 8Hz, J_2= 4Hz), 8.24 (2H, d, *J*= 8Hz), 7.96 (1H, t, *J*= 8Hz), 7.91 (1H, s), 7.85 (1H, dd, J_1= 8Hz, J_2= 4Hz), 7.53-7.45 (4H, m), 7.13 (1H, dd, J_1= 8Hz, J_2= 4Hz), 7.05 (2H, d, *J*= 8Hz), 4.81 (2H, d, *J*= 8Hz), 4.20 (2H, t, *J*= 4Hz), 2.83 (2H, t, *J*= 4Hz), 2.58 (4H, t, *J*= 4Hz), 1.66-1.60 (4H, m), 1.47-1.40 (3H, m), **(**$CDCl_3$, 100 MHz, δ with TMS=0**)** δ: 164.35, 164.37, 164.05, 161.16, 158.17, 139.36, 138.29, 130.70, 130.01, 128.85, 128.51, 120.52, 117.11, 114.56, 113.96, 109.61, 78.39, 75.83, 57.92, 56.16, 75.83, 29.72, 25.86, 24.13, **HRMS**: for $C_{32}H_{31}N_3O_2$, calculated $[M+H]^+$: 490.2495; observed $[M+H]^+$: 490.2480

4-(4-(2-(piperidin-1-yl)ethoxy)phenyl)-6-(3-(prop-2-yn-1-yloxy)phenyl)pyrimidin-2-amine (**VB15**):

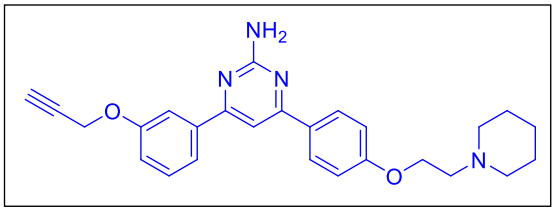

Yield 58%, ^{1}H NMR ($CDCl_3$, 400 MH_Z, δ with TMS=0): 7.99 (2H, d, *J*= 8Hz), 7.65-7.62 (2H, m), 7.39 (1H, t, *J*= 8Hz), 7.35 (1H, s), 7.08 (1H, dd, J_1= 8Hz, J_2= 4Hz), 6.97 (2H, d, *J*= 8Hz), 5.26 (2H, s), 4.75 (2H, d, *J*= 4Hz), 4.16 (2H, t, *J*= 4Hz), 2.80 (2H, t, *J*= 4Hz), 2.53 (5H, brs), 1.62-1.58 (4H, m), 0.97-0.92 (2H, m), **(**$CDCl_3$, 100 MH_Z, δ with TMS=0**)** δ: 165.75, 165.55, 163.60, 160.96, 158.07, 139.53, 131.02, 129.87, 128.67, 120.45, 117.08, 114.79, 113.50, 103.68, 78.51, 75.83, 66.01, 57.85, 56.03, 55.11, 25.87, 34.17, **HRMS**: for $C_{26}H_{28}N_4O_2$, calculated $[M+H]^+$: 429.2291; observed $[M+H]^+$: 429.2238

4.3.2 General protocol for the synthesis of Series-II (Scheme-II)

4.3.2.1 General procedure for the synthesis of a and b

For synthesis of **a,** to *p*-hydroxy benzaldehyde (0.5 g) morpholine or piperidine ethylchloride (1.2 eq) was added in the presence of potassium carbonate as base (2.4 eq) and acetone (30 mL) as solvent. For synthesis of **b,** to amino acetophenones (0.5 g) propargyl bromide (1.2 eq) was added in the presence of potassium carbonate as base (2.4 eq) and acetone (30 mL) as solvent. The reaction mixture was refluxed for 12 h at 60˚C. The progress of reaction was monitored via TLC. After completion of the reaction, excess of solvent was evaporated from the mixture using vacuum rotary evaporator, water (10 mL) was added and aqueous phase was extracted with ethyl acetate (10 mL × 3), and washed with brine, dried over anhydrous Na_2SO_4 and the organic solvent was concentrated under vacuum using rotary evaporator.

4.2.2.2 General procedure for the synthesis of c

To a mixture of **a** (1 eq) and **b** (1 eq) in methanol (20 mL), aqueous sodium hydroxide (20%) was added slowly with continuous stirring. The reaction mixture was stirred for 3 h at room temperature. The completion of reaction was monitored via TLC. After completion of reaction, excess of solvent was evaporated from the mixture using rotary evaporator. Chilled water was poured into the reaction mixture and precipitates of **c** were filtered and dried.

Scheme-II: Reaction scheme for the synthesis of target molecules

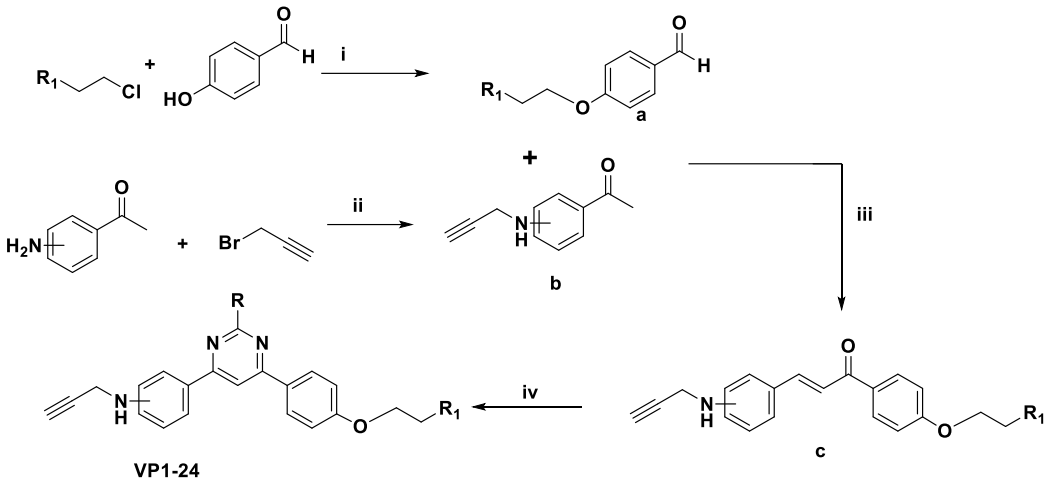

Reagents and Conditions: i) K_2CO_3, KI, acetone, reflux, 6 h; **ii)** K_2CO_3, acetone, reflux, 6 h; **iii)** CH_3OH, 10% NaOH aq., rt, stirring, 3 h; and **iv)** Na_2CO_3, CH_3CN, amidine/guanidine/benzamidine, reflux, 24h

4.3.2.3 General procedure for the synthesis of VP1-VP24

To a mixture of **c** (500 mg), and amidine (1.2 eq), anhydrous sodium carbonate (2.4 eq) was added in acetonitrile (5 mL) as solvent. The reaction mixture was refluxed for 24 h at 85˚ C. The progress of the reaction was monitored via TLC. After completion of the reaction, excess of solvent was evaporated under vacuum using rotary evaporator, water (10 mL) was added aqueous phase was extracted with ethyl acetate (3 × 10 mL), washed with brine, dried over anhydrous Na_2SO_4, and the organic solvent was concentrated under vacuum using rotary evaporator and purified via column chromatography (EtOAc:Pet ether). The final products were characterized by NMR spectroscopy and HRMS.

4.3.2.4 Spectral analysis

4-(4-(2-morpholinoethoxy)phenyl)-6-(4-(prop-2-yn-1-ylamino)phenyl)pyrimidin-2-amine (VP1):

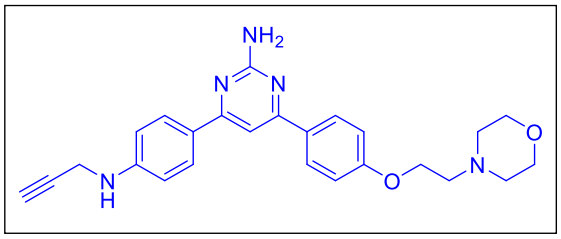

Yield 59%, ^{1}H NMR ($CDCl_3$, 300 MH_Z, δ with TMS=0): 7.98 (4H, t, *J* = 9Hz), 7.32 (1H, s), 6.98 (2H, d, *J* = 9Hz), 6.74 (2H, d, *J* = 9Hz), 5.05, (2H, s), 4.17 (2H, t, *J* =

6Hz), 4.00 (2H, brs), 3.74 (4H, brs), 2.81 (2H, d, *J* = 6Hz), 2.59 (4H, brs), 2.24 (1H, s), ^{13}C NMR **(**$CDCl_3$, 75 MHz, δ with TMS=0**)** 165.40, 165.28, 163.49, 160.71, 159.41, 131.13, 130.36, 128.36, 128.58, 115.00, 114.70, 102.86, 78.19, 75.89, 66.93, 65.89, 57.58, 55.85, 54.13, **HRMS**: for $C_{25}H_{27}N_5O_2$, calculated $[M+H]^+$: 430.2243; observed $[M+H]^+$: 430.2280

4-(2-methyl-6-(4-(2-morpholinoethoxy)phenyl)pyrimidin-4-yl)-N-(prop-2-yn-1-yl)aniline (VP2):

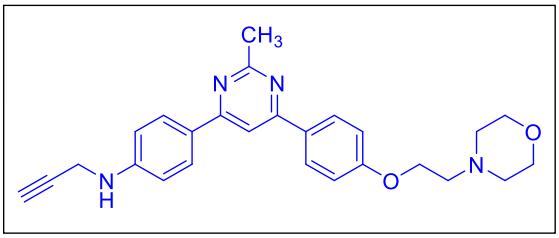

Yield 57%, ^{1}H NMR ($CDCl_3$, 300 MHz, δ with TMS=0): 8.04 (4H, t, *J* = 9Hz), 7.71 (1H, s), 7.00 (2H, d, *J* = 9Hz), 6.75 (2H, d, *J* = 9Hz), 4.17 (2H, brs), 4.00 (2H, brs), 3.73 (4H, brs), 2.82 (2H, brs), 2.78 (3H, s), 2.59 (4H, brs), 2.24 (1H, s), ^{13}C NMR **(**$CDCl_3$, 75 MHz, δ with TMS=0**)** 168.13, 164.30, 160.70, 149.02, 130.47, 128.67, 128.67, 128.55, 127.42, 114.84, 113.30, 107.83, 80.33, 71.66, 66.91, 65.91, 57.58, 54.13, 33.36, 22.69, **HRMS**: for $C_{26}H_{28}N_4O_2$, calculated $[M+H]^+$: 429.2291; observed $[M+H]^+$: 429.2280

4-(6-(4-(2-morpholinoethoxy)phenyl)-2-phenylpyrimidin-4-yl)-N-(prop-2-yn-1-yl)aniline (VP3):

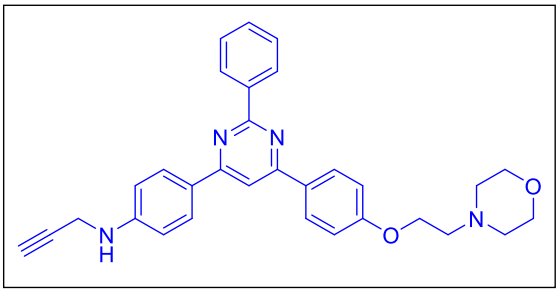

Yield 56%, ^{1}H NMR ($CDCl_3$, 400 MHz, δ with TMS=0): 8.69 (2H, dd, J_1 = 8Hz, J_2 = 4Hz), 8.21 (2H, d, *J* = 8Hz), 8.17 (2H, d, *J* = 8Hz), 7.80 (1H, s), 7.50 (3H, t, *J* = 8Hz), 7.02 (2H, d, *J* = 8Hz), 6.77 (2H, d, *J* = 8Hz), 3.98 (2H, brs), 3.74 (4H, t, *J* = 4Hz), 2.82 (2H, t, *J* = 4Hz), 2.59 (4H, t, *J* = 4Hz), 2.25 (1H, t, *J* = 4Hz), ^{13}C NMR **(**$CDCl_3$, 100 MHz, δ with TMS=0**)** 163.62, 160.81, 150.21, 138.66, 130.51, 130.45, 128.77,

128.66, 128.47, 128.46, 127.44, 114.83, 113.30, 108.07, 80.49, 71.77, 66.98, 65.88, 57.65, 54.19, 33.19, **HRMS**: for $C_{31}H_{30}N_4O_2$, calculated $[M+H]^+$: 491.2447; observed $[M+H]^+$: 491.2418

4-(4-(2-morpholinoethoxy)phenyl)-6-(3-(prop-2-yn-1-ylamino)phenyl)pyrimidin-2-amine (VP4):

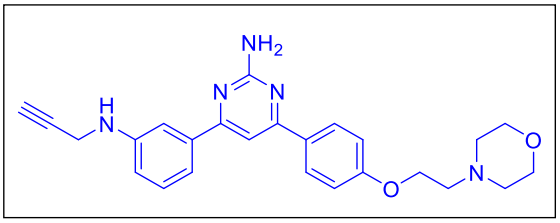

Yield 51%, ^{1}H NMR ($CDCl_3$, 300 MH_Z, δ with TMS=0): 7.99 (2H, d, *J* = 8Hz), 7.31 (4H, m), 6.98 (2H, d, *J* = 8Hz), 6.79 (1H, d, *J* = 9Hz), 5.18 (2H, s), 4.16 (2H, brs), 4.00 (2H, brs), 3.73 (4H, brs), 2.82 (2H, s), 2.59 (4H, brs), 2.22 (1H, s), ^{13}C NMR **(**$CDCl_3$, 75 MH_Z, δ with TMS=0**)** 166.27, 165.44, 163.47, 160.74, 147.33, 138.96, 130.34, 129.61, 128.62, 117.46, 115.36, 114.72, 112.17, 103.76, 80.82, 71.52, 66.91, 65.91, 57.58, 54.13, 33.73, **HRMS**: for $C_{25}H_{27}N_5O_2$, calculated $[M+H]^+$: 430.2243; observed $[M+H]^+$: 430.2274

3-(2-methyl-6-(4-(2-morpholinoethoxy)phenyl)pyrimidin-4-yl)-N-(prop-2-yn-1-yl)aniline (VP5):

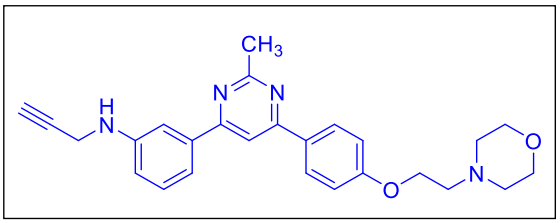

Yield 61%, ^{1}H NMR ($CDCl_3$, 300 MH_Z, δ with TMS=0): 8.07 (2H, d, *J* = 8Hz), 7.76 (1H,s), 7.43 (2H, brs) 7.33 (1H, t, *J* = 8Hz) 7.00 (2H, d, *J* = 9Hz), 6.80 (2H, d, *J* = 9Hz), 4.17 (2H, brs), 4.01 (2H, brs), 3.73 (4H, brs), 2.81 (5H, brs) 2.58 (4H, brs), 2.23 (1H, s), ^{13}C NMR **(**$CDCl_3$, 75 MH_Z, δ with TMS=0**)** 168.28, 164.92, 164.12, 160.88, 147.48, 138.71, 130.12, 129.76, 128.75, 117.50, 115.39, 114.89, 112.38, 109.43, 80.77, 71.53, 66.90, 65.92, 57.57, 54.13, 33.72, 26.51, **HRMS**: for $C_{26}H_{28}N_4O_2$, calculated $[M+H]^+$: 429.2291; observed $[M+H]^+$: 429.2319

3-(6-(4-(2-morpholinoethoxy)phenyl)-2-phenylpyrimidin-4-yl)-N-(prop-2-yn-1-yl)aniline (VP6):

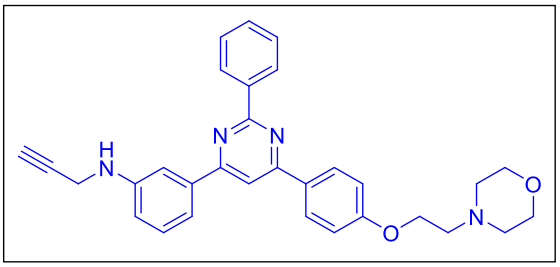

Yield 56%, ^{1}H NMR ($CDCl_3$, 400 MHz, δ with TMS=0): 8.70 (2H, d, *J* = 8Hz), 8.24 (2H, d, *J* = 8Hz), 7.89 (1H, s), 7.66 (1H, brs), 7.59 (1H, d, *J* = 8Hz), 7.49-7.54 (3H, m), 7.38 (1H, t, *J* = 8Hz), 7.04 (2H, d, *J* = 8Hz), 6.84 (1H, d, *J* = 8Hz), 4.19 (2H, t, *J* = 4Hz), 4.06 (2H, d, *J* = 4Hz), 3.75 (4H, t, *J* = 4Hz), 2.84 (2H, t, *J* = 4Hz), 2.60 (4H, t, *J* = 4Hz), 2.26 (1H, d, *J* = 4Hz), ^{13}C NMR **(**$CDCl_3$, 100 MHz, δ with TMS=0**)** 164.76, 164.30, 164.08, 161.06, 147.51, 138.78, 138.39, 130.60, 130.23, 129.81, 128.86, 128.50, 117.59, 115.66, 114.91, 112.51, 109.71, 80.85, 71.67, 67.02, 66.00, 57.67, 54.23, 33.84, **HRMS**: for $C_{31}H_{30}N_4O_2$, calculated $[M+H]^+$: 491.2447; observed $[M+H]^+$: 491.2414

4-(4-(2-morpholinoethoxy)phenyl)-6-(2-(prop-2-yn-1-ylamino)phenyl)pyrimidin-2-amine (VP7):

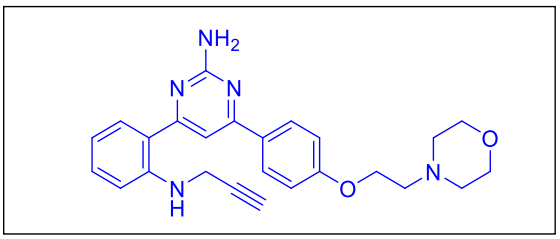

Yield 70%, ^{1}H NMR ($CDCl_3$, 300 MHz, δ with TMS=0): 7.99 (2H, d, *J* = 8Hz), 7.66 (1H, d, *J* = 9Hz), 7.32 (1H, s), 7.25 (1H, s), 6.98 (2H, d, *J* = 9Hz), 6.77-6.84 (2H, m), 5.11 (2H, s), 4.20 (2H, brs), 4.05 (2H, brs), 3.74 (4H, brs), 2.81 (2H, d, *J* = 4Hz), 2.59 (4H,brs), 2.23 (1H,s), ^{13}C NMR **(**$CDCl_3$, 75 MHz, δ with TMS=0**)** 167.74, 161.95, 160.77, 147.15, 131.60, 130.33, 129.59, 128.59, 116.85, 114.73, 11.99, 104.89, 80.85, 71.03, 66.92, 65.92, 57.57, 54.13, 32.85, **HRMS**: for $C_{25}H_{27}N_5O_2$, calculated $[M+H]^+$: 430.2243; observed $[M+H]^+$: 430.2239

2-(2-methyl-6-(4-(2-morpholinoethoxy)phenyl)pyrimidin-4-yl)-N-(prop-2-yn-1-yl)aniline (VP8):

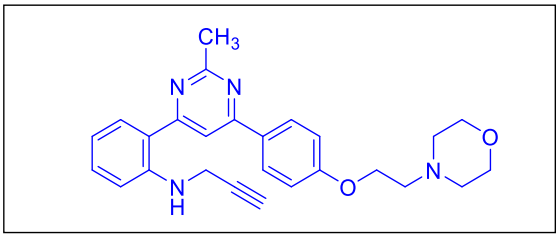

Yield 53%, ^{1}H NMR ($CDCl_3$, 400 MH_Z, δ with TMS=0): 8.06 (2H, d, *J* = 8Hz), 7.78 (1H, s), 7.74 (1H, d, *J* = 8Hz), 7.36 (1H, t, *J* = 8Hz), 7.01 (2H, d, *J* = 8Hz), 6.81 (2H, q, *J* = 8Hz), 4.21 (2H, t, *J* = 4Hz), 4.05 (2H, brs), 3.76 (4H, t, *J* = 4Hz), 2.89 (2H, brs), 2.79 (3H, s), 2.66 (4H, brs), 2.25 (1H, t, *J* = 4Hz), ^{13}C NMR **(**$CDCl_3$, 100 MH_Z, δ with TMS=0**)** 167.74, 161.95, 160.77, 147.15, 131.60, 130.33, 129.59, 128.59, 116.85, 114.73, 11.99, 104.89, 80.85, 71.03, 66.92, 65.92, 57.57, 54.13, 32.85, 26.51, **HRMS**: for $C_{26}H_{28}N_4O_2$, calculated $[M+H]^+$: 429.2291; observed $[M+H]^+$: 429.2238

2-(6-(4-(2-morpholinoethoxy)phenyl)-2-phenylpyrimidin-4-yl)-N-(prop-2-yn-1-yl)aniline (VP9):

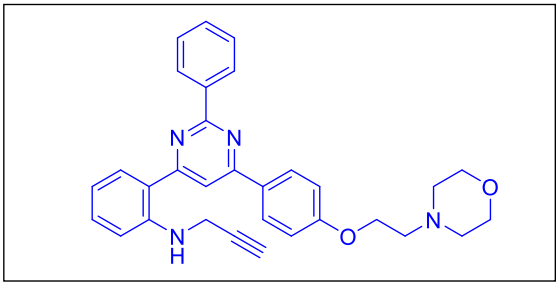

Yield 56%, ^{1}H NMR ($CDCl_3$, 400 MH_Z, δ with TMS=0): 8.55 (2H, t, *J* = 8Hz), 8.20-8.24 (2H, m), 7.88 (1H, d, *J* = 4Hz), 7.80 (1H, t, *J* = 8Hz), 7.51 (3H, d, *J* = 8Hz), 7.36-7.41 (1H, m), 7.02-7.05 (2H, m), 6.83 (2H, t, *J* = 8Hz), 4.21 (2H, t, *J* = 4Hz), 4.08 (2H, brs), 3.76 (4H, brs), 2.89 (2H, d, *J* = 4Hz), 2.66 (4H, brs), 2.29 (1H, t, *J* = 4Hz), ^{13}C NMR **(**$CDCl_3$, 100 MH_Z, δ with TMS=0**)** 166.67, 163.80, 161.95, 160.94, 147.89, 138.06, 130.75, 129.60, 128.88, 128.62, 128.42, 119.49, 116.86, 114.91, 114.58, 112.04, 110.66, 80.96, 76.80, 71.58, 66.75, 65.72, 57.56, 54.09**, HRMS**: for $C_{31}H_{30}N_4O_2$, calculated $[M+H]^+$: 491.2447; observed $[M+H]^+$: 491.2417

4-(4-(2-(piperidin-1-yl)ethoxy)phenyl)-6-(4-(prop-2-yn-1-ylamino)phenyl)pyrimidin-2-amine (VP10):

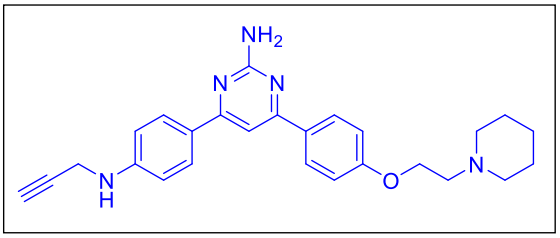

Yield 58%, ^{1}H NMR ($CDCl_3$, 400 MHz, δ with TMS=0): 8.02 (2H, d, *J* = 8Hz), 8.00 (2H, d, *J* = 8Hz), 7.36 (1H, s), 7.01 (2H, d, *J* = 8Hz), 6.77 (2H, d, *J* = 8Hz), 5.10 (2H,s), 4.19 (2H, t, *J* = 4Hz), 4.03 (2H, t, *J* = 4Hz), 2.82 (2H, t, *J* = 4Hz), 2.55 (4H, brs), 1.63 (4H, brs), 1.44 (3H, m), ^{13}C NMR **(**$CDCl_3$, 100 MHz, δ with TMS=0**)** 165.57, 165.12, 163.45, 160.73, 148.86, 130.45, 128.49, 128.42, 127.70, 114.69, 113.16, 102.30, 80.40, 71.62, 66.10, 57.87, 55.10, 33.38, 25.94, 24.19, **HRMS**: for $C_{26}H_{29}N_5O$, calculated $[M+H]^+$: 428.2450; observed $[M+H]^+$: 428.2473

4-(2-methyl-6-(4-(2-(piperidin-1-yl)ethoxy)phenyl)pyrimidin-4-yl)-N-(prop-2-yn-1-yl)aniline (VP11):

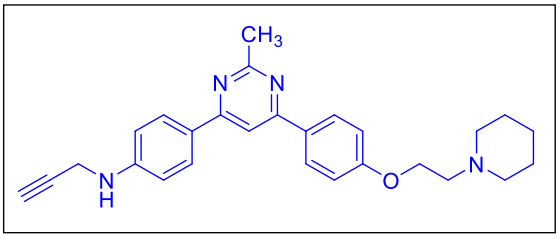

Yield 53%, ^{1}H NMR ($CDCl_3$, 400 MHz, δ with TMS=0): 8.09 (2H, d, *J* = 8Hz), 8.06 (2H, d, *J* = 8Hz), 7.74 (1H, s), 7.04 (2H, d, *J* = 8Hz), 6.79 (2H, d, *J* = 8Hz), 4.20 (2H, t, *J* = 4Hz), 4.03 (2H, t, *J* = 4Hz), 2.84 (1H, t, *J* = 4Hz), 2.82 (3H,s), 2.54 (4H, t, *J* = 4Hz), 2.27 (1H, t, *J* = 4Hz), 1.65 (4H, t, *J* = 4Hz), 1.48 (2H, t, *J* = 4Hz), ^{13}C NMR **(**$CDCl_3$, 100 MHz, δ with TMS=0) 168.10, 164.25, 163.80, 160.84, 148.97, 130.27, 128.62, 128.53, 127.47, 114.85, 113.30, 107.79, 80.33, 71.65, 66.07, 57.83, 55.09, 33.37, 26.53, 25.89, 24.16, **HRMS**: for $C_{27}H_{31}N_4O$, calculated $[M+H]^+$: 427.2498; observed $[M+H]^+$: 427.2532

4-(2-phenyl-6-(4-(2-(piperidin-1-yl)ethoxy)phenyl)pyrimidin-4-yl)-N-(prop-2-yn-1-yl)aniline (VP12):

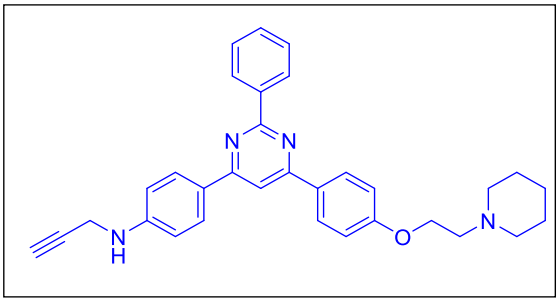

Yield 62%, ^{1}H NMR ($CDCl_3$, 400 MHz, δ with TMS=0): 8.73 (2H, d, *J* = 8Hz), 8.24 (2H, d, *J* = 8Hz), 8.20 (2H, d, *J* = 8Hz), 7.83 (1H, s), 7.54 (3H, t, *J* = 8Hz), 7.06 (2H, d, *J* = 8Hz), 6.80 (2H, d, *J* = 8Hz), 4.21 (2H, t, *J* = 4Hz), 4.01 (2H, brs), 2.84 (2H, t, *J* = 4Hz), 4.01 (4H, brs), 2.29 (1H, t, *J* = 4Hz), 1.66 (4H, t, *J* = 4Hz), 1.49 (2H, brs), ^{13}C NMR **(**$CDCl_3$, 100 MHz, δ with TMS=0**)** 164.10, 164.02, 163.61, 160.94, 149.13, 138.64, 130.31, 128.66, 128.60, 128.57, 128.41, 128.35, 127.42, 127.36, 114.79, 113.21, 107.96, 80.43, 71.67, 66.02, 57.84, 55.08, 33.33, 25.88, 24.17, **HRMS**: for $C_{32}H_{32}N_4O$, calculated $[M+H]^+$: 489.2654; observed $[M+H]^+$: 489.2651

4-(4-(2-(piperidin-1-yl)ethoxy)phenyl)-6-(3-(prop-2-yn-1-ylamino)phenyl)pyrimidin-2-amine (VP13):

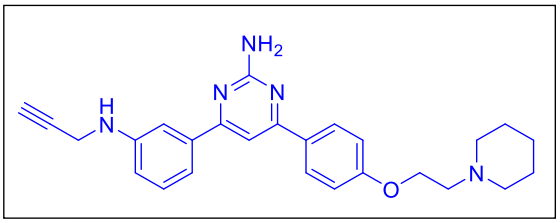

Yield 52%, ^{1}H NMR ($CDCl_3$, 400 MHz, δ with TMS=0): 8.00 (2H, d, *J* = 8Hz), 7.37 (1H, s), 7.89 (1H, s), 7.21 (1H, d, *J* = 8Hz), 7.15 (1H, d, *J* = 8Hz), 6.98 (2H, d, *J* = 12Hz), 6.78 (1H, d, *J* = 8Hz), 5.11 (2H, s), 4.16 (2H, t, *J* = 4Hz), 4.04 (2H, t, *J* = 4Hz), 3.95 (2H, t, *J* = 4Hz), 2.80 (2H, t, *J* = 4Hz), 2.73 (2H, t, *J* = 4Hz), 2.21 (2H, t, *J* = 4Hz), 1.57-1.62 (3H, m), 1.41 (2H, d, *J* = 4Hz), ^{13}C NMR **(**$CDCl_3$, 100 MHz, δ with TMS=0**)** 165.75, 165.55, 163.60, 160.96, 158.07, 139.53, 131.02, 129.87, 128.67, 120.45, 117.08, 114.79, 113.50, 103.68, 78.51, 75.83, 66.01, 57.85, 56.03, 55.11, 25.87, 34.17**, HRMS**: for $C_{26}H_{29}N_5O$, calculated $[M+H]^+$: 428.2450; observed $[M+H]^+$: 428.2440

3-(2-phenyl-6-(4-(2-(piperidin-1-yl)ethoxy)phenyl)pyrimidin-4-yl)-N-(prop-2-yn-1-yl)aniline (VP14):

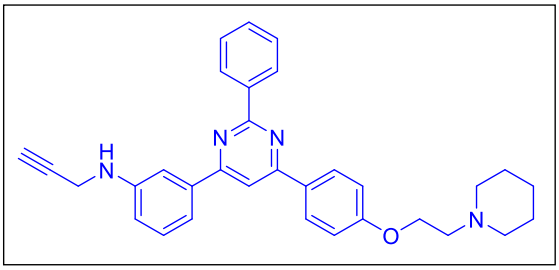

Yield 61%, ^{1}H NMR ($CDCl_3$, 300 MHz, δ with TMS=0): 8.69 (2H, d, *J* = 6Hz), 8.23 (2H, d, *J* = 9Hz), 7.89 (1H, s), 7.60 (2H, d, *J* = 9Hz), 7.51 (2H, d, *J* = 9Hz), 7.38 (2H, t, *J* = 9Hz), 7.04 (2H, d, *J* = 9Hz), 6.84 (1H, d, *J* = 9Hz), 4.20 (2H, t, *J* = 6Hz), 4.05 (2H, brs), 2.83 (2H, t, *J* = 6Hz), 2.55 (4H, brs), 2.26 (1H,s), 1.62 (4H, d, *J* = 6Hz), 1.42 (2H, brs), ^{13}C NMR **(**$CDCl_3$, 75 MHz, δ with TMS=0**)** 164.35, 164.37, 164.05, 161.16, 158.17, 139.36, 138.29, 130.70, 130.01, 128.85, 128.51, 120.52, 117.11, 114.56, 113.96, 109.61, 78.39, 75.83, 57.92, 56.16, 75.83, 29.72, 25.86, 24.13**,** $C_{32}H_{32}N_4O$, calculated $[M+H]^+$: 489.2654; observed $[M+H]^+$: 489.2695

4-(4-(2-(piperidin-1-yl)ethoxy)phenyl)-6-(2-(prop-2-yn-1-ylamino)phenyl)pyrimidin-2-amine (VP15):

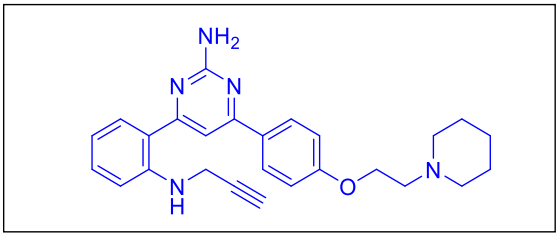

Yield 59%, ^{1}H NMR ($CDCl_3$, 400 MHz, δ with TMS=0): 8.40 (1H, brs), 8.01 (2H, d, *J* = 8Hz), 7.70 (1H, d, *J*= 8Hz), 7.37 (1H, t, *J*= 8Hz), 7.35 (1H, s), 7.01 (2H, d, *J* = 8Hz), 6.84 (2H, dd, J_1= 8Hz, J_2= 4Hz), 5.16 (2H, s), 4.23 (2H, t, *J* = 4Hz), 4.06 (2H, brs), 2.89 (2H, t, *J* = 6Hz), 2.62 (4H, brs), 2.26 (1H, brs), 1.69 (4H, t, *J* = 4Hz), 1.50 (2H, t, *J* = 4Hz), ^{13}C NMR **(**$CDCl_3$, 75 MHz, δ with TMS=0**)** 167.70, 165.36, 161.97, 160.74, 147.15, 131.56, 130.27, 129.58, 128.58, 120.28, 116.84, 114.73, 111.98, 104.85, 81.14, 71.02, 65.78, 57.64, 54.94, 32.85, 29.69, 25.58, **HRMS**: for $C_{32}H_{32}N_4O_1$, calculated $[M+H]^+$: 428.2450; observed $[M+H]^+$: 428.2460

2-(2-phenyl-6-(4-(2-(piperidin-1-yl)ethoxy)phenyl)pyrimidin-4-yl)-N-(prop-2-yn-1-yl)aniline (VP16):

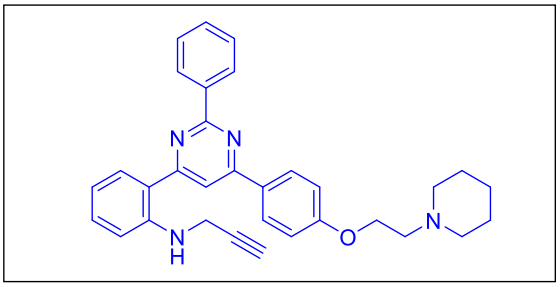

Yield 54%, ^{1}H NMR ($CDCl_3$, 400 MHz, δ with TMS=0): Yield 53%, ^{1}H NMR ($CDCl_3$, 400 MHz, δ with TMS=0): 8.70 (2H, dd, J_1= 8Hz, J_2= 4Hz), 8.24 (2H, d, J= 8Hz), 7.96 (1H, t, J= 8Hz), 7.91 (1H, s), 7.85 (1H, dd, J_1= 8Hz, J_2= 4Hz), 7.53-7.45 (4H, m), 7.13 (1H, dd, J_1= 8Hz, J_2= 4Hz), 7.05 (2H, d, J= 8Hz), 4.81 (2H, d, J= 8Hz), 4.20 (2H, t, J= 4Hz), 2.83 (2H, t, J= 4Hz), 2.58 (4H, t, J= 4Hz), 1.66-1.60 (4H, m), 1.47-1.40 (3H, m), **(**$CDCl_3$, 100 MHz, δ with TMS=0**)** δ: 164.35, 164.37, 164.05, 161.16, 158.17, 139.36, 138.29, 130.70, 130.01, 128.85, 128.51, 120.52, 117.11, 114.56, 113.96, 109.61, 78.39, 75.83, 57.92, 56.16, 75.83, 29.72, 25.86, 24.13, **HRMS**: for $C_{32}H_{32}N_4O$, calculated $[M+H]^+$: 489.2654; observed $[M+H]^+$: 489.2643

4-(6-(4-(2-(dimethylamino)ethoxy)phenyl)-2-phenylpyrimidin-4-yl)-N-(prop-2-yn-1-yl)aniline (VP17):

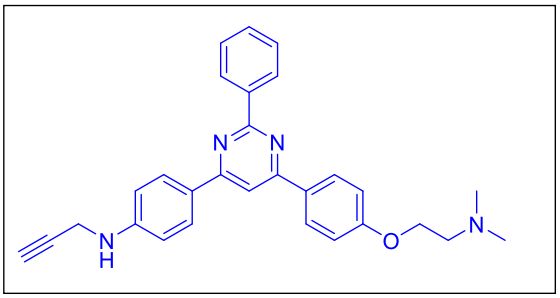

Yield 58%, ^{1}H NMR ($CDCl_3$, 400 MHz, δ with TMS=0): 8.72 (2H, d, J = 8Hz), 8.26 (2H, d, J = 8Hz), 8.23 (2H, d, J = 8Hz), 7.87 (1H, s), 7.53-7.57 (3H, m), 7.09 (2H, d, J = 8Hz), 6.83 (2H, d, J = 8Hz), 4.20 (2H, t, J = 4Hz), 4.05 (2H, brs), 2.85 (2H, t, J = 8Hz), 2.42 (6H, s), 2.29 (1H, brs), ^{13}C NMR ($CDCl_3$, 100 MHz, δ with TMS=0) 164.14, 164.07, 163.64, 160.87, 149.10, 138.60, 130.43, 130.31, 128.67, 128.59, 128.38, 128.33, 127.54, 114.77, 113.25, 108.02, 80.36, 71.67, 65.91, 58.05, 45.73, 33.38, 29.71 **HRMS**: for $C_{29}H_{28}N_4O$, calculated $[M+H]^+$: 449.2341; observed $[M+H]^+$: 449.2349

3-(6-(4-(2-(dimethylamino)ethoxy)phenyl)-2-phenylpyrimidin-4-yl)-N-(prop-2-yn-1-yl)aniline (VP18):

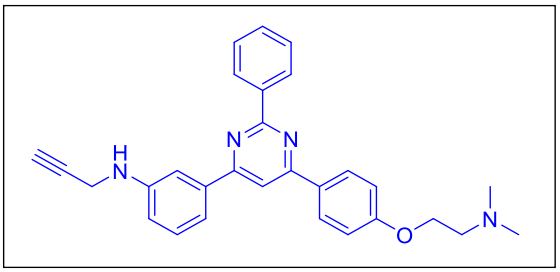

Yield 51%, ^{1}H NMR ($CDCl_3$, 400 MHz, δ with TMS=0): 8.69 (2H, dd, J_1 = 8Hz, J_2 = 4Hz), 8.24 (2H, dd, J_1 = 8Hz, J_2 = 4Hz), 7.98 (1H, s), 7.66 (1H, t, J = 8Hz), 7.59 (1H, d, J = 8Hz), 7.49-7.52 (3H, m), 7.38 (1H, t, J = 8Hz), 7.05 (2H, dd, J_1 = 8Hz, J_2 = 4Hz), 6.85 (1H, dd, J_1 = 8Hz, J_2 = 4Hz), 4.18 (2H, t, J = 4Hz), 4.05 (2H, d, J = 4Hz), 2.84 (2H, t, J = 8Hz), 2.40 (6H, s), 2.26 (1H, t, J = 4Hz), ^{13}C NMR ($CDCl_3$, 100 MHz, δ with TMS=0) 164.77, 164.30, 164.12, 161.04, 147.51, 138.79, 138.40, 130.59, 129.81, 128.85, 128.50, 124.10, 123.55, 117.61, 115.67, 114.89, 112.52, 109.73, 80.86, 71.67, 65.80, 57.96, 45.65, 33.84, **HRMS**: for $C_{29}H_{28}N_4O$, calculated $[M+H]^+$: 449.2341; observed $[M+H]^+$: 449.2334

4-(4-(2-(dimethylamino)ethoxy)phenyl)-6-(2-(prop-2-yn-1-ylamino)phenyl)pyrimidin-2-amine (VP19):

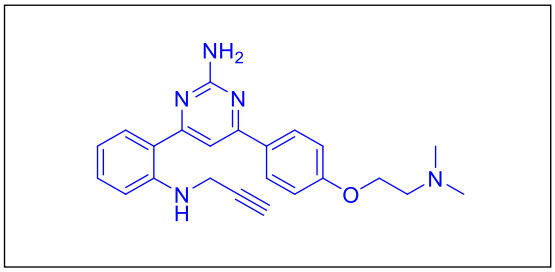

Yield 63%, ^{1}H NMR ($CDCl_3$, 400 MHz, δ with TMS=0): 8.03 (2H, d, J = 8Hz), 7.37 (1H, s), 7.66 (1H, t, J = 8Hz), 7.28-7.32 (1H, m), 7.20 (2H, dd, J_1 = 8Hz, J_2 = 4Hz), 7.15 (2H, dd, J_1 = 8Hz, J_2 = 4Hz), 7.03 (1H, d, J = 8Hz), 5.12 (2H, brs), 4.23 (2H, t, J = 4Hz), 4.07 (2H, d, J = 4Hz), 2.91 (2H, t, J = 4Hz), 2.47 (6H, s), 2.27 (1H, t, J = 4Hz), ^{13}C NMR ($CDCl_3$, 100 MHz, δ with TMS=0) 167.73, 165.32, 161.94, 160.62, 147.15, 146.46, 131.59, 130.41, 129.59, 128.60, 128.11, 127.66, 126.98, 125.65, 120.23, 116.85, 114.71, 111.98, 104.90, 81.13, 71.02, 65.61, 57.93, 46.05, 45.56, **HRMS**: for $C_{23}H_{25}N_5O$, calculated $[M+H]^+$: 388.2137; observed $[M+H]^+$: 388.2139

2-(6-(4-(2-(dimethylamino)ethoxy)phenyl)-2-methylpyrimidin-4-yl)-N-(prop-2-yn-1-yl)aniline (VP20):

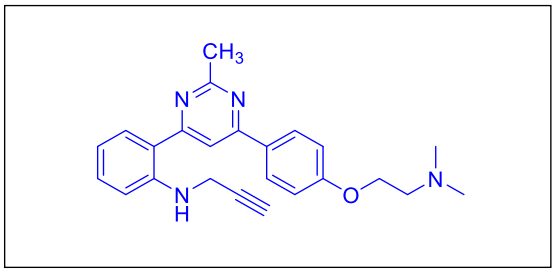

Yield 63%, ^{1}H NMR ($CDCl_3$, 400 MH_Z, δ with TMS=0): 8.03 (2H, d, *J* = 8Hz), 7.37 (1H, s), 7.66 (1H, t, *J* = 8Hz), 7.28-7.32 (1H, m), 7.20 (2H, dd, J_1 = 8Hz, J_2 = 4Hz), 7.15 (2H, dd, J_1 = 8Hz, J_2 = 4Hz), 7.03 (1H, d, *J* = 8Hz), 5.12 (2H, brs), 4.23 (2H, t, *J* = 4Hz), 4.07 (2H, d, *J* = 4Hz), 2.91 (2H, t, *J* = 4Hz), 2.47 (6H, s), 2.27 (1H, t, *J* = 4Hz), ^{13}C NMR ($CDCl_3$, 100 MH_Z, δ with TMS=0) 167.73, 165.32, 161.94, 160.62, 147.15, 146.46, 131.59, 130.41, 129.59, 128.60, 128.11, 127.66, 126.98, 125.65, 120.23, 116.85, 114.71, 111.98, 104.90, 81.13, 71.02, 65.61, 57.93, 46.05, 45.56, **HRMS**: for $C_{24}H_{26}N_4O$, calculated $[M+H]^+$: 387.2185; observed $[M+H]^+$: 387.2184

2-(6-(4-(2-(dimethylamino)ethoxy)phenyl)-2-phenylpyrimidin-4-yl)-N-(prop-2-yn-1-yl)aniline (VP21):

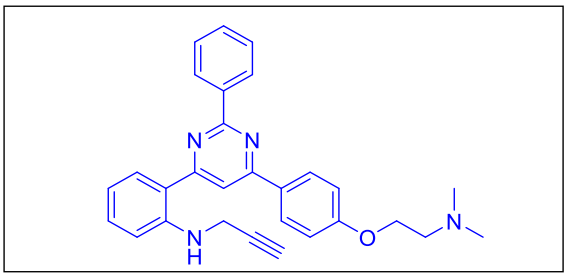

Yield 59%, ^{1}H NMR ($CDCl_3$, 400 MH_Z, δ with TMS=0): 8.62 (2H, d, *J* = 8Hz), 7.93 (1H, s), 8.26 (1H, d, *J* = 8Hz), 7.84 (1H, d, *J* = 8Hz), 7.57 (3H, m), 7.43 (1H, t, *J* = 8Hz), 7.10 (2H, d, *J* = 8Hz), 6.87 (2H, d, *J* = 8Hz), 4.22 (2H, t, *J* = 4Hz), 4.13 (2H, t, *J* = 4Hz), 2.87 (2H, t, *J* = 4Hz), 2.43 (6H, s), 2.33 (1H, t, *J* = 4Hz), ^{13}C NMR ($CDCl_3$, 100 MH_Z, δ with TMS=0) 166.58, 163.83, 162.89, 161.07, 147.84, 138.04, 132.03, 130.62, 129.51, 128.76, 128.58, 128.51, 128.35, 119.50, 116.79, 114.86, 111.97, 110.57, 80.91, 71.47, 65.92, 58.03, 45.71, 33.11, 29.70, 29.67, **HRMS**: for $C_{29}H_{28}N_4O$, calculated $[M+H]^+$: 449.2341; observed $[M+H]^+$: 449.2346

4-(2-phenyl-6-(4-(2-(pyrrolidin-1-yl)ethoxy)phenyl)pyrimidin-4-yl)-N-(prop-2-yn-1-yl)aniline (VP22):

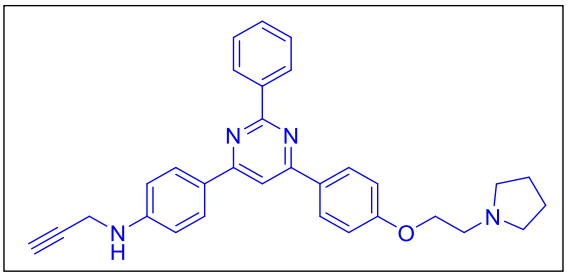

Yield 55%, ^{1}H NMR ($CDCl_3$, 400 MHz, δ with TMS=0): 8.69 (2H, dd, J_1 = 8Hz, J_2 = 4Hz), 8.24 (2H, dd, J_1 = 8Hz, J_2 = 4Hz), 7.84 (1H, s), 7.48-7.53 (3H, m), 7.06 (2H, dd, J_1 = 8Hz, J_2 = 4Hz), 6.81 (2H, t, J = 8Hz), 4.20 (2H, t, J = 4Hz), 4.03 (2H, t, J = 4Hz), 2.94 (2H, t, J = 4Hz), 2.65 (4H, t, J = 4Hz), 2.26 (1H, t, J = 4Hz), 1.82 (4H, t, J = 4Hz), ^{13}C NMR ($CDCl_3$, 100 MHz, δ with TMS=0) 164.26, 163.76, 161.08, 149.14, 138.67, 130.39, 128,74, 128.67, 128.45, 128.42, 127.65, 114.87, 113.33, 108.10, 80.84, 71.75, 67.29, 55.11, 54.86, 33.45, 23.58, **HRMS**: for $C_{31}H_{30}N_4O$, calculated $[M+H]^+$: 475.2498; observed $[M+H]^+$: 475.2491

3-(2-phenyl-6-(4-(2-(pyrrolidin-1-yl)ethoxy)phenyl)pyrimidin-4-yl)-N-(prop-2-yn-1-yl)aniline (VP23):

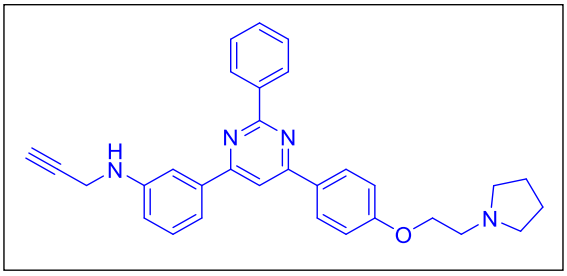

Yield 65%, ^{1}H NMR ($CDCl_3$, 400 MHz, δ with TMS=0): 8.69 (2H, d, J = 8Hz), 8.24 (2H, d, J = 8Hz), 7.90 (1H, s), 7.66 (1H, m), 7.59 (1H, dd, J_1 = 8Hz, J_2 = 4Hz), 7.47-7.54 (3H, m), 7.38 (1H, t, J = 8Hz), 7.05 (2H, d, J = 8Hz), 6.86 (1H, d, J = 8Hz), 4.27 (2H, t, J = 4Hz), 4.05 (2H, d, J = 4Hz), 3.36 (1H, t, J = 4Hz), 3.09 (2H, t, J = 4Hz), 2.84 (4H, brs), 1.89 (4H, t, J = 4Hz), ^{13}C NMR ($CDCl_3$, 100 MHz, δ with TMS=0) 164.79, 164.31, 164.08, 160.80, 147.51, 138.78, 138.38, 130.59, 129,82, 128.90, 128.50, 124.95, 124.10, 117.61, 115.68, 114.89, 112.52, 109.75, 80.84, 71.66, 66.31, 54.68, 54.61, 33.85, 29.79, **HRMS**: for $C_{31}H_{30}N_4O$, calculated $[M+H]^+$: 475.2498; observed $[M+H]^+$: 475.2497

2-(2-phenyl-6-(4-(2-(pyrrolidin-1-yl)ethoxy)phenyl)pyrimidin-4-yl)-N-(prop-2-yn-1-yl)aniline (VP24):

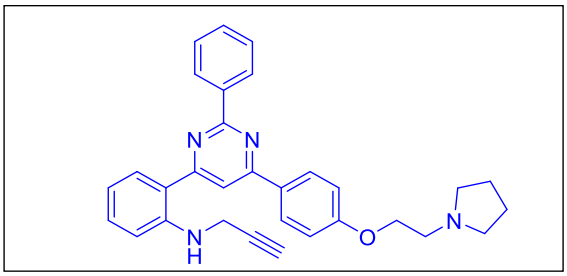

Yield 56%, ^{1}H NMR ($CDCl_3$, 400 MHz, δ with TMS=0): 8.55 (2H, d, *J* = 8Hz), 8.17 (2H, d, *J* = 8Hz), 7.45-7.52 (3H, m), 7.40 (1H, s), 7.27 (1H, d, *J* = 8Hz), 7.11 (2H, d, *J* = 8Hz), 7.02 (2H, d, *J* = 8Hz), 6.59 (1H, d, *J* = 8Hz), 4.25 (2H, t, *J* = 4Hz), 3.07 (2H, d, *J* = 4Hz), 2.82 (4H, t, *J* = 4Hz), 2.28 (2H, d, *J* = 4Hz), 2.01 (3H, t, *J* = 4Hz), 1.88 (4H, brs), ^{13}C NMR ($CDCl_3$, 100 MHz, δ with TMS=0) 167.55, 164.28, 163.21, 160.82, 139.39, 130.46, 128.81, 128.51, 128.38, 128.20, 127.74, 125.73, 124.95, 124.82, 124.12, 115.93, 114.84, 114.16, 113.21, 80.95, 66.41, 54.68, 54.57, 33.93, 32.02, 31.71, **HRMS**: for $C_{31}H_{30}N_4O$, calculated $[M+H]^+$: 475.2498; observed $[M+H]^+$: 475.2491

4.3.3 General Protocol for the synthesis of Series-III (Scheme-III)

4.3.3.1 General procedure for the synthesis of 3 and 4

To hydroxy substituted acetophenone (0.5 g) or benzaldehydes (0.5 g), propargyl bromide (1.2 eq) was added in the presence of potassium carbonate as base (2.4 eq) and acetone (30 mL) as solvent. The reaction mixture was refluxed overnight at 60˚C. The progress of reaction was monitored via TLC. After completion of the reaction, excess of solvent was evaporated from the mixture using vacuum rotary evaporator, water (10 mL) was added and aqueous phase was extracted with ethyl acetate (10 mL × 3), and washed with brine, dried over anhydrous Na_2SO_4 and the organic solvent was concentrated under vacuum using rotary evaporator.

4.3.3.2 General procedure for the synthesis of 5

To a mixture of **3** (1 eq) and **4** (1 eq) in methanol (20 mL), aqueous sodium hydroxide (20%) was added slowly with continuous stirring. The reaction mixture was stirred for 3 h at room temperature. The completion of reaction was monitored via TLC. After completion of reaction, excess of solvent was evaporated from the mixture

using rotary evaporator. Chilled water was poured into the reaction mixture and precipitates of **5** were filtered and dried. Further crude product was recrystallized from ethanol or purified using column chromatography as per requirement.

Synthetic scheme-III: Synthesis of target molecules of series-III

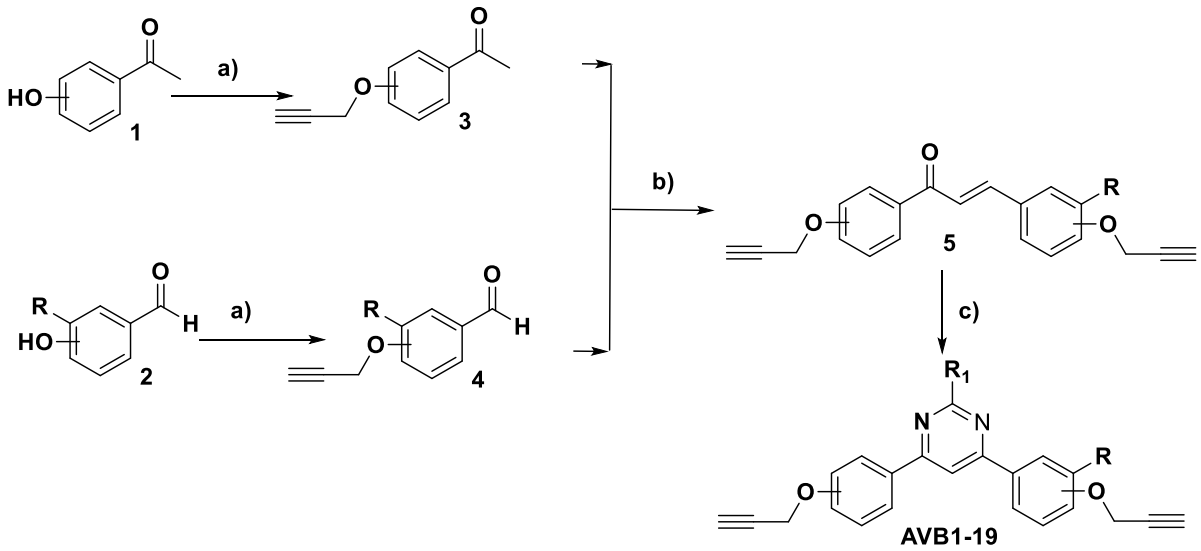

Reagents and conditions: a) Propargyl bromide (1.2 eq), K_2CO_3 (2 eq), acetone, reflux, 12h; **b)** CH_3OH as solvent, 10% NaOH aq., rt, stirring 1h; **c)** Amidines (1.5 eq), Na_2CO_3 (2.5 eq), CH_3CN as solvent, reflux, 24h

4.3.3.3 General procedure for the synthesis of AVB1-19

To a mixture of **5** (500 mg), and amidine (1.2 eq), anhydrous sodium carbonate (2.4 eq) was added in acetonitrile (10 mL) as solvent. The reaction mixture was refluxed for 24 h at 85˚ C. The progress of the reaction was monitored via TLC. After completion of the reaction, excess of solvent was evaporated under vacuum using rotary evaporator, water (10 mL) was added aqueous phase was extracted with ethyl acetate (3 × 10 mL), washed with brine, dried over anhydrous Na_2SO_4, and the organic solvent was concentrated under vacuum using rotary evaporator and purified via column chromatography (EtOAc:Pet ether). The final products were characterized by NMR spectroscopy and HRMS.

4.3.3.4 Spectral Analysis

4,6-bis(4-(prop-2-yn-1-yloxy)phenyl)pyrimidin-2-amine (AVB1):

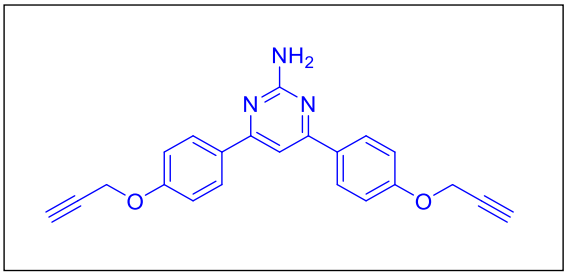

Yield: 55%; yellow solid, mp 139-141 °C; ^{1}H NMR ($CDCl_3$, 400 MHz, δ with TMS = 0): 8.02 (4H, d, *J* = 8Hz), 7.34 (1H, s), 7.06 (4H, d, *J* = 8Hz), 5.17 (2H, s), 4.76 (4H, d, *J* = 4Hz), 2.54 (2H, t, *J* = 4Hz), ^{13}C NMR ($CDCl_3$, 100 MHz, δ with TMS = 0) δ: 165.40, 163.57, 159.49, 131.16, 128.66, 115.25, 103.02, 76.81, 75.98, 55.92, **HRMS**: for $C_{22}H_{17}N_3O_2$, calculated $[M+H]^+$: 356.1399; observed $[M+H]^+$: 356.1369

2-methyl-4,6-bis(4-(prop-2-yn-1-yloxy)phenyl)pyrimidine (AVB2):

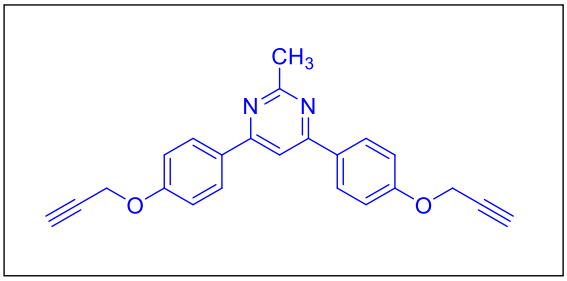

Yield: 60%; blue solid, mp 158-160 °C; ^{1}H NMR ($CDCl_3$, 400 MHz, δ with TMS = 0): 8.10 (4H, d, *J* = 8Hz), 7.76 (1H, s), 7.10 (4H, d, *J* = 8Hz), 4.76 (4H, d, *J* = 4Hz), 2.81 (3H, s), 2.55 (2H, t, *J* = 4Hz), ^{13}C NMR ($CDCl_3$, 100 MHz, δ with TMS = 0) δ: 168.34, 164.00, 159.59, 130.92, 128.71, 115.21, 108.55, 78.15, 75.90, 55.89, 26.49, **HRMS**: for $C_{23}H_{18}N_2O_2$, calculated $[M+H]^+$: 355.1447; observed $[M+H]^+$: 355.1405

2-phenyl-4,6-bis(4-(prop-2-yn-1-yloxy)phenyl)pyrimidine (AVB3):

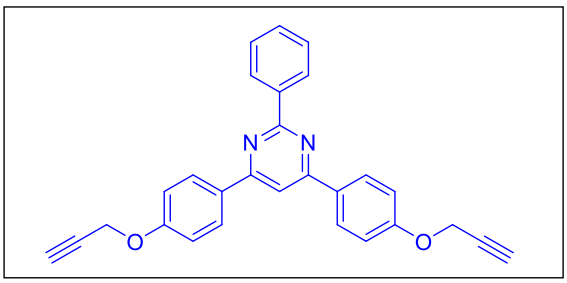

Yield: 65%; greenish solid, mp 148-150 °C; ^{1}H NMR ($CDCl_3$, 400MHz, δ with TMS=0) 8.73 (2H, d, *J* = 8Hz), 8.30 (4H, d, *J* = 8Hz), 7.92 (1H, s), 7.55 (3H, m), 7.18 (4H, d, *J* = 8Hz), 4.82 (4H, d, *J* = 4Hz), 2.59 (2H, t, *J* = 4Hz), ^{13}C NMR ($CDCl_3$, 100

MHz, δ with TMS=0): 163.90, 159.70, 138.32, 130.98, 130.51, 128.75, 128.40, 115.17, 108.78, 78.17, 75.92, 55.90, **HRMS**: for $C_{28}H_{20}N_2O_2$, calculated $[M+H]^+$: 417.1603; observed $[M+H]^+$: 417.1547

4-(3-(prop-2-yn-1-yloxy)phenyl)-6-(4-(prop-2-yn-1-yloxy)phenyl)pyrimidin-2-amine (AVB4):

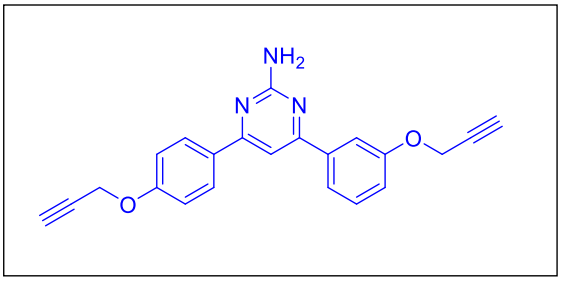

Yield: 65%; white solid, mp 139-141 °C; ^{1}H NMR ($CDCl_3$, 400 MHz, δ with TMS = 0): 8.02 (2H, d, *J* = 8Hz), 7.69-7.63 (2H, m), 7.42 (1H, d, *J* = 8Hz),7.37 (1H, s), 7.11 - 7.04 (3H, m), 5.25 (2H, s), 4.75 (4H, d, *J* = 4 Hz), 2.54 (2H, t, *J* = 4 Hz), ^{13}C NMR ($CDCl_3$, 100 MHz, δ with TMS = 0) δ: 165.66, 163.57, 159.59, 158.02, 139.47, 130.98, 129.90, 128.69, 120.45, 117.15, 115.11, 113.52 103.82, 78.49, 75.81, 56.04, 55.93, **HRMS**: for $C_{22}H_{17}N_3O_2$, calculated $[M+H]^+$: 356.1399; observed $[M+H]^+$: 356.1362

2-methyl-4-(3-(prop-2-yn-1-yloxy)phenyl)-6-(4-(prop-2-yn-1-yloxy)phenyl)pyrimidine (AVB5):

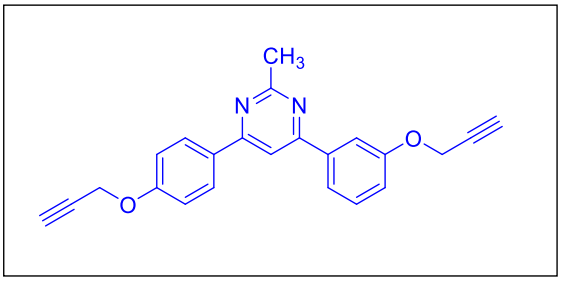

Yield: 63%; white solid, mp 116-118 °C; ^{1}H NMR ($CDCl_3$, 400MHz, δ with TMS=0) 8.15 (2H, d, *J* = 8Hz), 7.83 (1H, s), 7.78 (2H, d, *J* = 8Hz), 7.47 (1H, t, *J* = 8Hz), 7.15 (3H, m), 4.83 (4H, d, *J* = 4Hz), 2.86(3H, s), 2.58 (1H, t, *J* = 4Hz), ^{13}C NMR (CDCl3, 100 MHz, δ with TMS=0): 164.27, 158.10, 139.22, 129.98, 128.75, 120.49, 117.14, 115.24, 113.73, 109.44, 78.37, 78.19, 75.92, 75.72, 56.04, 55.88, 26.48, **HRMS**: for $C_{23}H_{18}N_2O_2$, calculated $[M+H]^+$: 355.1447; observed $[M+H]^+$: 355.1405

2-phenyl-4-(3-(prop-2-yn-1-yloxy)phenyl)-6-(4-(prop-2-yn-1-yloxy)phenyl)pyrimidine (AVB6):

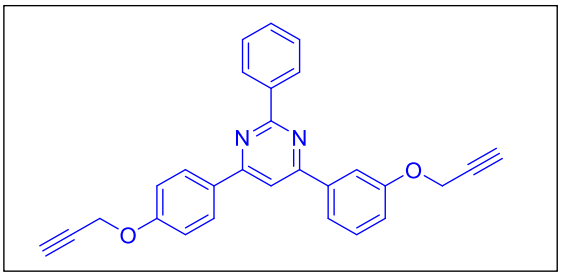

Yield: 60%; white solid, mp 147-148 °C; ^{1}H NMR ($CDCl_3$, 400 MHz, δ with TMS = 0): 8.72-8.70 (2H, m), 8.2 (2H, d, *J* = 8 Hz), 7.97-7.85 (3H, m), 7.54-7.48 (4H, m), 7.15 (3H, d, *J* = 8Hz), 4.83 (4H, d, *J* = 2.4 Hz), 2.59 (2H, m); ^{13}C NMR ($CDCl_3$, 100 MHz, δ with TMS = 0) δ: 164.38, 164.18, 164.11, 159.84, 158.18, 139.28, 138.20, 130.82, 130.72, 130.02, 128.87, 128.52, 120.50, 117.18, 115.24, 113.96, 109.70, 78.50, 76.06, 56.13, 55.95, , **HRMS**: for $C_{28}H_{20}N_2O_2$, calculated $[M+H]^+$: 417.1603; observed $[M+H]^+$: 417.1553

4-(2-(prop-2-yn-1-yloxy)phenyl)-6-(4-(prop-2-yn-1-yloxy)phenyl)pyrimidin-2-amine (AVB7):

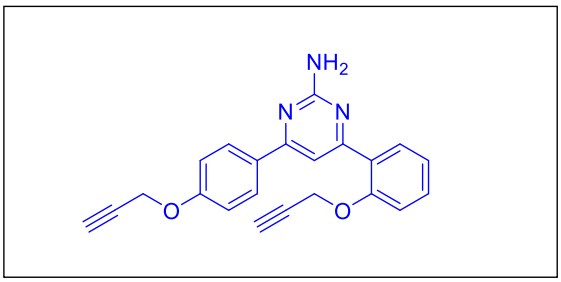

Yield: 64%; green solid, mp 134-136 °C; ^{1}H NMR ($CDCl_3$, 400MHz, δ with TMS=0) 8.07 (2H, d, *J* = 8Hz), 7.90 (1H, d, *J* = 8Hz), 7.66 (1H, s), 7.45 (1H, t, *J* = 8Hz), 7.18 (2H, d, *J* =8Hz), 7.09 (2H, d, *J* =8Hz), 5.15 (2H, brs), 4.79 (4H, t, *J* = 4Hz), 2.57 (2H, t, *J* = 4Hz), ^{13}C NMR ($CDCl_3$, 100 MHz, δ with TMS=0): 164.54, 164.29, 163.34, 159.39, 155.67, 131.21, 130.87, 128.72, 128.21, 122.15, 114.95, 113.54, 108.57, 78.46, 78.23, , 76.70, 75.83, 56.66, 55.85, 29.70, **HRMS**: for $C_{22}H_{17}N_3O_2$, calculated $[M+H]^+$: 356.1399; observed $[M+H]^+$: 356.1372

2-methyl-4-(2-(prop-2-yn-1-yloxy)phenyl)-6-(4-(prop-2-yn-1-yloxy)phenyl)pyrimidine (AVB8):

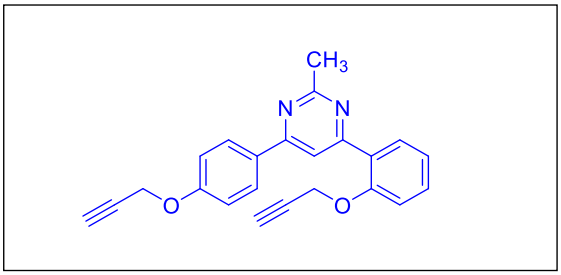

Yield: 58%; green solid, mp 132-134 °C; ^{1}H NMR ($CDCl_3$, 400MHz, δ with TMS=0) 8.15-8.12 (3H, m), 7.99 (1H, d, *J* = 8Hz), 7.47 (1H, t, *J* = 8Hz), 7.21-7.11 (4H, m), 4.80 (4H, d, *J* = 4Hz), 2.86 (3H, s), 2.58 (2H, t , *J* = 4Hz), ^{13}C NMR (CDCl3, 100 MHz, δ with TMS=0): 168.04, 163.14, 162.88, 159.49, 155.73, 131.22, 131.12, 131.08, 130.77, 128.85, 127.88, 122.30, 115.12, 114.64, 114.25, 113.34, 78.37, 78.19, 75.91, 75.86, 56.62, 55.86, 26.53, **HRMS**: for $C_{23}H_{18}N_2O_2$, calculated $[M+H]^+$: 355.1447; observed $[M+H]^+$: 355.1405

2-phenyl-4-(2-(prop-2-yn-1-yloxy)phenyl)-6-(4-(prop-2-yn-1-yloxy)phenyl)pyrimidine (AVB9):

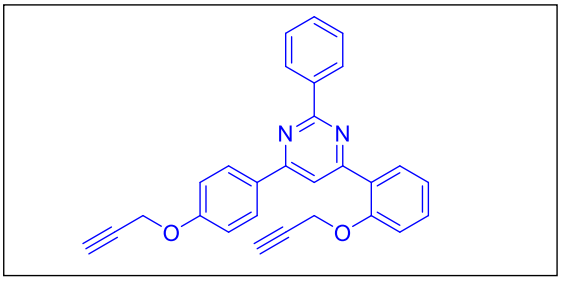

Yield: 65%; cream solid, mp 89-91 °C; ^{1}H NMR ($CDCl_3$, 400 MHz, δ with TMS = 0): 8.67 (2H, dd, J_{13} = 8 Hz; J_{12} = 4 Hz), 8.29-8.25 (4H, m), 7.52 - 7.46 (4H, m), 7.24 - 7.19 (1H, m), 7.15-7.11 (3H, m); 4.77 (4H, d, *J* = 4 Hz), 2.54 (2H, t , *J* = 4Hz), ^{13}C NMR ($CDCl_3$, 100 MHz, δ with TMS = 0) δ: 164.18, 163.16, 162.83, 159.66, 156.18, 138.51, 131.61, 131.22, 130.47, 128.98, 128.48, 127.86 122.34, 115.14, 114.86, 113.49, 78.48, 76.82, 56.73, 55.94, **HRMS**: for $C_{28}H_{20}N_2O_2$, calculated $[M+H]^+$: 417.1603; observed $[M+H]^+$: 417.1555

4,6-bis(3-(prop-2-yn-1-yloxy)phenyl)pyrimidin-2-amine (AVB10):

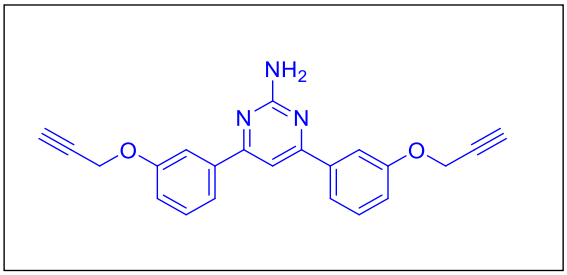

Yield: 57%; yellowish brown, mp 146-148 °C; ^{1}H NMR ($CDCl_3$, 400 MHz, δ with TMS = 0): 7.72 (2H, s), 7.69 (2H, d, *J* = 8Hz), 7.45 (3H, t, *J* = 8Hz), 7.14 (2H, d, *J* = 8Hz), 5.21 (2H, brs), 4.81 (4H, d, *J* = 4 Hz), 2.58 (2H, brs), ^{13}C NMR ($CDCl_3$, 100 MHz, δ with TMS = 0) δ: 165.84, 163.50, 157.98, 139.23, 129.86, 120.39, 117.22, 113.46, 104.53, 78.40, 75.74, 55.99, 29.86, **HRMS**: for $C_{22}H_{17}N_3O_2$, calculated $[M+H]^+$: 356.1399; observed $[M+H]^+$: 356.1367

2-phenyl-4,6-bis(3-(prop-2-yn-1-yloxy)phenyl)pyrimidine (AVB11):

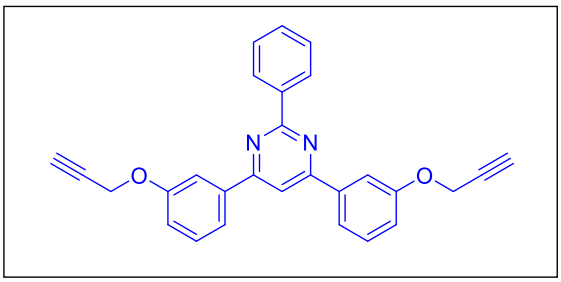

Yield: 59%; greenish yellow solid, mp 118-120 °C; ^{1}H NMR ($CDCl_3$, 400MHz, δ with TMS=0) 8.75 (2H, d, *J* = 8Hz), 8.01 (2H, d, *J* = 8Hz), 7.59 (1H, s), 7.57 (2H, d, *J* = 8Hz), 7.50-7.59 (4H, m), 7.20 (2H, d, *J* = 8Hz), 4.86 (4H, d, *J* = 4Hz), 2.62 (2H, t, *J* = 4Hz), ^{13}C NMR (CDCl3, 100 MHz, δ with TMS=0): 164.43, 164.35, 158.15, 139.05, 137.98, 130.74, 129.98, 128.48, 120.48, 117.28, 113.94, 110.51, 78.40, 75.86, 56.08, 29.71, **HRMS**: for $C_{28}H_{20}N_2O_2$, calculated $[M+H]^+$: 417.1603; observed $[M+H]^+$: 417.1603

4,6-bis(2-(prop-2-yn-1-yloxy)phenyl)pyrimidin-2-amine (AVB12):

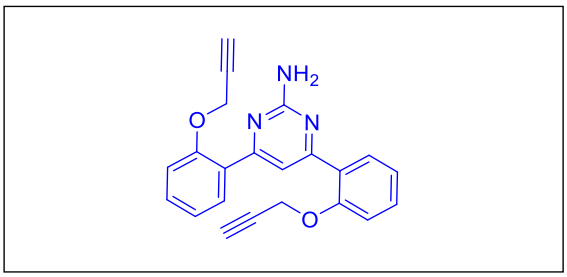

Yield: 64%; semi-solid; ^{1}H NMR ($CDCl_3$, 400MHz, δ with TMS=0) 7.83 (2H, d, *J* = 8Hz), 7.68 (1H, s), 7.44 (2H, t, *J* = 8Hz), 7.13-7.19 (4H, m), 5.47 (2H, brs), 4.80 (4H, d, *J* = 4Hz), 2.53 (2H, brs), ^{13}C NMR (CDCl3, 100 MHz, δ with TMS=0): 163.79, 163.19, 155.55, 131.04, 130.80, 128.25, 122.00, 113.73, 113.56, 78.58, 75.86, 56.47, 29.72, **HRMS**: for $C_{22}H_{17}N_3O_2$, calculated $[M+H]^+$: 356.1399; observed $[M+H]^+$: 356.1367

2-phenyl-4,6-bis(2-(prop-2-yn-1-yloxy)phenyl)pyrimidine (AVB13):

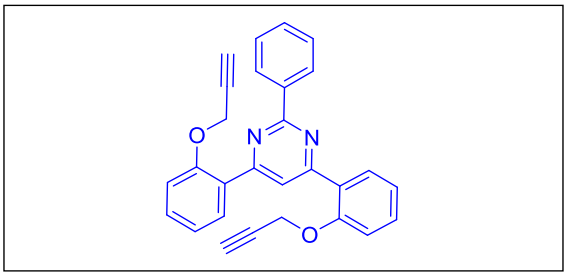

Yield: 68%; semi-solid; ^{1}H NMR ($CDCl_3$, 400MHz, δ with TMS=0) 8.69 (2H, d, *J* = 8Hz), 8.49 (1H, s), 8.24 (2H, d, *J* = 8Hz), 7.49-7.54 (5H, m), 7.22-7.27 (4H, m), 4.87 (4H, d, *J* = 4Hz), 2.55 (2H, brs), ^{13}C NMR (CDCl3, 100 MHz, δ with TMS=0): 164.08, 162.32, 156.01, 138.53, 131.70, 131.10, 130.27, 128.38, 128.29, 128.22, 122.15, 120.46, 113.56, 78.57, 75.95, 56.48, 29.74, **HRMS**: for $C_{28}H_{20}N_2O_2$, calculated $[M+H]^+$: 417.1603; observed $[M+H]^+$: 417.1603

4-(3-methoxy-4-(prop-2-yn-1-yloxy)phenyl)-6-(4-(prop-2-yn-1-yloxy)phenyl)pyrimidin-2-amine (AVB14):

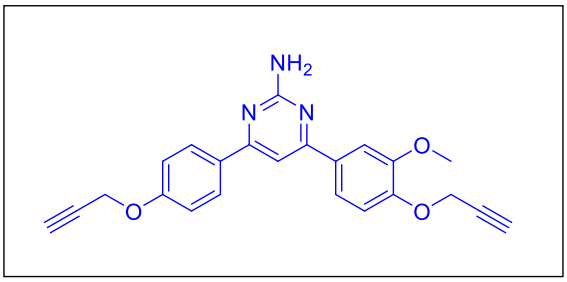

Yield: 60%; light brown solid, mp 118-120 °C; ^{1}H NMR ($CDCl_3$, 400 MHz, δ with TMS = 0): 8.04 (2H, d, *J* = 8Hz), 7.69 (1H, d, *J* = 8Hz), 7.60-7.58 (1H, m), 7.35 (1H, s), 7.12-7.06 (4H, m), 5.29 (2H, S), 4.83 (2H, d, *J* = 4Hz), 4.76 (2H, d, *J* = 4Hz), 3.99 (3H, s), 2.55 (2H, t, *J* = 4Hz), ^{13}C NMR ($CDCl_3$, 100 MHz, δ with TMS = 0) δ: 165.41, 163.47, 159.49, 149.78, 148.82, 131.73, 131.01, 128.63, 119.84, 115.04, 113.65,

110.48, 103.17, 78.19, 76.73, 75.09, 56.68, 56.06, 55.87, **HRMS**: for $C_{23}H_{19}N_3O_3$, calculated $[M+H]^+$: 386.1505; observed $[M+H]^+$: 386.1505

4-(3-methoxy-4-(prop-2-yn-1-yloxy)phenyl)-2-methyl-6-(4-(prop-2-yn-1-yloxy)phenyl)pyrimidine (AVB15):

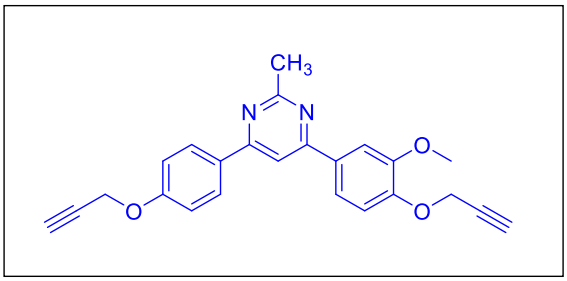

Yield: 60%; white solid, mp 132-134 °C; ^{1}H NMR ($CDCl_3$, 400 MHz, δ with TMS = 0): 8.10 (2H, d, *J* = 8H), 7.77 (2H, s), 7.66 (1H, dd, J_{13} = 8Hz, J_{12} = 4Hz), 7.15 – 7.09 (3H, m), 4.84 (2H, d, *J* = 4Hz), 4.77 (2H, d, *J* = 4Hz), 4.01 (3H, s), 2.82 (3H, s), 2.56-2.53 (2H, t, *J* = 4Hz), ^{13}C NMR ($CDCl_3$, 100 MHz, δ with TMS = 0) δ: 168.34, 164.05, 164.03, 157.60, 149.97, 148.97, 131.62, 130.88, 128.72, 119.93, 115.22, 113.83, 110.56, 108.74, 78.16 78.14, 76.18, 75.92, 56.71, 56.12, 55.80, 26.50, **HRMS**: for $C_{24}H_{20}N_2O_3$, calculated $[M+H]^+$: 385.1552; observed $[M+H]^+$: 385.1552

4-(3-methoxy-4-(prop-2-yn-1-yloxy)phenyl)-2-phenyl-6-(4-(prop-2-yn-1-yloxy)phenyl)pyrimidine (AVB16):

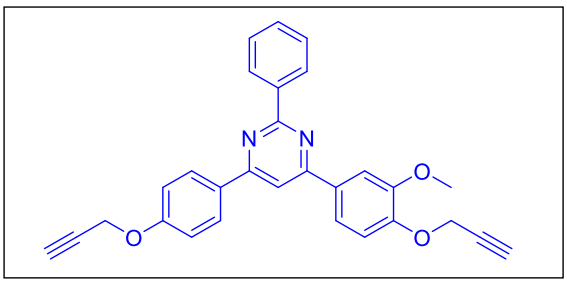

Yield: 70%; greenish white solid, mp 160-162 °C; ^{1}H NMR ($CDCl_3$, 400 MHz, δ with TMS = 0): 8.64 (2H, d, *J* = 8Hz), 8.45 (2H, d, *J* = 8 Hz), 8.29 (1H, s), 8.05 - 8.01 (2H, m), 7.58 - 7.52 (3H, m), 7.18 (3H, m), 4.88 (4H, d, *J*= 4 Hz), 4.00 (3H, s), 3.36 (2H, t, *J* = 4Hz), ^{13}C NMR ($CDCl_3$, 100 MHz, δ with TMS = 0) δ: 163.39, 163.31, 163.03, 159.47, 149.32, 148.96, 137.74, 130.39, 130.37, 129.81, 128.76, 128.36, 127.86, 120.19, 114.85, 113.59, 110.62, 108.89, 79.88, 78.67, 78.58, 77.84, 56.11, 55.72,

55.55, **HRMS**: for $C_{29}H_{22}N_2O_3$, calculated $[M+H]^+$: 447.1709; observed $[M+H]^+$: 447.1709

4-(3-ethoxy-4-(prop-2-yn-1-yloxy)phenyl)-6-(4-(prop-2-yn-1-yloxy)phenyl)pyrimidin-2-amine (AVB17):

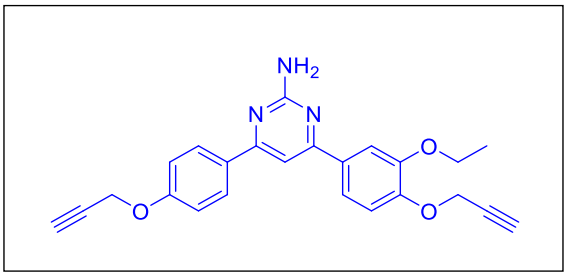

Yield: 65%; pale yellow solid, mp 162-164 °C; ^{1}H NMR ($CDCl_3$, 400MHz, δ with TMS=0) 8.05 (2H, d, *J* = 8Hz), 7.71 (1H, s), 7.62 (1H, d, *J* = 8Hz), 7.38 (1H, s), 7.16 (1H, d, *J* = 8Hz), 7.13 (2H, d, *J* = 8Hz), 5.21 (2H, brs), 4.87 (2H, d, *J* = 4Hz), 4.80 (2H, d, *J* = 4Hz), 4.26 (2H, q, *J* = 8Hz), 2.57 (2H, m), 1.53 (3H, t, *J* = 8Hz), ^{13}C NMR (CDCl3, 100 MHz, δ with TMS=0): 165.51, 165.36, 163.42, 159.47, 149.27, 149.12, 131.83, 131.05, 128.60, 119.83, 115.03, 114.42, 112.00, 103.20, 78.43, 78.17, 75.99, 75.66, 64.64, 56.85, 55.87, 30.27, 29.67, 14.86, **HRMS**: for $C_{24}H_{21}N_3O_3$, calculated $[M+H]^+$: 400.1661; observed $[M+H]^+$: 400.1661

4-(3-ethoxy-4-(prop-2-yn-1-yloxy)phenyl)-2-methyl-6-(4-(prop-2-yn-1-yloxy)phenyl)pyrimidine (AVB18):

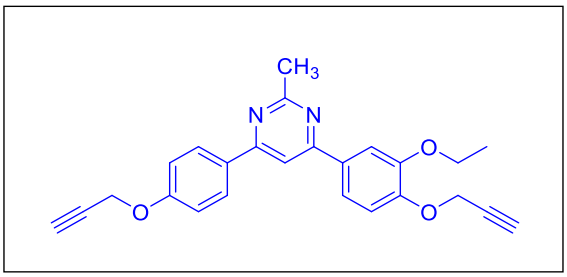

Yield: 60%; greenish yellow solid, mp 108-110 °C; ^{1}H NMR ($CDCl_3$, 400MHz, δ with TMS=0) 8.13 (2H, d, *J* = 8Hz), 7.79(2H, s), 7.67 (1H, d, *J* = 4Hz), 7.17 (1H, d, *J* = 4Hz), 7.13 (2H, d, *J* = 8Hz), 4.87 (2H, d, *J* = 4Hz), 4.80 (2H, d, *J* = 4Hz), 4.28 (2H, q, *J* = 8Hz), 2.85 (3H, s), 2.57 (2H, m), 1.56 (3H, t, *J* = 8Hz), ^{13}C NMR (CDCl3, 100 MHz, δ with TMS=0): 168.33, 164.13, 164.01, 159.59, 149.45, 149.27, 131.68, 130.91, 128.72, 119.94, 115.22, 114.56, 112.09, 108.78, 78.39, 78.14, 76.05, 75.91,

64.71, 56.85, 55.89, 26.50, 14.86, **HRMS**: for $C_{25}H_{23}N_2O_3$, calculated $[M+H]^+$: 399.1709; observed $[M+H]^+$: 399.1709

4-(3-ethoxy-4-(prop-2-yn-1-yloxy)phenyl)-2-phenyl-6-(4-(prop-2-yn-1-yloxy)phenyl)pyrimidine (AVB19):

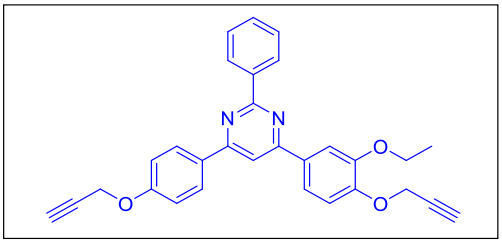

Yield: 67%; greenish yellow solid, mp 138-140 °C; ^{1}H NMR ($CDCl_3$, 400MHz, δ with TMS=0) 8.72 (2H, d, *J* = 8Hz), 8.30 (2H, d, *J* = 8Hz), 7.97 (1H, d, *J* = 4Hz), 7.91 (1H, s), 7.82 (1H, d, *J* = 8Hz), 7.57 (3H, m), 7.21 (1H, d, *J* = 8Hz), 7.19 (2H, d, *J* = 8Hz), 4.90 (2H, d, *J* = 4Hz), 4.83 (2H, d, *J* = 4Hz), 4.32 (2H, q, *J* = 8Hz), 2.58 (2H, dd, J_1 = 8Hz, J_2 = 4Hz), 1.58 (3H, d, *J* = 8Hz), ^{13}C NMR (CDCl3, 100 MHz, δ with TMS=0): 164.06, 159.72, 149.44, 149.41, 138.29, 131.75, 130.94, 130.54, 128.76, 128.42, 128.39, 120.03, 115.18, 114.52, 112.27, 109.02, 78.40, 78.16, 76.07, 75.93, 64.79, 56.86, 55.90, 14.88, **HRMS**: for $C_{30}H_{25}N_2O_3$, calculated $[M+H]^+$: 461.1865; observed $[M+H]^+$: 461.1865

4.4 Biological Studies

All the compounds were evaluated in free bases form for their in vitro biological assays.

4.4.1 Determination of hMAO inhibition activity

The MAO-A and MAO-B inhibitory potential of synthesized compounds was determined using Amplex® Red assay kit through fluorimetric method described by others and us (Kumar *et al.*, 2018; Zhou and Panchuk-Voloshina, 1997).

Briefly, 100 µL of sodium phosphate buffer (0.05 M, pH 7.4) containing the test drug and reference inhibitors, in various concentrations along with adequate amounts of recombinant hMAO (hMAO-A: 1.1 µg protein; specific activity: 150 nmol of p-tyramine oxidized to p-hydroxyphenylacetaldehyde/min/mg protein; hMAO-B: 7.5 µg protein; specific activity: 22 nmol of p-tyramine transformed/min/mg protein) enzyme, were incubated for 15 min at 37 °C in a flat-black-bottom 96-well plates (Tarsons) in an incubator. After the incubation period, the reaction was started by

adding (final concentrations) 200 µM Amplex® Red reagent, 1 U/mL horseradish peroxidase and 1 mM p-tyramine. After 30 min incubation in dark, the production of H_2O_2 was quantified at 37 °C in a multi-detection microplate fluorescence reader (Synergy^{HI}, Bio-Tek® Instruments) based on the fluorescence generated at excitation wavelength of 545 nm, and emission wavelength of 590 nm. Control experiments were carried out simultaneously by replacing the test drug with the vehicle. A direct reaction of test drug with the Amplex® Red reagent in a sodium phosphate buffer was performed to minimize the possibility of the test drugs to influence the fluorescence generated in the reaction mixture due to non-enzymatic inhibition. However, no significant modulation in the fluorescence was observed. The specific final fluorescence emission was calculated after subtraction of the background activity determined from vials containing all the components except the hMAO enzymes replaced by a sodium phosphate buffer solution.

4.4.2 Acetylcholinesterase inhibition assay

Acetylcholinesterase inhibition activity was determined using Amplex Red Acetylcholine/Acetylcholinesterase assay kit (A12217) purchased from the Molecular probes Inc. Invitrogen (Kalb *et al.*, 2013). Briefly, 100 µL of Tris-HCl buffer (0.05 M, pH 8.0) containing the synthesized test drugs and reference inhibitors, in various concentrations along with adequate amounts of recombinant AChE (0.2U/mL) enzyme, were incubated for 15 min at 37 °C in a flat bottom 96-well plates (Tarsons). Reaction was started by adding 100 µL of working solution of 400 µM Amplex Red reagent containing 2 U/mL horseradish peroxidase, 0.2 U/mL choline oxidase and 100 µM acetylcholine. After 30 min incubation in dark, the production of H_2O_2 and subsequent formation of resorufin from Amplex red dye was quantified at 37 °C in a multi-detection microplate fluorescence reader (Synergy^{HI}, Bio-Tek® Instruments) based on the fluorescence generated at excitation wavelength of 545 nm, and emission wavelength of 590 nm. Positive control experiment was carried out simultaneously by replacing the test drugs with the vehicle. Second positive control was carried out by using 20 mM H_2O_2. 1X reaction buffer without acetylcholinesterase was used as negative control. The specific final fluorescence emission was calculated after subtraction of the background activity, determined from wells containing all components except the AChE replaced by a 1X buffer solution. Each experiment was performed in triplicate (n=3).

4.4.3 BuChE inhibition assay

The procedure described by Ellman et al. was used for BuChE inhibition assays with minor modifications (Kumar *et al.*, 2018). BuChE were purchased from Sigma Aldrich (CAS No. 9001-80-5). Butyrylthiocholine iodide (BTCI), 5.5'-dithiobis (2-nitrobenzoic acid) (DTNB - Ellman's reagent) were purchased from Himedia. The assays were performed tris-HCl buffer (pH-8) and donepezil was used as standard compound. Six different concentrations of 20 µM, 10 µM, 1 µM, 0.1 µM, 0.01 µM, 0.001 µM of test compound were used to determine the IC_{50}. 50 µL (0.6 U/mL) and 20 µL of test or standard compounds were incubated in 96 well plates for 30 min. 100 µL (1.5 mM) of DTNB was added in the above solution. The substrate i.e. BTCI (30 mM, 10 µL) was added into it and absorbance was recorded immediately at 415 nm for 20 min at 1 min interval using Biotek plate reader. The IC_{50} values were calculated using absorbance obtained from the test and standard compounds. The assays were performed in triplicate and in three independent runs.

4.4.3 Reversibility inhibition studies

Reversibility inhibition studies of the most potent compounds on MAO-B and AChE were determined using earlier reported protocol by us (Kumar *et al.*, 2018; Minders *et al.*, 2015). Briefly, the test inhibitors were incubated with the MAO enzymes at concentrations of 10 × IC_{50} and 100 × IC_{50} at 37 °C for 30 min (negative control performed in the absence of inhibitor), and 4% DMSO was added as co-solvent to all incubations. After 30 min incubation period, the samples were subsequently diluted to 100–fold with the addition of tyramine substrate to achieve final inhibitor concentrations of 0.1 × IC_{50} and 1 x IC_{50} value, respectively. The residual MAO-B and AChE activities after dilutions were measured (n=3) and the residual enzyme activities were expressed as mean ± SD.

4.4.4 ROS production inhibition studies

Intracellular levels of ROS were determined using protocol described elsewhere (Kaur *et al.*, 2015), using non-fluorescent compound *2´,7´*-dichlorofluorescein diacetate (DCF-DA). It is permeable to cell membrane where it is hydrolyzed by intracellular esterases and further oxidized by ROS to a fluorescent compound 2,7-DCF. SH-SY5Y cells were seeded in 96 well plates ($1x10^4$ cells/ well) and left for 24 h in complete media at 37 °C. Then media was removed, washed with PBS and

cells were treated with the test compounds (without FBS) for 24 h at different concentrations (1 µM, 5 µM and 25 µM). After completion of experiment, cells were rinsed with PBS thrice and then treated with H_2DCF-DA (50 µM) and incubated for 30 min at 37 °C. Following incubation, cells were rinsed with PBS and fluorescence was detected at wavelength of 478 nm excitation and 518 nm emission.

4.4.5 Neuroprotective studies

The neuroprotective potential of compounds was determined against 6-OHDA neurotoxin using MTT assay (Liang *et al.*, 2011). For this SH-SY5Y cells were plated in 96 wells, at 10^6 cells/well density. The cells were cultured for 24h in DMEM/F-12 media containing 10% FBS and horse serum supplemented 1% penicillin antibiotic solution. Then cells were treated with the target compounds (at concentrations of 1-25 µM), 4h before 6-OHDA (12.5 µM). After 24 h incubation in the oven, at 37 °C and a 5% CO_2, 95% O_2 atmosphere, the tested compounds were replaced with 100 µL of MTT in media (0.5 mg/mL, final concentration). The cells were incubated for another 4h. After the removal of MTT, the formazan crystals were dissolved in DMSO. The amount of formazan was measured using a microculture plate reader with a test wavelength of 570 nm. Results were expressed as the mean ± SD of three independent experiments.

4.4.6 Cytotoxicity studies

With an aim to test the cytotoxicity of the synthesized compounds on neuronal cells, MTT assays were carried out with human neuroblastoma SH-SY5Y cells (Kumar *et al.*, 2018). Approximately 10,000 cells were seeded per well of 96 well plate in DMEM/F-12 media containing 10% FBS and horse serum supplemented 1% penicillin antibiotic solution for 24h and treated as indicated in the experimental design. Cells were treated with synthesized compounds at concentration of 1 µM, 5 µM and 25 µM for 24 h in humidified CO_2 incubator, maintained at 37 °C with 5% CO_2 and 95% humidity under serum-free conditions.

4.4.7 Metal-chelating study

Metal chelating studies were performed with a UV−vis spectrophotometer. The absorption spectra of each compound (50 µM, final concentration) alone or in the presence of $CuSO_4$, $FeSO_4$, and $FeCl_3$ (50 µM, final concentration) for 30 min in

20% (v/v) methanol/buffer (20 mM HEPES, 150 mM NaCl, pH = 7.4) were recorded at room temperature (Cai *et al.*, 2017).

4.4.8 Kinetic studies of AChE inhibition

To determine the mechanism of action of the most potent inhibitors of AChE, kinetic study was performed using *ee*AChE with the help of earlier reported protocols (Bolea *et al.*, 2011; Yan *et al.*, 2017). Linewevaer-Burk double reciprocal graph was plotted at different concentrations of substrate ACh (0.1 mM- 1 mM) by using same methodology reported for the *in vitro* inhibition study of AChE. Progress curves were analyzed by steady state turnover of substrate and values of linear regression were fitted according to Lineweaver-Burk replots using Origin software. Different concentrations of inhibitors (1 nM -100 µM) were used for kinetic study. The plots were assessed by weighted least-square analysis that assumed the variance of initial velocity (v) to be constant for whole data set. Slopes of the reciprocal of initial velocity (v) were then plotted against the reciprocal of concentration of substrate to evaluate K_i data.

4.5 Animal studies

Wistar albino young male rats in the age group of 5-6 months were used for all the experiments. The rats were purchased from IIIM, Jammu. All rats were caged in the group of four under controlled conditions with temperature of 25 ± 2˚ C and day/night cycle of 12:12 h with ad libitum access to food and water. Rats were handled strictly according to the guidelines of the Institutional animal ethics committee (IAEC), Guru Nanak Dev University, Amritsar. These rats were acclimated for 5 days prior to any experimental analysis. Rats were divided into two groups: 1) Group I (G1) which was treated with hydrochloric salt of VP15 (10 mg/kg, p.o.) and 2) Group II (G2) which was treated with hydrochloric salt of VP15 (20 mg/kg, p.o.). The rats in each group were intragastrically (i.g.) administered corresponding drug dosage via making solution in water for 4 consecutive days. One hour after the last dose, the rats were sacrificed and dissected for collection of brain tissues.

4.5.1 *In vivo* blood-brain barrier permeability

In vivo blood-brain barrier permeability of VP15 was evaluated via determining levels of VP15 in the brain tissue of wistar rats after oral administration (Bystrowska *et al.*, 2012; Geerts *et al.*, 2005; Li and Bartlett, 2014). The animals were decapitated

and the brain tissues were dissected, and frozen on dry ice. Frozen tissues were weighed, thawed at room temperature and homogenized in mixture of chloroform and methanol (2:1; v/v) in proportion 1 gm tissue per 2 mL of mixture. The samples were shaken for 10 min on an oscillating shaker. The samples were then centrifuged for 10 min at 2,000 × *g* and the lower organic layer was collected. The organic phase was evaporated to dryness and the residues were recollected in 2 mL of methanol and subjected to LCMS (Agilent 1260 Infinity, USA, system equipped with 1260VL infinity quater-nary pumps, autosampler, a thermostat compartment) analysis. For LC Chromolith high resolution RP18e column (100 × 4.6 mm, Merck, Germany) guarded by a Chromolith RP18e (10 × 4.6 mm) was used. The mobile phase consisted of MeCN and 0.1% (v/v) formic acid in water. For MS, triple-quadrupole tandem mass spectrometry (MS/MS) was carried out on an Agilent 6410 tandem triple quadrupole mass spectrometer (TQD-MS) equipped with an ESI ion source operating in both positive and negative ion mode.

Stock solution for reference compound (VP15) was diluted to appropriate concentrations for construction of calibration curves. The stocks and working solutions were stored at +4^{o}C. The average peak area values for each analyte were plotted against corresponding concentrations of the analytes (expressed in ng/mL). Data was obtained using proprietary software from the instrument manufacturer. Peak area and quantitative data were generated by Software Quantitative Analysis (Agilent Technologies, Santa Clara).

4.6 Computational studies

4.6.1 Molecular docking studies

Docking studies can provide some valuable information on ligand's orientation and its interactions at the receptor site. To determine the mode of interaction of the synthesized ligands at the active site of hMAO-A and AChE enzymes, molecular docking studies were performed using Maestro 11.1 (Schrödinger LLC) (Friesner *et al.*, 2006). X-ray crystal structures of different enzymes were imported from the protein data bank (www.rscb.org). Proteins were prepared using "protein preparation wizard" application of Schrödinger suite 2017. Energy was minimized using OPLS2005 force field. Ligands were drawn in ChemBio Draw Ultra-12 and prepared using ligand preparation application in Schrödinger suite 2017. For each

compound, the top-score docking poses were chosen for final ligand-target interaction analysis employing XP interaction visualizer of Maestro 11.1 software. Validation of the docking procedure was done by re-docking the co-crystalized ligand into the active site of the enzymes. Qikprop application of Schrodinger suit was used to determine the drug like and ADME properties of the compounds (Release, 2017).

4.6.2 Molecular dynamics simulation studies

In order to investigate the behavior and stability of the most potent inhibitors (observed from *in vitro* studies) into the active site of the MAO and AChE, molecular dynamic (MD) simulation was utilized. The docking complex of most potent inhibitors with respective enzymes were used. MD simulations were performed using Desmond standard protocol (Release, 2014). Complex was solvated by TIP3P water model and then naturalized by adding 0.15M Na^+ and Cl^- ions. The thickness of water layer was set to 10 Å. Before the MD simulations the systems were minimized with a maximum iteration of 2000 steps. Then, the systems were submitted to 30 ns MD simulation for equilibration and production MD run. Temperature and pressure were assigned on 300 K and 1.01325 bar, respectively using Isothermal–isobaric (NPT) ensemble. Cut-off radios of 9 Å was used for Coulomb interactions.

Chapter- 5
Results and Discussion

‘Single-site-targeting’ drugs have failed to render sufficient neuroprotective and/or neurorestorative activity. AD is reported to originate through multiple pathogenic factors and hence the one-drug-one-target strategy has limited success for its treatment. Multitarget-based drug discovery is the alternative approach in which a single compound can bind to multiple targets so as to manage multiple symptoms. Thus, in the current research work we designed and synthesized multi-targeted ligands by incorporating propargylamine moiety of rasagiline (MAO inhibitor, neuroprotective), benzylpiperidine moiety of donepezil (acetylcholinesrase inhibitor) attached with a heterocyclic moiety.

5.1 Design and selection of heterocyclic scaffold for synthesis

For the designing of target compounds, a library of different heterocyclic moieties containing pharmacophore or its mimicking substituents was generated. Docking was performed at AChE (PDB ID: 1EVE), MAO-A (PDB ID: 2BXR) and MAO-B (PDB ID: 2BYB) to find the most suitable heterocyclic moieties which can simultaneously target these enzymes. For this purpose, the top-score docking poses were chosen for final ligand-target interactions. In addition to above criteria, ADMET studies were performed using qikprop module of Maestro 11.1. This ADMET screening of molecules minimizes the chances of failure of compounds in early pre-clinical studies. From this library top 10 molecules were identified having most favorable drug-like ADMET characteristics along with docking scores (Table 5.1). For drug like characteristics of the designed molecules, Lipinski rule was followed in ADMET selection. QPP Caco model was used to predict the permeability to gut-blood barrier. Orally administered drug must cross this barrier for entering into blood circulation. The acceptable range for QPP Caco was chosen higher than 500 nM/s. More the value of QPP Caco, more is the permeability. QPlogBBB was another model used to predict the blood-brain barrier permeability of the molecules. The range selected for this purpose was from -3.0 to 1.2.

In these studies, 4,6-diphenylpyrimidine was found to be the most suitable core moiety for binding to AChE and MAO simultaneously. Based on the ADMET profile and docking scores, the 4,6-diphenylpyrimidine scaffold was found to show favorable characteristics of drug like molecules and this scaffold was selected for synthesis, biological screening and structure-activity relationship studies.

Table 5.1 Docking score and ADMET profile of designed compounds with different heterocyclic moieties

Structure	Docking score (Kcal/mol)			QPlog P o/w	QPlog HERG	QPP Caco	QPLogBB	Oral absorption (%)
	AChE	MAO-A	MAO-B					
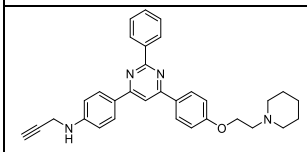	-11.27	-8.59	-10.97	7.1	-9.294	1329	-0.04	100
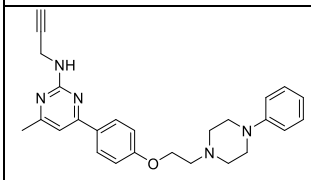	-11.23	-7.96	-9.38	5.4	-8.34	951	-0.06	100
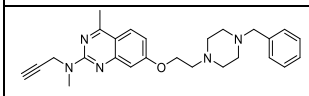	-10.87	-4.39	-9.18	4.6	-8.693	343	0.501	100
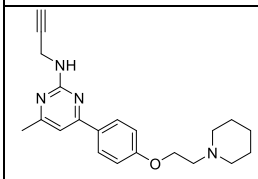	-9.52	-10.5	-12.18	4.38	-7.12	1012	0.02	100
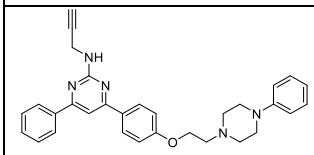	-10.71	-4.9	-8.78	6.82	-9.50	1110	-0.04	100
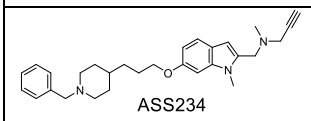 ASS234	-10.77	-5.52	-11.67	6.68	-8.88	550	0.637	100
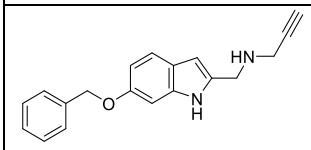	-8.37	-9.85	-9.65	4.19	-7.51	1114	0.161	100
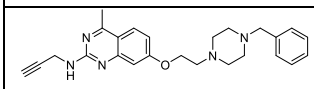	-10.84	-6.01	-8.41	3.93	-8.69	184	0.166	90
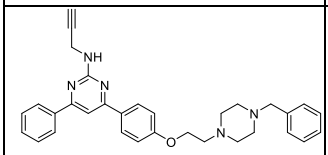	-10.76	-2.73	---	6.2	-10.38	258	0.189	80
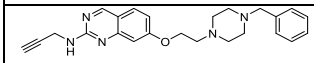	-10.53	-4.72	-9.09	3.82	-8.83	194	0.202	90
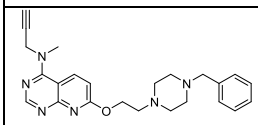	-8.07	-4.36	-5.91	6.21	-10.38	258	0.189	80
Donepezil	-12.03	-5.83	-9.69	4.44	-6.80	867	0.092	100

5.2 Results from compounds based on Series-I

5.2.1 Synthesis of target molecules of Series-I

All the compounds were synthesized as per reaction procedures described in Scheme-I. Briefly, *O*-alkylated acetophenones **(1)** and benzaldehydes **(2)** were synthesized from corresponding hydroxy acetophenones or benzaldehydes by refluxing these with suitable alkyl halides in the presence of potassium carbonate and acetone as solvent. *O*-alkylated acetophenones **(1)** and benzaldehydes **(2)** were reacted through aldol condensation to get the intermediate chalcones (**3)**.

Scheme-I: Reaction scheme for the synthesis of target molecules

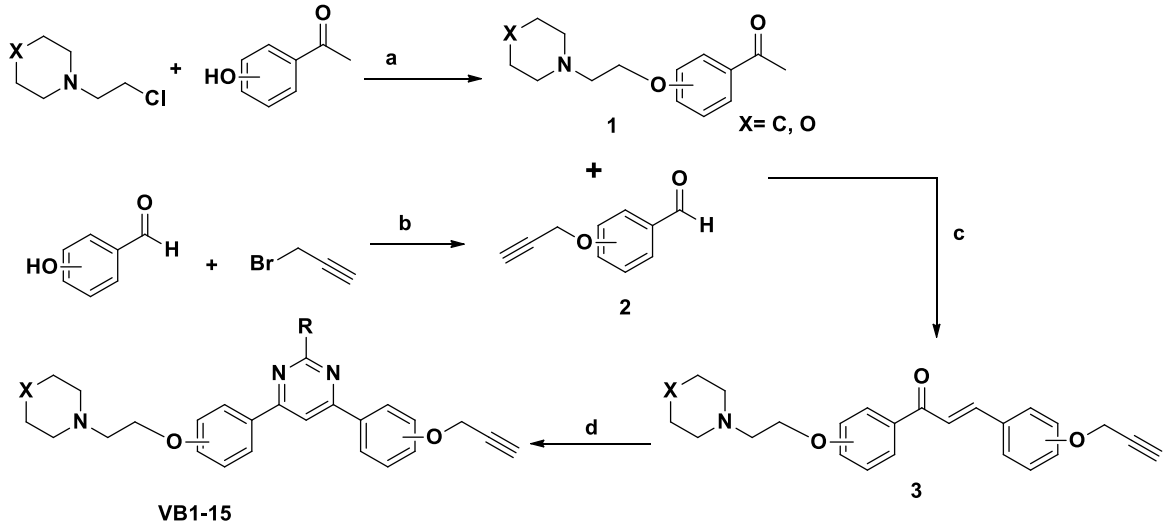

Reagents and Conditions: a) K_2CO_3, KI, acetone, reflux, 6 h; **b)** K_2CO_3, acetone, reflux, 6 h; **c)** CH_3OH, 10% NaOH aq., rt, stirring, 3 h; and **d)** Na_2CO_3, CH_3CN, amidine/guanidine/benzamidine, reflux, 24h

In the final step chalcones (**3)** were reacted with various amidines in the presence of sodium carbonate to obtain the target compounds 4,6-diphenylpyrimidine derivatives **(VB1-VB15).** All the final products were characterized by IR, ^{1}H NMR, ^{13}C NMR, ESI-MS and HRMS.

5.2.2 Biological studies of series-I

5.2.2.1 MAO, AChE and BuChE enzyme inhibition studies

MAO inhibition potential of the 4,6-diphenylpyrimidine derivatives (**VB1-VB15**) was evaluated through fluorimetric method using recombinant human MAO-A and MAO-B enzymes and Amplex® Red assay kit (Chimenti *et al.*, 2010). Similarly, acetylcholinesterase inhibition activity was determined using Amplex Red

Acetylcholine/Acetylcholinesterase assay kit (A12217) purchased from the Molecular probes Inc. Invitrogen. The results of MAO inhibition studies are described in **Table 5.2** in terms of IC_{50} values expressed in nano molar concentrations. Morpholine or piperidine ethyl chains (R_1) were used as meta or para substituents at one of the phenyl rings. To develop structure activity relationship profile of 4,6-diphenylpyrimidines, three amidines were used with R as $-NH_2$, $-CH_3$ or $-C_6H_5$. Similarly, second phenyl ring was substituted with a propargyl group at ortho/meta/para positions. MAO-A, MAO-B and AChE inhibitory activities of some of the intermediate chalcones were also evaluated to compare them with the final products. Clorgyline, pargyline and donepezil were used as standard inhibitors for MAO-A, MAO-B and AChE enzymes, respectively. All the compounds were found selective towards MAO-A isoform with IC_{50} values varying from 18 nM to 2430 nM. MAO-B inhibition activities of these compounds were found in the range of 7313 nM to 14850 nM. These compounds were also found to be the potent inhibitors of AChE with IC_{50} values in nano molar range. However, most of the compounds displayed BuChE inhibitory activity in the micro molar range (0.66 µM to 161.6 µM**)**. **VB1** was found to be the most potent MAO-A inhibitor with IC_{50} value of 18.34 ± 0.38 nM and selectivity index (SI) of 540 over MAO-B. **VB1** was also found to be the most potent BuChE inhibitor in the series with IC_{50} value of 0.666 ± 0.03 µM**.** Similarly, **VB8** was found to be the most potent AChE inhibitor with IC_{50} value of 9.54 ± 0.07 nM. **VB3** was also found potent inhibitor of both AChE and MAO-A with IC_{50} values of 18.92 ± 0.29 nM and 28.33 ± 3.22 nM, respectively. All the chalcone intermediates were found less active as compared to the corresponding final products.

Table 5.2 Results of the MAO, AChE and BuChE inhibition studies of synthesized compounds

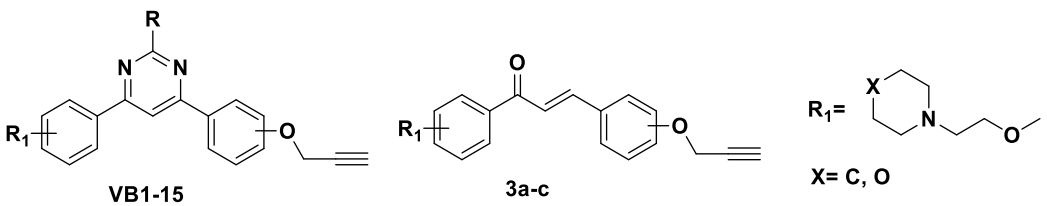

Entry Name	R_1	R	Propargyl group position	X	IC_{50} values (mean ± S.E. nM)			IC_{50} values (mean±S.E. µM)	MAO SI
					hMAO-A	hMAO-B	*ee*AChE	*eq*BuChE	
VB1	C4	NH_2	C4	O	18.34 ± 0.38	9910.14 ± 32.83	30.46 ± 0.23	0.666 ± 0.03	540
VB2	C4	C_6H_5	C4	O	86.35 ± 0.42	6915.62 ± 26.72	39.83 ± 0.39	14.84 ± 0.27	80
VB3	C4	CH_3	C4	O	28.33 ± 3.22	8409.53 ± 25.69	18.92 ± 0.29	14.98 ± 0.31	297
VB4	C4	C_6H_5	C4	C	103.42 ± 11.43	8376.28 ± 23.73	24.69 ± 0.76	19.72 ± 0.27	81
VB5	C4	CH_3	C4	C	752.63 ± 14.34	12140.12 ± 100.64	765.14 ± 3.51	54.46 ± 1.42	16
VB6	C4	C_6H_5	C3	O	2140.12± 50.43	14850.34 ± 80.62	1841.56 ± 27.67	8.216 ± 0.10	7
VB7	C4	NH_2	C3	O	230.12 ± 7.22	7313.76 ± 65.32	20.45. ± 0.17	16.65 ± 0.17	32
VB8	C4	CH_3	C3	O	1010 ± 70.42	12185.94 ± 190.86	9.54 ± 0.07	13.75 ± 0.23	12
VB9	C4	NH_2	C2	O	890.45 ± 8.32	8875.37 ± 110.52	2390.23 ± 20.72	161.6 ± 5.88	10
VB10	C4	C_6H_5	C2	O	690.34 ± 20.32	12305.63 ± 87.72	30105.12±70.14	22.68 ± 0.36	18
VB11	C3	C_6H_5	C4	O	2430.23 ± 45.33	8974.73 ± 93.73	2269.82 ± 32.01	14.66 ± 0.20	4
VB12	C3	NH_2	C4	O	360.33 ± 2.34	8738.97 ± 51.73	1438.54 ± 27.67	23.48 ± 0.18	24
VB13	C3	CH_3	C4	O	450.44 ± 5.13	8469.63 ± 83.72	717.88 ± 7.54	15.27 ± 0.11	19
VB14	C4	C_6H_5	C3	C	1320.22 ± 30.22	9565.83 ± 120.53	2093.71 ± 15.69	15.95 ± 0.12	7
VB15	C4	NH_2	C3	C	1040.12 ± 40.12	7706.23 ± 95.73	1441.42 ± 20.33	34.79 ± 0.27	7
3a	C4	----	C4	O	260.12 ± 13.12	9320.12 ± 24.22	20427.18±22.15	**----**	36
3b	C4	----	C2	O	313.23 ± 17.22	8110.11 ± 40.11	**	**----**	26
3c	C3	----	C4	O	532.42 ± 19.23	7809.02 ± 35.13	**	**----**	15
Clorgyline					4.39 **±** 1.02	**-----**	**----**	**----**	**----**
Pargyline					**----**	0.15 ± 0.02	**----**	**----**	**----**
Donepezil					**----**	**----**	11.32 ± 0.001	1.28 ± 0.04	----

**Inactive or showed less than 50% inhibitory activity at 50 µM concentration and precipitated at higher concentrations. IC_{50} values of BuChE are expressed in µM. MAO SI= IC_{50} of MAO-B / IC_{50} of MAO-A.

5.2.2.2 Reversibility inhibition studies

First generation MAO inhibitors were irreversible in nature and associated with severe side effects. Reversibility of the target compound is frequently considered in designing and development of new class of inhibitors. Thus, to determine the reversible inhibition of the enzyme by the most active and selective compounds i.e.

VB1, VB3 and **VB8**, reversibility inhibition studies were performed using earlier reported protocol by us and others (Kumar *et al.*, 2018; Minders *et al.*, 2015; Mostert *et al.*, 2012). All the tested compounds were found reversible inhibitors of both MAO-A and AChE enzymes. Upon treatment of MAO-A and AChE with the test compounds at concentrations of 10 x IC_{50} and 100 x IC_{50} activity was reduced to minimum. Upon 100 times dilution with the substrate solution, recovery of more than 75% enzymatic activity was achieved as shown in Fig. 5.1A and Fig. 5.1B for MAO-A and AChE respectively. Thus, it can be concluded that the tested compounds were found to be reversible inhibitors of MAO-A and AChE.

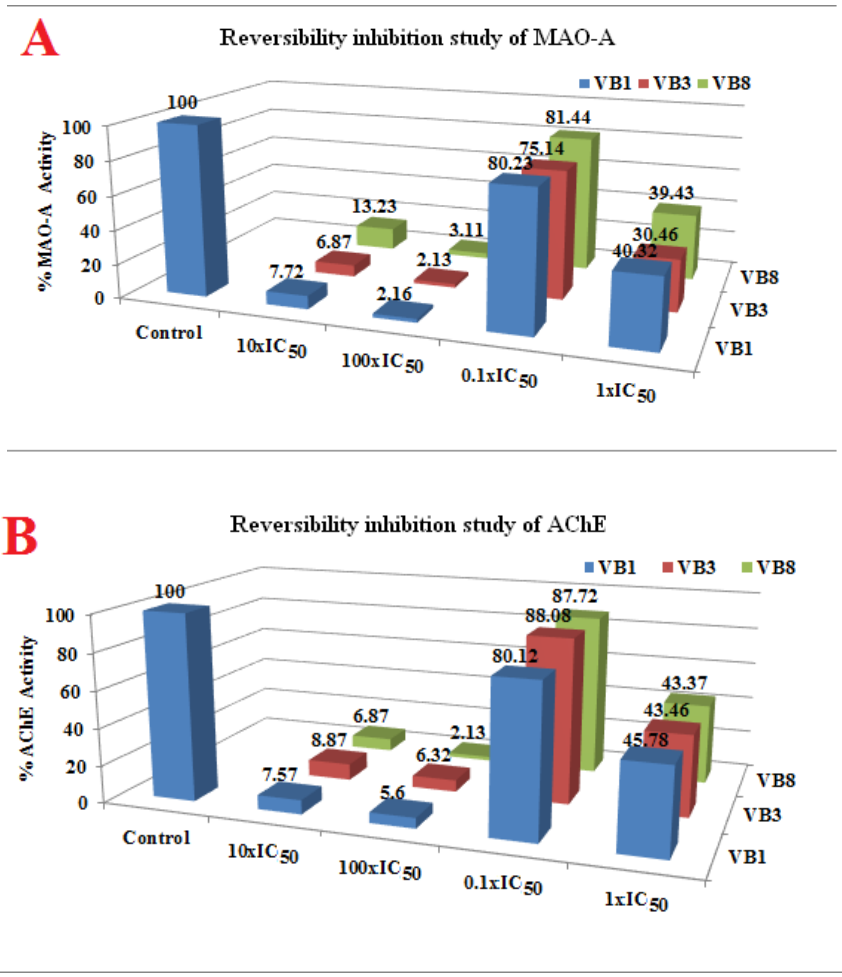

Fig. 5.1 (A) Reversibility inhibition studies of the most potent and selective inhibitors with MAO-A enzyme; (B) Reversibility inhibition studies with AChE enzyme.

5.2.2.3 Intracellular ROS determination

It is a well-known fact that monoamine oxidase mediated oxidative metabolism of mono amines lead to the production of H_2O_2 as a byproduct (Pizzinat *et al.*, 1999;

Sturza *et al.*, 2014). Subsequently, H_2O_2 get converted to the free radicals (ȮH, $\dot{O}_2$) through Fenton's reaction which contribute to the oxidative stress. Uncontrolled increase in the concentrations of the free radicals, initiate free radical-mediated chain reactions that causes oxidative damage to the cell membranes, lipid peroxidation and DNA strand breakdown. Thus, prevention of ROS generation along with the MAO inhibition is important strategy to reduce or eliminate neurotoxicity in neurodegenerative disorders.

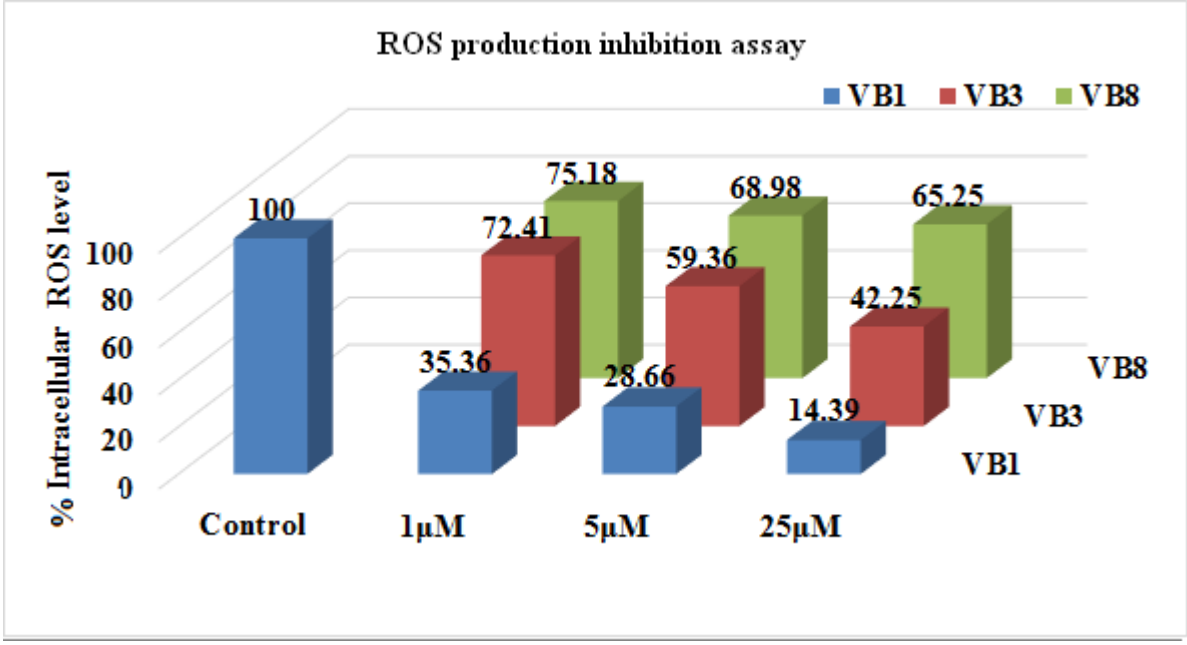

Fig. 5.2 ROS production inhibition studies of VB1, VB2 and VB3 against SH-SY5Y cells

Intracellular ROS level of SH-SY5Y cells was determined using non-fluorescent compound 2',7'-dichlorofluorescein diacetate (DCF-DA). It is permeable and oxidized by ROS to a fluorescent compound 2,7-DCF. **VB1** was found to be the most potent ROS inhibitor and reduced the intracellular ROS level to 35.36% and 14.39% at 1 µM and 25 µM concentration respectively (Fig. 5.2). **VB3** and **VB8** also reduced the ROS levels to 42.25% and 65.25% respectively at 25 µM concentrations.

5.2.2.4 Neuroprotective studies

The most potent compounds (**VB1**, **VB3** and **VB8**) were evaluated for their neuroprotective potential against 6-hydroxydopamine (6-OHD) neurotoxin in the SH-SY5Y neuroblastoma cells. But none of the tested compounds showed

promising neuroprotective potential at low concentrations (Fig. 5.3). **VB8** was found to be the most potent amongst the tested compounds and displayed recovery of cells up to 61.77% at 25 µM concentration as compared to the 6-OHD which reduced the cell viability to less than 50% at 12.5 µM.

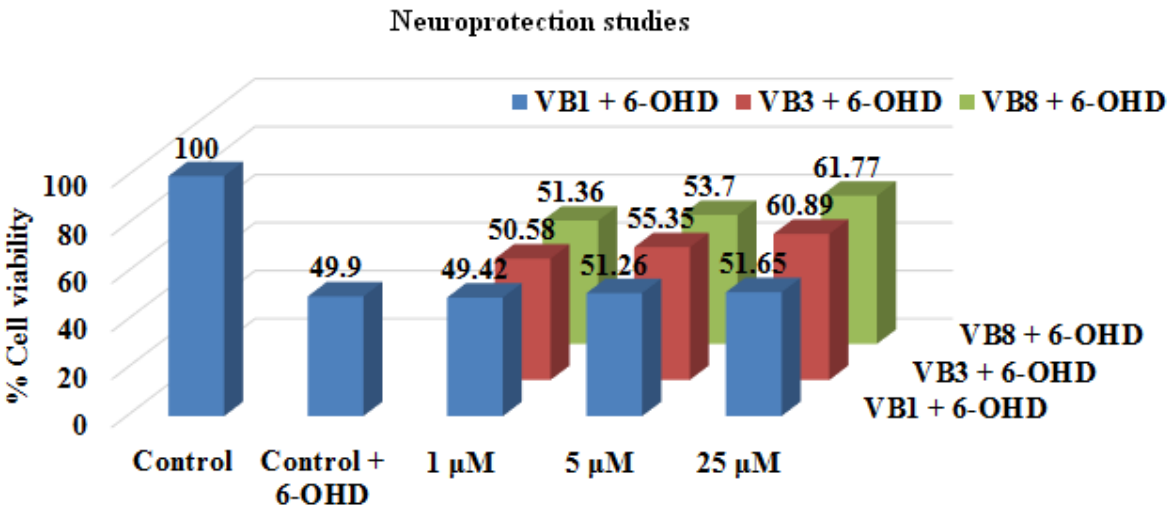

Fig. 5.3 Neuroprotective studies of the most potent and selective MAO-A and AChE inhibitors

5.2.2.5 Cytotoxicity studies

The cytotoxic effects of the most active compounds (**VB1, VB3 and VB8**) were evaluated against human neuroblastoma (SH-SY5Y) cells because of their similarity to the dopaminergic neurons (Xie *et al.*, 2010). The test compounds were incubated at 1 µM, 5 µM and 25 µM concentrations and were analyzed after 24h treatment time. The percentage cell viability was measured using MTT assay. As depicted in Fig. 5.4, the compounds were found non-toxic against the tested cells even at 25 µM concentrations. It has been observed that as concentration of the compounds increases, the percentage cell viability also increases. Least cell viability of 80% was observed with **VB8** at 1 µM concentration. Thus, keeping in view the nano molar IC_{50} values obtained for enzyme inhibition, the current series of compounds were found to be non-toxic to the tissue cells.

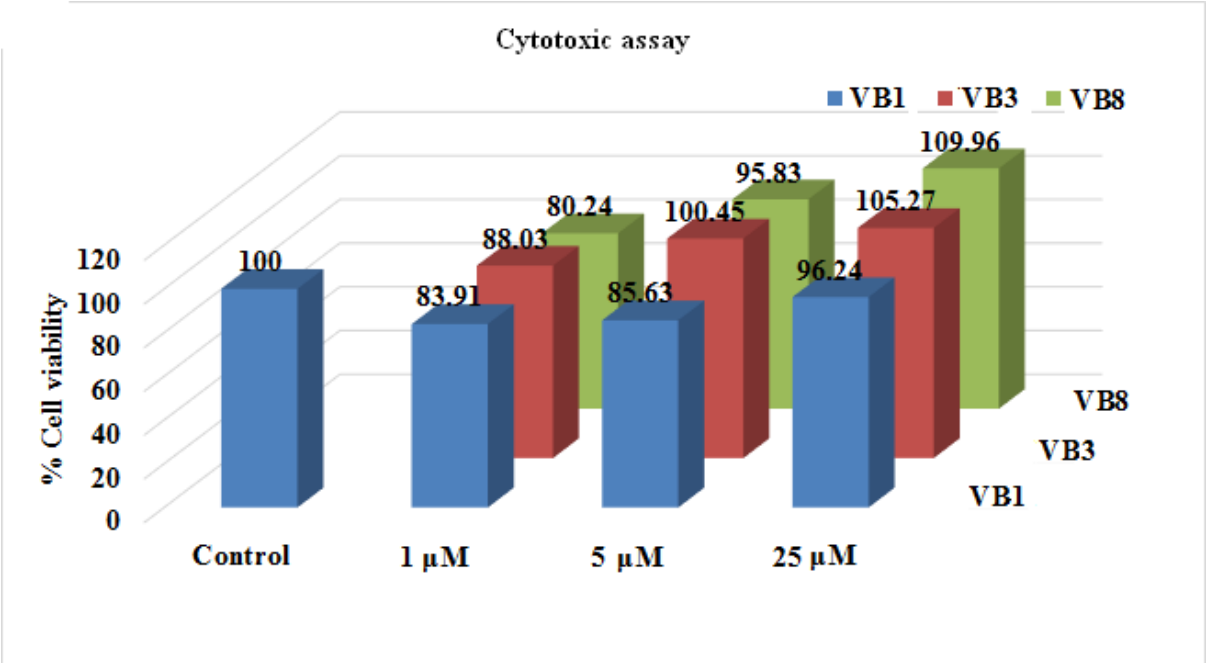

Fig. 5.4 Cytotoxicity studies of **VB1**, **VB3** and **VB8** against SH-SY5Y cells at 1 µM, 5 µM and 25 µM.

5.2.2.6 Metal chelating studies

Metal chelating studies of the most potent compounds i.e. **VB1, VB3** and **VB8** were performed with UV−vis spectrophotometer. The absorption spectra of each compound (50 µM, final concentration) alone or in the presence of $CuSO_4$, $FeSO_4$, and $FeCl_3$ (50 µM, final concentration) was recorded. In metal chelating studies, compounds were found ineffective against metals and does not form any chelates with the metal salts.

5.2.2.7 Kinetic studies of AChE inhibition

To determine the mechanism of inhibition of AChE, kinetic study was carried out with the most potent inhibitor of AChE i.e. **VB8** using eeAChE. The reciprocal Lineweaver-Burk plots (Fig. 5.5) illustrate increased slope (decreased V_{max}) and higher intercepts (K_m) with the increasing concentration of **VB8.** The intersection point of the Lineweaver-Burk reciprocal plots was located in the second quadrant, which indicate that the inhibition mode of **VB8** was mixed-type inhibition. Thus, it can be concluded that **VB8** binds to both CAS and PAS of AChE simultaneously.

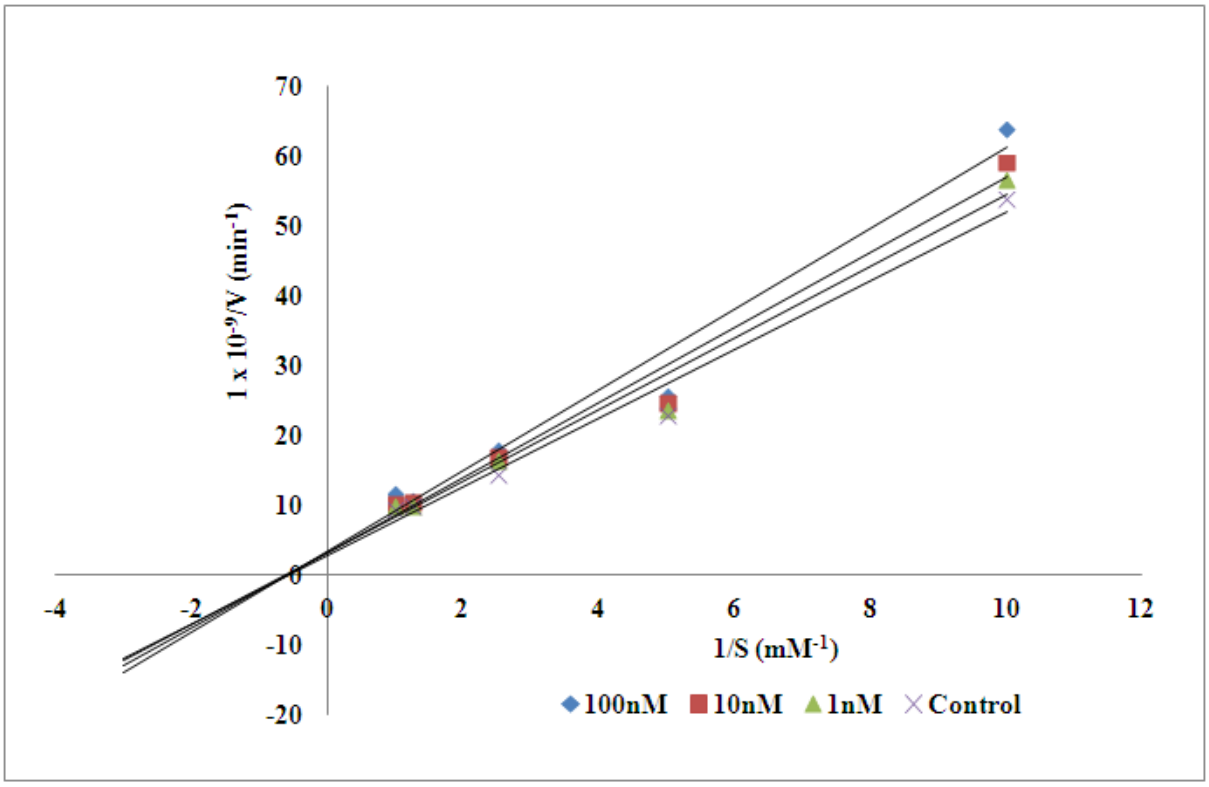

Fig. 5.5 Kinetic study for the mechanism of *ee*AChE inhibition by **VB8**. Overlaid Lineweaver−Burk reciprocal plots of AChE initial velocity at increasing substrate concentration (0.1−1 mM) in the absence or presence of **VB8** are shown.

5.2.3 Computational studies

5.2.3.1 Molecular docking studies

The most potent compounds (**VB1, VB3** and **VB8**) were subjected to molecular docking studies to find the interaction pattern of the molecules with the amino acid lining and their orientation at the active site of the receptors. Compounds were docked at the active site of hMAO-A (PDB ID- 2BXR and 2Z5X) (De Colibus *et al.*, 2005; Son *et al.*, 2008) and AChE (PDB ID- 1EVE) (Cheung *et al.*, 2012). The X-ray crystal structures were imported from the protein data bank using Maestro 11.1 (Schrödinger LLC). The docking procedure employed was first validated by redocking the co-crystallized ligands into the MAO and AChE models and the process was found suitable for the current study. Three most potent compounds (**VB1, VB3** and **VB8**) were docked at the structure of MAO-A (2BXR and 2Z5X) enzymes co-crystallized with clorgyline and harmine.

All the compounds were found to accommodate nicely to the active site of MAO-A delineated by hydrophobic residues Tyr69, Phe208, Arg296, Ile335, Leu337, Phe352, Tyr407, Trp441,

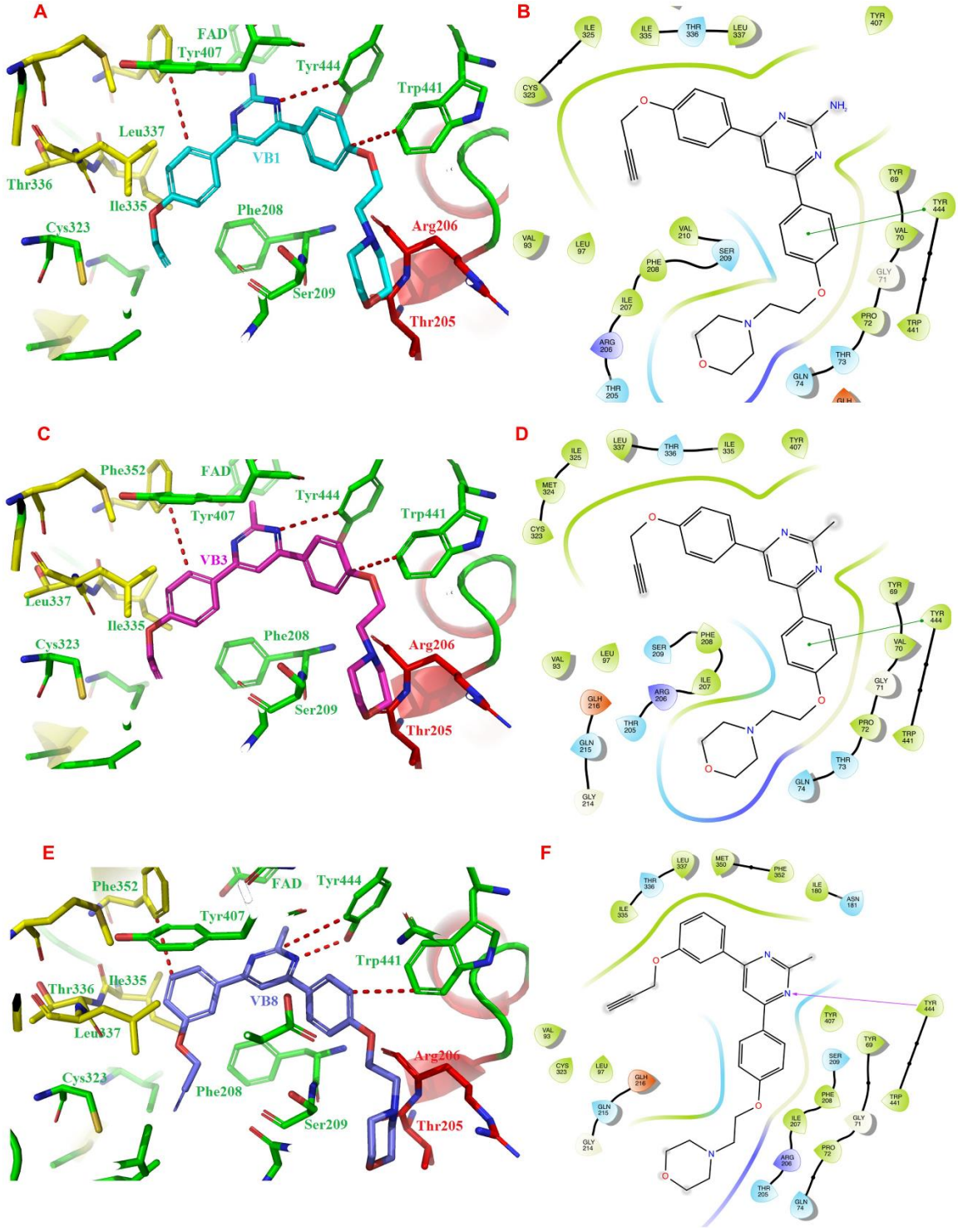

Fig. 5.6 A) Binding pattern (3D) of **VB1** with the amino acid residues at the active site of MAO-A (2BXR) and B) Binding interactions (2D) of **VB1** with various amino acids of MAO-A active cavity, C) Binding pattern (3D) of **VB3** with the amino acid residues at the active site of MAO-A (2BXR), D) Binding interactions (2D) of **VB3** with various amino acids of MAO-A active cavity, E) Binding pattern (3D) of **VB8** with the amino acid residues at the active site of MAO-A (2BXR), and F) Binding interactions (2D) of **VB8** with various amino acids of MAO-A active cavity

Tyr444 and FAD. Most of the interactions observed were hydrophobic and π-π aromatic stacking which showed hydrophobic nature of the MAO-A active site. Pyrimidine moiety was aligned towards the FAD co-factor while 4-(2-phenoxyethyl)morpholine fragment was exposed to the outer part of the active site cavity lined by the polar amino acid residues Thr205 and Arg206. The (prop-2-yn-1-yloxy)benzene fragment of **VB1** showed π-π aromatic interaction with Phe352 while pyrimidine ring showed π-π aromatic interaction with Tyr444. 4-(2-phenoxyethyl)morpholine showed π-π aromatic interaction with Trp441. **VB3** and **VB8** also showed interactions with the same set of amino acids at the active cavity of the enzyme (Fig. 5.6). The only difference observed in the conformation of **VB8** was the orientation of propargyl group. In case of **VB1** and **VB3** propargyl group was oriented towards rest of the molecule to the inner side of the cavity while in **VB8**, it was directed away from the rest of the molecule towards outer side of the cavity (Fig. 5.6). This difference in the conformation of **VB8** might be responsible for its lower activity towards MAO-A (Fig. 5.6). Propargylamino group of clorgyline is reported to interact with FAD co-factor and form strong covalent bond. These strong interactions might be responsible for the irreversible nature of clorgyline. As evident from Fig. 5.6, in **VB1**, **VB3** and **VB8** pyrimidine ring is aligned close to the FAD while propargyl group is oriented away from the FAD co-factor. These conformations of the ligands at the active site negate any possibility of covalent bond formation between the propargyl group and FAD. Thus, these ligands may not form strong covalent bond with the enzyme and hence display reversible inhibition activity. Son *et al.* reported a very high-resolution structure of human MAO-A co-crystallized with a reversible MAO-A inhibitor harmine which was different from the structure reported by Colibus *et al*. We have also performed docking studies of reversible MAO-A inhibitor VB1 with PDB-2Z5X (Fig. 5.7). In this case, it also has been observed that pyrimidine ring was aligned towards the FAD co-factor and the propargyl group was directed towards outer part of the cavity aligned with amino acid resides Val484 and Thr487 (Fig. 5.7). These observations further strengthen our claim that the propargyl group may not be able to form strong covalent bond with the FAD and hence current series of compounds behave as reversible inhibitors.

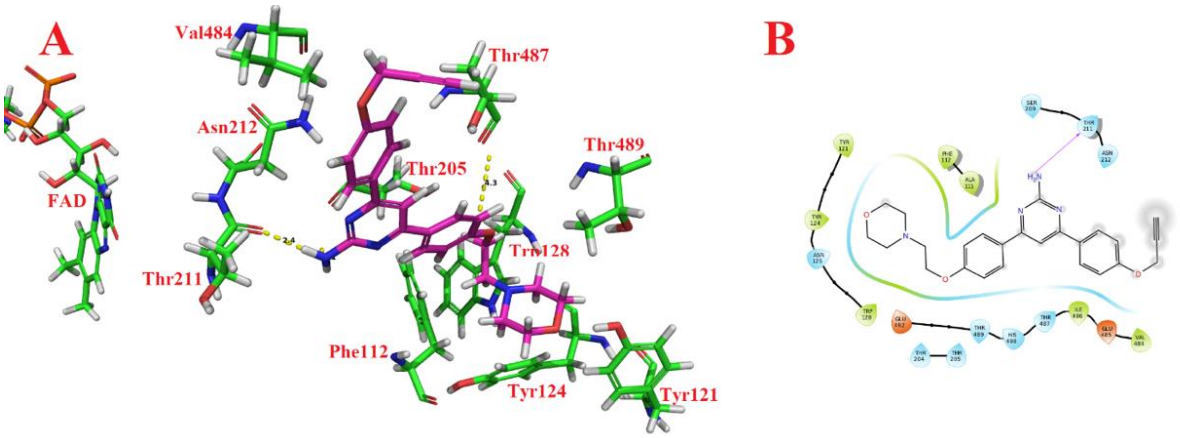

Fig. 5.7 A) Binding pattern (3D) of VB1 with the amino acid residues at the active site of MAO-A (2Z5X), and B) Binding interactions (2D) of VB1 with various amino acids of MAO-A active cavity.

Similarly, the most potent compounds (**VB1, VB3** and **VB8**) were docked in the crystal structure of AChE (1EVE) enzyme co-crystallized with donepezil (Fig. 5.8). All the compounds were accommodating nicely to the active site as well as the peripheral anionic site (PAS) of AChE as done by the standard inhibitor donepezil. The AChE anionic site, composed of Trp84, Tyr130, Phe330 and Phe331 residues while peripheral anionic site (PAS) consists of five amino acids-Tyr70, Asp72, Tyr121, Trp279 and Tyr334. The increased chain length between the phenyl and morpholine ring, as compared to the N-benzylpiperidine moiety of donepezil, pushed the 4-(2-phenoxyethyl)morpholine fragment of **VB1** and **VB3** inside the CAS of AChE. The morpholine moiety was aligned towards the narrowest part of the active site cavity. However, for **VB8,** the binding alignment was inverted and 4-(2-phenoxyethyl)morpholine fragment was aligned towards the 2,3-dihydroinden-1-one fragment of the donepezil (Fig. 5.9). Thus the (prop-2-yn-1-yloxy)benzene fragment of **VB8** was oriented towards CAS of AChE.

Comparison of the binding patterns (predicted) of donepezil and **VB8** reveals the plausible reason of its high potency for AChE. Donepezil showed π−π aromatic interactions of N-benzylpiperidine fragment with Trp84 residue and cation−π interactions with Phe331 and Tyr334 residues. The 2,3-dihydroinden-1-one fragment of the donepezil showed π−π stacking with Trp279.

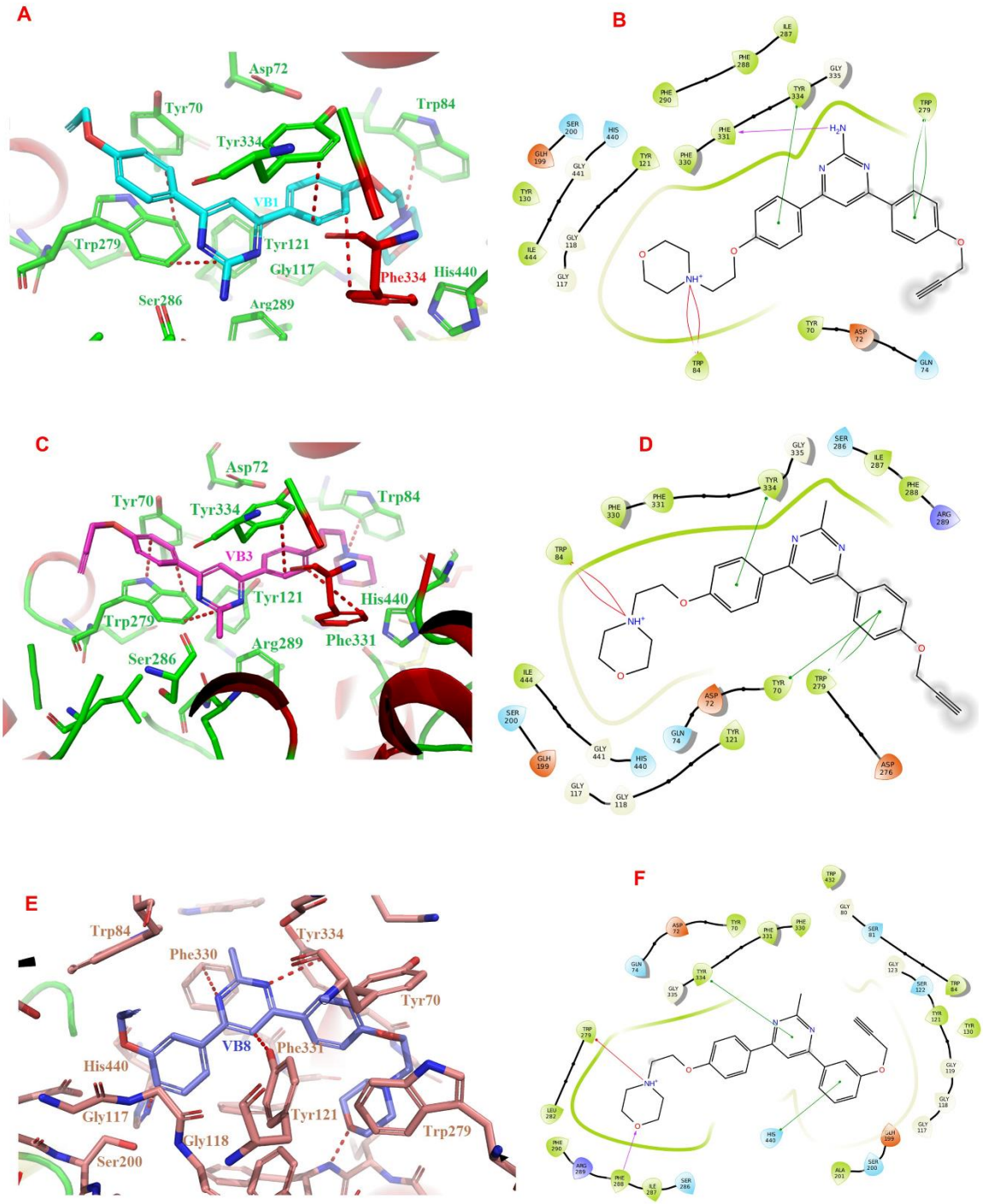

Fig. 5.8 A) Binding pattern (3D) of **VB1** with the amino acid residues at the active site of AChE (1EVE), B) Binding interactions (2D) of **VB1** with various amino acids of AChE active cavity, and C) A) Binding pattern (3D) of **VB3** with the amino acid residues at the active site of AChE (1EVE), D) Binding interactions (2D) of **VB3** with various amino acids of AChE active cavity, E) Binding pattern (3D) of **VB8** with the amino acid residues at the active site of AChE (1EVE), and F) Binding interactions (2D) of **VB8** with various amino acids of AChE active cavity

VB1 and **VB3** preserved most of the interactions of the donepezil with the same set of amino acid residues. These compounds showed cation−π interactions with Trp84 and π−π stacking with Trp279, Phe331 and Tyr334 residues. Similarly**,** pyrimidine fragment of **VB8** showed π−π aromatic stacking with Phe331 and Tyr334. However, 4-(2-phenoxyethyl)morpholine fragment was aligned in the opposite direction as compared to the benzylpiperidine moiety of donepezil and displayed cation−π interactions with the Trp279 residue and hydrogen bonding interactions with the Phe288 residue through oxygen atom of the morpholine ring (Fig. 5.8). Furthermore, the (prop-2-yn-1-yloxy)benzene fragment of **VB8** showed additional aromatic π−π stacking with His440 residue, not observed for **VB1**, **VB3** and donepezil.

Compounds **VB1**, **VB3** and **VB8** were superimposed with donepezil at the active site of AChE (Fig. 5.9). The (prop-2-yn-1-yloxy)benzene fragments of **VB1** and **VB3** were oriented towards 2,3-dihydroinden-1-one fragment of the donepezil in PAS of AChE while 4-(2-phenoxyethyl)morpholine fragment overlap with the N-benzylpiperidine moiety of donepezil and oriented towards CAS. Pyrimidine rings of **VB1** and **VB3** showed good overlap with the dihydroindenone part of donepezil. Surprisingly, **VB8** showed reverse orientation and its (prop-2-yn-1-yloxy)benzene fragment overlapped with the benzylpiperidine moiety of the donepezil aligned towards CAS of AChE. The 4-(2-phenoxyethyl)morpholine moiety of **VB8** oriented towards 2,3-dihydroinden-1-one fragment of donepezil and accommodate in the PAS of AChE. The pyrimidine ring of **VB8** overlapped with the piperidine ring of donepezil while (prop-2-yn-1-yloxy)benzene fragment overlapped with the benzylic ring. Thus, altered orientation and additional interactions at the active site might be responsible for the high potency of **VB8** towards AChE enzyme.

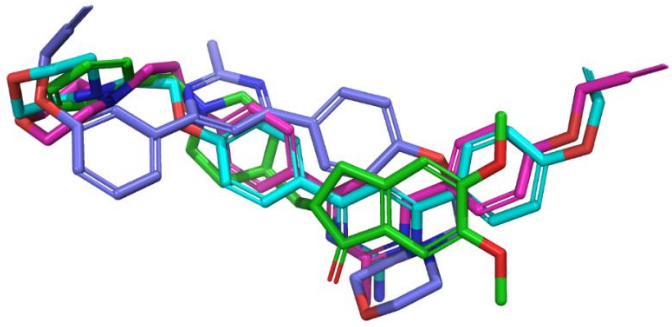

Fig. 5.9 Superimposed poses of **VB1** (cyan), **VB3** (pink) and **VB8** (violet) with donepezil (green) at the active site of AChE (1EVE).

5.2.3.2 Molecular dynamics simulation studies

Molecular dynamics (MD) simulations were performed to study the protein–ligand interactions and to determine the thermodynamic stability of the docked compounds at the active pocket of the enzymes. The protein–ligand docked complexes of the most active compounds **VB1** with MAO-A and **VB8** with AChE were used for MD simulations. The MD simulation studies were conducted for 30 ns and the interaction pattern of the test compound with different amino acids was analyzed. MD simulations yielded stable trajectories for **VB1** with MAO-A in the first 20 ns, as noted by the time evolution of the potential energy and the root-mean-square deviation (RMSD) of the protein backbone, which ranged from 0.6 to 1.0 Å (Fig. 5.10). There were no major structural alterations and the pyrimidine moiety adopted similar orientation in the active site of MAO-A (Fig. 5.10) as obtained during the docking studies. In particular, the 4-(2-phenoxyethyl)morpholine fragment of **VB1** was stacked against Tyr444 and Arg206. After the time interval of 22 ns, there was a sudden hike in the RMSD and thereafter it showed stable trajectory up to 30 ns. RMSD oscillates in the range of 2 Å to 3 Å in this time interval. In the MD simulations studies, it has been observed that **VB1** preserved most of the interactions observed during the docking studies. In addition, some new interactions with various amino acid residues were also observed (Fig. 5.10). In the MD simulations, π-π aromatic interaction with Tyr444 was retained. The NH_2 group present on the pyrimidine fragment move more towards Tyr407 and formed a hydrogen bond with it. The nitrogen atom of the morpholine ring formed hydrogen bonds with Pro72 and Arg206 through water bridge formation. It demonstrates the structural integrity of the MAO-A-VB1 complex, and displayed similar binding features as done by clorgyline.

The MD simulations of AChE-VB8 complex was performed to determine the binding stability of **VB8** at CAS and PAS of AChE. The complex yielded stable trajectories from 2 ns to 30 ns, as noted by the time evolution of the potential energy and the root-mean-square deviation (RMSD) of the protein backbone. The RMSD values for AChE-VB8 complex ranged from 1.6 to 2.0 Å (Fig. 5.11). For the initial 2s, the RMSD value increase from 0.8 to 1.6 and thereafter it remained stable up to 30 ns.

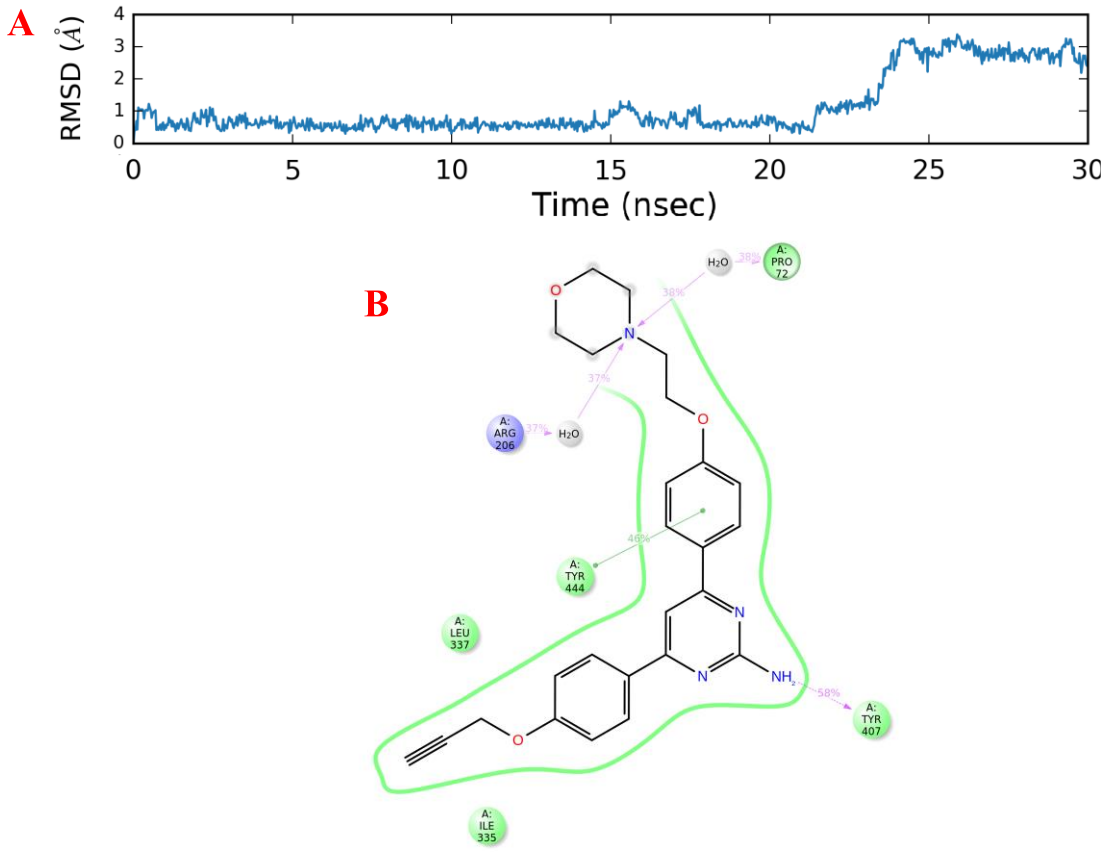

Fig. 5.10 A) RMSD graph of MD studies of **VB1** with MAO-A for 30 ns, and **B**) interactions of **VB1** with the active site residues of MAO-A after 30 ns MD simulation studies

Analyzing the MD trajectory of AChE-VB8 complex, it can be concluded that **VB8** showed strong tendency to be localized in the binding region of AChE. Nitrogen atom of the pyrimidine ring form hydrogen-bond with Tyr121. In the PAS of AChE, the protonated nitrogen atom of morpholine moiety maintained the initial cation−π interaction (from comparison of Fig. 5.8 and Fig. 5.11) throughout the MD simulations interval, indicating stable binding of **VB8** with AChE. In addition, morpholine ring formed hydrogen bonding with the Glu278 residue through water bridge formation. The (prop-2-yn-1-yloxy)benzene fragment aligned towards CAS of AChE and showed aromatic π-π interaction of **VB8** with Tyr330 and Trp84. The MD simulations of **VB8** does not indicate any abrupt local force that could potentially break up the inhibitor or can even delocalize it from the binding site of AChE. Thus, from the MD simulations studies of AChE-VB8 complex, it can be concluded that

the complex is stable and this stability might be responsible for the high *in vitro* potency of **VB8** for AChE.

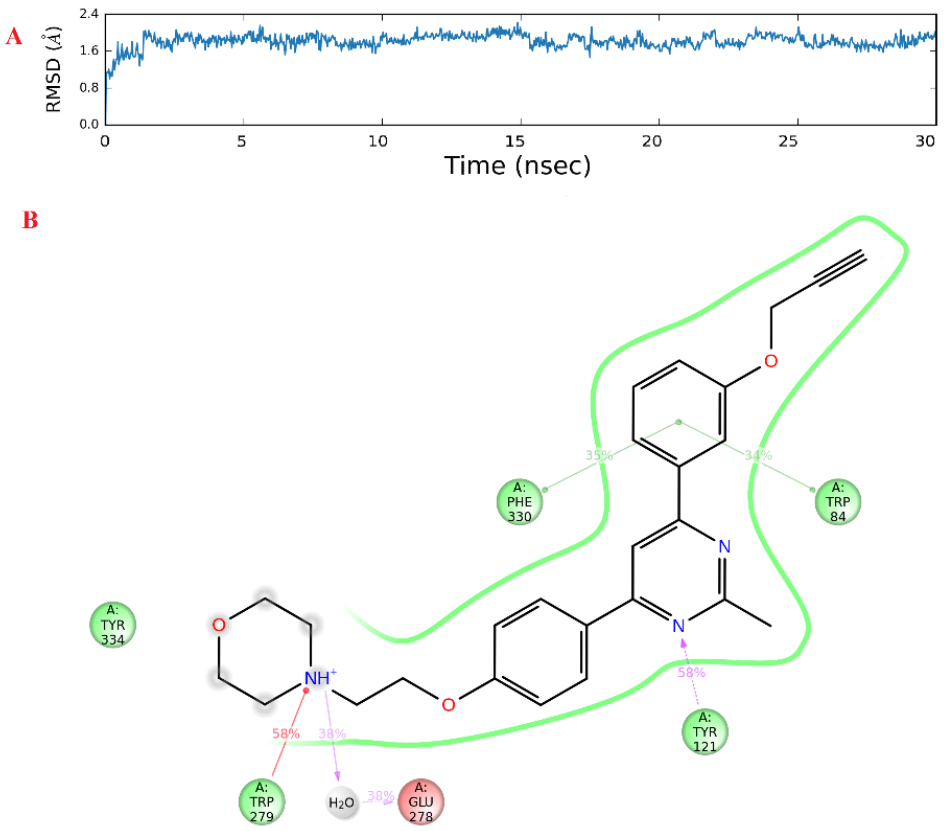

Fig. 5.11 A) RMSD graph of MD simulations studies of **VB8** with AChE for 30 ns, and **B**) interactions of **VB8** with the active site residues of AChE during 30 ns MD simulation studies

5.2.3.3 ADME properties

To determine the drug like characteristics of the synthesized compounds, ADME parameters of these compounds were determined using Qikprop application of Schrodinger. **VB1** displayed very good drug-like profile with LogP value less than 5 and QPlogBB value as -0.65. In addition, **VB1** showed optimum oral absorption and blood-brain barrier permeability. **VB3** and **VB8** also showed 100 % oral absorption and QPlogBB in the optimum range to cross the blood brain barrier.

Table 5.3: Physiochemical properties of the most potent MAO-A selective and AChE inhibitors

Name	Mol. Wt.	Log P	HB donor	HB acceptor	% human oral absorption	QPlogBB (Optimum range -3.0 – 1.2)	BBB permeability predicted
VB1	430.505	3.94	3	8	96	-0.65	+ve
VB3	429.518	5.06	1	7	100	0.22	+ve
VB8	429.518	5.09	1	7	100	0.28	+ve

+ve = high blood-brain barrier permeability, HB = Hydrogen bond, QPlogBB = qualitatively predicted logarithmic ratio between the concentration of a compound in the brain and blood, LogP = partition coefficient of a molecule between an aqueous and lipophilic phase (octanol and water)

5.2.4 SAR studies of series-I

In the series-I, three different amidines have been used with R as $-NH_2$, $-CH_3$ or $-C_6H_5$ (Table 5.2). One of the rings of diphenylpyrimidines is optionally substituted with the morpholine or piperidine ethyl chain while other phenyl ring is functionalized with a propargyl group at ortho, meta or para positions. The effect of different substituents on the activity is analyzed as reported in the Table 5.2. The compounds were evaluated for MAO-A, MAO-B, *ee*AChE and eqBuChE inhibitory activities using enzymatic assays. All the compounds were found selective for MAO-A isoform with IC_{50} values in nano molar range and with moderate to very high selectivity index. It has been observed that the compounds with morpholine ethyl chain and propargyl group at para positions of both the phenyl rings showed high potency for MAO-A isoform and *ee*AChE. **VB1** with R as $-NH_2$ was found to be the most potent MAO-A inhibitor with IC_{50} value of 18.34 nM and it also showed potent *ee*AChE inhibitory activity with IC_{50} value of 30.46 nM. **VB1** was also found to be the most potent BuChE inhibitor in the series with IC_{50} value of 0.666 ± 0.03 µM. **VB3** with R as $-CH_3$ also showed strong inhibition potential against MAO-A and *ee*AChE with IC_{50} values of 28.33 nM and 18.92 nM respectively. Replacement of $-NH_2$ with C_6H_5 in **VB2** reduces MAO-A activity by 5-folds. Shifting of propargyl group from para position to meta position (**VB7**) reduces MAO-A inhibitory activity by more than 12-folds but there was no effect on the *ee*AChE inhibitory activity. Similarly, in **VB8** meta propargyl group reduces MAO-A inhibitory activity by 35-folds when compared to **VB3**. However, **VB8** was found to be the most potent *ee*AChE inhibitor in the series

with IC_{50} values of 9.54 nM. In general, replacement of morpholine ring with the piperidine ring reduces MAO-A inhibitory activity (**VB4** and **VB5**). Shifting of morpholine substituent from para (**VB1**) to meta position (**VB12**) decreases MAO-A activity by 19-folds and *ee*AChE activity by 47-folds. It has been found that compounds with a propargyl substitution at the ortho and meta positions were less active towards MAO-A as compared to the para substituents. The current series of compounds displayed high selectivity index towards AChE as compared to BuChE (Table 5.2). **VB1** was found to be the most potent BuChE inhibitor however, it showed SI of 22-folds for AChE. In the current series of compounds, VB8 displayed highest SI of about 10^3 for AChE. Replacement of amino group with methyl or phenyl groups (**VB2** and **VB3**) decreases BuChE inhibitory activity by about 22-folds. Shifting of propargyl group from para (**VB1**) to ortho (**VB9**) position drastically reduced the activity by about 240-folds. Similarly, shifting of morpholine ring from para (**VB1**) to meta position (**VB12**) decreases BuChE activity by 35-folds. Thus **VB1, VB3** and **VB8** were found to be the most promising compounds amongst the reported series of compounds.

5.3 Results from compounds based on Series-II

5.3.1 Synthesis of target molecules of Series-II

All the compounds were synthesized as per reaction procedures described in Scheme-II. Briefly, O-alkylated benzaldehydes **(I)** and propargylamine substituted acetophenons **(II)** were synthesized from corresponding hydroxy benzaldehydes and amino acetophenones by refluxing these with suitable alkyl halides in the presence of potassium carbonate and acetone as solvent. O-alkylated benzaldehydes **(I)** and propargylamine substituted acetophenones **(II)** were further reacted through aldol condensation to get the intermediate chalcones **(III).** In the final step chalcones **(III)** were reacted with various amidines in the presence of sodium carbonate to obtain the target compounds 4,6-diphenylpyrimidine derivatives **(VP1-VP24).** All the final products were characterized by ^{1}H NMR, ^{13}C NMR, ESI-MS and HRMS.

Scheme-II: Reaction scheme for the synthesis of target molecules

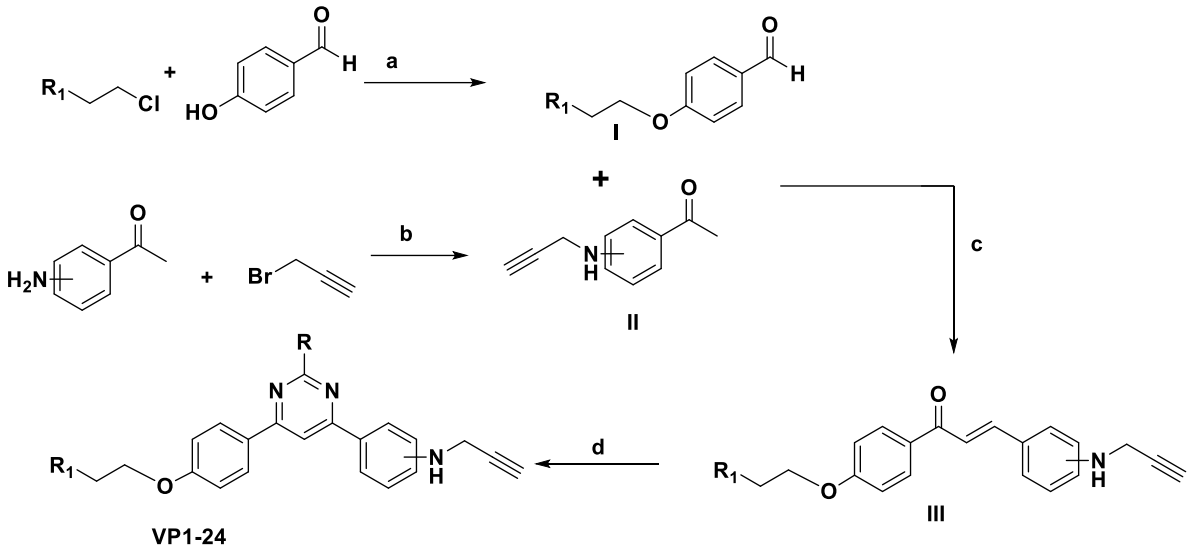

Reagents and Conditions: a) K_2CO_3, KI, acetone, reflux, 6 h; **b)** K_2CO_3, acetone, reflux, 6 h; **c)** CH_3OH, 10% NaOH aq., rt, stirring, 3 h; and **d)** Na_2CO_3, CH_3CN, amidine/guanidine/benzamidine, reflux, 24h

5.3.2 Biological studies of series-II

5.3.2.1 hMAO and ChEs inhibition studies

MAO inhibition potential of the synthesized 4,6-diphenylpyrimidine derivatives (**VP1-VP15**) was evaluated through fluorimetric method using recombinant human MAO-A and MAO-B enzymes and Amplex® Red assay kit (Chimenti *et al.*, 2010). Similarly, acetylcholinesterase inhibition activity was determined using Amplex Red Acetylcholine/Acetylcholinesterase assay kit (A12217) purchased from the Molecular probes Inc. Invitrogen. The results of MAO inhibition studies are described in Table 5.4 in terms of IC_{50} values expressed in micromolar concentrations. Morpholine, piperidine, pyrollidine or *N,N*-dimethyl ethyl chains (R) were used as para substituents at one of the phenyl ring. To develop structure activity relationship profile of 4,6-diphenylpyrimidines, three amidines were used with R_1 as $-NH_2$, $-CH_3$ or $-C_6H_5$. Similarly, second phenyl ring was substituted with a propargylamine group at ortho/meta/para positions. Clorgyline, pargyline and donepezil were used as standard inhibitors for MAO-A, MAO-B and ChEs (AChE and BuChE) enzymes, respectively. **VP1** was found to be the most potent MAO-B inhibitor in the series with an IC_{50} value of 0.04 ± 0.002 µM with high selectivity over MAO-A (248 fold). Similarly, **VP15** with an IC_{50} value of 0.04 ± 0.003 µM and selectivity index of 626 (over BuChE) was found to be the most potent AChE inhibitor in this series.

Table 5.4. Results of the MAO and ChEs inhibition studies of synthesized compounds

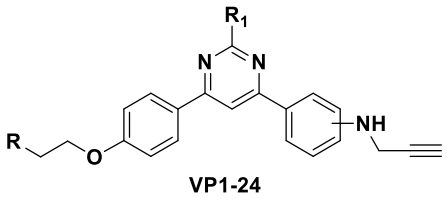

VP1-24

Entry Name	R	R_1	Propargyl group position	IC_{50} values (mean ± S.E. μM)			
				hMAO-A	hMAO-B	*ee*AChE	hBuChE
VP1	Morpholine	NH_2	C4	9.94 ± 0.11	0.04 ± 0.002	7.21 ± 0.15	**
VP2	Morpholine	CH_3	C4	18.11 ± 0.35	0.06 ± 0.004	7.18 ± 0.08	**
VP3	Morpholine	C_6H_5	C4	13.36 ± 0.18	0.66 ± 0.04	6.23 ± 0.11	30.51 ± 0.25
VP4	Morpholine	NH_2	C3	11.33 ± 0.24	0.09 ± 0.005	3.61 ± 0.06	38.19 ± 0.58
VP5	Morpholine	CH_3	C3	10.49 ± 0.22	0.23 ± 0.02	2.97 ± 0.05	37.17 ± 0.37
VP6	Morpholine	C_6H_5	C3	19.56 ± 0.38	0.66 ± 0.025	0.24 ± 0.03	21.18 ± 0.33
VP7	Morpholine	NH_2	C2	**	0.82 ± 0.03	0.07 ± 0.002	**
VP8	Morpholine	CH_3	C2	17.14 ± 0.25	2.53 ± 0.15	6.77 ± 0.13	**
VP9	Morpholine	C_6H_5	C2	10.98 ± 0.25	1.51 ± 0.05	4.30 ± 0.06	**
VP10	Piperidine	NH_2	C4	21.31 ± 0.48	0.83 ± 0.04	1.21 ± 0.03	11.25 ± 0.11
VP11	Piperidine	CH_3	C4	24.34 ± 0.53	1.49 ± 0.07	0.49 ± 0.02	12.18 ± 0.17
VP12	Piperidine	C_6H_5	C4	**	1.18 ± 0.11	1.87 ± 0.08	18.10 ± 0.13
VP13	Piperidine	NH_2	C3	22.15 ± 0.39	0.57 ± 0.04	0.19 ± 0.005	10.45 ± 0.21
VP14	Piperidine	C_6H_5	C3	24.45 ± 0.35	3.08 ± 0.15	0.05 ± 0.002	13.32 ± 0.11
VP15	Piperidine	NH_2	C2	13.61 ± 0.75	0.37 ± 0.03	0.04 ± 0.003	25.03 ± 0.33
VP16	Piperidine	C_6H_5	C2	**	0.80 ± 0.03	16.56 ± 0.08	**
VP17	N,N-diCH_3	C_6H_5	C4	21.16 ± 0.57	**	12.37 ± 0.19	40.17 ± 0.57
VP18	N,N-diCH_3	C_6H_5	C3	12.97 ± 0.61	20.23 ± 0.57	14.21 ± 0.25	**
VP19	N,N-diCH_3	NH_2	C2	7.26 ± 0.23	24.14 ± 0.78	8.10 ± 0.23	**

VP20	N,N-diCH_3	CH_3	C2	10.70 ± 033	10.15 ± 0.15	12.26 ± 0.35	**
VP21	N,N-diCH_3	C_6H_5	C2	**	24.39 ± 0.88	11.67 ± 0.39	**
VP22	Pyrrolidine	C_6H_5	C4	**	24.78 ± 0.49	11.95 ± 0.27	**
VP23	Pyrrolidine	C_6H_5	C3	15.17 ± 0.57	**	14.57 ± 0.26	**
VP24	Pyrrolidine	C_6H_5	C2	12.16 ± 0.30	23.81 ± 0.54	12.48 ± 0.18	**
Clorgyline				4.39 ± 1.02nM	-----	----	----
Pargyline				----	0.015 ± 0.002	----	----
Donepezil				----	----	0.011 ± 0.001	1.28 ± 0.04

5.3.2.2 Reversibility inhibition studies on MAO-B

First generation MAO inhibitors were irreversible in nature and associated with severe side effects. Reversibility of the target compound is frequently considered in designing and development of new class of inhibitors. Thus, to determine the reversible inhibition of the enzyme by the most active and selective compounds i.e. **VP1, VP3, VP14** and **VP15**, reversibility inhibition studies were performed using earlier reported protocol by us and others (Kumar *et al.*, 2018; Minders *et al.*, 2015). In reversibility inhibition study against MAO-B, all tested compounds were found to be irreversible inhibitors of MAO-B.

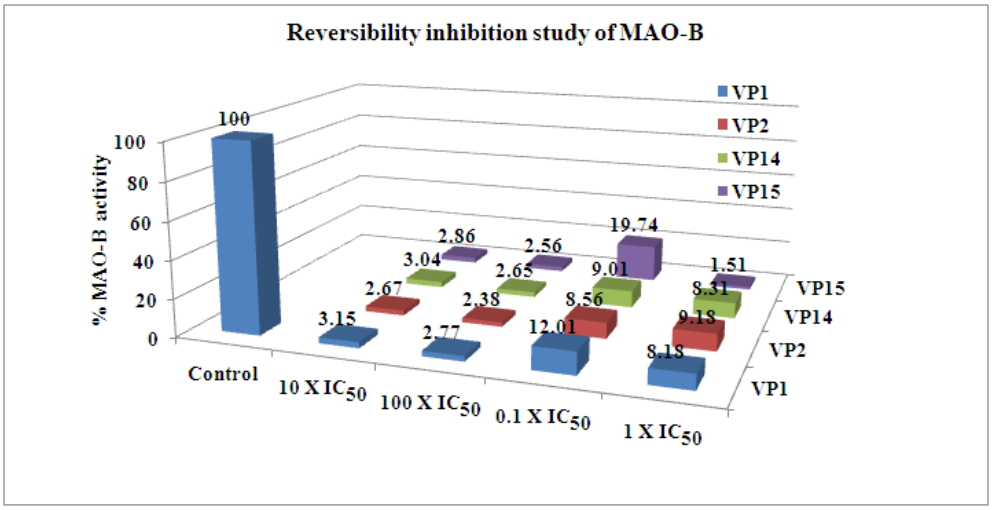

Fig. 5.12 Reversibility inhibition studies of the most potent and selective inhibitors with MAO-B

On incubation of MAO-B enzyme with 10 X IC_{50} and 100 X IC_{50}, the enzyme activity was reduced to the minimal level. Further, after diluting to 100 times (final concentrations of compound in reaction 0.1 X IC_{50} and 1 X IC_{50}) with substrate, the activity of enzyme was not recovered significantly. Maximum activity upto 19.74% was recovered in case of compound **VP14.** Thus, it can be concluded that the synthesized compounds are irreversible inhibitors of MAO-B.

5.3.2.3 Intracellular ROS determination

It is a well-known fact that monoamine oxidase mediated oxidative metabolism of mono amines lead to the production of H_2O_2 as a byproduct (Pizzinat *et al.*, 1999; Sturza *et al.*, 2014). Subsequently, H_2O_2 get converted to the free radicals (ȮH, $Ȯ_2$) through Fenton's reaction which contribute to the oxidative stress. Uncontrolled increase in the concentrations of the free radicals initiate free radical-mediated chain reactions, that causes oxidative damage to the cell membranes, lipid peroxidation and DNA strand breakdown. Thus, prevention of ROS generation along with the MAO inhibition is important strategy to reduce or eliminate neurotoxicity in neurodegenerative disorders.

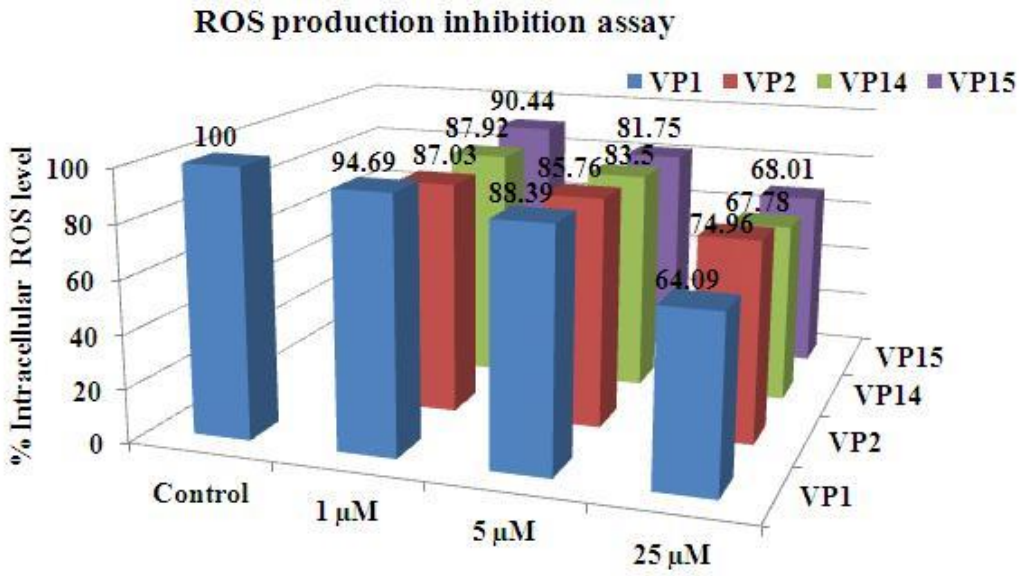

Fig. 5.13 ROS production inhibition studies of VP1, VP2, VP14 and VP15 against SH-SY5Y cells

Intracellular ROS level of SH-SY5Y cells was determined using non-fluorescent compound 2´,7´-dichlorofluorescein diacetate (DCF-DA). It is permeable and oxidized by ROS to a fluorescent compound 2,7-DCF. The intracellular ROS level

of SH-SY5Y cells was not altered significantly at lower concentration (1 µM and 5 µM) by test compounds. Although at 25 µM concentration, intracellular ROS level was reduced to 64% by **VP1**. **VP14** and **VP15** also reduced the ROS level upto 67% and 68% respectively.

5.3.2.4 Neuroprotective studies

Compound **VP1, VP2, VP14** and **VP15** were also evaluated for their neuroprotective properties against 6-hydroxydopamine (6-OHD) induced neuronal damage at SH-SY5Y cells. All the compounds displayed good neuroprotective profile against 6-OHD neurotoxin. **VP14** displayed the best neuroprotective profile against it by recovering cells upto 90% at 25 µM concentration. At lower concentrations (1 µM and 5 µM) also, **VP14** protected the cells upto 83% as compared to control. VP1, VP2 and VP15 also protected the cells upto 64.95%, 77.68% and 77.15% respectively at 25 µM concentration. Thus, it can be concluded that these compounds also act as neuroprotective agents against stress induced neuronal damage.

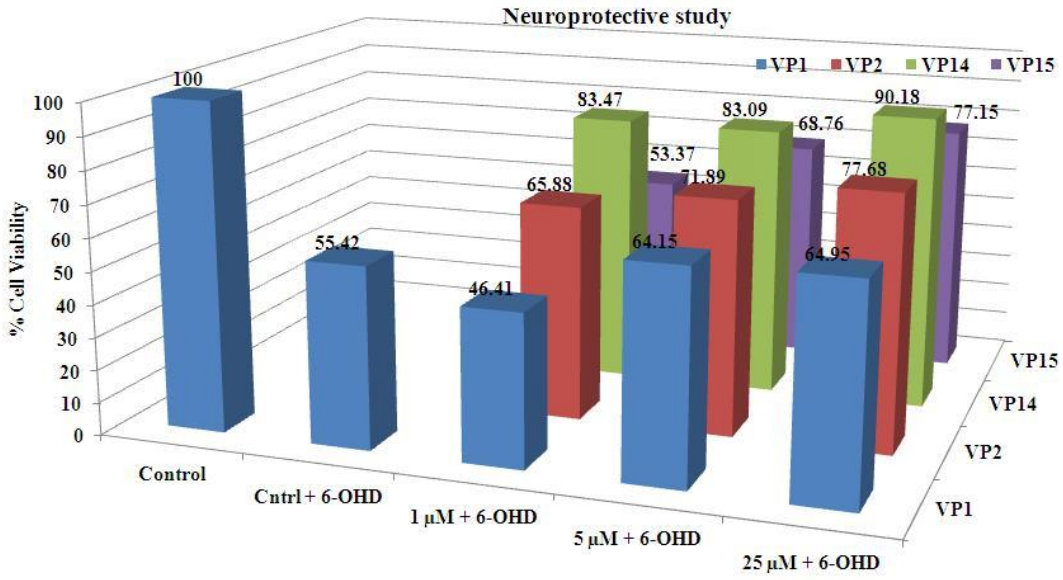

Fig. 5.14 Neuroprotective studies of the most potent and selective MAO-A and AChE inhibitors

5.3.2.5 Cytotoxicity studies

The cytotoxic effects of the most active compounds (**VP1, VP2, VB14 and VB15**) were evaluated against human neuro-blastome (SH-SY5Y) cells because of their

similarity to the dopaminergic neurons (Xie *et al.*, 2010). The test compounds were incubated at 1 µM, 5 µM and 25 µM concentrations and were analyzed after 24h treatment time. The percentage cell viability was measured using MTT assay. As depicted in Fig. 5.15, the compounds were found non-toxic against human neuroblastome (SH-SY5Y) cells. Compounds did not show any significant cytotoxic profile against SH-SY5Y cells. Maximum reduction in cell viability was observed in case of **VP1** (72.95%) at 25 µM concentration, however the concentration is very high as compared to its IC_{50}. At lower concentration these compounds did not show any significant cytotoxicity. Thus, it can be concluded that the target compounds are non-cytotoxic to neuronal cells.

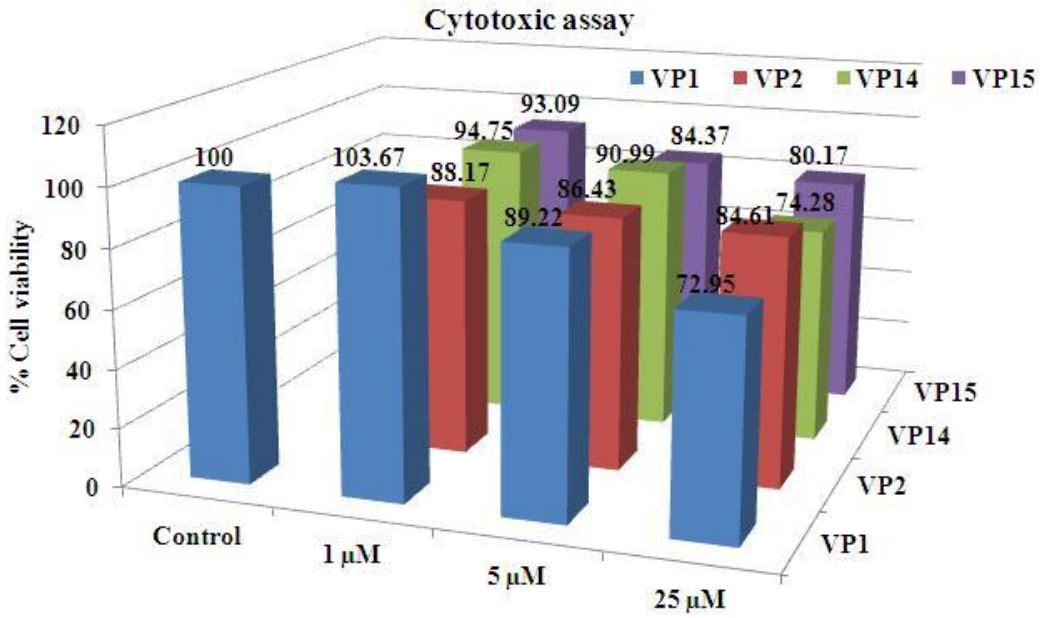

Fig. 5.15 Cytotoxicity studies of **VP1, VP2, VP14** and **VP15** against SH-SY5Y cells at 1 µM, 5 µM and 25 µM.

5.3.2.6 Metal chelating studies

Metal chelating studies of the most potent compounds i.e. **VP1, VP2, VP14** and **VB15** were performed using a UV−vis spectrophotometer. The absorption spectra of each compound (50 µM, final concentration) alone or in the presence of $CuSO_4$, $FeSO_4$, and $FeCl_3$ (50 µM, final concentration) after incubation period of 30 min at room temperature in 20% (v/v) methanol/buffer (20 mM HEPES, 150 mM NaCl, pH = 7.4) was recorded. In metal chelating studies, compounds were found ineffective against metals and does not form any chelates with the metal salts.

5.3.2.7 Kinetic studies of AChE inhibition

To determine the mechanism of inhibition of AChE, kinetic study was carried out with the most potent inhibitor of AChE i.e. **VP15** using ***ee*AChE**. The reciprocal Lineweaver-Burk plots (Fig. 5.16) illustrate increased slope (decreased V_{max}) and higher intercepts (K_m) with the increasing concentration of **VP15.** The intersection point of the Lineweaver-Burk reciprocal plots was located in the third quadrant, which indicate that the inhibition mode of **VP15** was mixed-type inhibition. Thus, it can be concluded that **VP15** binds to both CAS and PAS of AChE simultaneously.

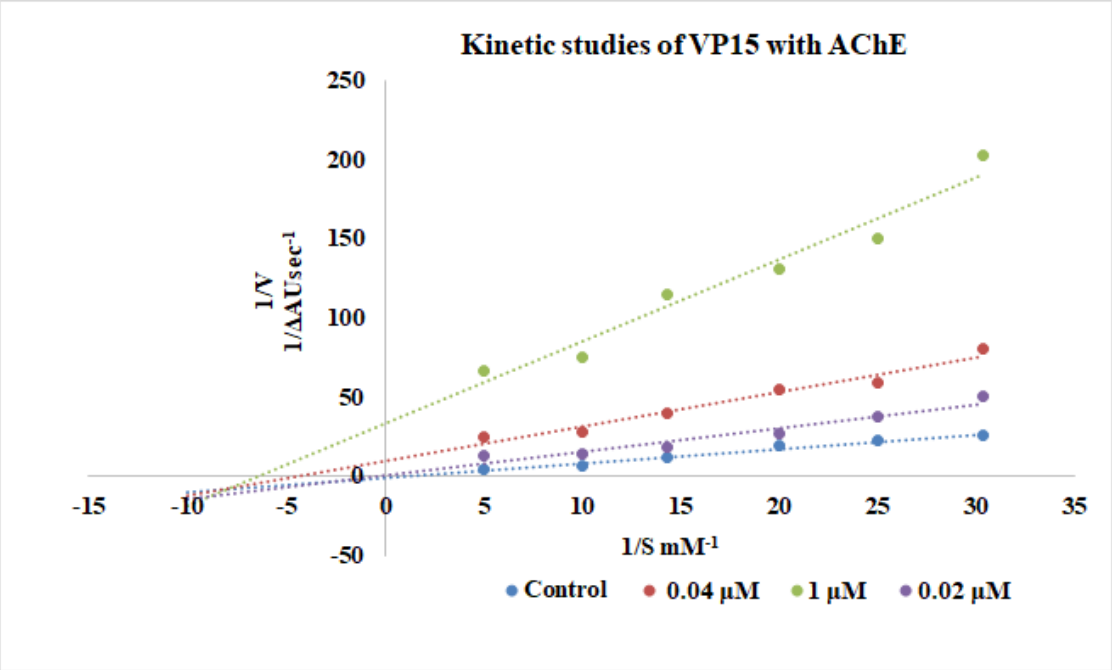

Fig. 5.16 Kinetic study on the mechanism of *ee*AChE inhibition by **VP15**. Overlaid Lineweaver−Burk reciprocal plots of AChE initial velocity at increasing substrate concentration (0.1−1 mM) in the absence or presence of **VP15** are shown.

5.3.2.8 *in vivo* blood-brain barrier permeability

VP15.HCl (10 and 20 mg/kg test compound dissolved in water) was administered orally for four consecutive days to the corresponding treatment groups G1 an G2 (n = 4). After 1 h of last dose on fourth day, rats were sacrificed and their brain tissues were collected. LCMS analysis of the brain samples is reported in Fig. 5.17(a) and Table 5.5. Calibration curve for VP15 was constructed using concentrations ranging between 10 to 500 PPB ($R^2 = 0.9939$) as shown in Fig. 5.17(b) and Table 5.5. LCMS analysis for G1 and G2 groups were performed and brain concentration of VP15

a)

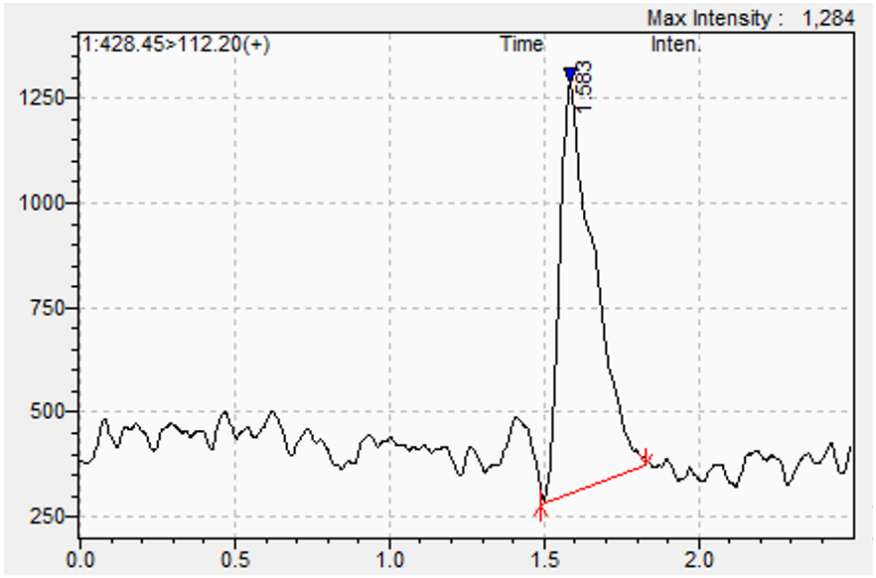

b)

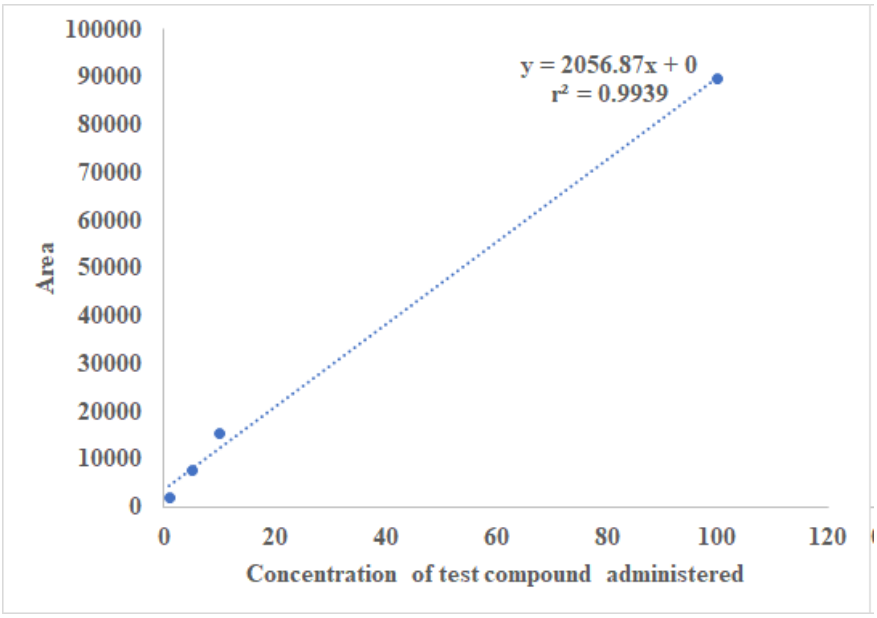

Fig. 5.17 a) MRM graph of VP15 with m/z 428.45/112.20 mass peaks and **b)** standard curve graph for VP15 at different concentrations

was averaged as reported in Table 5.5. For G1 group, 10 mg/kg dose of VP15.HCl was administered and 1.38 ng/mL concentration of VP15 was detected in the brain. Similarly, G2 group was administered a dosage of 20 mg/kg of and 2.95 ng/mL concentration of the same compound was detected in the brain. As evident from Table 5.5, with increase in the dose of VP15.HCl, the increased level of the test compound was detected in the brain. Hence, from these studies it can be concluded that after oral administration, the compound is able to cross the blood-brain barrier and reach the target site in brain tissue.

Table: 5.5 Calibration curve and LC-MS/MS analysis of compound VP15 from brain tissues samples of rats

Vial	Sample Name	Injected volume (µL)	Retention Time (Min)	Area	Concentration (ng/mL)
1	1 PPB	5	1.434	2023	0.983
2	5 PPB	5	1.583	7687	3.737
3	10 PPB	5	1.598	15565	7.568
4	100 PPB	5	1.605	89626	43.574
5	G1 (10 mg/kg)	10	1.825	2840	1.381
6	G2 (20 mg/kg)	10	1.845	6068	2.950

5.3.3 Computational studies of series-II

5.3.3.1 Molecular docking studies

The most potent compounds (**VP1, VP2, VP14** and **VB15**) were subjected to molecular docking studies to find the interaction pattern of the molecules with the amino acid lining and their orientation at the active site of the receptor. Compounds were docked at the active site of hMAO-B (PDB ID- 2BYB) (De Colibus *et al.*, 2005) and AChE (PDB ID- 1EVE) (Cheung *et al.*, 2012). The X-ray crystal structures were imported from the protein data bank using Maestro 11.1 (Schrödinger LLC). The docking procedure employed was first validated by redocking the co-crystallized ligands into the MAO-B and AChE models and the process was found suitable for the docking studies. Two most potent compounds (**VP1 and VP2**) were docked at the crystal structure of MAO-B (2BYB) co-crystallized with deprenyl. The active site of MAO-B comprises an entrance cavity and substrate cavity separated by the side chain of Ile199, which serves as a “gate” between these two cavities. The position of FAD co-factor is also highly conserved to the substrate cavity.

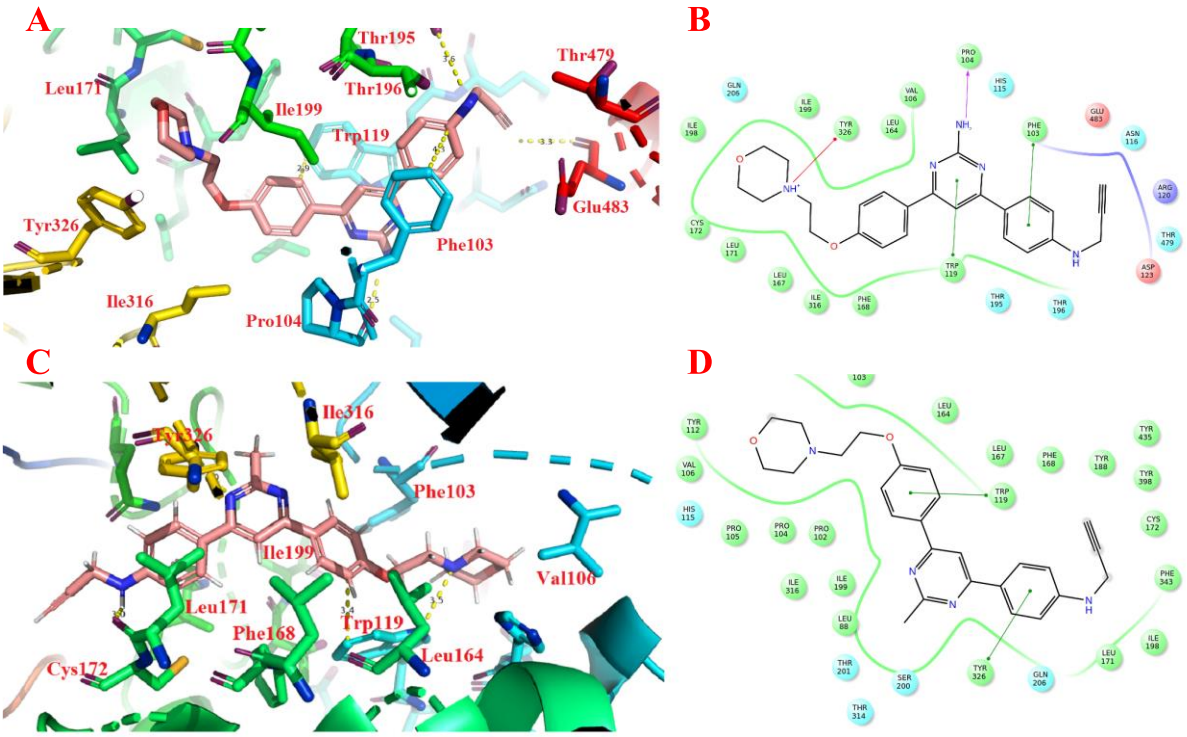

Fig. 5.18 A) Binding pattern (3D) of **VP1** with the amino acid residues at the active site of MAO-B (2BYB), B) Binding interactions (2D) of **VP1** with various amino acids of MAO-B active cavity, C) Binding pattern (3D) of **VP2** with the amino acid residues at the active site of MAO-B (2BYB), and D) Binding interactions (2D) of **VP2** with various amino acids of MAO-B active cavity.

The docking orientations of the compounds **VP1** and **VP2** showed that the pyrimidine moiety in both the compounds interact with the Ile199 and keep this residue in open gate conformation. 4-(2-phenoxyethyl)morpholine fragment of **VP1** accommodated in the substrate cavity of MAO-B while the phenyl ring containing propargylamine moiety was oriented towards the entrance cavity. In case of **VP2**, the binding orientation of compound was reversed and phenyl ring containing propargylamine moiety is accommodated in the substrate cavity of MAO-B, while 4-(2-phenoxyethyl)morpholine fragment was oriented towards entrance cavity. Thus, these compounds block both substrate as well as entrance cavity of MAO-B. The protonated nitrogen atom of morpholine in **VP1** showed cation-π interaction with Tyr326. The presence of NH_2 group facilitated hydrogen bonding with Pro104. Pyrimidine ring and phenyl ring containing propargylamine moiety showed π-π stacking with Trp119 and Phe103 respectively. In case of **VP2**, propargylamine containing phenyl ring formed π-π stacking with residue Tyr326 while phenyl ring

attached to morpholine group formed π-π stacking with Trp199. The pyrimidine moiety in both the compounds was keeping Ile199 in “open-gate” conformation and block the substrate and entrance cavities of MAO-B at same time.

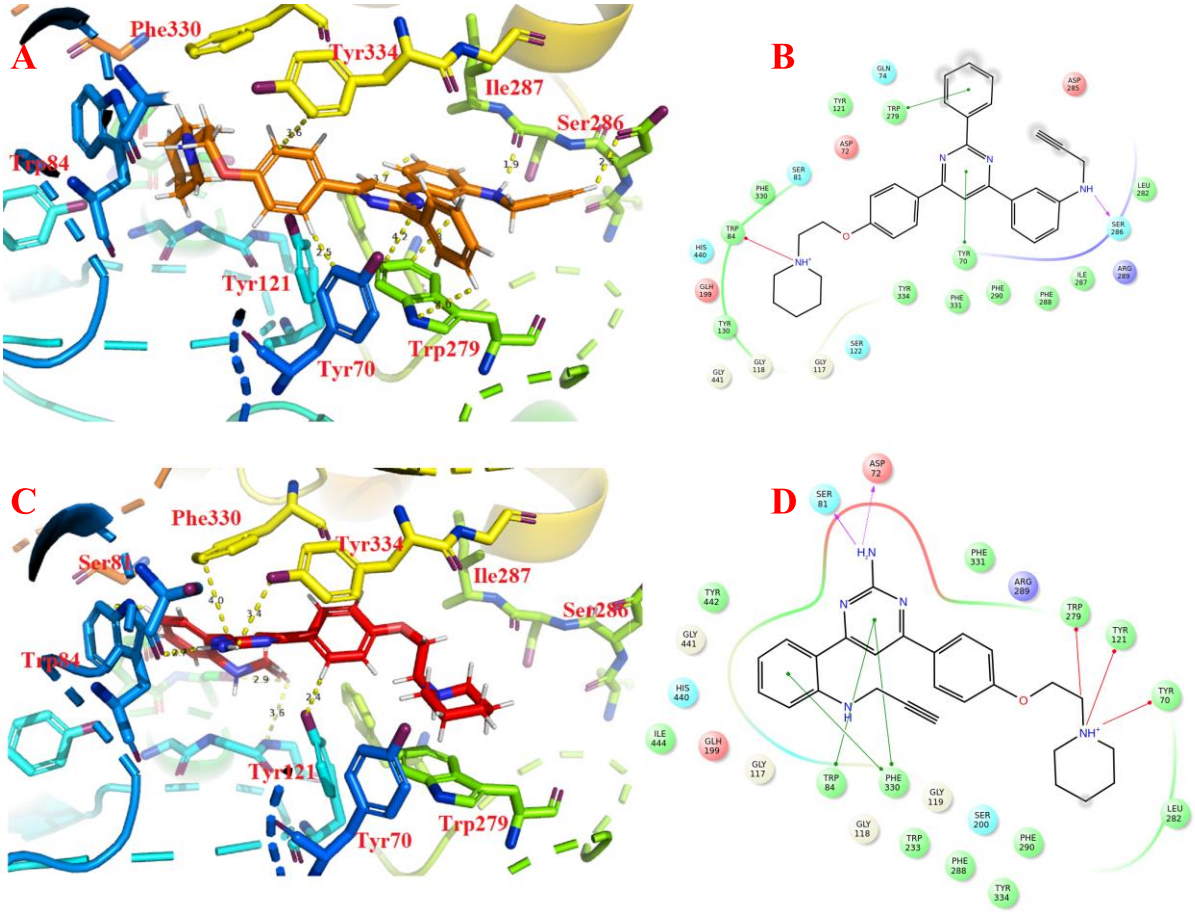

Fig. 5.19 A) Binding pattern (3D) of **VP14** with the amino acid residues at the active site of AChE (1EVE), B) Binding interactions (2D) of **VP14** with various amino acids of AChE active cavity, C) A) Binding pattern (3D) of **VP15** with the amino acid residues at the active site of AChE (1EVE), and D) Binding interactions (2D) of **VP15** with various amino acids of AChE active cavity.

Most potent AChE inhibitors, **VP14** and **VP15,** were subjected to docking against AChE (PDB ID- 1EVE co crystallized with donepezil) to determine their binding alignment at the active site of enzyme. The compounds were well accommodated in the catalytic active site (CAS) aligned with amino acid residues Trp84, Tyr130, Phe330, and Phe331 and peripheral anionic site (PAS) aligned by amino acid residues Tyr70, Asp72, Tyr121, Trp279, Ser286, Phe330 and Tyr334.

The extended chain length between the phenyl and morpholine ring, as compared to the N-benzylpiperidine moiety of donepezil, pushes the compounds further inside

the CAS of AChE. 4-(2-phenoxyethyl)piperidine fragment of **VP14** was aligned inside the CAS of AChE and pyrimidine ring as well as unsubstituted phenyl ring attached to the pyrimidine ring occupy PAS of AChE and interact with Tyr70 and Trp279 respectively. Protonated nitrogen atom of piperidine group in **VP14** formed cation-π interaction with Trp84 and phenyl ring of 4-(2-phenoxyethyl) fragment formed π-π stacking with Tyr334 of CAS. The nitrogen atom of propargylamine group extended outside the PAS and formed hydrogen bond with Ser286. In case of **VP15,** the orientation of the compound is reversed as compared to **VP14**. In this case, phenyl ring containing propargylamine group was oriented towards PAS while 4-(2-phenoxyethyl)piperidine fragment was aligned inside CAS of AChE. The protonated nitrogen atom of piperidine moiety in **VP15** formed cation-π interactions with Tyr70, Tyr121 and Trp279 residues of PAS. In addition, NH_2 group present on the pyrimidine ring of **VP15** formed hydrogen bonds with Asp72 and Ser81. Pyrimidine ring of **VP15** also formed the π-π stackings with Trp84 and Phe330 residues of CAS. Phenyl ring containing propargylamine group also formed π-π stacking with Phe330 residue of CAS.

5.3.3.2 Molecular dynamics simulation studies

Molecular dynamics simulation (MD) studies were performed to study the protein–ligand interactions and to determine the thermodynamic stability of the docked compounds at the active pocket of the enzymes. The protein–ligand docked complexes of the most active compounds **VP1** & **VP2** with MAO-B and **VP14** & **VP15** with AChE were used for MD simulations. The MD simulation studies were conducted for 30 ns and the interaction pattern of the test compounds with different amino acids was analyzed. MD simulations yielded stable trajectories for **VP1** & **VP2** with MAO-B, as noted by the time evolution of the potential energy and the root-mean-square deviation (RMSD) of the protein backbone. In case of **VP1** after initial 5 ns interval stable trajectory was observed for it ranging from 1.5 Å to 2 Å (Fig. 5.20). In case of **VP2** RMSD ranged from 0.8 Å to 1.4 Å for first 15 ns interval, however at 15 ns there was sudden hike in the RMSD and thereafter it showed stable trajectory up to 30 ns. RMSD oscillates in the range of 1.6 Å to 2.2 Å in this time interval (Fig. 5.20). There were not any major structural alterations observed in the binding pattern of **VP1** & **VP2** at binding site of MAO-B and the pyrimidine moiety adopted the similar orientation in the active site of MAO-B as obtained in the docking

studies. Interactions (cation−π interaction of protonated nitrogen of morpholine ring with Tyr326 and π –π interaction of propargylamine containing ring with Phe103) of **VP1** with various amino acids of MAO-B like Tyr326 and Phe103 were maintained throughout the interval of MD study. It showed the stable binding of **VP1** at the substrate and entrance cavity of MAO-B. similarly in case of **VP2**, the initial interactions observed in docking studies like π-π stacking were conserved. While there were little changes observed in the rotatable bonds between morpholine and benzene ring attached. The compact orientation of bonds observed in case of docking studies were found extended, which lead to the breakage of π-π stacking of Trp119 with benzene ring and it formed the hydrogen bonding with nitrogen atom of morpholine ring. In case of both compounds, overall orientation of compounds at active site of MAO-B were conserved, which proves the stable binding of these compounds to MAO-B and possibly explains their irreversible binding nature to the enzyme.

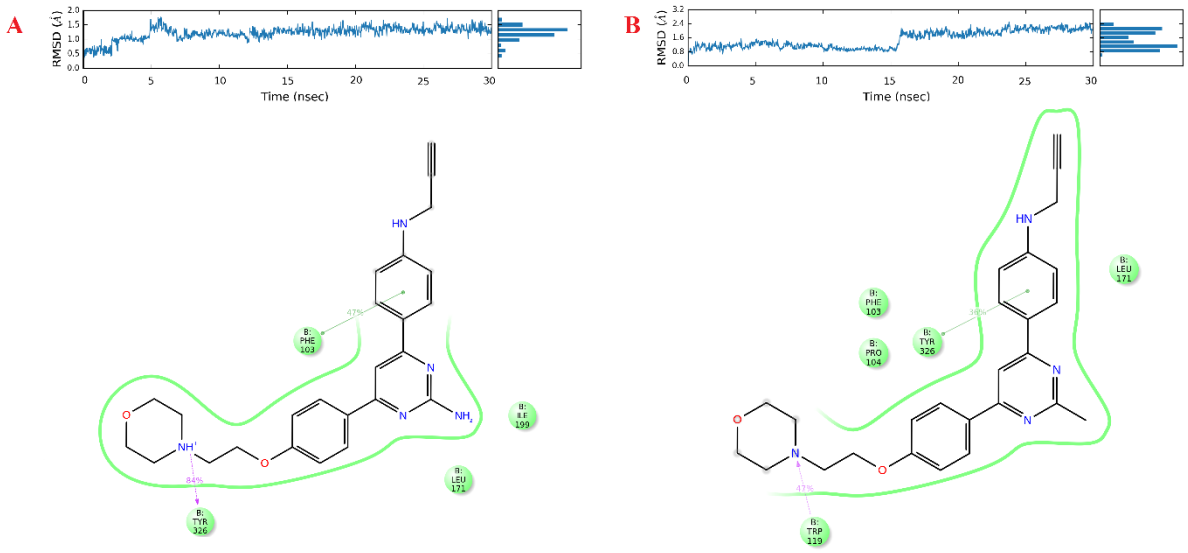

Fig. 5.20 A) RMSD graph and interaction diagram of **VP1** with MAO-B after MD studies of 30 ns, and **B**) RMSD graph and interaction diagram of **VP2** with MAO-B after MD studies of 30 ns.

Similarly, docking complexes of **VP14** & **VP15** with AChE were used for MD simulations to determine their binding stability at active site of enzyme. In case of **VP14** after initial 8 ns interval stable trajectory was observed, determined through RMSD of the protein backbone ranging from 1.6 Å to 2.2 Å. In the first 8 ns interval, RMSD trajectory ranged from 0.9 Å to 1.3 Å. In case of **VP15** RMSD kept oscillating

from 0.8 Å to 2 Å throughout the MD study time interval. Analyzing these MD trajectories of AChE-VP14 and AChE-VP15 complexes, it can be concluded that these compounds (**VP14** and **VP15**) had strong tendency to be localized in the binding region of AChE. In case of **VP15,** nitrogen atom of pyrimidine ring and propargylamine group formed hydrogen bond with Tyr121 and Ser200, respectively. In the CAS of AChE, pyrimidine ring of **VP15** maintained its π-π interaction with Trp84.

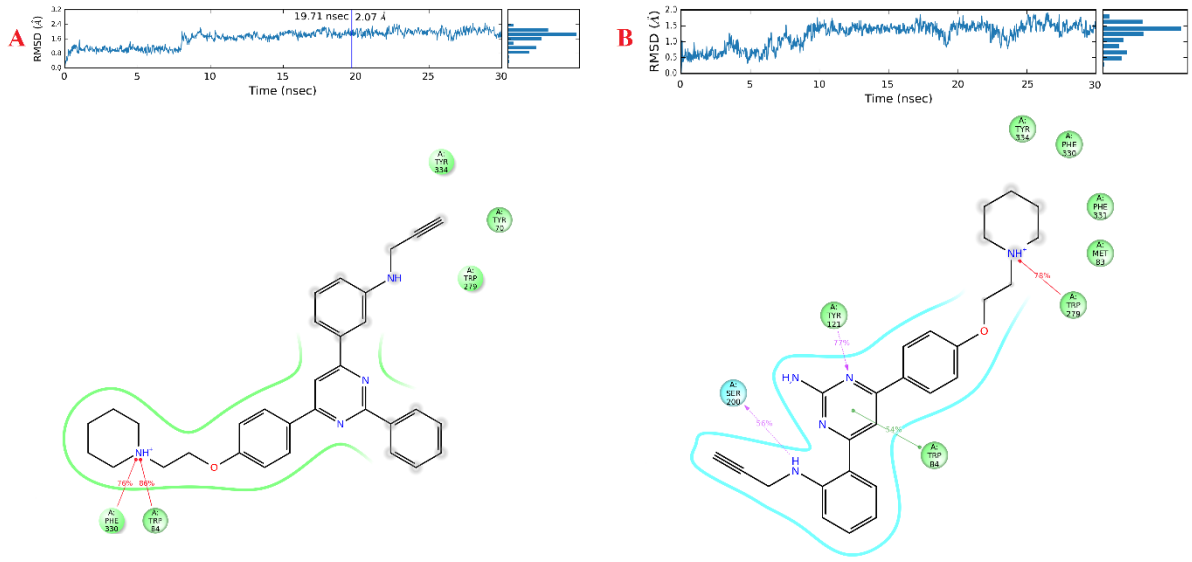

Fig. 5.21- A) RMSD graph and interaction diagram of **VP14** with AChE for 30 ns, and **B**) RMSD graph and interaction diagram of **VP15** with AChE for 30 ns MD simulation studies

The protonated nitrogen atom of piperidine ring, aligned toward PAS of AChE, maintained its initial cation-π interaction with Trp279 throughout the MD interval indicating stable binding of **VP15** at CAS and PAS of AChE without any major structural alignment changes in binding. Similarly, in case of **VP14**, protonated nitrogen atom of piperidine ring aligned toward CAS of AChE, maintained the initial cation-π interaction with Trp84 and formed additional cation-π interaction with Phe330. Propargylamine group containing ring kept aligned toward CAS of AChE aligned by Trp279 and Tyr70 amino acid residues. Thus, from these studies, it can be concluded that, MD simulations of **VP14** and **VP15** does not indicate any abrupt local force that could potentially break up the inhibitors or can even delocalize these from the binding site of AChE.

5.3.3.3 ADME properties

To determine the drug like characteristics of the synthesized compounds, ADME parameters of these compounds were determined using Qikprop application of Schrodinger. **VP1** displayed very good drug-like profile with LogP value less than 5 and QPlogBB value as -0.87. In addition, **VP1** showed optimum oral absorption and blood-brain barrier permeability. **VP2** and **VP14** also showed 100 % oral absorption and QPlogBB in the optimum range to cross the blood brain barrier.

Table 5.6: Physiochemical properties of the most potent and selective MAO-B and AChE inhibitors

Name	**Mol. Wt.**	**Log P**	**HB donor**	**HB acceptor**	**% human oral absorption**	**QPlogBB (**Optimum range -3.0 **–** 1.2)	**BBB permeability predicted**
VP1	429.52	3.59	4	8	90.74	-0.87	+ve
VP2	428.53	4.82	2	7	100	-0.004	+ve
VP14	488.63	7.11	2	6	100	-0.04	+ve
VP15	427.55	4.31	4	6	95.61	-0.79	+ve

+ve = high blood-brain barrier permeability, HB = Hydrogen bond, QPlogBB = qualitatively predicted logarithmic ratio between the concentration of a compound in brain and blood, LogP = partition coefficient of a molecule between an aqueous and lipophilic phase (octanol and water)

5.3.3.4 SAR studies of series-II

In the series-II, a number of diphenylpyrimidine derivatives have been synthesized with different substituents at three aromatic rings. One of the aromatic rings is substituted with morpholine-, piperidine-, *N, N*-dimethyl-, and pyrrolidine- (R groups) ethyl chain at the para position. In the series-I, we have screened different *O*-propargylated pyrimidines and realized that morpholinethyl chain at the para position was most effective for MAO and AChE inhibitory activities. Thus, in series-II, the position of ethyl chain is fixed at the para position of the phenyl ring. The pyrimidine ring is substituted with $–NH_2$, $-CH_3$, and C_6H_5- (R_1) functionalities while, third aromatic ring is optionally substituted with a propargylamine group at ortho,

meta and para positions. The synthesized compounds were screened for MAO-A, MAO-B, *ee*AChE and hBuChE inhibitory activities using enzymatic assays. As evident from **Table 5.4**, the compounds with morpholine and piperidine substituents were found to be selective inhibitors of MAO-B isoform with IC_{50} values in nanomolar to sub micromolar range with very high selectivity index while compounds with *N,N*-dimethyl and pyrrolidine substituents were found to be equipotent for MAO-A and MAO-B isoforms. This series of compounds were also found to be potent inhibitors of AChE and BuChE enzymes with IC_{50} values in nanomolar to low micromolar range. **VP1** with R as morpholine, R_1 as $-NH_2$ and propargylamine group at para position of the aromatic ring displayed potent MAO-B inhibition and high selectivity over MAO-A (248 fold). **VP1** was found to be the most potent MAO-B inhibitor in the series with an IC_{50} value of 0.04 ± 0.002 µM. Replacing R_1 with $-CH_3$ in **VP2** slightly reduced the MAO-B inhibitory activity to 0.06 ± 0.004 µM while substitution of R_1 with C_6H_5- in **VP3** reduced the MAO-B inhibition activity by more than 16-folds as compared to **VP1**. Shifting of propargylamine group from para to meta position in **VP4** and **VP5** also reduced MAO-B inhibitory activity by 2-fold and 4-fold when compared with **VP1** and **VP2** respectively. However, in **VP6** no change in the MAO-B inhibitory activity was observed. Substitution of propargylamine group at ortho position further reduced MAO-B inhibitory activity in **VP7, VP8 and VP9.** Replacement of morpholine ring with piperidine ring in **VP10, VP11 and VP12** reduced MAO-B inhibitory activity by 21-fold, 25-fold and 2-folds when compared with corresponding morpholine derivatives **VP1, VP2 and VP3** respectively. Similarly, piperidine containing derivatives with propargylamine group at meta and ortho position of the third aromatic ring showed reduced activity for MAO-B isoform (**VP13** to **VP16)**. Surprisingly, when morpholine and piperidine rings are replaced with *N,N*-dimethyl and pyrrolidine moieties, most of the compounds displayed more selectivity towards MAO-A as compared to MAO-B except **VP21** and **VP22. VP17** was found to be selective towards MAO-A isoform with an IC_{50} value of 21.16 ± 0.57 µM. **VP18** and **VP20** were found to be equipotent for both MAO-A and MAO-B while **VP19** showed 3-fold more potency towards MAO-A as compared to MAO-B. Similarly, **VP23** and **VP24** were found to be selective inhibitors of MAO-A isoform with IC_{50} values of 15.17 ± 0.57 µM and 12.16 ± 0.30 µM respectively.

This series of compounds were also found to be potent inhibitors of eeAChE and hBuChE enzymes and most of the compounds displayed high selectivity index for eeAChE. **VP1, VP2** and **VP3** showed almost similar potency towards AChE. Shifting of propargylamine group to meta and ortho positions (**VP4** to **VP9)** increased the AChE and BuChE inhibition activities and **VP7** with R_1 as $-NH_2$ and propargylamine group at ortho position displayed an IC_{50} value of 0.07 ± 0.002 µM for AChE with high selectivity index. Replacement of morpholine with piperidine ring (**VP10** to **VP16)** significantly improved the inhibitory activities of the compounds and **VP15** with an IC_{50} value of 0.04 ± 0.003 µM and selectivity index of 626 (over BuChE) was found to be the most potent AChE inhibitor in this series. Similarly, **VP13** was found to be the most potent BuChE inhibitor in this series with an IC_{50} value of 10.45 ± 0.21 µM. Other changes in the substitution pattern like replacement with N,N-dimethyl group or with pyrrolidine ring further reduced the AChE and BuChE inhibition activities.

5.4 Results from compounds based on Series-III

5.4.1 Synthesis of target molecules of Series-III

All the compounds were synthesized as per reaction procedures described in Scheme-III. Briefly, *O*-propargylated acetophenones **(3)** and benzaldehydes **(4),** optionally substituted at ortho, meta and para positions, were synthesized from corresponding hydroxy acetophenones or benzaldehydes by refluxing these with suitable propargyl bromide in the presence of potassium carbonate and acetone as solvent. *O*-propagylated acetophenones **(3)** and benzaldehydes **(4)** were reacted through aldol condensation to get the intermediate chalcones (**5)**. In the final step these propargyl substituted chalcones (**5)** were reacted with various amidines in the presence of sodium carbonate to obtain the target compounds 4,6-diphenylpyrimidine derivatives **(AVB1-AVB19).** All the final products were characterized by IR, ^{1}H NMR, ^{13}C NMR, ESI-MS and HRMS.

Scheme-III: Reaction scheme for the synthesis of target molecules

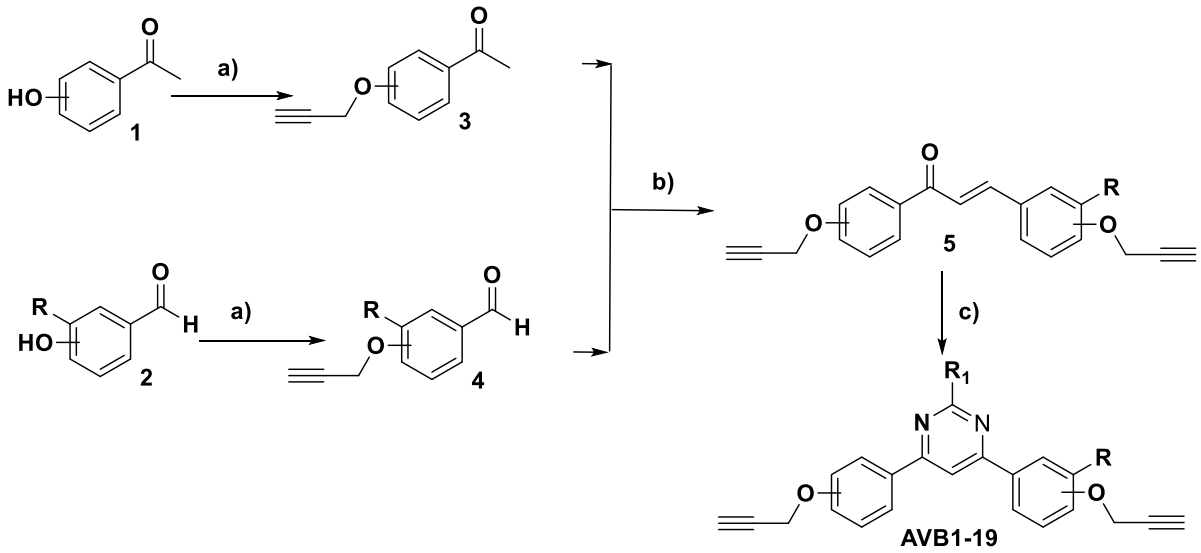

Reagents and conditions: a) Propargyl bromide (1.2 eq), K_2CO_3 (2 eq), acetone, reflux, 12h; **b)** CH_3OH as solvent, 10% NaOH aq., rt, stirring 1h; **c)** Amidines (1.5 eq), Na_2CO_3 (2.5 eq), CH_3CN as solvent, reflux, 24h

5.4.2 Biological studies of series-III

5.4.2.1 hMAO and AChE inhibition studies

MAO and AChE inhibition potential of the synthesized compounds (**AVB1**−**AVB19**) was evaluated through fluorimetric method using Amplex Red assay kits purchased from the Molecular Probes, Inc. /Invitrogen. The results of MAO and AChE inhibition studies are expressed in the form of IC_{50} values (µM) described in **Table 5.7**. Both the phenyl rings of synthesized diphenylpyrimidine derivatives were substituted with propargyl groups at ortho/meta/para positions. Different amidines were used with R_1 as $-NH_2$, or $-CH_3$ or $-C_6H_5$ so as to develop structure activity relationship profile of this series of compounds. Clorgyline, pargyline, and donepezil were used as standard inhibitors for MAO-A, MAO-B, and AChE enzymes, respectively. All of the synthesized compounds were found to be potent inhibitors of MAO-B isoform (Selective over MAO-A) and AChE with IC_{50} values in low micromolar range. Compound **AVB4** was found to be the most potent MAO-B inhibitor with IC_{50} value of 1.49 ± 0.09 µM exhibiting 17-folds selectivity over MAO-A. It also showed potent inhibition of AChE with IC_{50} value of 1.74 ± 0.07 µM. In the reported series, **AVB1** was found to be the most potent AChE inhibitor with an IC_{50} value of 1.35 ±0.03 µM and displayed MAO-B inhibitory activity with an IC_{50} value of 3.30 ± 1.17 µM. As evident from Table 5.7, all the compounds were found to be selective for MAO-B isoform.

Table 5.7. Results of MAO-A, MAO-B and AChE inhibition studies of the synthesized compounds

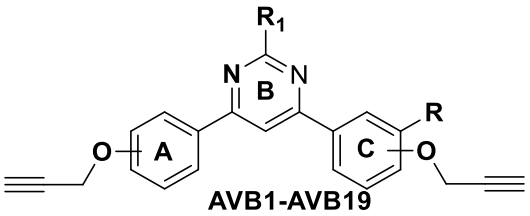

AVB1-AVB19

Entry Name	Propargyl at ring A	Propargyl at ring C	R	R_1	IC_{50} values (mean ± S.E. µM)			MAO Selectivity
					hMAO-A	hMAO-B	eeAChE	
AVB1	C4	C4	H	NH_2	32.06 ± 1.19	3.30 ± 1.17	1.35 ±0.03	MAO-B
AVB2	C4	C4	H	CH_3	34.15 ± 2.03	7.83 ± 0.57	1.76 ± 0.06	MAO-B
AVB3	C4	C4	H	C_6H_5	25.57 ± 1.18	12.26 ± 0.99	7.53 ± 0.23	MAO-B
AVB4	C4	C3	H	NH_2	24.06 ± 0.71	1.49 ± 0.09	1.74 ± 0.07	MAO-B
AVB5	C4	C3	H	CH_3	21.14 ± 1.40	8.09 ± 0.54	5.88 ± 0.07	MAO-B
AVB6	C4	C3	H	C_6H_5	25.83 ± 1.92	17.69 ± 1.13	4.39 ± 0.16	MAO-B
AVB7	C4	C2	H	NH_2	28.55 ± 0.77	22.12 ± 1.68	1.81 ± 0.02	MAO-B
AVB8	C4	C2	H	CH_3	23.19 ± 1.87	18.07 ± 1.75	2.56 ± 0.13	MAO-B
AVB9	C4	C2	H	C_6H_5	22.02 ± 1.03	14.44 ± 0.78	7.25 ± 0.16	MAO-B
AVB10	C3	C3	H	NH_2	***	22.09 ± 0.94	6.99 ± 0.09	MAO-B
AVB11	C3	C3	H	C_6H_5	***	23.44 ± 1.17	6.73 ± 0.18	MAO-B
AVB12	C2	C2	H	NH_2	***	11.13 ± 0.16	5.19 ± 0.21	MAO-B
AVB13	C2	C2	H	C_6H_5	***	13.78 ± 0.22	8.12 ± 0.19	MAO-B
AVB14	C4	C4	OCH_3	NH_2	***	20.03 ± 1.18	4.58 ± 0.08	MAO-B
AVB15	C4	C4	OCH_3	CH_3	24.99 ± 2.13	21.08 ± 1.83	5.92 ± 0.18	MAO-B
AVB16	C4	C4	OCH_3	C_6H_5	24.93 ± 1.17	15.71 ± 0.95	6.99 ± 0.16	MAO-B
AVB17	C4	C4	OCH_2CH_3	NH_2	***	14.01 ± 1.07	7.05 ± 0.14	MAO-B
AVB18	C4	C4	OCH_2CH_3	CH_3	***	10.97 ± 0.82	6.38 ± 0.09	MAO-B
AVB19	C4	C4	OCH_2CH_3	C_6H_5	***	29.03 ± 1.33	6.94 ± 0.16	MAO-B
Clorgyline					4.39 ± 1.02 nM	nd	nd	
Pargyline					nd	0.15 ± 0.02	nd	
Donepezil					nd	nd	0.03 ± 0.001	

***Inactive or showed less than 50% inhibitory activity at 50 µM concentration and precipitated at higher concentrations. [nd] not determined

5.4.2.2 Reversibility inhibition studies

To determine whether the synthesized compounds are reversible or irreversible inhibitors of the target enzymes, the most active compounds i.e. **AVB1** and **AVB4** were subjected to reversibility inhibition studies (Kumar *et al.*, 2018; Minders *et al.*, 2015). Both the compounds were found to be the reversible inhibitors of MAO-B and AChE enzymes.

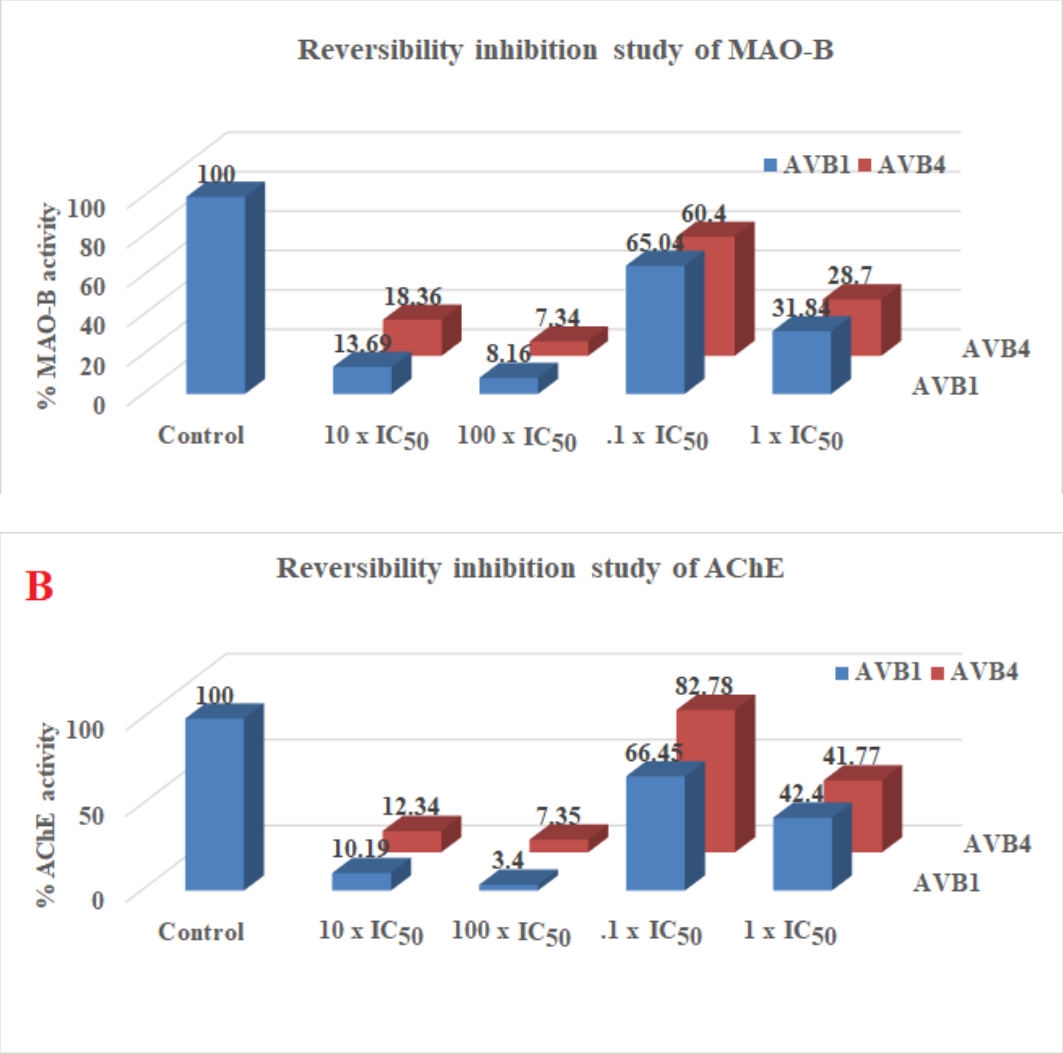

Fig. 5.22 Reversibility inhibition studies of **AVB1** and **AVB4** with **A)** MAO-B enzyme and **B)** AChE enzyme.

Compound **AVB1** showed recovery in the enzyme activity by up to 65.04% and 66.45% for MAO-B and AChE respectively, while compound **AVB4** showed

recovery in the enzyme activity up to 60.4% and 82.78% for MAO-B and AChE respectively (Fig. 5.22). Thus, it can be concluded that the synthesized compounds are reversible inhibitors of both MAO-B and AChE enzymes.

5.4.2.3 ROS inhibition studies

From literature survey, it is clear that MAO mediated metabolism of various monoamines leads to the production of H_2O_2 which further get converted into free radicals through Fenton's reaction and induces oxidative stress. Increased levels of these free radicals, initiate free radical-mediated chain reactions that may cause oxidative damage to the cell membranes, DNA strand breakdown and neuronal cell death. Thus, prevention of ROS generation along with MAO inhibition is considered as an added advantage to prevent neurotoxicity in neurodegenerative diseases. The most potent compounds in the series i.e. **AVB1** and **AVB4** were evaluated for their ROS production inhibition potential against SH-SY5Y cells after 24 h interval treatment. For activity evaluation, 2',7'-dichlorofluorescein diacetate (DCF-DA), a non-fluorescent compound was used. DCF-DA in the presence of reactive oxygen species is oxidized to 2,7-DCF which is a fluorescence emitting agent.

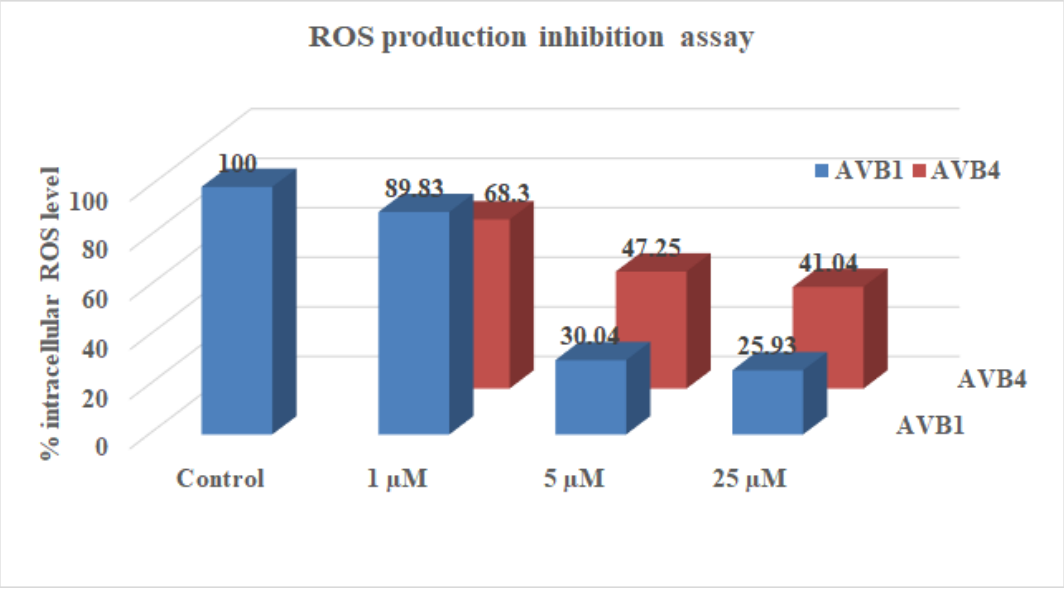

Fig. 5.23 ROS inhibition studies of compound **AVB1** and **AVB4** on SH-SY5Y cells after treatment for 24 h.

Compound **AVB1** significantly reduced the ROS levels to 30.04 % and 25.93 % at 5 µM and 25 µM concentrations, respectively in the SH-SY5Y cells. Similarly, compound **AVB4** reduced the ROS levels up to 47.25% and 41.04% at 5 µM and

25 µM concentrations, respectively in the SH-SY5Y cells. Thus, from these results, it is apparent that this series of compounds with two propargyl moieties can act as potent ROS production inhibitors and hence may protect the neuronal cells.

5.4.2.4 Neuroprotective effects

The most potent AChE and MAO-B inhibitors i.e **AVB1** and **AVB4** were evaluated for their neuroprotective potential against 6-hydroxydopamine (6-OHDA) neurotoxin in SH-SY5Y cells. These compounds showed mild neuroprotective potential against 6-OHDA. Highest cell viability of 66.6% was observed for compound **AVB1** as compared to the 6-OHDA treated cells (48.52%). As the concentration of the compounds increased from 5 µM to 25 µM, the cell viability was further reduced as shown in Fig. 5.24.

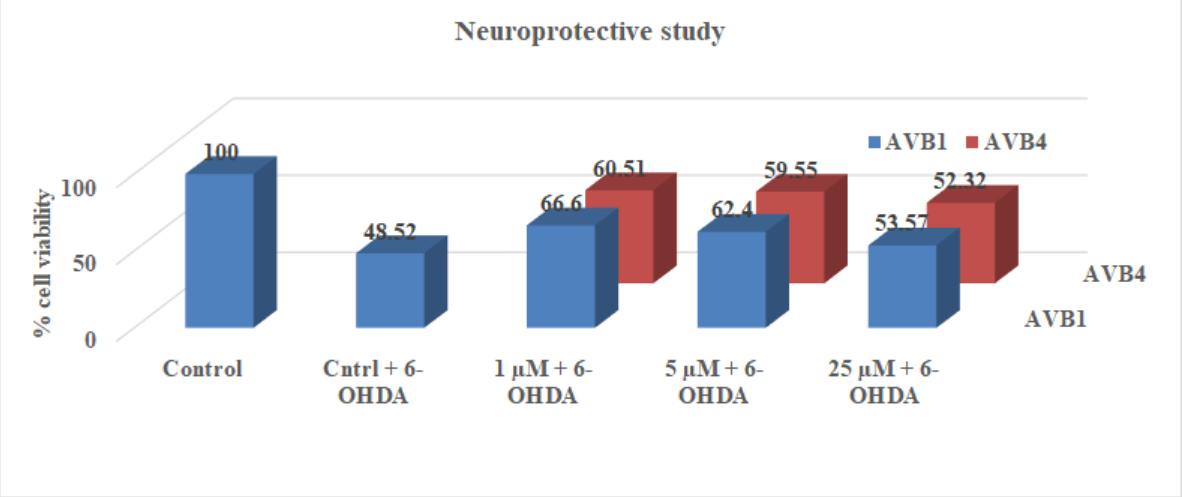

Fig. 5.24 Neuroprotective studies of **AVB1** and **AVB4** on SH-SY5Y cells.

5.4.2.5 Metal chelation studies

Metal-chelating studies of **AVB1** and **AVB4** were performed with a UV−vis spectrophotometer. The absorption spectra of each compound (50 µM, final concentration) alone or in the presence of $CuSO_4$, $FeSO_4$, and $FeCl_3$ (50 µM, final concentration) was recorded. In metal chelating studies, none of the compounds formed any metal chelate with any of the above metal salts. Thus, these compounds are ineffective against metal salts and did not show any metal chelating properties.

5.4.2.6 Cytotoxicity studies

Cytotoxicity of the most potent inhibitors (**AVB1 and AVB4**) was determined against SH-SY5Y cells using MTT assay. The test compounds at 1 µM, 5 µM and 25 µM concentrations were incubated with SH-SY5Y cells and cell viability was determined after 24 h time interval using MTT assay. As depicted in Fig. 5.25, the compounds were found non-toxic at the lower concentrations. As the concentration of the compounds increased, there was slight decrease in cell viability. Least cell viability of 69.17% was observed for **AVB4** at 25 µM concentration. At lower concentration of 1 µM, cell viability of 87.34% was observed as compared to the control. Thus, keeping in view the IC_{50} values of the compounds which are in low micromolar range, the current series of compounds were found to be nontoxic to the tissue cells.

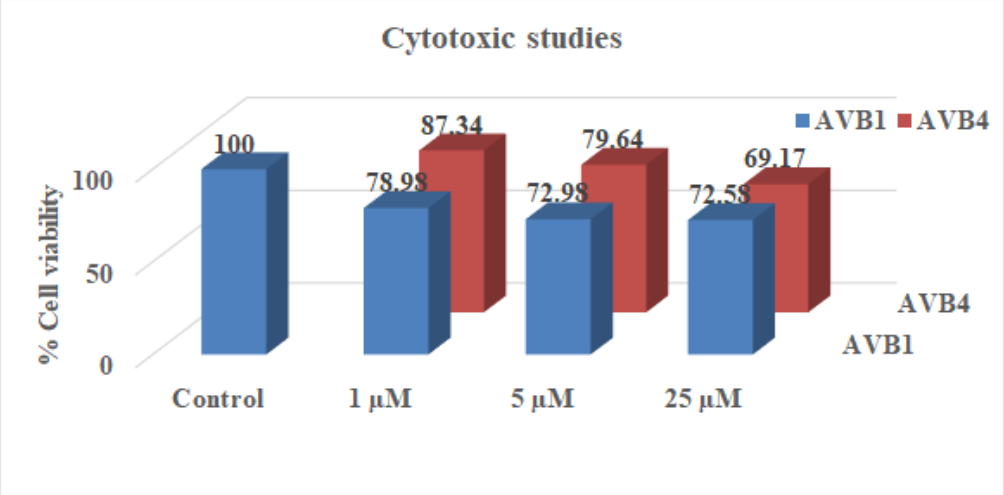

Fig. 5.25 Cytotoxicity studies of **AVB1** and **AVB4** on the SH-SY5Y cells after treatment for 24 h.

5.4.2.7 Kinetic studies of AChE inhibition of AVB4

To determine the mechanism of inhibition of AChE, kinetic study was carried out with the most potent inhibitor of AChE (**AVB4)** using eeAChE. The reciprocal Lineweaver-Burk plots (Fig. 5.26) illustrates the increased slope (decreased V_{max}) and higher intercepts (K_m) with the increasing concentration of **AVB4.** The intersection point of the Lineweaver-Burk reciprocal plots was located in the third quadrant, which indicate that **AVB4** is mixed type inhibitor. **AVB4** might be binding to PAS and CAS of AChE simultaneously and inhibit the binding of substrate to active site. Binding of **AVB4** with the PAS and CAS is further supported by docking and molecular dynamics simulation studies.

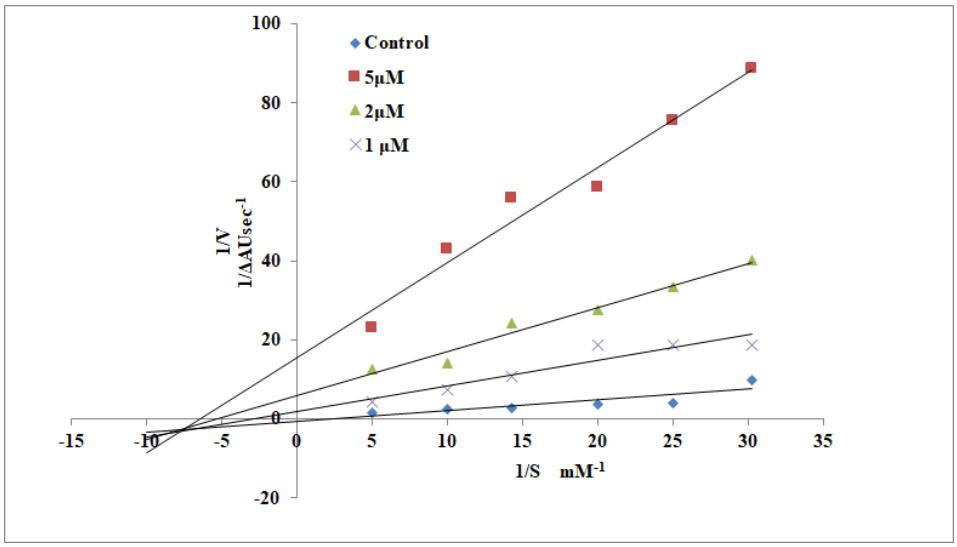

Fig. 5.26 Kinetic study on the mechanism of *ee*AChE inhibition by **AVB4**. Overlaid Lineweaver−Burk reciprocal plots of AChE initial velocity at increasing substrate concentration (0.1−1 mM) in the absence or presence of **AVB4** are shown.

5.4.3 Computational studies

5.4.3.1 Molecular docking and simulation studies

Docking of the ligands and molecular dynamics simulations in the active site of the receptors may provide crucial information about the orientations of the ligands and their interactions with various amino acid residues at the receptor site. Most active compounds obtained in the series were docked at the respective active sites of the receptor isoforms. Maestro 11.1 (Schrödinger LLC) software was used for carrying out the docking studies and compounds **AVB1** and **AVB4** were docked at the hMAO-B (PDB ID-2BYB) (De Colibus *et al.*, 2005) and AChE (PDB ID-1EVE) (Cheung *et al.*, 2012) crystal structures imported from the protein data bank. The docking procedures were first validated by accurately redocking the co-crystallized ligands into the MAO models. The active site of MAO-B is divided into two different compartments, an entrance cavity and a substrate cavity separated by the side chain of Ile199 which serves as a “gate” between the two cavities. The docking orientations of the compound **AVB1** and **AVB4** showed that the pyrimidine moiety in both the compounds interacts with the Ile199 and keep this gate residue in open gate conformation. Phenyl ring with propargyl group at meta position in **AVB4** is oriented towards FAD co factor and accommodated in the substrate cavity while the phenyl ring with para propargyl group is aligned in the entrance cavity. In **AVB1** both the phenyl rings contain propargyl groups at the para positions and one of the

propargyl group is oriented towards the FAD co factor. The NH_2 group in **AVB1** showed hydrogen bonding with Phe168 and Cys172. In **AVB4** pyrimidine ring remain close to the entrance cavity and NH_2 group formed hydrogen bonds with Cys172 and Tyr188. The pyrimidine ring in **AVB1** form π-π stacking with Tyr326 while in **AVB4** propargyl containing phenyl ring interacts with Tyr326 as shown in **Fig**. **5.27**. The inner phenyl ring of **AVB4** in the substrate displayed π-π interactions with Phe343. The increased MAO-B activity of **AVB4** as compared to **AVB1** might be due to the additional π-π stacking of **AVB4** with Tyr326 and Phe343.

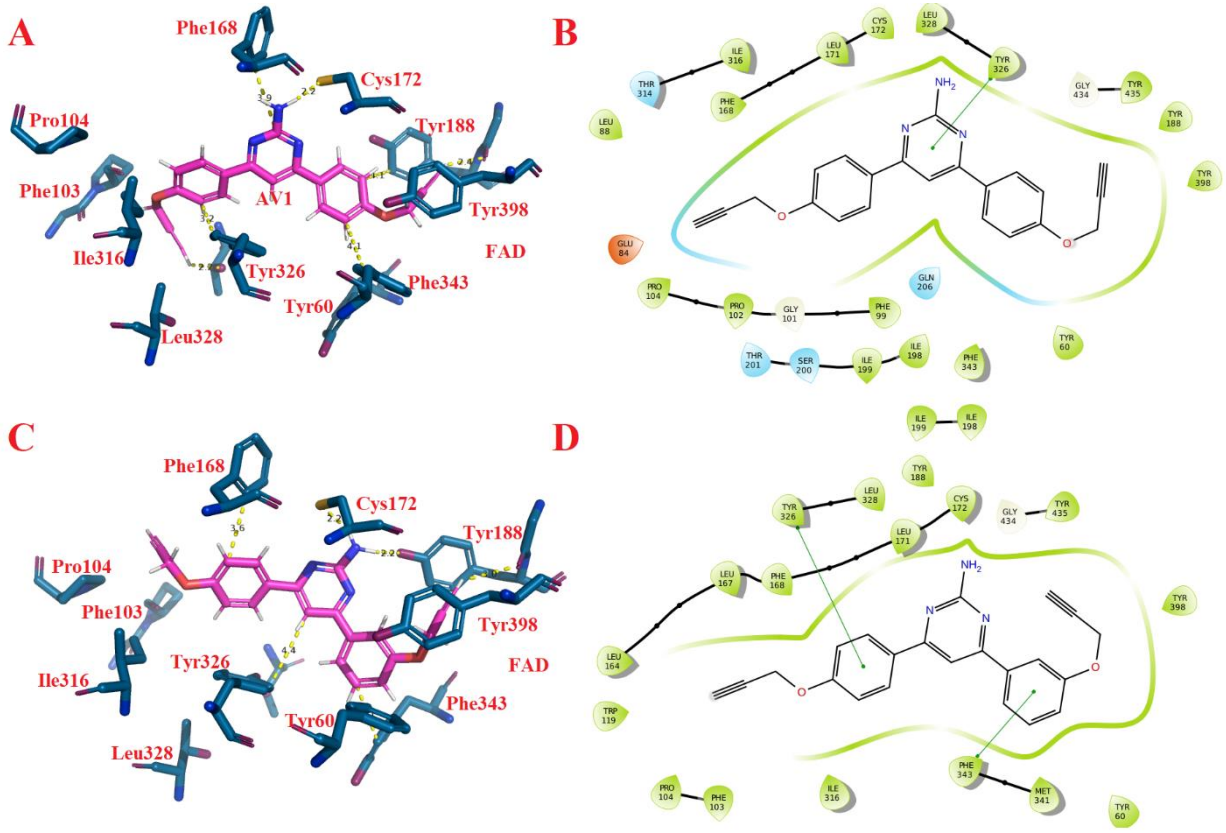

Fig. 5.27 A) Binding pattern (3D) of **AVB1** with the amino acid residues at the active site of MAO-B (2BYB)**, B)** binding interactions (2D) of **AVB1** with various amino acids of MAO-B active cavity, **C**) Binding pattern (3D) of **AVB4** with the amino acid residues at the active site of MAO-B (2BYB)**,** and **D)** binding interactions (2D) of **AVB4** with various amino acids of MAO-B active cavity.

Similarly, both of these compounds i.e. **AVB1** and **AVB4** were docked against AChE (PDB ID- 1EVE co crystallized with donepezil) to determine their binding alignment at the active site of enzyme. The active site of AChE is divided into two compartments; i) catalytic active site (CAS) composed of Trp84, Tyr130, Phe330,

Phe331 residues and, ii) peripheral anionic site (PAS) consists of amino acids-Tyr70, Asp72, Tyr121, Trp279, and Tyr334. The compounds were found to interact both with CAS as well as with PAS of AChE. Pyrimidine ring in **AVB1** and **AVB4** accommodated in PAS and NH_2 group formed hydrogen bonds with Asp72. In case of **AVB1,** one of the phenyl rings with a propargyl group is accommodated in the CAS and showed π-π interactions with Trp84. In **AVB4,** phenyl ring with para proparyl group is oriented towards PAS and displayed π-π stacking with Tyr334. An additional hydrogen bond interaction of *O*-propargylated group with Phe288 in PAS was observed in **AVB1**.

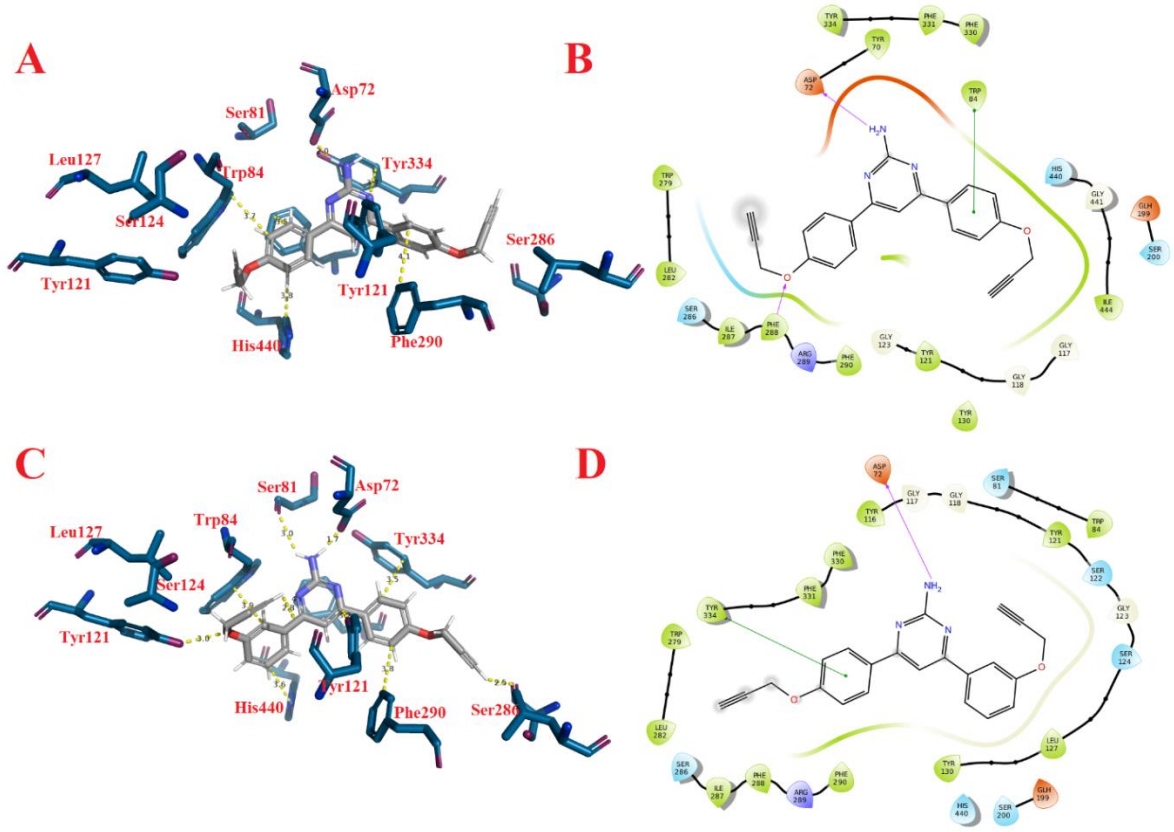

Fig. 5.28 A) Binding pattern (3D) of **AVB1** with the amino acid residues at the active site of AChE (1EVE)**, B)** binding interactions (2D) of **AVB1** with various amino acids of AChE active cavity, **C**) Binding pattern (3D) of **AVB4** with the amino acid residues at the active site of AChE (1EVE)**,** and **D)** binding interactions (2D) of **AVB4** with various amino acids of AChE active cavity.

5.4.3.2 Molecular dynamic simulation studies

In order to investigate the binding stability of the potent inhibitors into the active site of the MAO-B and AChE, molecular dynamic (MD) simulations studies were

performed. For this docking complexes of **AVB1** and **AVB4** with MAO-B and AChE were used. The MD simulations studies were conducted for 30 ns and the interaction pattern of the test compounds with different amino acids was analyzed. MD simulations studies of **AVB4** with MAO-B yielded the stable trajectory from 3 ns to 30 ns, oscillating in between 0.8 Å to 1.2 Å (Fig. 5.29). For the initial 2 ns time interval, a sharp hike was observed in RMSD from 0.4 Å to 1.6 Å, which stabilized to 1.2 Å after 3 ns interval. The pyrimidine ring of AVB4 maintained its initial π-π interaction with Tyr326 throughout MD time interval.

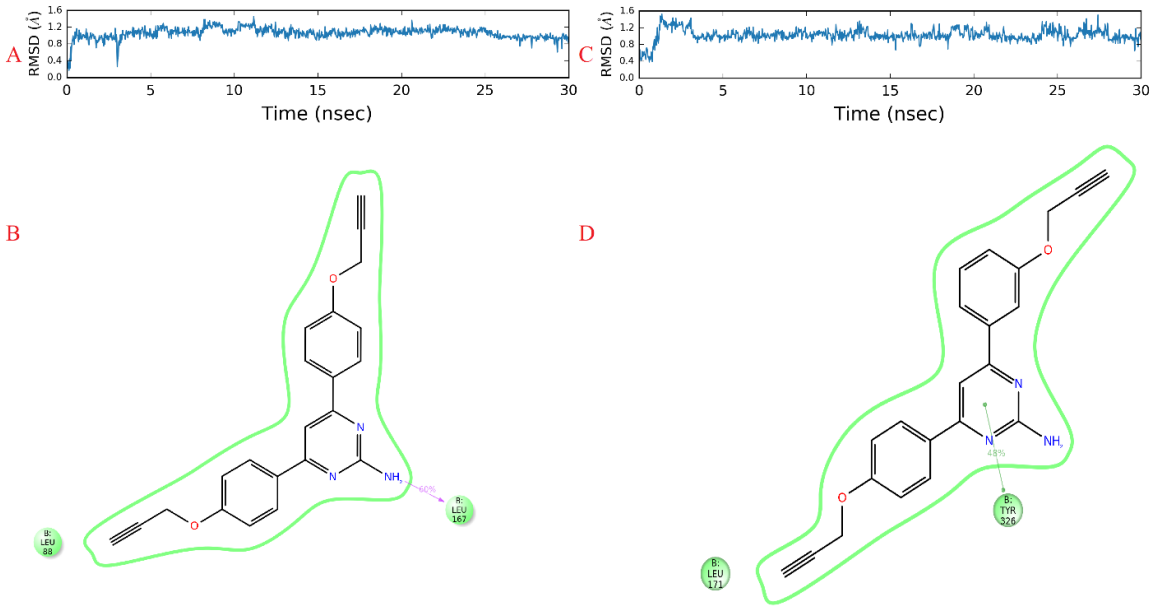

Fig. 5.29 A) RMSD graph of MD simulations studies of **AVB1** with MAO-B for 30 ns, **B**) interactions of **AVB1** with the active site residues of MAO-B during 30 ns MD simulations studies, **C)** RMSD graph of MD simulations studies of **AVB4** with MAO-B for 30 ns, and **D**) interactions of **AVB4** with the active site residues of MAO-B during 30 ns MD simulation studies

Similarly, docking complexes of **AVB1** and **AVB4** with AChE were used for MD simulations to determine their binding stability at the active site of enzyme (Fig. 5.30). In case of **AVB4,** a stable trajectory was observed after the initial 3 ns interval which was determined through RMSD of the protein backbone ranging from 0.8 Å to 1.2 Å. For the first 3 ns time interval, a hike in RMSD trajectory was observed from 0.4 Å to 0.8 Å. In case of **AVB1,** RMSD kept oscillating from 0.4 Å to 1.2 Å throughout the MD simulations studies of 30 ns. Analyzing these MD trajectories of AChE-AVB1 and AChE-AVB4 complexes, it can be concluded that these

compounds (**AVB1** and **AVB4**) had strong tendency to be localized in the binding region of AChE. One of the propargyl substituted ring of **AVB1** maintained its initial π-π interaction with Trp84. Similarly, for **AVB4** the initial interactions such as hydrogen bond formation of pyrimidine ring with Tyr121 and π-π interactions of pyrimidine ring with Trp84 were maintained throughout the MD simulations time interval. Thus, from these studies, it can be concluded that, MD simulations of **AVB1** and **AVB4** does not indicate any abrupt local force that could potentially break up the inhibitors or can even delocalize these from the binding site of AChE.

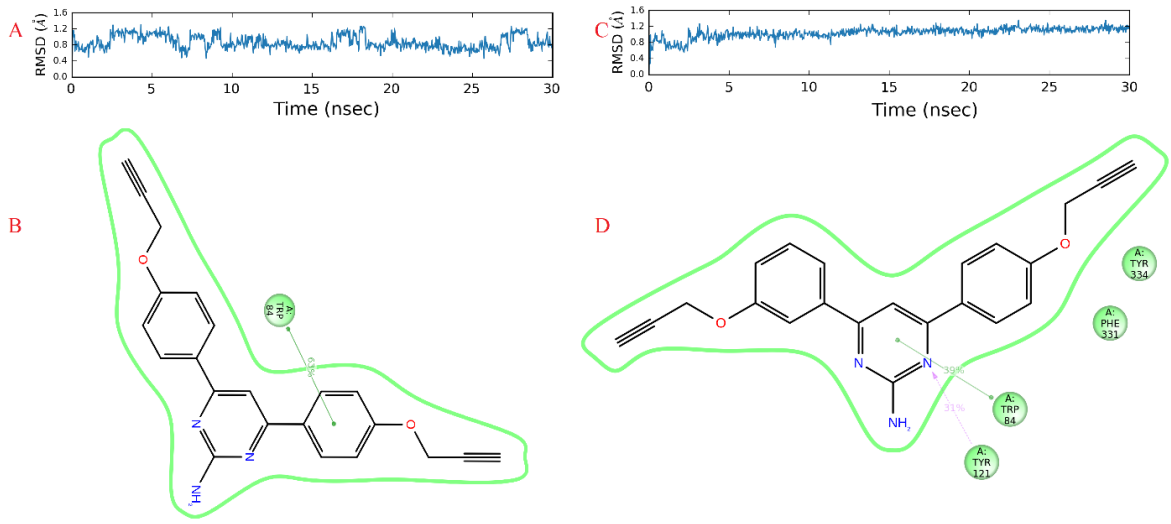

Fig. 5.30 A) RMSD graph of MD simulations studies of **AVB1** with AChE for 30 ns, **B**) interactions of **AVB1** with the active site residues of AChE during 30 ns MD simulation studies, **C)** RMSD graph of MD simulations studies of **AVB4** with AChE for 30 ns, and **D**) interactions of **AVB4** with the active site residues of AChE during 30 ns MD simulation studies

5.4.3.3 Physiochemical properties

In order to assess the drug-like characteristics of the most active compounds (**AVB1** and **AVB4**), various physicochemical parameters of these compounds have been evaluated. Both the compounds are bearing good drug like properties and follows the Lipinski's rule of five. The logP value of both the compounds is less than five and hydrogen bond donor and acceptor atoms are also less than five. Both the compounds, showed the 100% human oral absorption in Qikprop studies. The QPlogBB value is also in optimum range which proves that these compounds can cross the blood-brain barrier. Thus, it can be concluded that both of these

compounds have optimum chemical skeleton to be developed as potential drug molecules.

Table 5.8. Physiochemical properties of some of the potent and selective MAO inhibitors.

Compound number	**Mol. Wt.**	**Log P**	**HB donor**	**HB acceptor**	**% human oral absorption**	**QPlogBB (**Optimum range -3.0 to 1.2)	**BBB permeability predicted**
AVB1	355.39	4.52	3	4	100	-0.934	+ve
AVB4	355.39	4.51	3	4	100	-0.93	+ve

+ ve = blood-brain barrier permeable; - ve = no permeability to the blood-brain barrier

5.4.3.4 SAR studies

In the series-III, biphenylpyrimidines containing two propargyl groups were designed and synthesized. A total of 19 compounds were synthesized and evaluated against MAO-A, MAO-B and AChE enzymes. Most of the compounds of this series were found to be selective inhibitors of MAO-B isoform and also displayed potent AChE inhibitory activities. As evident from Table 5.7, **AVB1** with propargyl groups at the para positions of the phenyl rings and a NH_2 group on the pyrimidine ring displayed IC_{50} values of 1.74 ± 0.07 µM and 1.35 ±0.03 µM for MAO-B and AChE respectively. **AVB1** was found to be the most potent AChE inhibitor in the reported series of compounds. Replacement of NH_2 with CH_3 in **AVB2** reduced MAO-B inhibitory activity by more than 2-folds but retained AChE inhibition activity. Replacing NH_2 with phenyl ring in **AVB3** further reduced the MAO-B inhibitory activity by almost 4-folds and AChE inhibition activity by more than 5-folds. Shifting of one of the propargyl group from para (**AVB1**) to meta position (**AVB4**) significantly increased MAO-B inhibitory activity by more than 2-folds and retained AChE inhibition activity. **AVB4** was found to be the most potent MAO-B inhibitor in the series with an IC_{50} value of 1.49 ± 0.09 µM. Replacement of NH_2 group of **AVB4** by CH_3 (**AVB5**) and phenyl (**AVB6**) groups reduced the MAO-B inhibitory activity by more than 5-folds and 12-folds respectively and AChE inhibitory activity was reduced by about 3-folds. Shifting of propargyl group from meta (**AVB4**) to ortho position (**AVB7** to **AVB9**) of the phenyl ring proved detrimental and the MAO-B

inhibitory activity was found to be reduced by more than 14-folds. Similarly, reduced MAO-B inhibitory activity was observed when both the phenyl rings were substituted by propargyl groups at the meta positions (**AVB10** and **AVB11**) and at ortho positions (**AVB12** and **AVB13**). Presence of additional substituents at the phenyl ring (**AVB14** and **AVB19**) were also found unfavorable for the MAO-B and AChE inhibitory activitie

Chapter- 6
Summary and Conclusion

Alzheimer's disease (AD) is multifactorial in nature, and different enzymes including MAO, AChE, and amyloid beta are implicated in its pathogenesis. The pathomechanism of AD is complex and single target drugs proved to be ineffective for the treatment of the disease. Thus, a multitarget directed approach is being explored for the development of effective drug candidates for the treatment of AD. A drug active on multiple targets may be characterized by an improved efficacy when compared with a highly selective pharmacological agent. Multitarget activities may potentiate efficacy either additively or synergistically and be less prone to the drug resistance. In the current research studies, we have designed, synthesized and screened three different series of 4,6-diphenylpyrimidines as multipotent inhibitors of monoamine oxidase and acetylcholinesterase enzymes for the treatment of Alzheimer's disease.

With an aim of developing dual/multipotent inhibitors, 4,6-diphenylpyrimidines were optionally substituted with propargyl group and an ethyl chain containing a cyclic or acyclic tertiary nitrogen atom (piperidine/morpholine/pyrrolidine/N,N-dimethyl) as potential pharmacophores for MAO and AChE enzymes. In the first series of target compounds, one of the phenyl rings of diphenylpyrimidines was optionally substituted with a morpholine or piperidine ethyl chain while other phenyl ring was functionalized with an *O*-propargyl group at ortho, meta, or para positions. These compounds were found to be potent inhibitors of both MAO and AChE enzymes with IC_{50} values in sub-micro molar to nano molar range. Compound **VB1** was found to be the most potent MAO-A and BuChE inhibitor with IC_{50} values of 18.34 541 ± 0.38 nM and 0.66 ± 0.03 µM, respectively. It also displayed potent AChE inhibitory activity with an IC_{50} value of 30.46 ± 0.23 nM. **VB3** was another promising compound in this series with IC_{50} values of 28.33 ± 3.22 nM and 18.92 ± 0.29 nM against MAO-A and AChE, respectively. **VB8** was found to be the most potent AChE inhibitor with an IC_{50} value of 9.54 ± 0.07 nM and displayed very high SI (103) for AChE over BuChE. These compounds were found to be reversible inhibitors of MAO and AChE enzymes and non-toxic to the human neuroblastoma SH-SY5Y cells. In ROS inhibition studies compound **VB1** was found to reduce intracellular ROS level significantly (upto 65% reduction at 1µM concentration). In the molecular simulation studies, the most potent MAO inhibitor i.e. **VB1** and most potent AChE inhibitor i.e. **VB8** were found quite stable in the active sites of the enzymes. These compounds

also displayed neuroprotective potential against 6-hydroxydopamine (6-OHDA) induced neurotoxicity in SH-SY5Y cells.

Series-II was designed on the basis of structure-activity relationship analysis of the first series of compounds. It has been observed that the compounds with piperidine/morpholine ethyl chain at the para position of the phenyl ring were more active as compared to the meta and ortho derivatives. Thus in the second series of compounds, the position of piperidine/morpholine/pyrrolidine/N,N-dimethyl ethyl chain was fixed at the para position of one of the phenyl ring of diphenylpyrimidine and other ring was optionally substituted with propargylamine group. In this series, compound **VP15** was found to be a multi-potent inhibitor of MAO-B and AChE with IC_{50} values of 0.37 ± 0.03 µM and 0.04 ± 0.003 µM respectively. **VP15** was found to be selective for MAO-B with SI of 270 over MAO-A. It also displayed SI of 625 for AChE over BuChE. **VP15** was found irreversible inhibitor of MAO-B. **VP1** was found to be the most potent MAO-B inhibitor in the series with an IC_{50} value of 0.04 ± 0.002 µM with high SI over MAO-A (248 fold). These compounds were found irreversible inhibitors of MAO-B. Most potent compounds of this series were found to have potential neuroprotective properties. Compound **VB14** was found most potent neuroprotective agent with recovery of cell viability upto 83% at 1µM concentration. Similarly, **VP1**, **VP2** and **VP15** also showed cell viability recovery to 64%, 71% and 68% respectively at 5 µM concentration.

In the series-III of target compounds, both the phenyl rings of diphenylpyrimidines were substituted with *O*-propargyl groups. Different derivatives have been synthesized with *O*-propargyl groups substituted at ortho, meta and para positions of the phenyl rings. In the third series of compounds, **AVB1** and **AVB4** were found to be the most potent inhibitors of AChE and MAO-B with IC_{50} values of 1.35 ±0.03 µM and 1.49 ± 0.09 µM respectively. In the reversible inhibition studies, the lead compounds were found to be reversible inhibitors of MAO-B and AChE enzymes. In the ROS protection inhibition studies, **AVB1** and **AVB4** displayed good activity in SH-SY5Y cells and **AVB1** reduced the ROS levels up to 30% at 5 µM. This series of compounds were also found to be non-toxic to the SH-SY5Y cells in the cytotoxicity studies.

Thus, from the present study it can be concluded that 4,6-diphenylpyrimidine derivatives can act as potential lead for the development of effective drug candidate for the treatment of AD. Compound **VB3** and **VP15** were found to be the most potent dual inhibitors of MAO and AChE. Initial studies for blood-brain barrier permeability has been conducted *in vivo* with **VP15** using wistar male rats. The compound was detected in the LCMS analysis of the extracts of rat brain tissues. Detail studies need to be performed for other lead compounds too. In docking studies from binding mode of compounds it was observed that pyrimidine moiety of compounds was oriented toward FAD co-factor. Thus, if propargyl group is substituted at option available between two nitrogen atoms of pyrimidine, it can bind to FAD co-factor and can give more potent MAO inhibition along with AChE inhibition.

References

Agis-Torres, A., Sollhuber, M., Fernandez, M., and Sanchez-Montero, J. (2014). Multi-target-directed ligands and other therapeutic strategies in the search of a real solution for Alzheimer's disease. *Current Neuropharmacology,* **12:** 2-36.

Albuquerque, E., Santos, M., Alkondon, M., Pereira, E., and Maelicke, A. (2001). Modulation of nicotinic receptor activity in the central nervous system: a novel approach to the treatment of Alzheimer disease. *Alzheimer Disease & Associated Disorders,* **15:** S19-S25.

Alzheimer's, A. (2013). 2013 Alzheimer's disease facts and figures. *Alzheimer's & Dementia,* **9:** 208-245.

Alzheimer's, A. (2017). 2017 Alzheimer's disease facts and figures. *Alzheimer's & Dementia,* **13:** 325-373.

Alzheimer, A. (1907). *A Characteristic Disease of the Cerebral Cortex: Meeting of South-West Germany Psychiatrists Held in Tubingen on November 3rd and 4th, 1906*.

Amouyal-Barkate, K., Bagheri-Charabiani, H., Montastruc, J. L., Moulias, S., and Vellas, B. (2000). Abnormal movements with donepezil in Alzheimer disease. *Annals of Pharmacotherapy,* **34:** 1347-1347.

Anand, P., and Singh, B. (2013). A review on cholinesterase inhibitors for Alzheimer's disease. *Archives of Pharmacal Research,* **36:** 375-399.

Andres, A. M., Soldevila, M., Navarro, A., Kidd, K. K., Oliva, B., and Bertranpetit, J. (2004). Positive selection in MAOA gene is human exclusive: determination of the putative amino acid change selected in the human lineage. *Human Genetics,* **115:** 377-386.

Avramovich-Tirosh, Y., Amit, T., Bar-Am, O., Zheng, H., Fridkin, M., and Youdim, M. B. (2007). Therapeutic targets and potential of the novel brain-permeable multifunctional iron chelator–monoamine oxidase inhibitor drug, M-30, for the treatment of Alzheimer's disease1. *Journal of neurochemistry,* **100:** 490-502.

Bar-Am, O., Amit, T., Weinreb, O., Youdim, M. B., and Mandel, S. (2010). Propargylamine containing Compounds as modulators of proteolytic cleavage of amyloid protein precursor: involvement of MAPK and PKC activation. *Journal of Alzheimer's Disease,* **21:** 361-371.

Bar-Am, O., Amit, T., and Youdim, M. B. (2007). Aminoindan and hydroxyaminoindan, metabolites of rasagiline and ladostigil, respectively,

exert neuroprotective properties in vitro. *Journal of Neurochemistry,* **103:** 500-508.

Barnham, K. J., Masters, C. L., and Bush, A. I. (2004). Neurodegenerative diseases and oxidative stress. *Nature Rreviews Drug Discovery,* **3:** 205.

Bartus, R. T., Dean, R. r., Beer, B., and Lippa, A. S. (1982). The cholinergic hypothesis of geriatric memory dysfunction. *Science, 217*(4558), 408-414.

Bautista-Aguilera, O. M., Samadi, A., Chioua, M., Nikolic, K., Filipic, S., Agbaba, D., Soriano, E., de Andres, L., Rodríguez-Franco, M. I., and Alcaro, S. (2014). N-Methyl-N-((1-methyl-5-(3-(1-(2-methylbenzyl) piperidin-4-yl) propoxy)-1 H-indol-2-yl) methyl) prop-2-yn-1-amine, a New Cholinesterase and Monoamine Oxidase Dual Inhibitor. *Journal of Medicinal Chemistry,* **57:** 10455-10463.

Bernardo, A., Harrison, F. E., McCord, M., Zhao, J., Bruchey, A., Davies, S. S., Roberts II, L. J., Mathews, P. M., Matsuoka, Y., and Ariga, T. (2009). Elimination of GD3 synthase improves memory and reduces amyloid-β plaque load in transgenic mice. *Neurobiology of Aging,* **30:** 1777-1791.

Bickel, U., Thomsen, T., Weber, W., Fischer, J. P., Bachus, R., Nitz, M., and Kewitz, H. (1991). Pharmacokinetics of galanthamine in humans and corresponding cholinesterase inhibition. *Clinical Pharmacology & Therapeutics,* **50:** 420-428.

Binda, C., Mattevi, A., and Edmondson, D. E. (2011). Structural properties of human monoamine oxidases A and B. *International Review of Neurobiology,* **100:** 1-11.

Binda, C., Newton-Vinson, P., Hubálek, F., Edmondson, D. E., and Mattevi, A. (2002). Structure of human monoamine oxidase B, a drug target for the treatment of neurological disorders. *Nature Structural and Molecular Biology,* **9:** 22-26.

Binda, C., Wang, J., Pisani, L., Caccia, C., Carotti, A., Salvati, P., Edmondson, D. E., and Mattevi, A. (2007). Structures of human monoamine oxidase B complexes with selective noncovalent inhibitors: safinamide and coumarin analogs. *Journal of Medicinal Chemistry,* **50:** 5848-5852.

Birks, J. S., Chong, L. Y., and Grimley Evans, J. (2015). Rivastigmine for Alzheimer's disease. *The Cochrane Library*, **10:** 1-206.

Bolea, I., Gella, A., and Unzeta, M. (2013). Propargylamine-derived multitarget-directed ligands: fighting Alzheimer's disease with monoamine oxidase inhibitors. *Journal of Neural Transmission,* **120:** 893-902.

Bolea, I., Juarez-Jimenez, J., de los Rıos, C., Chioua, M., Pouplana, R., Luque, F. J., Unzeta, M., Marco-Contelles, J., and Samadi, A. (2011). Synthesis, biological evaluation, and molecular modeling of donepezil and N-[(5-(benzyloxy)-1-methyl-1 H-indol-2-yl) methyl]-N-methylprop-2-yn-1-amine hybrids as new multipotent cholinesterase/monoamine oxidase inhibitors for the treatment of Alzheimer's disease. *Journal of Medicinal Chemistry,* **54:** 8251-8270.

Bollen, E., and Prickaerts, J. (2012). Phosphodiesterases in neurodegenerative disorders. *IUBMB life,* **64:** 965-970.

Bonivento, D., Milczek, E. M., McDonald, G. R., Binda, C., Holt, A., Edmondson, D. E., and Mattevi, A. (2010). Potentiation of ligand binding through cooperative effects in monoamine oxidase B. *Journal of Biological Chemistry,* **285:** 36849-36856.

Bortolato, M., Chen, K., and Shih, J. C. (2008). Monoamine oxidase inactivation: from pathophysiology to therapeutics. *Advanced Drug Delivery Reviews,* **60:** 1527-1533.

Brown, D. R., and Kozlowski, H. (2004). Biological inorganic and bioinorganic chemistry of neurodegeneration based on prion and Alzheimer diseases. *Dalton Transactions,* **0:** 1907-1917.

Brufani, M., Filocamo, L., Lappa, S., and Maggi, A. (1997). New acetylcholinesterase inhibitors. *Drugs of the Future,* **22:** 397-410.

Bryant, C., Ouldred, E., Jackson, S., and Kinirons, M. (1998). Purpuric rash with donepezil treatment. *British Medical Journal,* **317:** 787.

Burch, D., Asgharnejad, M., Gerson, W., Fielding, R. M., and Azzaro, A. J. (2014). Lack of tyramine pressor response effect with oral CX157: A specific reversible MAOI. *Clinical Pharmacology in Drug Development,* **3**: 4-12.

Burns, A., Rossor, M., Hecker, J., Gauthier, S., Petit, H., Möller, H.-J., Rogers, S., and Friedhoff, L. (1999). The Effects of Donepezil in Alzheimer's Disease–Results from a Multinational Trial1. *Dementia and Geriatric Cognitive Disorders,* **10:** 237-244.

Bystrowska, B., Adamczyk, P., Moniczewski, A., Zaniewska, M., Fuxe, K., and Filip, M. (2012). LC/MS/MS evaluation of cocaine and its metabolites in different brain areas, peripheral organs and plasma in cocaine self-administering rats. *Pharmacological Reports,* **64:** 1337-1349.

Cai, P., Fang, S.-Q., Yang, X.-L., Wu, J.-J., Liu, Q.-H., Hong, H., Wang, X.-B., and Kong, L.-Y. (2017). Rational Design and Multibiological Profiling of Novel Donepezil–Trolox Hybrids against Alzheimer's Disease, with Cholinergic, Antioxidant, Neuroprotective, and Cognition Enhancing Properties. *ACS Chemical Neuroscience,* **8**: 2496-2511.

Cai, Z. (2014). Monoamine oxidase inhibitors: promising therapeutic agents for Alzheimer's disease. *Molecular Medicine Reports,* **9**: 1533-1541.

Camacho, I. E., Serneels, L., Spittaels, K., Merchiers, P., Dominguez, D., and De Strooper, B. (2004). Peroxisome proliferator-activated receptor γ induces a clearance mechanism for the amyloid-β peptide. *Journal of Neuroscience,* **24:** 10908-10917.

Caricasole, A., Copani, A., Caraci, F., Aronica, E., Rozemuller, A. J., Caruso, A., Storto, M., Gaviraghi, G., Terstappen, G. C., and Nicoletti, F. (2004). Induction of Dickkopf-1, a negative modulator of the Wnt pathway, is associated with neuronal degeneration in Alzheimer's brain. *Journal of Neuroscience,* **24:** 6021-6027.

Cavalli, A., Bolognesi, M. L., Minarini, A., Rosini, M., Tumiatti, V., Recanatini, M., and Melchiorre, C. (2008). Multi-target-directed ligands to combat neurodegenerative diseases. *Journal of Medicinal Chemistry,* **51:** 347-372.

Cecilia Rodrigues Simoes, M., Pereira Dias Viegas, F., Soares Moreira, M., de Freitas Silva, M., Maximo Riquiel, M., Mattos da Rosa, P., Rosa Castelli, M., Henrique dos Santos, M., Gomes Soares, M., and Viegas, C. (2014). Donepezil: an important prototype to the design of new drug candidates for Alzheimer's disease. *Mini Reviews in Medicinal Chemistry,* **14**: 2-19.

Chen, J. J., Swope, D. M., and Dashtipour, K. (2007). Comprehensive review of rasagiline, a second-generation monoamine oxidase inhibitor, for the treatment of Parkinson's disease. *Clinical Therapeutics,* **29:** 1825-1849.

Cheung, J., Rudolph, M. J., Burshteyn, F., Cassidy, M. S., Gary, E. N., Love, J., Franklin, M. C., and Height, J. J. (2012). Structures of human

acetylcholinesterase in complex with pharmacologically important ligands. *Journal of Medicinal Chemistry,* **55:** 10282-10286.

Chimenti, F., Carradori, S., Secci, D., Bolasco, A., Bizzarri, B., Chimenti, P., Granese, A., Yanez, M., and Orallo, F. (2010). Synthesis and inhibitory activity against human monoamine oxidase of N1-thiocarbamoyl-3, 5-di (hetero) aryl-4, 5-dihydro-(1H)-pyrazole derivatives. *European Journal of Medicinal Chemistry,* **45:** 800-804.

Christen, Y. (2000). Oxidative stress and Alzheimer disease. *The American Journal of Clinical Nutrition,* **71:** 621S-629S.

Coyle, J. T., Price, D. L., and Delong, M. R. (1983). Alzheimer's disease: a disorder of cortical cholinergic innervation. *Science,* **219:** 1184-1190.

Cummings, J. L., Ross, W., Absher, J., Gornbein, J., and Hadjiaghai, L. (1995). Depressive symptoms in Alzheimer disease: assessment and determinants. *Alzheimer Disease & Associated Disorders,* **9:** 87-93.

Czarnecka, K., Chufarova, N., Halczuk, K., Maciejewska, K., Girek, M., Skibiński, R., Jończyk, J., Bajda, M., Kabziński, J., and Majsterek, I. (2018). Tetrahydroacridine derivatives with dichloronicotinic acid moiety as attractive, multipotent agents for Alzheimer's disease treatment. *European Journal of Medicinal Chemistry,* **145:** 760-769.

Czollner, L., Frantsits, W., Küenburg, B., Hedenig, U., Fröhlich, J., and Jordis, U. (1998). New kilogram-synthesis of the anti-alzheimer drug (−)-galanthamine. *Tetrahedron Letters,* **39:** 2087-2088.

d'Abramo, C., Massone, S., Zingg, J.-M., Pizzuti, A., Marambaud, P., Dalla Piccola, B., Azzi, A., Marinari, U. M., Pronzato, M. A., and Ricciarelli, R. (2005). Role of peroxisome proliferator-activated receptor γ in amyloid precursor protein processing and amyloid β-mediated cell death. *Biochemical Journal,* **391:** 693-698.

Davis, K. L., Thal, L. J., Gamzu, E. R., Davis, C. S., Woolson, R. F., Gracon, S. I., Drachman, D. A., Schneider, L. S., Whitehouse, P. J., and Hoover, T. M. (1992). A double-blind, placebo-controlled multicenter study of tacrine for Alzheimer's disease. *New England Journal of Medicine,* **327:** 1253-1259.

De Colibus, L., Li, M., Binda, C., Lustig, A., Edmondson, D. E., and Mattevi, A. (2005). Three-dimensional structure of human monoamine oxidase A (MAO

A): relation to the structures of rat MAO A and human MAO B. *Proceedings of the National Academy of Sciences,* **102:** 12684-12689.

Denya, I., Malan, S. F., Enogieru, A. B., Omoruyi, S. I., Ekpo, O. E., Kapp, E., Zindo, F. T., and Joubert, J. (2018). Design, synthesis and evaluation of indole derivatives as multifunctional agents against Alzheimer's disease. *MedChemComm,* **9**: 357-370.

Du, H., Guo, L., Fang, F., Chen, D., Sosunov, A. A., McKhann, G. M., Yan, Y., Wang, C., Zhang, H., and Molkentin, J. D. (2008). Cyclophilin D deficiency attenuates mitochondrial and neuronal perturbation and ameliorates learning and memory in Alzheimer's disease. *Nature Medicine,* **14:** 1097.

Du, L., Bakish, D., Ravindran, A., and Hrdina, P. D. (2004). MAO-A gene polymorphisms are associated with major depression and sleep disturbance in males. *Neuroreport,* **15:**, 2097-2101.

Eagger, S. A., Levy, R., and Sahakian, B. J. (1991). Tacrine in Alzheimer's disease. *The Lancet,* **337:** 989-992.

Francis, P. T., Palmer, A. M., Snape, M., and Wilcock, G. K. (1999). The cholinergic hypothesis of Alzheimer’s disease: a review of progress. *Journal of Neurology, Neurosurgery & Psychiatry,* **66:** 137-147.

Friesner, R. A., Murphy, R. B., Repasky, M. P., Frye, L. L., Greenwood, J. R., Halgren, T. A., Sanschagrin, P. C., and Mainz, D. T. (2006). Extra precision glide: Docking and scoring incorporating a model of hydrophobic enclosure for protein− ligand complexes. *Journal of Medicinal Chemistry,* **49:** 6177-6196.

Fuller, R. W. (1978). Selectivity among monoamine oxidase inhibitors and its possible importance for development of antidepressant drugs. *Progress in Neuro-Psychopharmacology,* **2:** 303-311.

Garcia-Alloza, M., Gil-Bea, F., Diez-Ariza, M., Chen, C.-H., Francis, P. T., Lasheras, B., and Ramirez, M. (2005). Cholinergic–serotonergic imbalance contributes to cognitive and behavioral symptoms in Alzheimer’s disease. *Neuropsychologia,* **43:** 442-449.

Gauthier, S. (2002). Advances in the pharmacotherapy of Alzheimer's disease. *Canadian Medical Association Journal,* **166:** 616-623.

Geerts, H., Guillaumat, P.-O., Grantham, C., Bode, W., Anciaux, K., and Sachak, S. (2005). Brain levels and acetylcholinesterase inhibition with galantamine and donepezil in rats, mice, and rabbits. *Brain Research,* **1033:** 186-193.

Goedert, M., Spillantini, M., Jakes, R., Rutherford, D., and Crowther, R. (1989). Multiple isoforms of human microtubule-associated protein tau: sequences and localization in neurofibrillary tangles of Alzheimer's disease. *Neuron,* **3**: 519-526.

Goedert Michel, and Spillantini, M. G. (2006). A century of Alzheimer's disease. *Science,* **314:** 777-781.

Gura, T. (2008). Hope in Alzheimer's fight emerges from unexpected places. *Nature Medicine,* **14:** 894-894.

Haass, C., Lemere, C. A., Capell, A., Citron, M., Seubert, P., Schenk, D., Lannfelt, L., and Selkoe, D. J. (1995). The Swedish mutation causes early-onset Alzheimer's disease by β-secretase cleavage within the secretory pathway. *Nature Medicine,* **1:**1291.

Hardy, J. (1997). Amyloid, the presenilins and Alzheimer's disease. *Trends in Neurosciences,* **20:** 154-159.

Hardy, J. (2006). Alzheimer's disease: the amyloid cascade hypothesis: an update and reappraisal. *Journal of Alzheimer's Disease,* **9:** 151-153.

Hardy, J., and Selkoe, D. J. (2002). The amyloid hypothesis of Alzheimer's disease: progress and problems on the road to therapeutics. *Science,* **297:** 353-356.

Harel, M., Schalk, I., Ehret-Sabatier, L., Bouet, F., Goeldner, M., Hirth, C., Axelsen, P., Silman, I., and Sussman, J. (1993). Quaternary ligand binding to aromatic residues in the active-site gorge of acetylcholinesterase. *Proceedings of the National Academy of Sciences,* **90:** 9031-9035.

Hashimoto, M., Imamura, T., Tanimukai, S., Kazui, H., and Mori, E. (2000). Urinary incontinence: an unrecognised adverse effect with donepezil. *The Lancet,* **356:** 568.

Hooper, C., Killick, R., and Lovestone, S. (2008). The GSK3 hypothesis of Alzheimer's disease. *Journal of Neurochemistry,* **104:** 1433-1439.

Hroudová, J., Singh, N., Fišar, Z., and Ghosh, K. K. (2016). Progress in drug development for Alzheimer's disease: An overview in relation to mitochondrial energy metabolism. *European Journal of Medicinal Chemistry*, **121:** 774-784.

Hu, J., Huang, Y.-D., Pan, T., Zhang, T., Su, T., Li, X., Luo, H.-B., and Huang, L. (2018). Design, Synthesis, and Biological Evaluation of Dual-Target Inhibitors of Acetylcholinesterase (AChE) and Phosphodiesterase 9A (PDE9A) for the Treatment of Alzheimer's Disease. *ACS Chemical Neuroscience*, **10:** 537-551.

Hubálek, F., Binda, C., Khalil, A., Li, M., Mattevi, A., Castagnoli, N., and Edmondson, D. E. (2005). Demonstration of isoleucine 199 as a structural determinant for the selective inhibition of human monoamine oxidase B by specific reversible inhibitors. *Journal of Biological Chemistry,* **280:** 15761-15766.

Hughes, R. E., Nikolic, K., and Ramsay, R. R. (2016). One for all? Hitting multiple Alzheimer's disease targets with one drug. *Frontiers in Neuroscience,* **10:** 177.

Inestrosa, N. C., Alvarez, A., Perez, C. A., Moreno, R. D., Vicente, M., Linker, C., Casanueva, O. I., Soto, C., and Garrido, J. (1996). Acetylcholinesterase accelerates assembly of amyloid-β-peptides into Alzheimer's fibrils: possible role of the peripheral site of the enzyme. *Neuron,* **16:** 881-891.

Jakob-Roetne, R., and Jacobsen, H. (2009). Alzheimer's disease: from pathology to therapeutic approaches. *Angewandte Chemie International Edition,* **48:** 3030-3059.

Jiang, X.-Y., Chen, T.-K., Zhou, J.-T., He, S.-Y., Yang, H.-Y., Chen, Y., Qu, W., Feng, F., and Sun, H.-P. (2018). Dual GSK-3β/AChE Inhibitors as a New Strategy for Multitargeting Anti-Alzheimer's Disease Drug Discovery. *ACS Medicinal Chemistry Letters,* **9:** 171-176.

Kalb, A., von Haefen, C., Sifringer, M., Tegethoff, A., Paeschke, N., Kostova, M., Feldheiser, A., and Spies, C. D. (2013). Acetylcholinesterase inhibitors reduce neuroinflammation and-degeneration in the cortex and hippocampus of a surgery stress rat model. *PLoS One,* **8:** e62679.

Kaur, N., Dhiman, M., Perez-Polo, J. R., and Mantha, A. K. (2015). Ginkgolide B revamps neuroprotective role of apurinic/apyrimidinic endonuclease 1 and mitochondrial oxidative phosphorylation against Aβ25–35-induced neurotoxicity in human neuroblastoma cells. *Journal of Neuroscience Research,* **93:** 938-947.

Kilgore, M., Miller, C. A., Fass, D. M., Hennig, K. M., Haggarty, S. J., Sweatt, J. D., and Rumbaugh, G. (2010). Inhibitors of class 1 histone deacetylases reverse contextual memory deficits in a mouse model of Alzheimer's disease. *Neuropsychopharmacology,* **35:** 870.

Kitamura, Y., Shimohama, S., Koike, H., Kakimura, J.-i., Matsuoka, Y., Nomura, Y., Gebicke-Haerter, P. J., and Taniguchi, T. (1999). Increased expression of cyclooxygenases and peroxisome proliferator-activated receptor-γ in Alzheimer's disease brains. *Biochemical and Biophysical Research Communications,* **254:** 582-586.

Klafki, H.-W., Staufenbiel, M., Kornhuber, J., and Wiltfang, J. (2006). Therapeutic approaches to Alzheimer's disease. *Brain,* **129:** 2840-2855.

Knapp, M. J., Knopman, D. S., Solomon, P. R., Pendlebury, W. W., Davis, C. S., Gracon, S. I., Apter, J. T., Lazarus, C. N., Baker, K. E., and Barnett, M. (1994). A 30-week randomized controlled trial of high-dose tacrine in patients with Alzheimer's disease. *Jama,* **271:** 985-991.

Kumar, A., Nisha, C. M., Silakari, C., Sharma, I., Anusha, K., Gupta, N., Nair, P., Tripathi, T., and Kumar, A. (2016). Current and novel therapeutic molecules and targets in Alzheimer's disease. *Journal of the Formosan Medical Association,* **115:** 3-10.

Kumar, B., Gupta, V., and Kumar, V. (2015). A Perspective on Monoamine Oxidase Enzyme as Drug Target: Challenges and Opportunities. *Current Drug Targets*, **18:** 87-97.

Kumar, B., Kumar, M., Dwivedi, A. R., and Kumar, V. (2018). Synthesis, Biological Evaluation and Molecular Modeling Studies of Propargyl-Containing 2, 4, 6-Trisubstituted Pyrimidine Derivatives as Potential Anti-Parkinson Agents. *ChemMedChem,* **13:** 705-712.

Kumar, B., Mantha, A. K., and Kumar, V. (2016). Recent developments on the structure–activity relationship studies of MAO inhibitors and their role in different neurological disorders. *RSC Advances,* **6:** 42660-42683.

Kumar, B., Sheetal, Mantha, A. K., and Kumar, V. (2018). Synthesis, Biological Evaluation and Molecular Modeling Studies of Phenyl-/Benzhydrylpiperazine Derivatives as Potential MAO Inhibitors. *Bioorgnic Chemistry,* **77:** 252-262.

Kumar, D., Gupta, S. K., Ganeshpurkar, A., Gutti, G., Krishnamurthy, S., Modi, G., and Singh, S. K. (2018). Development of Piperazinediones as dual inhibitor

for treatment of Alzheimer's disease. *European Journal of Medicinal Chemistry,* **150**: 87-101.

Kung, H. F. (2012). The β-amyloid hypothesis in Alzheimer's disease: seeing is believing. *ACS Medicinal Chemistry Letters,* **3:** 265-267.

Li, P., and Bartlett, M. G. (2014). A review of sample preparation methods for quantitation of small-molecule analytes in brain tissue by liquid chromatography tandem mass spectrometry (LC-MS/MS). *Analytical Methods,* **6:** 6183-6207.

Liang, Z., Shi, F., Wang, Y., Lu, L., Zhang, Z., Wang, X., and Wang, X. (2011). Neuroprotective effects of tenuigenin in a SH-SY5Y cell model with 6-OHDA-induced injury. *Neuroscience Letters,* **497:** 104-109.

Lin, M. T., and Beal, M. F. (2006). Mitochondrial dysfunction and oxidative stress in neurodegenerative diseases. *Nature,* **443:** 787-795.

Lipton, S. A. (2005). The molecular basis of memantine action in Alzheimer's disease and other neurologic disorders: low-affinity, uncompetitive antagonism. *Current Alzheimer Research,* **2:** 155-165.

Marco-Contelles, J., do Carmo Carreiras, M., Rodríguez, C., Villarroya, M., and Garcia, A. G. (2006). Synthesis and pharmacology of galantamine. *Chemical Reviews,* **106:** 116-133.

Marco-Contelles, J., Unzeta, M., Bolea, I., Esteban, G., Ramsay, R. R., Romero, A., Martínez-Murillo, R., Carreiras, M. C., and Ismaili, L. (2016). ASS234, as a new multi-target directed Propargylamine for Alzheimer's Disease therapy. *Frontiers in Neuroscience,* **10:** 294.

Masters, C. L., Bateman, R., Blennow, K., Rowe, C. C., Sperling, R. A., and Cummings, J. L. (2015). Alzheimer's Disease. *Nature Reviews Disease Primers,* **1:** 1-18.

Mattson, M. P. (1997). Cellular actions of beta-amyloid precursor protein and its soluble and fibrillogenic derivatives. *Physiological reviews,* **77:** 1081-1132.

Mattson, M. P. (2004). Pathways towards and away from Alzheimer's disease. *Nature,* **430:** 631.

Melchor, J. P., Pawlak, R., and Strickland, S. (2003). The tissue plasminogen activator-plasminogen proteolytic cascade accelerates amyloid-β (Aβ) degradation and inhibits Aβ-induced neurodegeneration. *Journal of Neuroscience,* **23:** 8867-8871.

Milczek, E. M., Binda, C., Rovida, S., Mattevi, A., and Edmondson, D. E. (2011). The ‘gating’residues Ile199 and Tyr326 in human monoamine oxidase B function in substrate and inhibitor recognition. *FEBS Journal,* **278:** 4860-4869.

Minders, C., Petzer, J. P., Petzer, A., and Lourens, A. C. (2015). Monoamine oxidase inhibitory activities of heterocyclic chalcones. *Bioorganic and Medicinal Chemistry Letters,* **25:** 5270-5276.

Mohamed, T., and Rao, P. (2011). Alzheimer's disease: emerging trends in small molecule therapies. *Current Medicinal Chemistry,* **18:** 4299-4320.

Mohs, R. C., Doody, R., Morris, J., Ieni, J., Rogers, S., Perdomo, C., and Pratt, R. (2001). A 1-year, placebo-controlled preservation of function survival study of donepezil in AD patients. *Neurology,* **57:** 481-488.

Morawski, M., Schilling, S., Kreuzberger, M., Waniek, A., Jäger, C., Koch, B., Cynis, H., Kehlen, A., Arendt, T., and Hartlage-Rübsamen, M. (2014). Glutaminyl cyclase in human cortex: correlation with (pGlu)-amyloid-β load and cognitive decline in Alzheimer's disease. *Journal of Alzheimer's Disease,* **39:** 385-400.

Morphy, R., and Rankovic, Z. (2005). Designed multiple ligands. An emerging drug discovery paradigm. *Journal of Medicinal Chemistry,* **48:** 6523-6543.

Mostert, S., Mentz, W., Petzer, A., Bergh, J. J., and Petzer, J. P. (2012). Inhibition of monoamine oxidase by 8-[(phenylethyl) sulfanyl] caffeine analogues. *Bioorganic and Medicinal Chemistry,* **20:** 7040-7050.

Mucke, L., and Selkoe, D. J. (2012). Neurotoxicity of amyloid β-protein: synaptic and network dysfunction. *Cold Spring Harbor Perspectives in Medicine*, a006338.

Müller, T. J., Braun, R., and Ansorge, M. (2000). A Novel Three-Component One-Pot Pyrimidine Synthesis Based upon a Coupling− Isomerization Sequence. *Organic Letters,* **2:** 1967-1970.

Munoz-Torrero, D. (2008). Acetylcholinesterase inhibitors as disease-modifying therapies for Alzheimer's disease. *Current Medicinal Chemistry,* **15:** 2433-2455.

Naoi, M., and Maruyama, W. (2009). Functional mechanism of neuroprotection by inhibitors of type B monoamine oxidase in Parkinson's disease. *Expert Reviews on Neurotherapeutics,* **9:** 1233-1250.

Nolte, H.-J., Rosenberry, T. L., and Neumann, E. (1980). Effective charge on acetylcholinesterase active sites determined from the ionic strength

dependence of association rate constants with cationic ligands. *Biochemistry,* **19:** 3705-3711.

Oliveira Pedrosa, M. d., da Cruz, D., Marques, R., Viana, O., de Moura, R. O., Ishiki, H. M., Barbosa, F., Maria, J., Diniz, M. F., and Scotti, M. T. (2017). Hybrid Compounds as Direct Multitarget Ligands: A Review. *Current Topics in Medicinal Chemistry,* **17:** 1044-1079.

Onor, M. L., Trevisiol, M., and Aguglia, E. (2007). Rivastigmine in the treatment of Alzheimer's disease: an update. *Clinical Interventions in Aging,* **2:** 17.

Oset-Gasque, M. J. s., and Marco-Contelles, J. (2018). Alzheimer's Disease, the "One-Molecule, One-Target" Paradigm, and the Multitarget Directed Ligand Approach. *ACS Chemical Neuroscience,* **9:** 401-403.

Pákáski, M., and Kálmán, J. (2008). Interactions between the amyloid and cholinergic mechanisms in Alzheimer's disease. *Neurochemistry International,* **53:** 103-111.

Pérez-Torres, S., Cortés, R., Tolnay, M., Probst, A., Palacios, J. M., and Mengod, G. (2003). Alterations on phosphodiesterase type 7 and 8 isozyme mRNA expression in Alzheimer's disease brains examined by in situ hybridization. *Experimental Neurology,* **182:** 322-334.

Pérez-Torres, S., and Mengod, G. (2003). *cAMP-specific phosphodiesterases expression in Alzheimer's disease brains.* Paper presented at the International Congress Series.

Pizzinat, N., Copin, N., Vindis, C., Parini, A., and Cambon, C. (1999). Reactive oxygen species production by monoamine oxidases in intact cells. *Naunyn-Schmiedeberg's Archives of Pharmacology,* **359:** 428-431.

Polinsky, R. J., Holmes, K. V., Brown, R. T., and Weise, V. (1989). CSF acetylcholinesterase levels are reduced in multiple system atrophy with autonomic failure. *Neurology,* **39:** 40-40.

Proskurnina, N., and Yakovleva, A. (1952). Alkaloids of Galanthus woronowi. II. Isolation of a new alkaloid. *Zh Obschchei Khim (J Gen Chem),* **22:** 1899-1902.

Racchi, M., Mazzucchelli, M., Porrello, E., Lanni, C., and Govoni, S. (2004). Acetylcholinesterase inhibitors: novel activities of old molecules. *Pharmacological Research,* **50:** 441-451.

Release, Q. S. (2017). 1: QikProp. *Schrödinger, LLC, New York, NY*.

Release, S. (2014). 1: Desmond Molecular Dynamics System, version 3.7. *DE Shaw Research, New York, NY, Maestro-Desmond Interoperability Tools, version, 3*.

Reyes, A. E., Perez, D. R., Alvarez, A., Garrido, J., Gentry, M. K., Doctor, B. P., and Inestrosa, N. C. (1997). A monoclonal antibody against acetylcholinesterase inhibits the formation of amyloid fibrils induced by the enzyme. *Biochemical and Biophysical Research Communications,* **232:** 652-655.

Riederer, P., Danielczyk, W., and Grünblatt, E. (2004). Monoamine oxidase-B inhibition in Alzheimer's disease. *Neurotoxicology,* **25:** 271-277.

Sachs, J. N., and Engelman, D. M. (2006). Introduction to the membrane protein reviews: the interplay of structure, dynamics, and environment in membrane protein function. *Annual Review of Biochemistry,* **75:** 707-712.

Saido, T. C., Iwatsubo, T., Mann, D. M., Shimada, H., Ihara, Y., and Kawashima, S. (1995). Dominant and differential deposition of distinct β-amyloid peptide species, AβN3 (pE), in senile plaques. *Neuron,* **14:** 457-466.

Saito, K., Elce, J. S., Hamos, J. E., and Nixon, R. A. (1993). Widespread activation of calcium-activated neutral proteinase (calpain) in the brain in Alzheimer disease: a potential molecular basis for neuronal degeneration. *Proceedings of the National Academy of Sciences,* **90:** 2628-2632.

Samadi, A., Chioua, M., Bolea, I., de los Ríos, C., Iriepa, I., Moraleda, I., Bastida, A., Esteban, G., Unzeta, M., and Gálvez, E. (2011). Synthesis, biological assessment and molecular modeling of new multipotent MAO and cholinesterase inhibitors as potential drugs for the treatment of Alzheimer's disease. *European Journal of Medicinal Chemistry,* **46:** 4665-4668.

Samadi, A., de los Ríos, C., Bolea, I., Chioua, M., Iriepa, I., Moraleda, I., Bartolini, M., Andrisano, V., Gálvez, E., and Valderas, C. (2012). Multipotent MAO and cholinesterase inhibitors for the treatment of Alzheimer's disease: synthesis, pharmacological analysis and molecular modeling of heterocyclic substituted alkyl and cycloalkyl propargyl amine. *European Journal of Medicinal Chemistry,* **52:** 251-262.

Samanta, M. K., Wilson, B., Santhi, K., Kumar, K. S., and Suresh, B. (2006). Alzheimer disease and its management: a review. *American Journal of Therapeutics,* **13:** 516-526.

Sanchez-Mejia, R. O., Newman, J. W., Toh, S., Yu, G.-Q., Zhou, Y., Halabisky, B., Cissé, M., Scearce-Levie, K., Cheng, I. H., and Gan, L. (2008). Phospholipase A 2 reduction ameliorates cognitive deficits in a mouse model of Alzheimer's disease. *Nature Neuroscience,* **11:** 1311.

Sang, Z., Wang, K., Xue, H., Cao, M., Tan, Z., and Liu, W. (2018). Design, synthesis and evaluation of novel ferulic acid derivatives as multi-target-directed ligands for the treatment of Alzheimer's disease. *ACS Chemical Neuroscience*, **10:** 1008-1024.

Sano, M., Ernesto, C., Thomas, R. G., Klauber, M. R., Schafer, K., Grundman, M., Woodbury, P., Growdon, J., Cotman, C. W., and Pfeiffer, E. (1997). A controlled trial of selegiline, alpha-tocopherol, or both as treatment for Alzheimer's disease. *New England Journal of Medicine,* **336:** 1216-1222.

Sastre, M., Dewachter, I., Landreth, G. E., Willson, T. M., Klockgether, T., Van Leuven, F., and Heneka, M. T. (2003). Nonsteroidal anti-inflammatory drugs and peroxisome proliferator-activated receptor-γ agonists modulate immunostimulated processing of amyloid precursor protein through regulation of β-secretase. *Journal of Neuroscience,* **23:** 9796-9804.

Sastre, M., Roßner, S., Bogdanovic, N., Rosen, E., Dewachter, I., Borghgraef, P., Evert, B., Dumitrescu-Ozimek, L., Thal, D., and Landreth, G. (2005). NSAIDs repress BACE1 gene promoter activity by activation of PPARgamma. *Aktuelle Neurologie,* **32:** V66.

Saura, J., Luque, J., Cesura, A., Da Prada, M., Chan-Palay, V., Huber, G., Löffler, J., and Richards, J. (1994). Increased monoamine oxidase B activity in plaque-associated astrocytes of Alzheimer brains revealed by quantitative enzyme radioautography. *Neuroscience,* **62:** 15-30.

Savini, L., Gaeta, A., Fattorusso, C., Catalanotti, B., Campiani, G., Chiasserini, L., Pellerano, C., Novellino, E., McKissic, D., and Saxena, A. (2003). Specific targeting of acetylcholinesterase and butyrylcholinesterase recognition sites. Rational design of novel, selective, and highly potent cholinesterase inhibitors. *Journal of Medicinal Chemistry,* **46:** 1-4.

Saxena, A., Redman, A. M., Jiang, X., Lockridge, O., and Doctor, B. (1997). Differences in active site gorge dimensions of cholinesterases revealed by binding of inhibitors to human butyrylcholinesterase. *Biochemistry,* **36:** 14642-14651.

Scheuner, D., Eckman, C., Jensen, M., Song, X., Citron, M., Suzuki, N., Bird, T., Hardy, J., Hutton, M., and Kukull, W. (1996). Secreted amyloid β–protein similar to that in the senile plaques of Alzheimer's disease is increased in vivo by the presenilin 1 and 2 and APP mutations linked to familial Alzheimer's disease. *Nature Medicine,* **2:** 864.

Schilling, S., Zeitschel, U., Hoffmann, T., Heiser, U., Francke, M., Kehlen, A., Holzer, M., Hutter-Paier, B., Prokesch, M., and Windisch, M. (2008). Glutaminyl cyclase inhibition attenuates pyroglutamate Aβ and Alzheimer's disease–like pathology. *Nature Medicine,* **14:** 1106.

Selkoe, D. J. (2001). Alzheimer's disease: genes, proteins, and therapy. *Physiological Reviews,* **81:** 741-766.

Selkoe, D. J., and Schenk, D. (2003). Alzheimer's disease: molecular understanding predicts amyloid-based therapeutics. *Annual Review of Pharmacology and Toxicology,* **43:** 545-584.

Shih, J., and Thompson, R. (1999). Monoamine oxidase in neuropsychiatry and behavior. *American Journal of Human Genetics,* **65:** 593.

Small, G. W., and Greenfield, S. (2015). Current and future treatments for Alzheimer disease. *American Journal of Geriatric Psychiatry,* **23:** 1101-1105.

Son, S.-Y., Ma, J., Kondou, Y., Yoshimura, M., Yamashita, E., and Tsukihara, T. (2008). Structure of human monoamine oxidase A at 2.2-Å resolution: the control of opening the entry for substrates/inhibitors. *Proceedings of the National Academy of Sciences,* **105:** 5739-5744.

Soreq, H., and Seidman, S. (2001). Acetylcholinesterase—new roles for an old actor. *Nature Reviews Neuroscience,* **2:** 294.

Sramek, J. J., Frackiewicz, E. J., and Cutler, N. R. (2000). Review of the acetylcholinesterase inhibitor galanthamine. *Expert Opinion on Investigational Drugs,* **9:** 2393-2402.

Sterling, J., Herzig, Y., Goren, T., Finkelstein, N., Lerner, D., Goldenberg, W., Miskolczi, I., Molnar, S., Rantal, F., and Tamas, T. (2002). Novel dual inhibitors of AChE and MAO derived from hydroxy aminoindan and phenethylamine as potential treatment for Alzheimer's disease. *Journal of Medicinal Chemistry,* **45:** 5260-5279.

Stocchi, F., Vacca, L., Grassini, P., De Pandis, M., Battaglia, G., Cattaneo, C., and Fariello, R. (2006). Symptom relief in Parkinson disease by safinamide

Biochemical and clinical evidence of efficacy beyond MAO-B inhibition. *Neurology,* **67:** S24-S29.

Sturza, A., Noveanu, L., Duicu, O., Angoulvant, D., and Muntean, D. M. (2014). 0209: Monoamine oxidases as novel sources of reactive oxygen species in experimental diabetes. *Archives of Cardiovascular Diseases,* **6:** 15.

Sugimoto, H., Iimura, Y., Yamanishi, Y., and Yamatsu, K. (1995). Synthesis and structure-activity relationships of acetylcholinesterase inhibitors: 1-benzyl-4-[(5, 6-dimethoxy-1-oxoindan-2-yl) methyl] piperidine hydrochloride and related compounds. *Journal of Medicinal Chemistry,* **38:** 4821-4829.

Sugimoto, H., Tsuchiya, Y., Sugumi, H., Higurashi, K., Karibe, N., Iimura, Y., Sasaki, A., Araki, S., Yamanishi, Y., and Yamatsu, K. (1992). Synthesis and structure-activity relationships of acetylcholinesterase inhibitors: 1-benzyl-4-(2-phthalimidoethyl) piperidine, and related derivatives. *Journal of Medicinal Chemistry,* **35:** 4542-4548.

Sugimoto, H., Tsuchiya, Y., Sugumi, H., Higurashi, K., Karibe, N., Iimura, Y., Sasaki, A., Kawakami, Y., and Nakamura, T. (1990). Novel piperidine derivatives. Synthesis and anti-acetylcholinesterase activity of 1-benzyl-4-[2-(N-benzoylamino) ethyl] piperidine derivatives. *Journal of Medicinal Chemistry,* **33:** 1880-1887.

Sugimoto, H., Yamanish, Y., Iimura, Y., and Kawakami, Y. (2000). Donepezil hydrochloride (E2020) and other acetylcholinesterase inhibitors. *Current Medicinal Chemistry,* **7:** 303-339.

Summers, W. K., Majovski, L. V., Marsh, G. M., Tachiki, K., and Kling, A. (1986). Oral tetrahydroaminoacridine in long-term treatment of senile dementia, Alzheimer type. *New England Journal of Medicine,* **315:** 1241-1245.

Szegletes, T., Mallender, W. D., Thomas, P. J., and Rosenberry, T. L. (1999). Substrate binding to the peripheral site of acetylcholinesterase initiates enzymatic catalysis. Substrate inhibition arises as a secondary effect. *Biochemistry,* **38:** 122-133.

Talesa, V. N. (2001). Acetylcholinesterase in Alzheimer's disease. *Mechanisms of Ageing and Development,* **122:** 1961-1969.

Tariot, P. N., Cohen, R. M., Sunderland, T., Newhouse, P. A., Yount, D., Mellow, A. M., Weingartner, H., Mueller, E. A., and Murphy, D. L. (1987). L-deprenyl in Alzheimer's disease: preliminary evidence for behavioral change with

monoamine oxidase B inhibition. *Archives of General Psychiatry,* **44:** 427-433.

Thomas, T. (2000). Monoamine oxidase-B inhibitors in the treatment of Alzheimers disease. *Neurobiology of Aging,* **21:** 343-348.

Tsopelas, N. D., and Marin, D. B. (2001). 32 - Cholinergic Treatments of Alzheimer's Disease. In P. R. Hof & C. V. Mobbs (Eds.), *Functional Neurobiology of Aging* (pp. 475-486). San Diego: Academic Press.

Van Duinen, S. G., Castano, E. M., Prelli, F., Bots, G., Luyendijk, W., and Frangione, B. (1987). Hereditary cerebral hemorrhage with amyloidosis in patients of Dutch origin is related to Alzheimer disease. *Proceedings of the National Academy of Sciences,* **84:** 5991-5994.

Viegas, F. P., Simões, M. C. R., da Rocha, M. D., Castelli, M. R., Moreira, M. S., and Viegas Jr, C. (2011). Doença de Alzheimer: caracterização, evolução e implicações do processo neuroinflamatório. *Revista Virtual de Química,* **3:** 286-306.

Vitale, R. M., Rispoli, V., Desiderio, D., Sgammato, R., Thellung, S., Canale, C., Vassalli, M., Carbone, M., Ciavatta, M. L., and Mollo, E. (2018). In Silico Identification and Experimental Validation of Novel Anti-Alzheimer's Multitargeted Ligands from a Marine Source Featuring a "2-Aminoimidazole plus Aromatic Group" Scaffold. *ACS Chemical Neuroscience,* **9:** 1290-1303.

Wang, L., Esteban, G., Ojima, M., Bautista-Aguilera, O. M., Inokuchi, T., Moraleda, I., Iriepa, I., Samadi, A., Youdim, M. B., and Romero, A. (2014). Donepezil+ propargylamine+ 8-hydroxyquinoline hybrids as new multifunctional metal-chelators, ChE and MAO inhibitors for the potential treatment of Alzheimer's disease. *European Journal of Medicinal Chemistry,* **80:** 543-561.

Weinreb, O., Amit, T., Bar-Am, O., and Youdim, M. B. (2010). Rasagiline: a novel anti-Parkinsonian monoamine oxidase-B inhibitor with neuroprotective activity. *Progress in Neurobiology,* **92:** 330-344.

Weinreb, O., Mandel, S., Bar-Am, O., Yogev-Falach, M., Avramovich-Tirosh, Y., Amit, T., and Youdim, M. B. (2009). Multifunctional neuroprotective derivatives of rasagiline as anti-Alzheimer's disease drugs. *Neurotherapeutics,* **6:** 163-174.

Weinstock, M., Gorodetsky, E., Poltyrev, T., Gross, A., Sagi, Y., and Youdim, M. (2003). A novel cholinesterase and brain-selective monoamine oxidase

inhibitor for the treatment of dementia comorbid with depression and Parkinson's disease. *Progress in Neuro-Psychopharmacology and Biological Psychiatry,* **27:** 555-561.

Więckowska, A., Wichur, T., Godyń, J., Bucki, A., Marcinkowska, M., Siwek, A., Więckowski, K., Zaręba, P., Knez, D., and Głuch-Lutwin, M. (2018). Novel Multitarget-Directed Ligands Aiming at Symptoms and Causes of Alzheimer's Disease. *ACS Chemical Neuroscience,* **9:** 1195–1214.

Winblad, B., Engedal, K., Soininen, H., Verhey, F., Waldemar, G., Wimo, A., Wetterholm, A.-L., Zhang, R., Haglund, A., and Subbiah, P. (2001). A 1-year, randomized, placebo-controlled study of donepezil in patients with mild to moderate AD. *Neurology,* **57:** 489-495.

Winblad, B., Grossberg, G., Frölich, L., Farlow, M., Zechner, S., Nagel, J., and Lane, R. (2007). IDEAL A 6-month, double-blind, placebo-controlled study of the first skin patch for Alzheimer disease. *Neurology,* **69:** S14-S22.

Wright, C. I., Geula, C., and Mesulam, M. M. (1993). Neuroglial cholinesterases in the normal brain and in Alzheimer's disease: relationship to plaques, tangles, and patterns of selective vulnerability. *Annals of Neurology: Official Journal of the American Neurological Association and the Child Neurology Society,* **34:** 373-384.

Wu, M.-Y., Esteban, G., Brogi, S., Shionoya, M., Wang, L., Campiani, G., Unzeta, M., Inokuchi, T., Butini, S., and Marco-Contelles, J. (2015). Donepezil-like multifunctional agents: Design, synthesis, molecular modeling and biological evaluation. *European Journal of Medicinal Chemistry*, **121:** 864-879.

Xie, H.-r., Hu, L.-s., and Li, G.-y. (2010). SH-SY5Y human neuroblastoma cell line: in vitro cell model of dopaminergic neurons in Parkinson's disease. *Chinese Medical Journal,* **123:** 1086-1092.

Xu, Y., Zhang, J., Wang, H., Mao, F., Bao, K., Liu, W., Zhu, J., Li, X., Zhang, H., and Li, J. (2018). Rational Design of Novel Selective Dual-Target Inhibitors of Acetylcholinesterase and Monoamine Oxidase B as Potential Anti-Alzheimer's Disease Agents. *ACS Chemical Neuroscience*, **10:** 482-496.

Yamada, M., and Yasuhara, H. (2004). Clinical pharmacology of MAO inhibitors: safety and future. *Neurotoxicology,* **25:** 215-221.

Yan, J., Hu, J., Liu, A., He, L., Li, X., and Wei, H. (2017). Design, synthesis, and evaluation of multitarget-directed ligands against Alzheimer's disease based

on the fusion of donepezil and curcumin. *Bioorganic and Medicinal Chemistry,* **25:** 2946-2955.

Yiannopoulou, K. G., and Papageorgiou, S. G. (2013). Current and future treatments for Alzheimer's disease. *Therapeutic Advances in Neurological Disorders,* **6:** 19-33.

Yogev-Falach, M., Bar-Am, O., Amit, T., Weinreb, O., and Youdim, M. B. (2006). A multifunctional, neuroprotective drug, ladostigil (TV3326), regulates holo-APP translation and processing. *The FASEB Journal,* **20:** 2177-2179.

Youdim, M. B., Bar Am, O., Yogev-Falach, M., Weinreb, O., Maruyama, W., Naoi, M., and Amit, T. (2005). Rasagiline: neurodegeneration, neuroprotection, and mitochondrial permeability transition. *Journal of Neuroscience Research,* **79:** 172-179.

Youdim, M. B., Edmondson, D., and Tipton, K. F. (2006). The therapeutic potential of monoamine oxidase inhibitors. *Nature Reviews Neuroscience,* **7:** 295.

Zhang, Y.-w., Thompson, R., Zhang, H., and Xu, H. (2011). APP processing in Alzheimer's disease. *Molecular Brain,* **4:** 3.

Zheng, H., Weiner, L. M., Bar-Am, O., Epsztejn, S., Cabantchik, Z. I., Warshawsky, A., Youdim, M. B., and Fridkin, M. (2005). Design, synthesis, and evaluation of novel bifunctional iron-chelators as potential agents for neuroprotection in Alzheimer's, Parkinson's, and other neurodegenerative diseases. *Bioorganic and Medicinal Chemistry,* **13:** 773-783.

Zheng, H., Youdim, M. B., and Fridkin, M. (2010). Site-activated chelators targeting acetylcholinesterase and monoamine oxidase for Alzheimer's therapy. *ACS Chemical Biology,* **5:** 603-610.

Zheng, W., and Monnot, A. D. (2012). Regulation of brain iron and copper homeostasis by brain barrier systems: implication in neurodegenerative diseases. *Pharmacology & Therapeutics,* **133:** 177-188.

Zhou, M., and Panchuk-Voloshina, N. (1997). A one-step fluorometric method for the continuous measurement of monoamine oxidase activity. *Analytical Biochemistry,* **253:** 169-174.

Appendices

List of Publications

Publications from thesis

1. 4, 6-Diphenylpyrimidine Derivatives as Dual Inhibitors of Monoamine Oxidase and Acetylcholinesterase for the Treatment of Alzheimer's Disease

   Bhupinder Kumar, Ashish Ranjan Dwivedi, Bibekananda Sarkar, Sukesh Kumar Gupta, Sairam Krishnamurthy, Anil K. Mantha, Jyoti Parkash, and Vinod Kumar, ACS Chemical Neuroscience, 2019, 10, 252-261; Impact Factor- 4.22
2. Dipropargyl Substituted Diphenylpyrimidines as Dual Inhibitors of Monoamine Oxidase and Acetylcholinesterase

   Bhupinder Kumar, Vijay Kumar, Vikash Prashar, Suresh Saini, Ashish Ranjan Dwivedi, Binu Bajaj, Devashish Mehta, Jyoti Parkash and Vinod Kumar*; European Journal of Medicinal Chemistry, 2019, 177, 221-234; Impact Factor- 4.82
3. Recent Developments on the Structure-Activity Relationship Studies of MAO Inhibitors and Their Role in Different Neurological Disorders

   Bhupinder Kumar, Sheetal, Anil K. Mantha and Vinod Kumar*; RSC Advances; 2016, 6, 42660-42683; Impact Factor- 3.09
4. A Perspective on Monoamine Oxidase Enzyme as Drug Target: Challenges and Opportunities

   Bhupinder Kumar, Vivek Prakash Gupta and Vinod Kumar*; Current Drug Targets, 2017, 18, 87-97; Impact Factor- 3.11

Allied Publications

5. Synthesis, Biological Evaluation and Molecular Modeling Studies of Phenyl-/Benzhydrylpiperazine Derivatives as Potential MAO Inhibitors

   Bhupinder Kumar, Sheetal, Anil K Mantha and Vinod Kumar*, Bioorganic Chemistry, 2018, 77, 252-262. Impact Factor: 3.93
6. Synthesis, Biological Evaluation and Molecular Modeling Studies of Propargyl Containing 2,4,6-trisubstituted Pyrimidine Derivatives as Potential anti-Parkinson agents

Bhupinder Kumar, Mohit Kumar, Ashish Ranjan Dwivedi, and Vinod Kumar*, ChemMedChem, 2018, 13, 705-712. Impact Factor: 3.01

7. Chitosan-supported copper as an efficient and recyclable heterogeneous catalyst for A3/decarboxylative A3-coupling reaction
   Pavneet Kaur, **Bhupinder Kumar**, Vinod Kumar, Rakesh Kumar; Tetrahedron Letter, 2018, 59, 1986-1991. Impact Factor: 2.12
8. Synthesis and Biological Evaluation of Pyrimidine Bridged Combretastatin Derivatives as Potential Anticancer Agents and Mechanistic Studies
   Bhupinder Kumar, Praveen Sharma, Vivek Prakash Gupta, Madhu Khullar, Sandeep Singh, Nilambra Dogra and Vinod Kumar; Bioorganic Chemistry, 2018, 78, 130-140. Impact Factor: 3.93
9. Promising Targets in Anti-cancer Drug Development: Recent Updates
   Bhupinder Kumar, Sandeep Singh, Ira Skvortsova and Vinod Kumar*, Current Medicinal Chemistry, 2017, 27, 4729-4752, Impact Factor: 3.25
10. Mechanisms of Tubulin Binding Ligands to Target Cancer Cells: Updates on Their Therapeutic Potential and Clinical Trials
    Bhupinder Kumar, Rakesh Kumar, Ira Skvortsova, and Vinod Kumar*; Current Cancer Drug Targets; 2017, 17, 357-375, Impact Factor- 3.0
11. Targeting Cancer Stem Cells Pathways for the Effective Treatment of Cancer**,** Ashish Ranjan Dwivedi, Amandeep Thakur, Vijay Kumar, **Bhupinder Kumar**, Ira Skvortsova and Vinod Kumar; Cur. Drug Targets, 2019, Accepted; Impact Factor- 3.11
12. Regioselective Alkylation of 1,2,4-triazole Using Ionic Liquids Under Microwave Conditions
    Ramandeep Kaur, **Bhupinder Kumar**, Ashish Ranjan Dwivedi, Vinod Kumar*; Green Processing and Synthesis; 2016, 5, 233-237. Impact Factor- 1.15
13. Recent Developments on 1,2,4-Triazole Nucleus in Anticancer Compounds: A Review.
    Ramandeep Kaur, AR Dwivedi, **Bhupinder Kumar**, Vinod Kumar; Anticancer Agents Med Chem. 2016, 16(4): 465-489, Impact Factor- 2.56

List of Patents Filed

1. Pyrimidine Bridged Biaryl Derivatives as Multi-Targeting Agents for the Treatment of Neurological Disorders; Application number 201811008301
2. Single Step Process for the Direct Preparation of Aromatic Amines from Aromatic Halides and Azides; Application number 201911006109

List of Conferences/workshops and Symposiums

1. Award presentation entitled “Design, Synthesis and Screening of Phenylpiperazine and 1-Benzhydrylpiperazine Derivatives as Putative MAO inhibitors” **Bhupinder Kumar**, Shelly Pathania and Vinod Kumar in a “51st Annual Convention of Chemists 2014” **(Won prize: Prof P.Sengupta Memorial Award)** held on December 9-12, 2014 at Department of Chemistry, Kurukshetra University, Kurukshetra, Haryana, India.
2. Presented a poster entitled “4,6-diphenylpyrimidine derivatives as Dual Inhibitors of Monoamine Oxidase and Acetylcholinesterase for the Treatment of Alzheimer’s Disease” at international conference “Frontiers in Chemical Sciences” held on December 6-8, 2018 at Department of Chemistry, Indian Institute of Technology Guwahati.
3. Attended an International conference on “Nascent Developments in Chemical Sciences: Opportunities for Academia-Industry Collaboration (NDCS-2015)” and a poster was presented entitled “Design, Synthesis and Screening of 1-Benzhydrylpiperazine Derivatives as Putative MAO Inhibitors” **Bhupinder Kumar** and Vinod Kumar; held on Oct. 16-18, 2015 at Department of Chemistry, BITS-Pilani, Rajasthan.
4. Attended a Three-Day National Workshop on ‘Drug Design, Molecular Docking, Virtual Screening and Pharmacoinformatics’ held at Department of Pharmaceutical Sciences and Natural Products in collaboration with Schrödinger INC. USA on Nov. 26-28, 2015 at Central University of Punjab, City Campus, Mansa Road, Bathinda.
5. Poster presentation entitled “Design, Synthesis and Evaluation of Pyrimidine Bridged Combretastatin Derivatives as Putative Antiproliferative Agents” **Bhupinder Kumar**, Sapna, Sandeep Singh and Vinod Kumar; in the International Symposium on Current Trends in Drug Discovery and Research (CTDDR)” held at CDRI Lucknow from Feb. 25-28, 2016.
6. Poster presented by student entitled “*In Silico* Screening of 1-Benzhydrylpiperazine Derivatives as Putative MAO inhibitors” **Bhupinder Kumar** and Vinod Kumar in a Seminar on “Recent Trends in Molecular Medicine” December 5, 2014 at Central University of Punjab, Centre for Genetic Diseases and Molecular Medicine, Bathinda, Punjab, India.
7. Organized (Member organizing committee) a Three-Day National Workshop

on '"Advanced Workshop on Molecular Docking, Virtual Screening and Computational Biology" held at Department of Pharmaceutical Sciences and Natural Products in collaboration with Schrödinger INC. USA on Nov. 15-17, 2017 at Central University of Punjab, City Campus, Mansa Road, Bathinda.

8. Attended a Two-Day National Workshop on 'Cytokine analysis and phenotyping of B/T cells using Flow Cytometry' held by Centre for Human Genetics and Molecular Medicine in collaboration with BD Biosciences on Jan. 21-22, 2016 at Central University of Punjab, City Campus, Mansa Road, Bathinda.
9. Presented poster at One Day National Workshop on 'Training the Trainers-Water Quality and Health' held on Feb. 11, 2015 at Central University of Punjab, City Campus, Mansa Road, Bathinda.
10. Attended seminar on "The evolving Importance of Intellectual Property Rights" held on Jan. 30,2016 at Central University of Punjab, City Campus, Mansa Road, Bathinda.
11. Bhupinder Kumar participated in DST and CII sponsored one day workshop on "Prime Minister's Fellowship Scheme for Doctoral Research" organized on May 3,2017 at Central University of Punjab, City Campus, Mansa Road, Bathinda.
12. Attended a One-Day National Workshop on 'GC-MS instrumentation and sample preparation techniques' held by Central instrumentation laboratory in collaboration with Toshvin Analytical Pvt. Ltd. Mumbai, on Jan. 11, 2019 at Central University of Punjab, City Campus, Mansa Road, Bathinda

Spectral data of representative compounds

B2P106

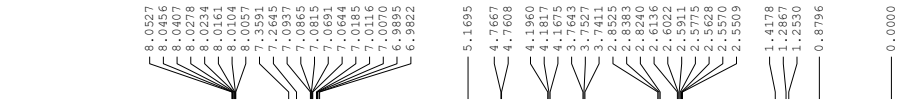

BRUKER
AVANCE II 400 NMR
Spectrometer
SAIF
Panjab University
Chandigarh

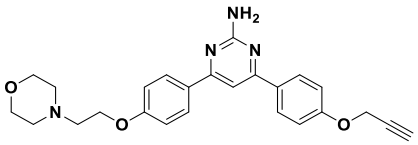

VB-1

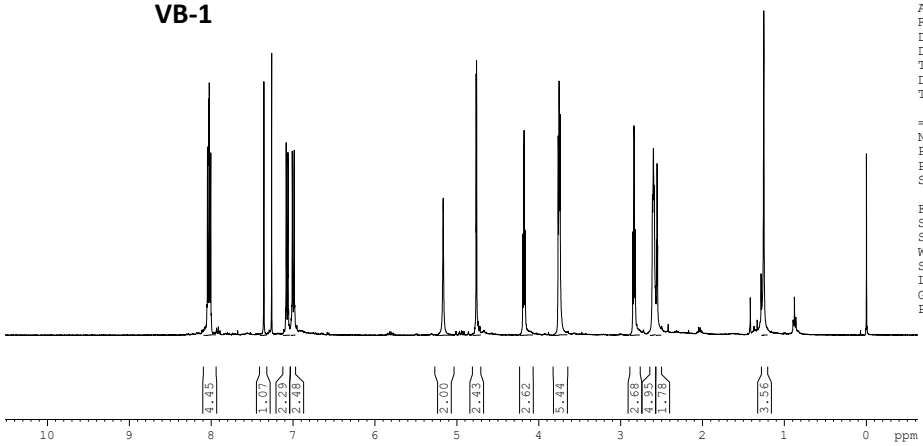


```
Current Data Parameters
NAME          Jan14-2017
EXPNO                161
PROCNO                 1

F2 - Acquisition Parameters
Date_           20170115
Time               14.00
INSTRUM            spect
PROBHD   5 mm PABBO BB-
PULPROG             zg30
TD                 65536
SOLVENT            CDCl3
NS                     8
DS                     2
SWH            12019.230 Hz
FIDRES          0.183399 Hz
AQ             2.7263477 sec
RG                   287
DW                41.600 usec
DE                 6.00 usec
TE                292.9 K
D1            1.00000000 sec
TD0                    1

======== CHANNEL f1 ========
NUC1                  1H
P1                 10.90 usec
PL1                -3.00 dB
SFO1         400.1324710 MHz

F2 - Processing parameters
SI                 32768
SF           400.1300077 MHz
WDW                   EM
SSB                    0
LB                  0.30 Hz
GB                     0
PC                  1.00
```

manishkumarmanu1986@gmail.com

B2P106

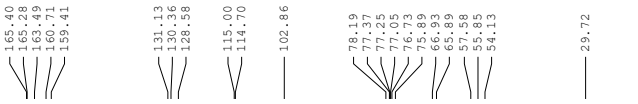

BRUKER
AVANCE II 400 NMR
Spectrometer
SAIF
Panjab University
Chandigarh

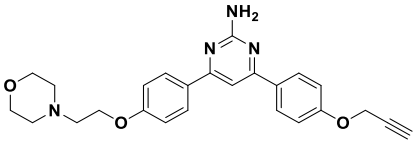

VB-1


```
Current Data Parameters
NAME          Jan14-2017
EXPNO                162
PROCNO                 1

F2 - Acquisition Parameters
Date_           20170115
Time               14.30
INSTRUM            spect
PROBHD   5 mm PABBO BB-
PULPROG           zgpg30
TD                 65536
SOLVENT            CDCl3
NS                   512
DS                     4
SWH            29761.904 Hz
FIDRES          0.454131 Hz
AQ             1.1010548 sec
RG                   724
DW                16.800 usec
DE                 6.00 usec
TE                293.4 K
D1            2.00000000 sec
d11           0.03000000 sec
DELTA         1.89999998 sec
TD0                    1

======== CHANNEL f1 ========
NUC1                 13C
P1                 9.60 usec
PL1               -2.00 dB
SFO1        100.6228298 MHz

======== CHANNEL f2 ========
CPDPRG2          waltz16
NUC2                  1H
PCPD2             80.00 usec
PL2               -3.00 dB
PL12              14.31 dB
PL13              18.00 dB
SFO2        400.1316005 MHz

F2 - Processing parameters
SI                 32768
SF          100.6127690 MHz
WDW                   EM
SSB                    0
LB                  1.00 Hz
GB                     0
PC                  1.40
```

manishkumarmanu1986@gmail.com

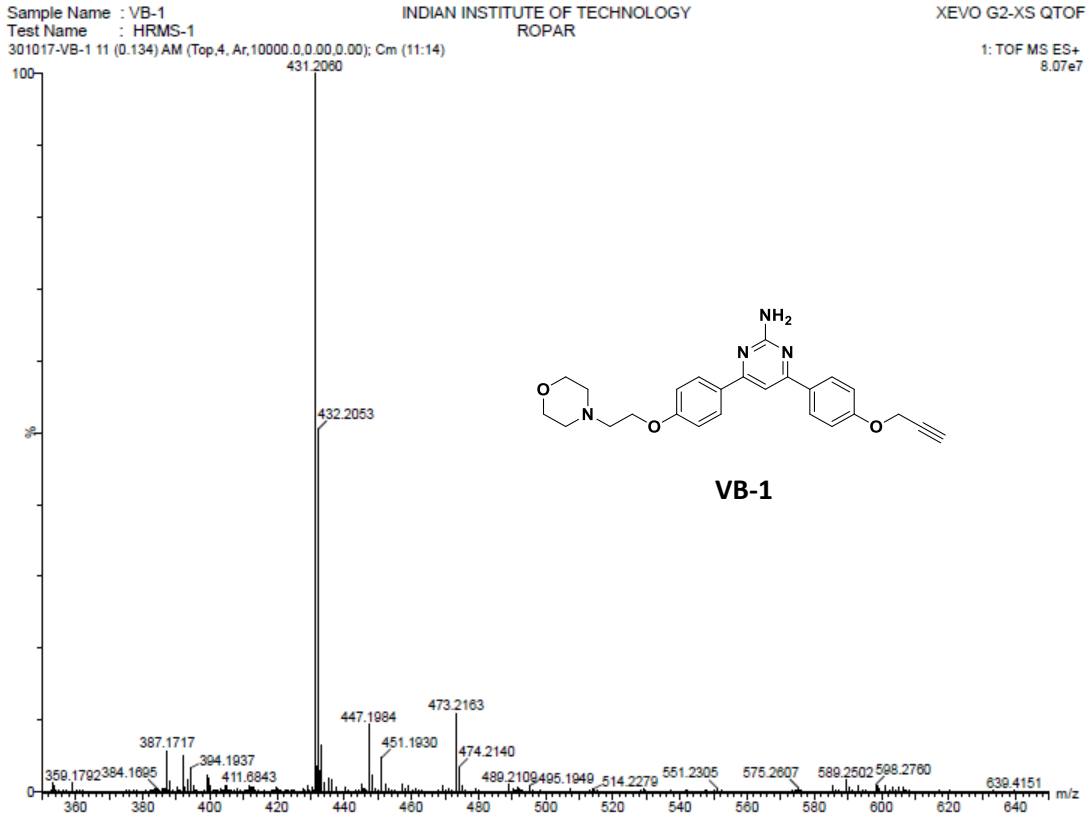
Sample Name : VB-1
Test Name : HRMS-1
INDIAN INSTITUTE OF TECHNOLOGY
ROPAR
XEVO G2-XS QTOF
301017-VB-1 11 (0.134) AM (Top,4, Ar,10000.0,0.00,0.00); Cm (11:14)
1: TOF MS ES+
8.07e7
100
%
0
431.2060
432.2053
473.2163
447.1984
451.1930
474.2140
387.1717
394.1937
359.1792
384.1695
411.6843
489.2109
495.1949
514.2279
551.2305
575.2607
589.2502
598.2760
639.4151
m/z
360
380
400
420
440
460
480
500
520
540
560
580
600
620
640
NH2
N
N
O
N
O
O
VB-1

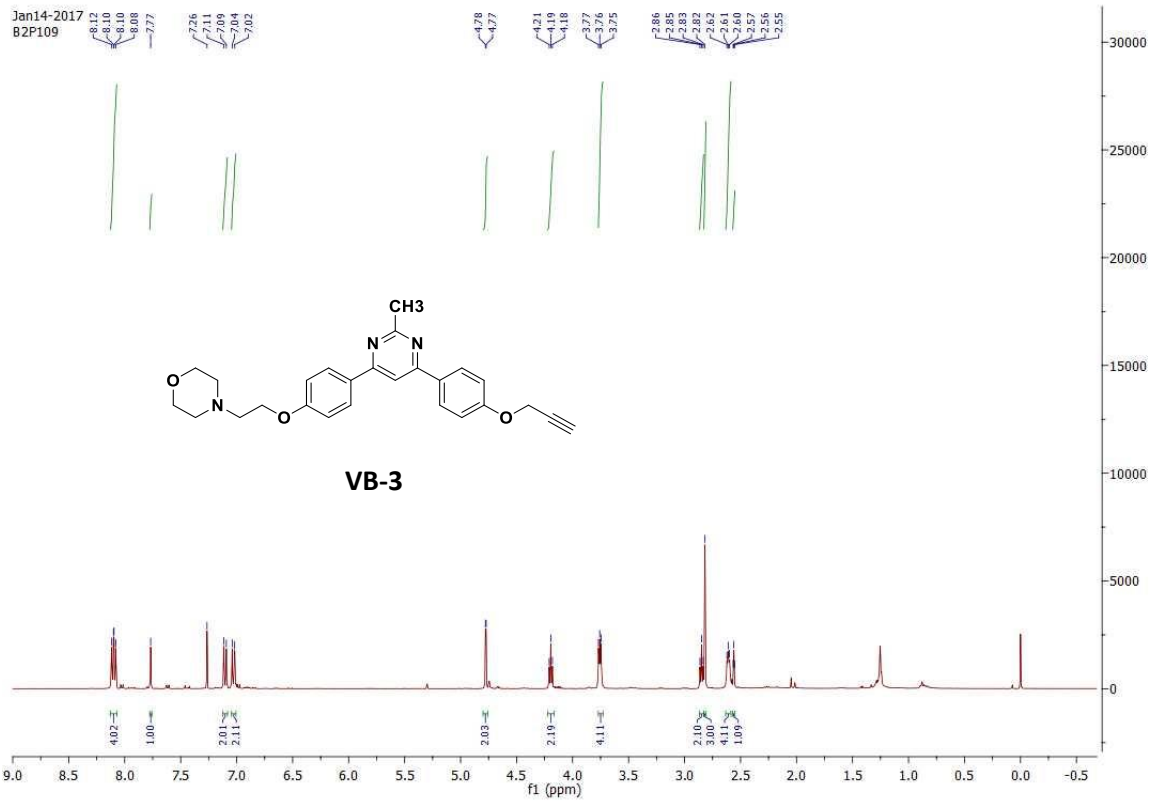

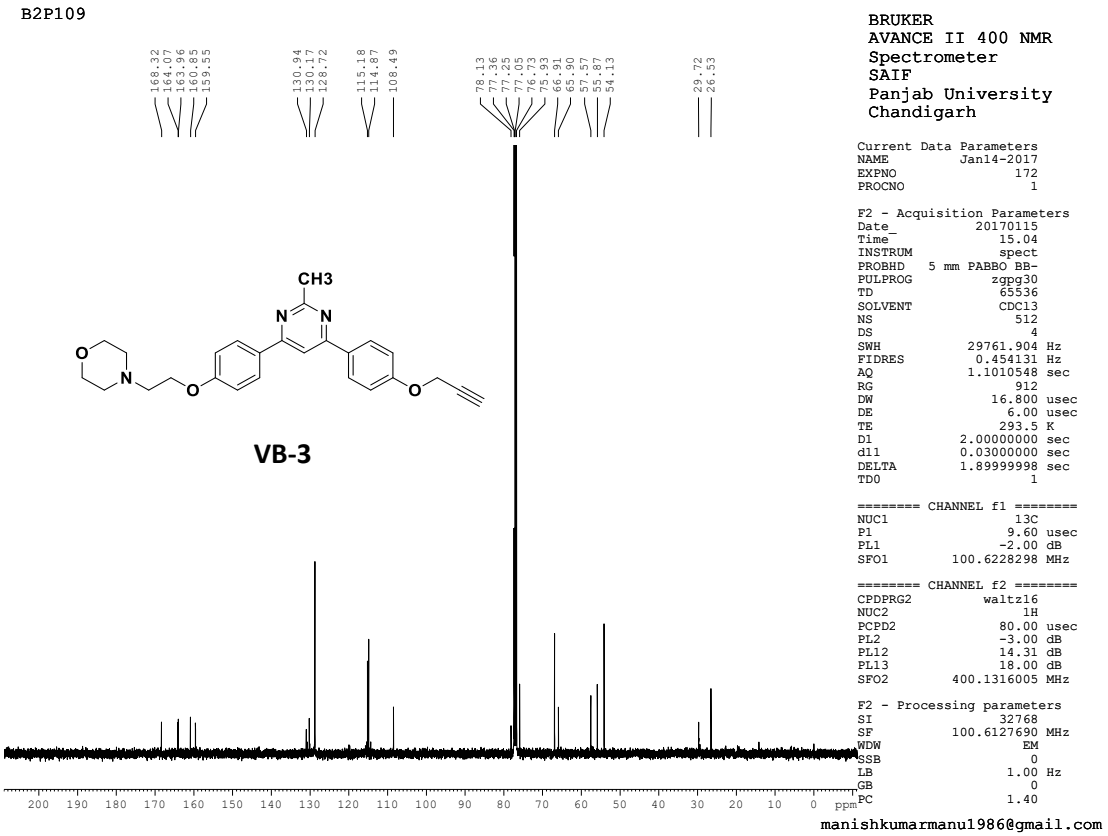

BRUKER
AVANCE II 400 NMR
Spectrometer
SAIF
Panjab University
Chandigarh

```
Current Data Parameters
NAME          Jan14-2017
EXPNO                172
PROCNO                 1

F2 - Acquisition Parameters
Date_           20170115
Time               15.04
INSTRUM            spect
PROBHD   5 mm PABBO BB-
PULPROG          zgpg30
TD                65536
SOLVENT           CDCl3
NS                  512
DS                    4
SWH           29761.904 Hz
FIDRES         0.454131 Hz
AQ            1.1010548 sec
RG                  912
DW               16.800 usec
DE                6.00 usec
TE                293.5 K
D1           2.00000000 sec
d11          0.03000000 sec
DELTA        1.89999998 sec
TD0                   1

======== CHANNEL f1 ========
NUC1                 13C
P1                  9.60 usec
PL1                -2.00 dB
SFO1        100.6228298 MHz

======== CHANNEL f2 ========
CPDPRG2          waltz16
NUC2                 1H
PCPD2             80.00 usec
PL2                -3.00 dB
PL12               14.31 dB
PL13               18.00 dB
SFO2        400.1316005 MHz

F2 - Processing parameters
SI                32768
SF          100.6127690 MHz
WDW                  EM
SSB                   0
LB                 1.00 Hz
GB                    0
PC                 1.40
```

manishkumarmanu1986@gmail.com

Sample Name : VB-3
Test Name : HRMS-1

INDIAN INSTITUTE OF TECHNOLOGY
ROPAR

XEVO G2-XS QTOF

301017-VB-3 9 (0.117) AM (Top,4, Ar,10000.0,0.00,0.00); Cm (8:14-21:38)

1: TOF MS ES+
7.39e7

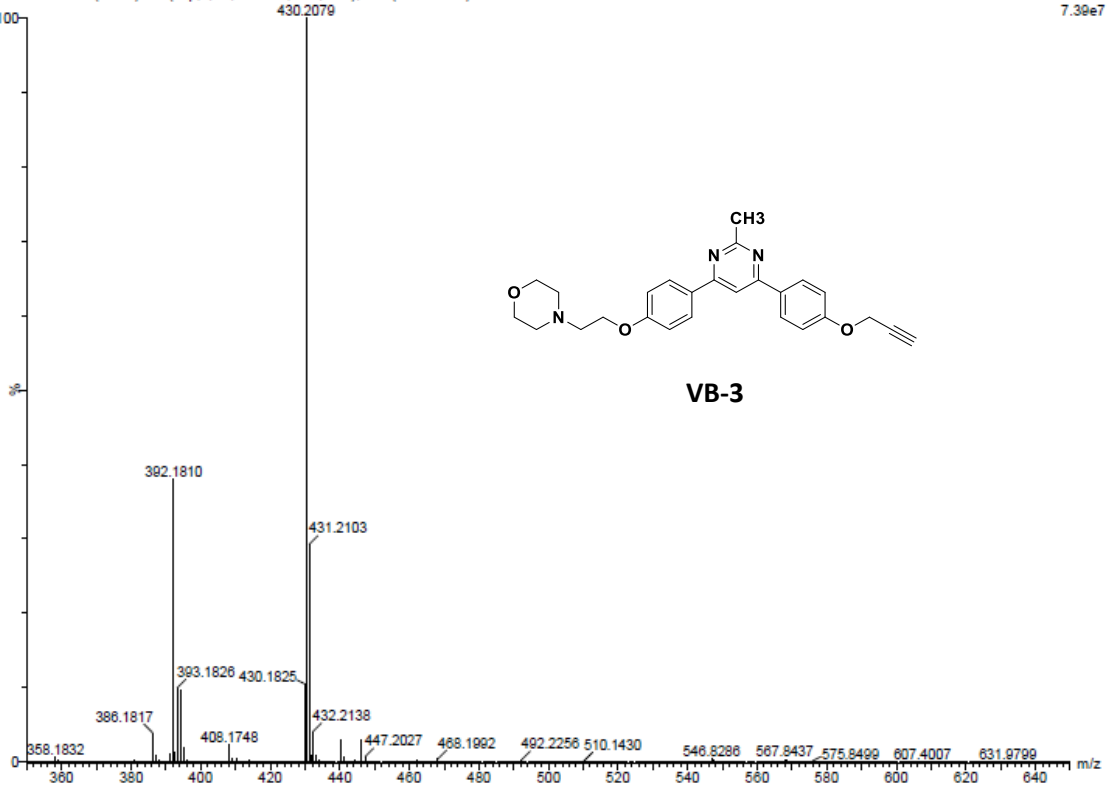

VB-3

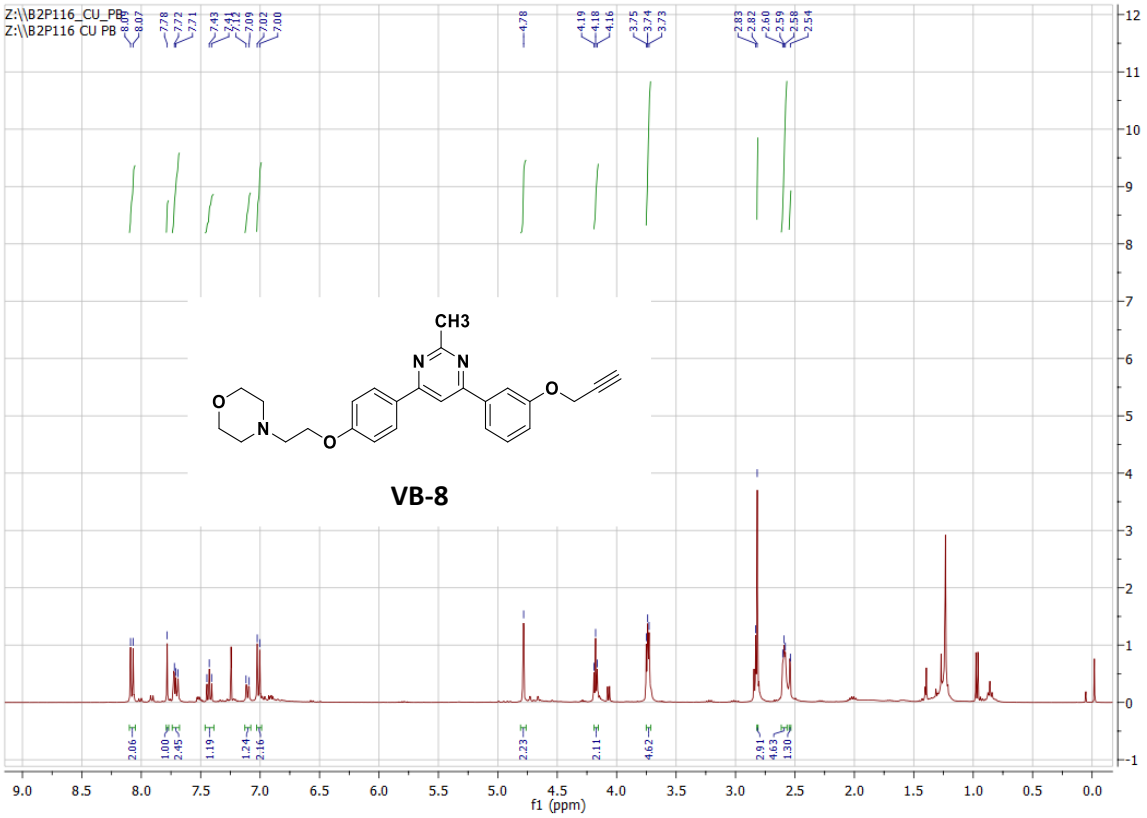
Z:\\B2P116_CU_PB
Z:\\B2P116 CU PB
CH3
N
N
O
N
O
O
VB-8
f1 (ppm)

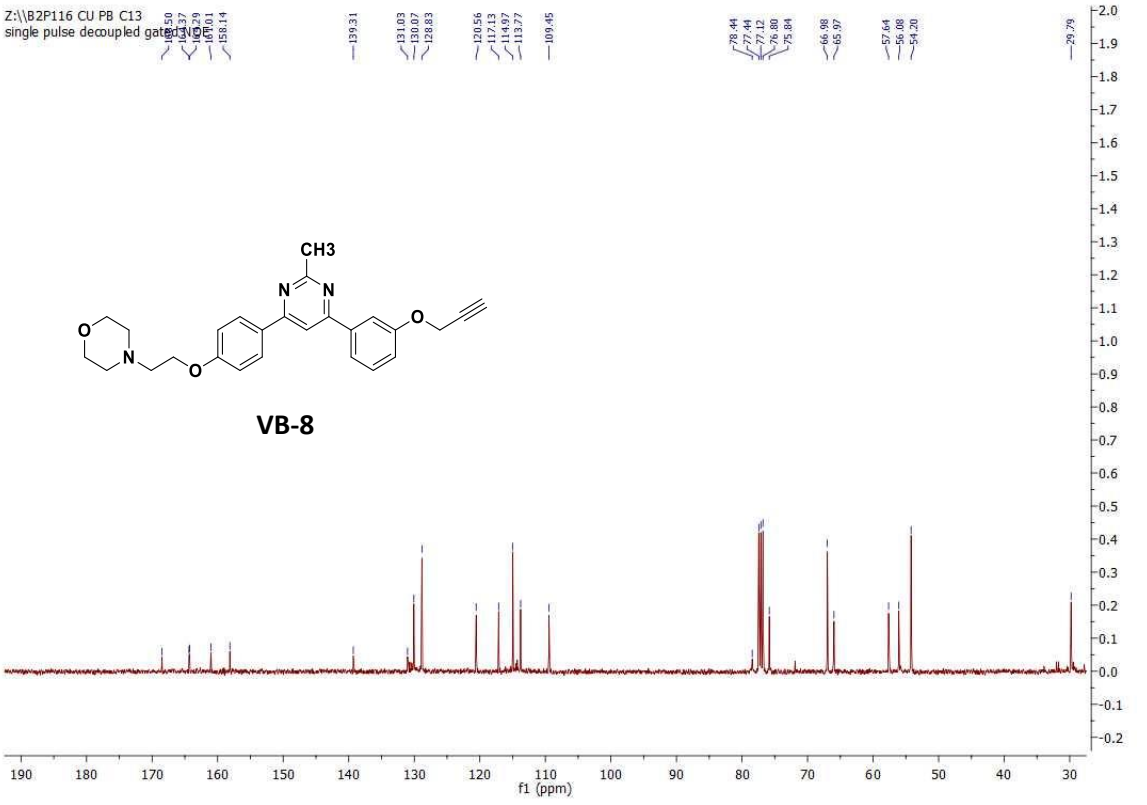
Z:\\B2P116 CU PB C13
single pulse decoupled gated NOE
CH3
N
N
O
N
O
O
VB-8
f1 (ppm)

Sample Name : VB-8
Test Name : HRMS-1
INDIAN INSTITUTE OF TECHNOLOGY
ROPAR
XEVO G2-XS QTOF
301017-VB-8 9 (0.117) AM2 (Ar,13000.0,0.00,0.00); Cm (9:11)
1: TOF MS ES+
5.33e7

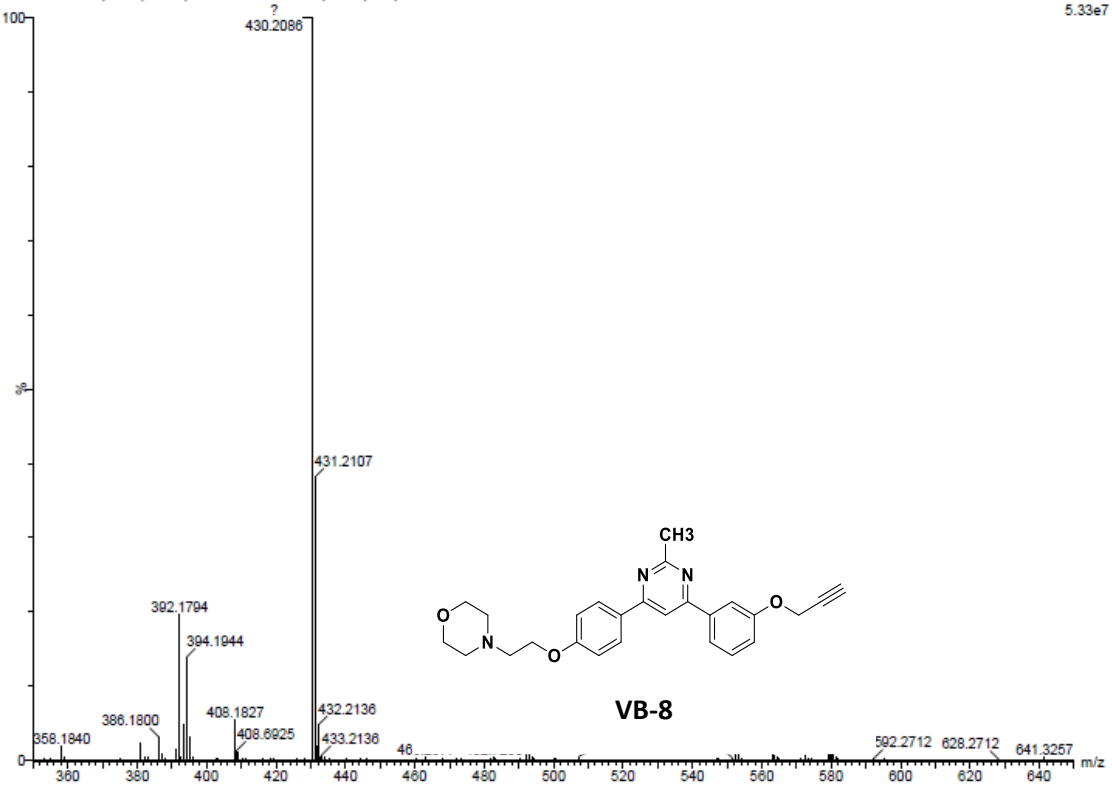

VB-8

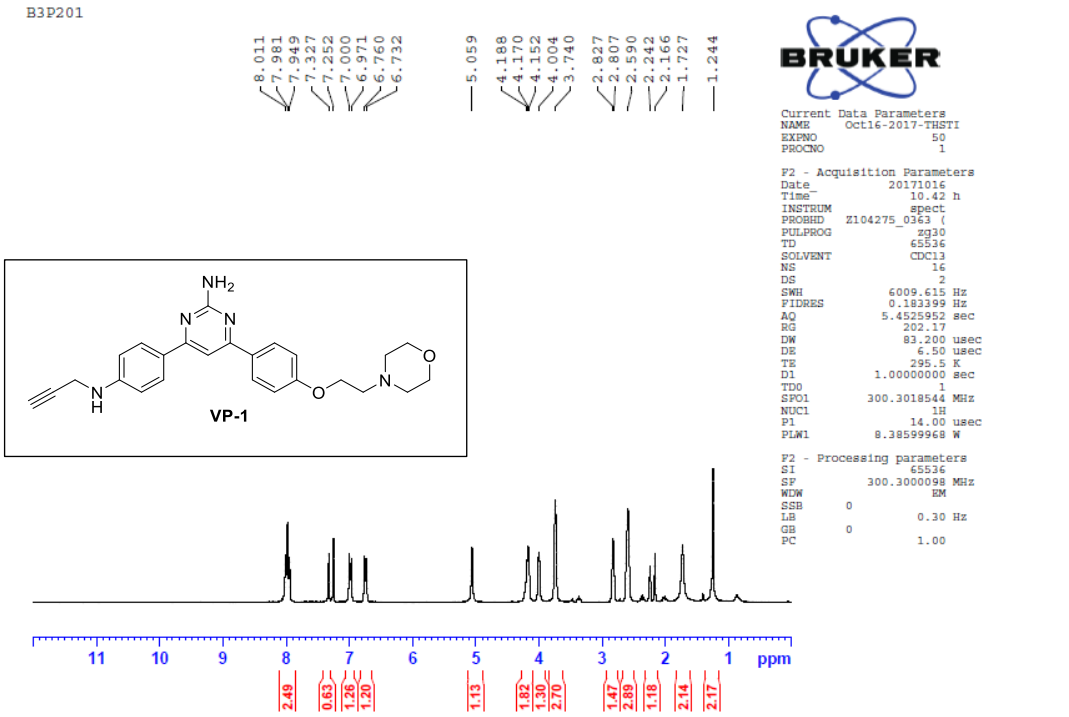
B3P201
8.011
7.981
7.949
7.327
7.252
7.000
6.971
6.760
6.732
5.059
4.188
4.170
4.152
4.004
3.740
2.827
2.807
2.590
2.242
2.166
1.727
1.244
BRUKER
Current Data Parameters
NAME Oct16-2017-THSTI
EXPNO 50
PROCNO 1
F2 - Acquisition Parameters
Date_ 20171016
Time 10.42 h
INSTRUM spect
PROBHD Z104275_0363 (
PULPROG zg30
TD 65536
SOLVENT CDCl3
NS 16
DS 2
SWH 6009.615 Hz
FIDRES 0.183399 Hz
AQ 5.4525952 sec
RG 202.17
DW 83.200 usec
DE 6.50 usec
TE 295.5 K
D1 1.00000000 sec
TD0 1
SFO1 300.3018544 MHz
NUC1 1H
P1 14.00 usec
PLW1 8.38599968 W
F2 - Processing parameters
SI 65536
SF 300.3000098 MHz
WDW EM
SSB 0
LB 0.30 Hz
GB 0
PC 1.00
NH2
N
N
N
H
O
N
O
VP-1
11
10
9
8
7
6
5
4
3
2
1
ppm
2.49
0.63
1.26
1.20
1.13
1.82
1.30
2.70
1.47
2.89
1.18
2.14
2.17
NH2
N
N
N
H
O
N
O
VP-1

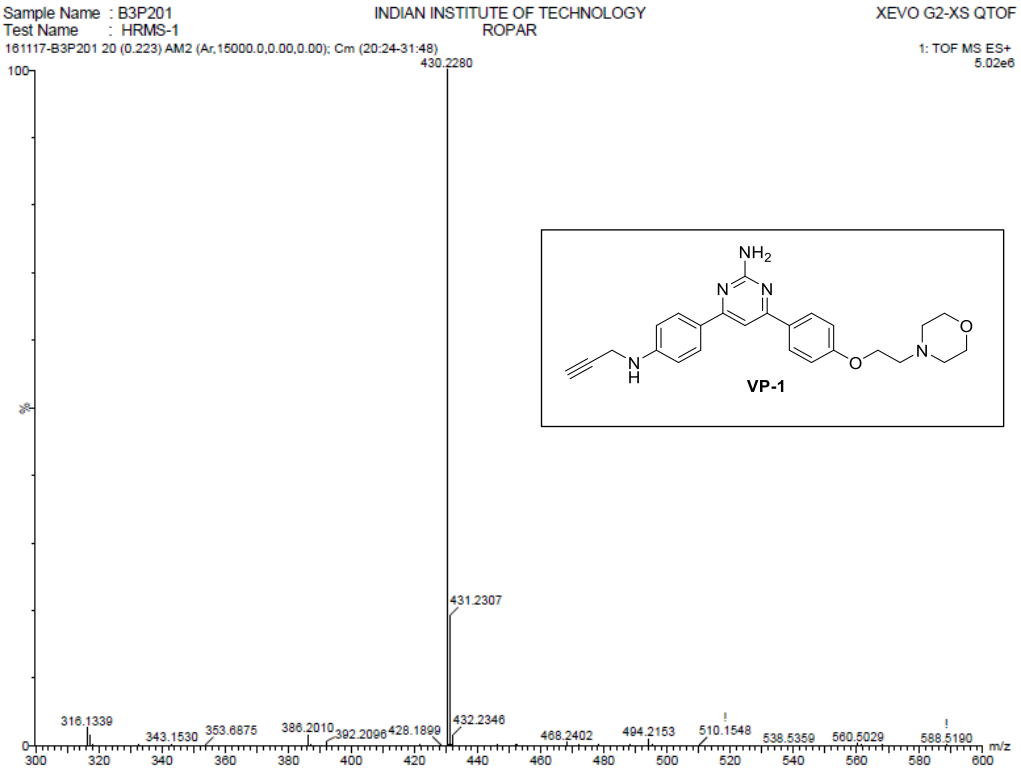
Sample Name : B3P201
Test Name : HRMS-1
INDIAN INSTITUTE OF TECHNOLOGY
ROPAR
XEVO G2-XS QTOF
161117-B3P201 20 (0.223) AM2 (Ar,15000.0,0.00,0.00); Cm (20:24-31:48)
1: TOF MS ES+
5.02e6
100
%
0
430.2280
431.2307
432.2346
316.1339
343.1530
353.6875
386.2010
392.2096
428.1899
468.2402
494.2153
510.1548
538.5359
560.5029
588.5190
300
320
340
360
380
400
420
440
460
480
500
520
540
560
580
600
m/z
NH2
N
N
N
H
O
N
O
VP-1

B3P202

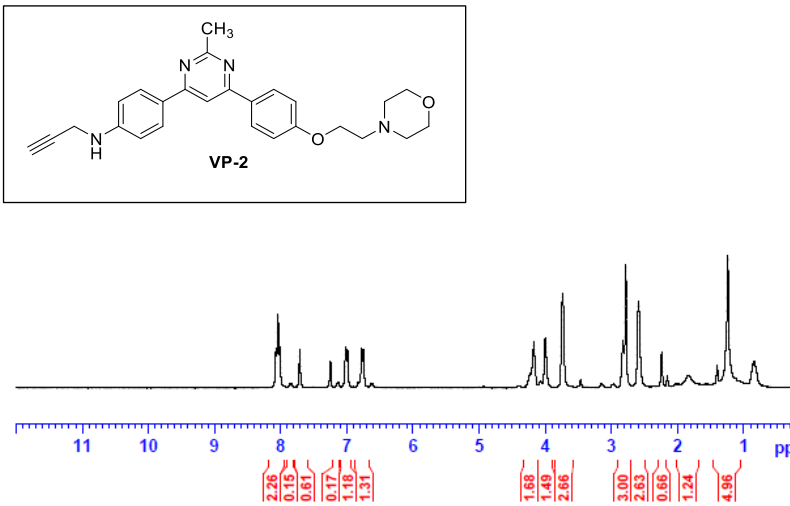

BRUKER

```
Current Data Parameters
NAME      Oct16-2017-THSTI
EXPNO              110
PROCNO               1

F2 - Acquisition Parameters
Date_          20171016
Time_             11.37 h
INSTRUM           spect
PROBHD    Z104275_0363 (
PULPROG           zg30
TD               65536
SOLVENT          CDCl3
NS                  16
DS                   2
SWH            6009.615 Hz
FIDRES         0.183399 Hz
AQ             5.4525952 sec
RG               202.17
DW               83.200 usec
DE                6.50 usec
TE               295.8 K
D1            1.00000000 sec
TD0                  1
SFO1         300.3018544 MHz
NUC1               1H
P1               14.00 usec
PLW1          8.38599968 W

F2 - Processing parameters
SI               65536
SF          300.3000107 MHz
WDW                EM
SSB       0
LB                0.30 Hz
GB        0
PC                1.00
```

B3P202-13C

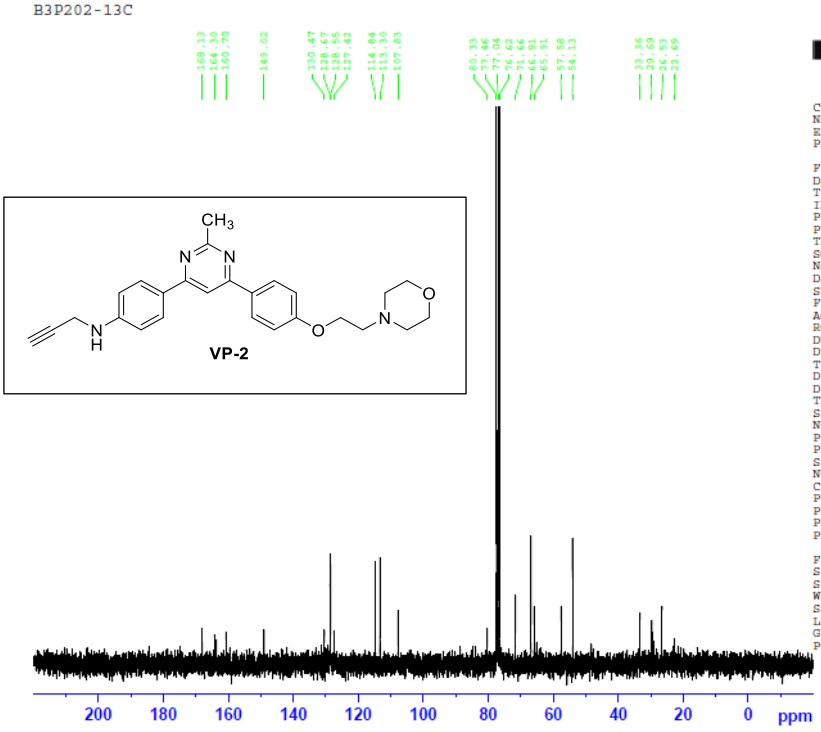

BRUKER

```
Current Data Parameters
NAME      May03-2018-THSTI
EXPNO              130
PROCNO               1

F2 - Acquisition Parameters
Date_          20180504
Time_             11.37 h
INSTRUM           spect
PROBHD    Z104275_0363 (
PULPROG         zgpg30
TD               65536
SOLVENT          CDCl3
NS                 350
DS                   4
SWH           18115.941 Hz
FIDRES         0.552855 Hz
AQ             1.8087935 sec
RG                14.65
DW               27.600 usec
DE                6.50 usec
TE               298.3 K
D1            2.00000000 sec
D11           0.03000000 sec
TD0                  1
SFO1         75.5180461 MHz
NUC1               13C
P1               10.00 usec
PLW1         44.50699997 W
SFO2        300.3012012 MHz
NUC2               1H
CPDPRG[2        waltz16
PCPD2            90.00 usec
PLW2          8.38599968 W
PLW12         0.20043489 W
PLW13         0.10045800 W

F2 - Processing parameters
SI               32768
SF          75.5104951 MHz
WDW                EM
SSB       0
LB                1.00 Hz
GB        0
PC                1.40
```

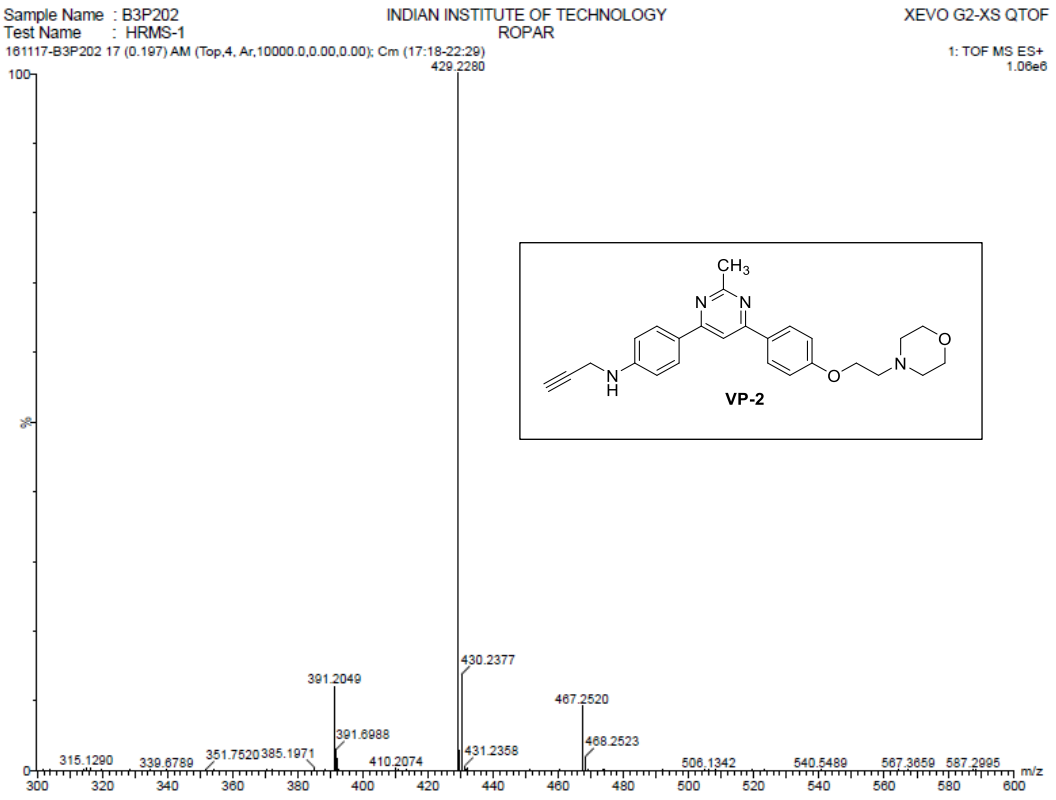
Sample Name : B3P202
Test Name : HRMS-1
INDIAN INSTITUTE OF TECHNOLOGY
ROPAR
XEVO G2-XS QTOF
161117-B3P202 17 (0.197) AM (Top,4, Ar,10000.0,0.00,0.00); Cm (17:18-22:29)
1: TOF MS ES+
1.06e6
429.2280
430.2377
391.2049
467.2520
391.6988
468.2523
315.1290
339.6789
351.7520
385.1971
410.2074
431.2358
506.1342
540.5489
567.3659
587.2995
%
m/z
VP-2

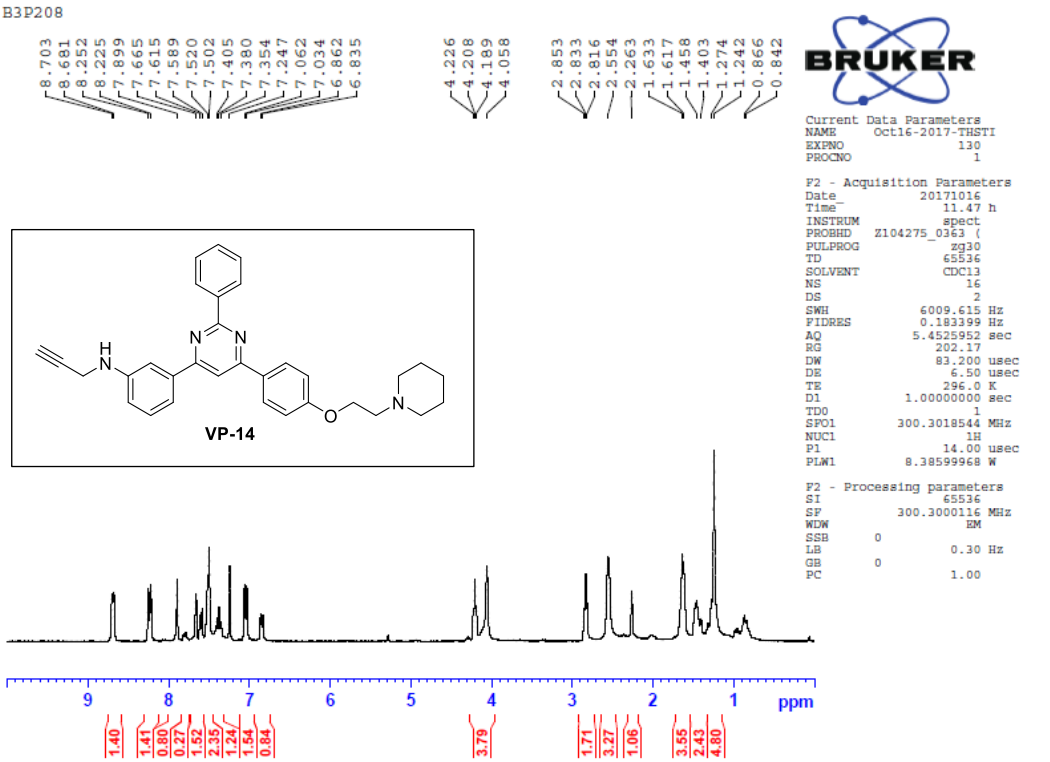
B3P208
8.703
8.681
8.252
8.225
7.899
7.665
7.615
7.589
7.520
7.502
7.405
7.380
7.354
7.247
7.062
7.034
6.862
6.835
4.226
4.208
4.189
4.058
2.853
2.833
2.816
2.554
2.263
1.633
1.617
1.458
1.403
1.274
1.242
0.866
0.842
BRUKER
Current Data Parameters
NAME Oct16-2017-THSTI
EXPNO 130
PROCNO 1
F2 - Acquisition Parameters
Date_ 20171016
Time 11.47 h
INSTRUM spect
PROBHD Z104275_0363 (
PULPROG zg30
TD 65536
SOLVENT CDCl3
NS 16
DS 2
SWH 6009.615 Hz
FIDRES 0.183399 Hz
AQ 5.4525952 sec
RG 202.17
DW 83.200 usec
DE 6.50 usec
TE 296.0 K
D1 1.00000000 sec
TD0 1
SFO1 300.3018544 MHz
NUC1 1H
P1 14.00 usec
PLW1 8.38599968 W
F2 - Processing parameters
SI 65536
SF 300.3000116 MHz
WDW EM
SSB 0
LB 0.30 Hz
GB 0
PC 1.00
VP-14
9
8
7
6
5
4
3
2
1
ppm
1.40
1.41
0.80
0.27
1.52
2.35
1.24
1.54
0.84
3.79
1.71
3.27
1.06
3.55
2.43
4.80

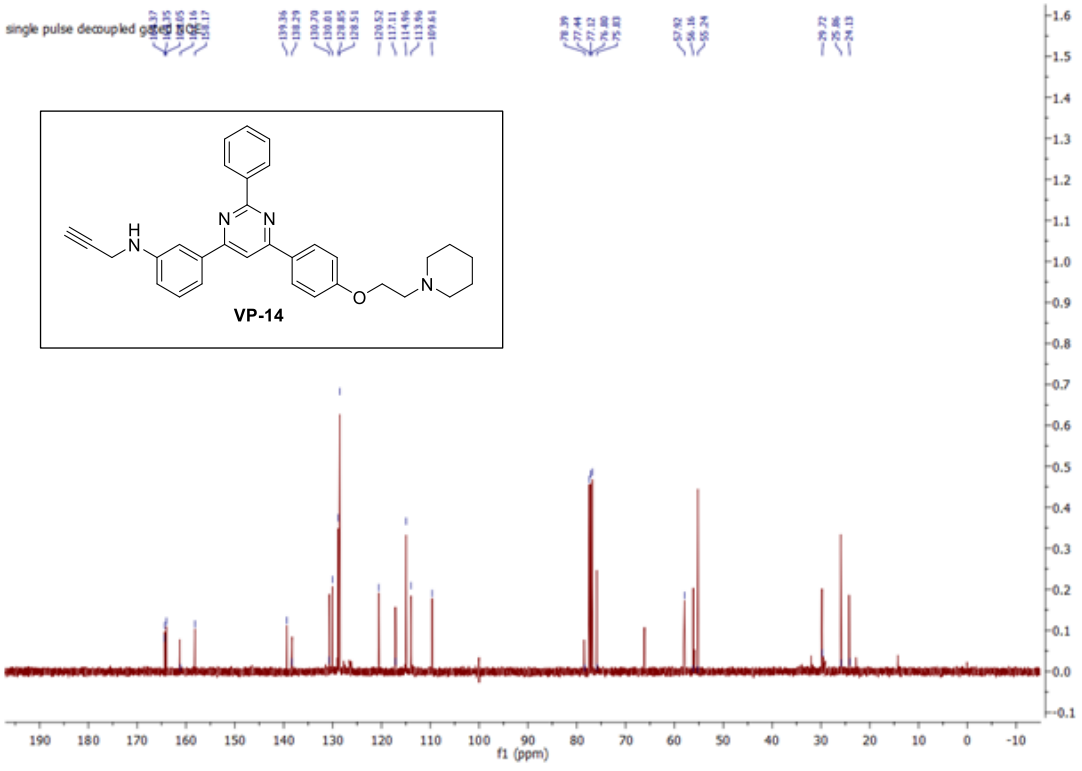
single pulse decoupled gated NOE
VP-14
190
180
170
160
150
140
130
120
110
100
90
80
70
60
50
40
30
20
10
0
-10
f1 (ppm)

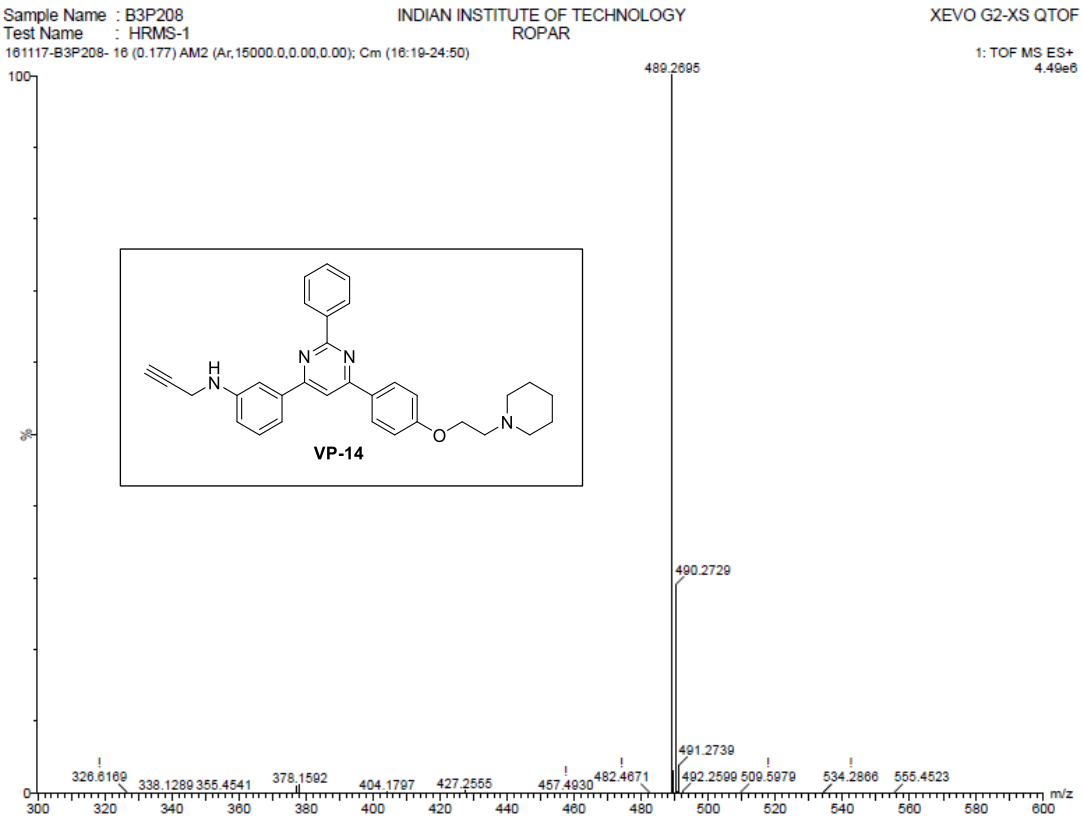
Sample Name : B3P208
Test Name : HRMS-1
INDIAN INSTITUTE OF TECHNOLOGY
ROPAR
XEVO G2-XS QTOF
161117-B3P208- 16 (0.177) AM2 (Ar,15000.0,0.00,0.00); Cm (16:19-24:50)
1: TOF MS ES+
4.49e6
100
%
0
489.2695
490.2729
491.2739
326.6169
338.1289
355.4541
378.1592
404.1797
427.2555
457.4930
482.4671
492.2599
509.5979
534.2866
555.4523
300
320
340
360
380
400
420
440
460
480
500
520
540
560
580
600
m/z
VP-14

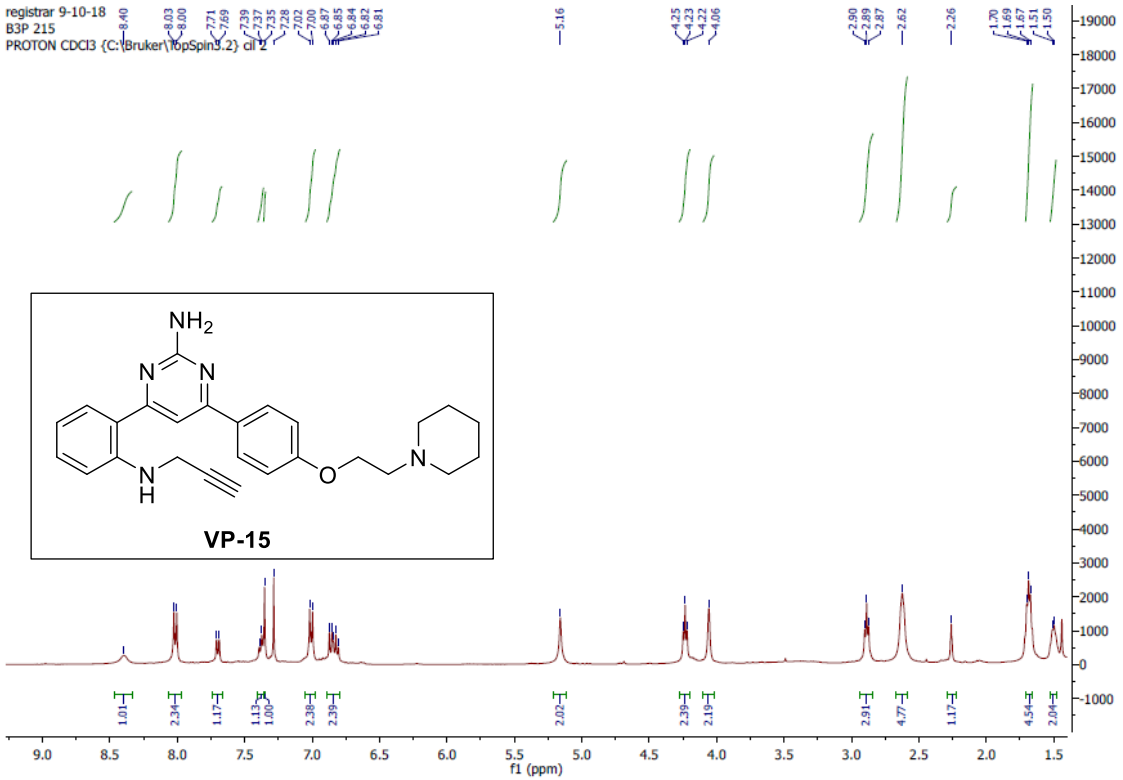
registrar 9-10-18
B3P 215
PROTON CDCl3 {C:\Bruker\TopSpin3.2} cil 2
VP-15
f1 (ppm)

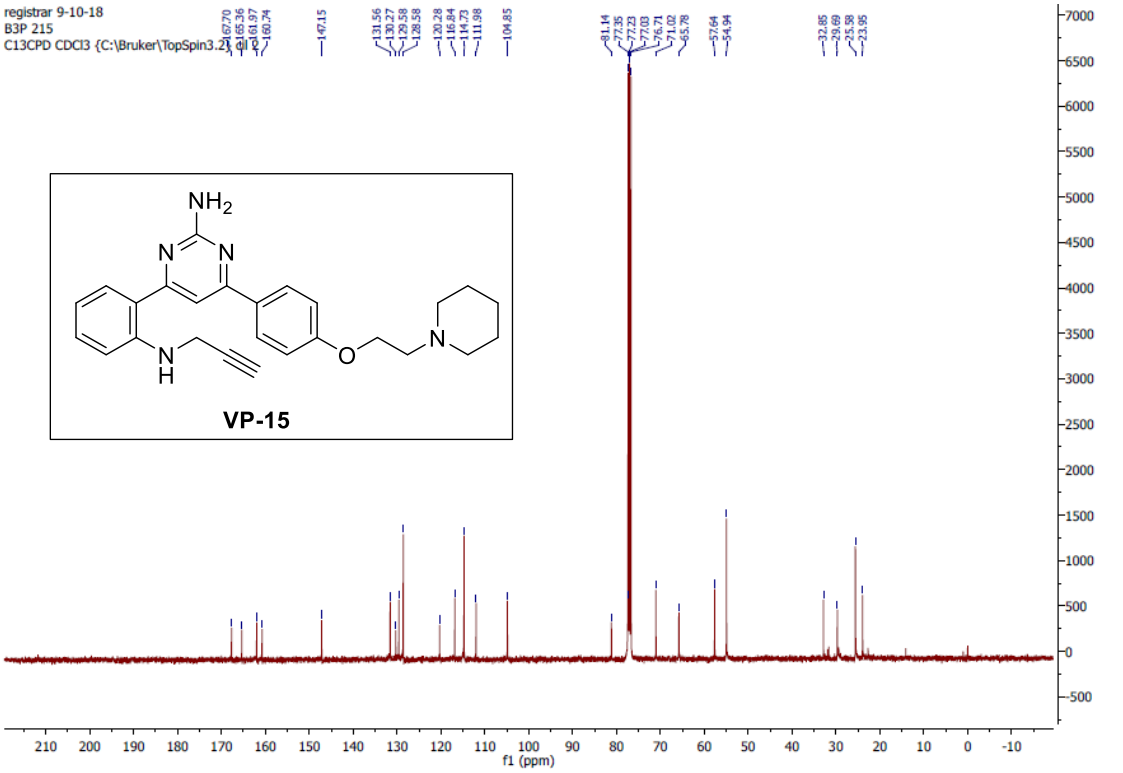
registrar 9-10-18
B3P 215
C13CPD CDCl3 {C:\Bruker\TopSpin3.2} cil 2
VP-15
f1 (ppm)

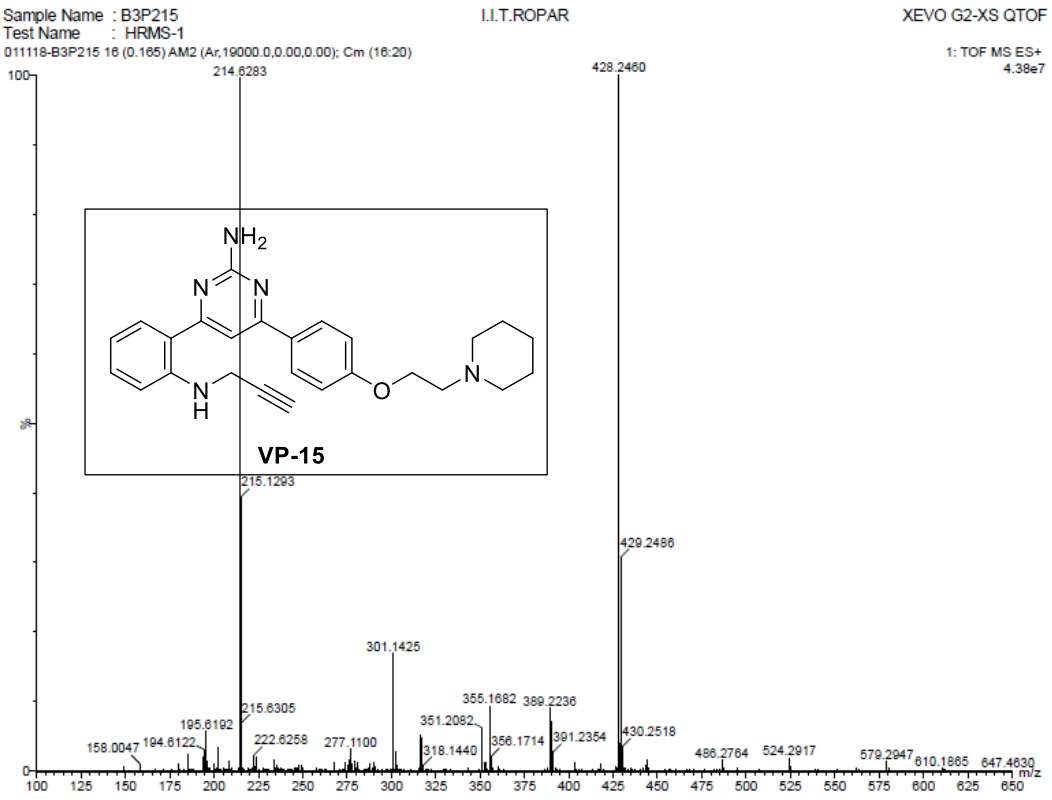
Sample Name : B3P215
Test Name : HRMS-1
I.I.T.ROPAR
XEVO G2-XS QTOF
011118-B3P215 16 (0.165) AM2 (Ar,19000.0,0.00,0.00); Cm (16:20)
1: TOF MS ES+
4.38e7
VP-15
214.6283
428.2460
215.1293
429.2486
301.1425
355.1682
389.2236
215.6305
351.2082
195.6192
391.2354
430.2518
158.0047
194.6122
222.6258
277.1100
318.1440
356.1714
486.2764
524.2917
579.2947
610.1865
647.4630
%
m/z

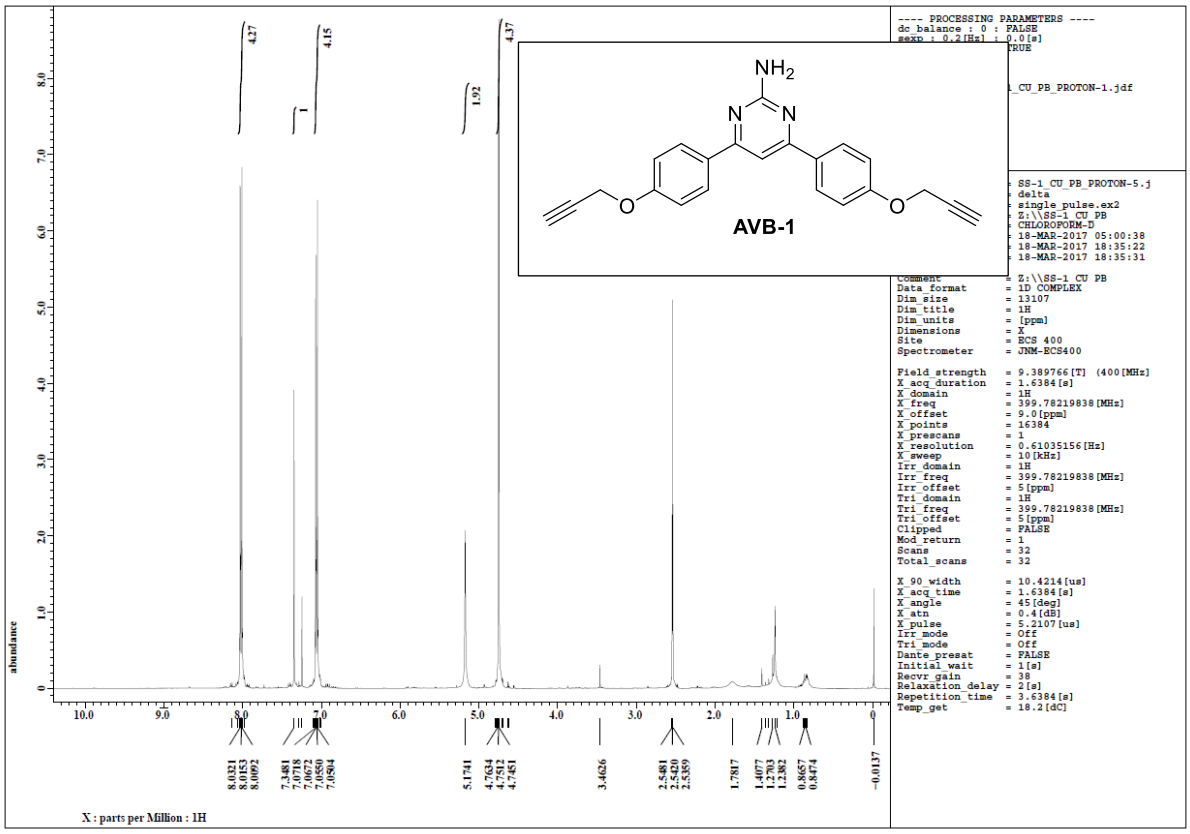
AVB-1
X : parts per Million : 1H

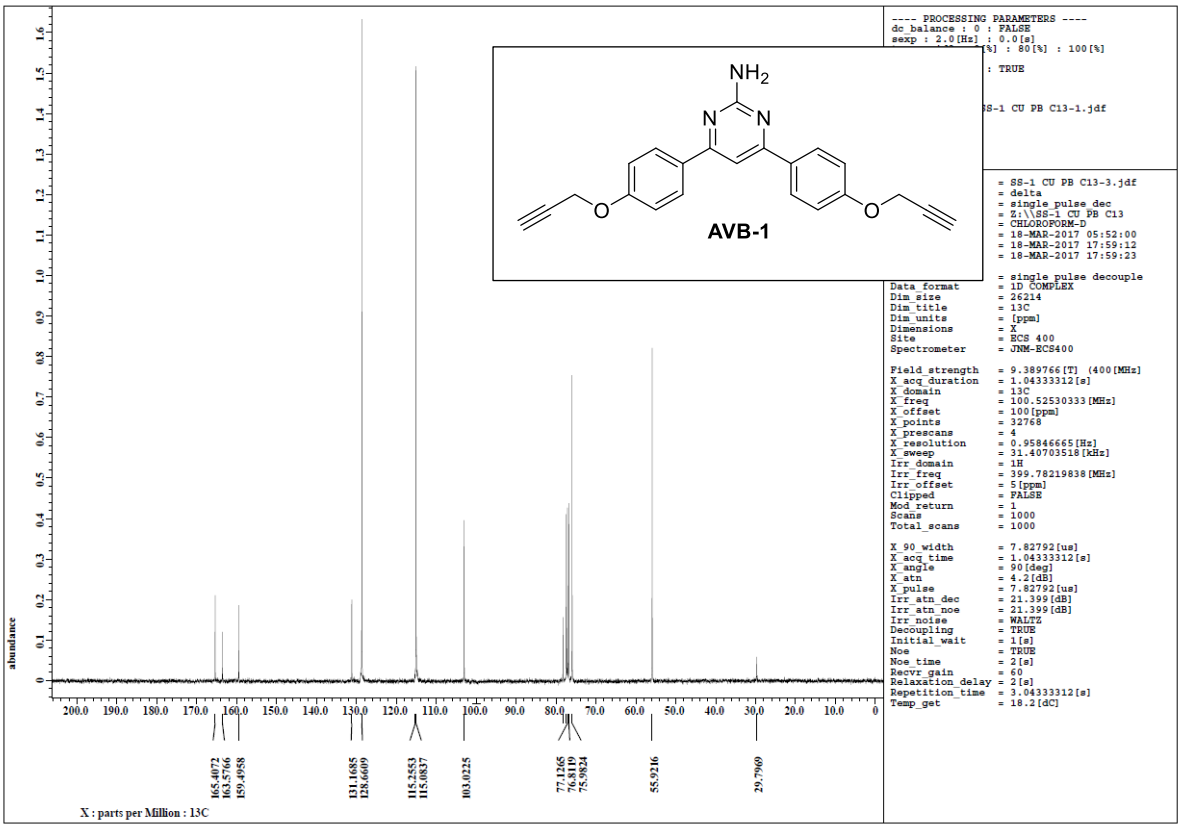
AVB-1
X : parts per Million : 13C

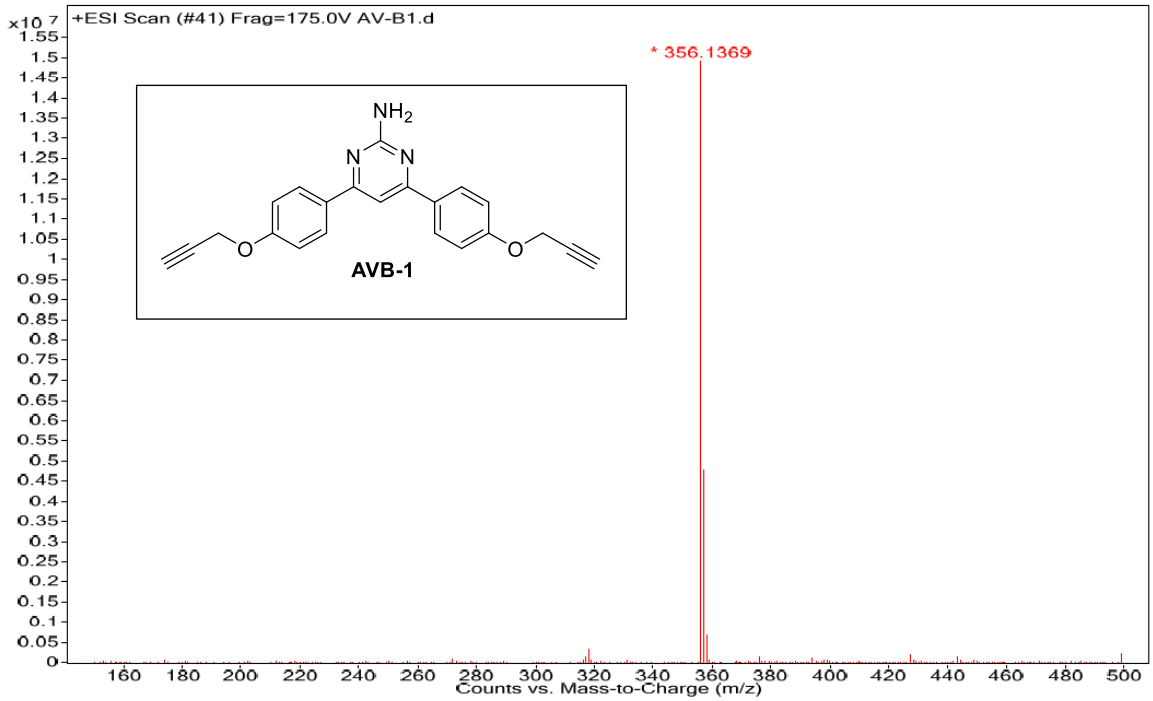
+ESI Scan (#41) Frag=175.0V AV-B1.d
x10 7
* 356.1369
NH2
N
N
O
O
AVB-1
Counts vs. Mass-to-Charge (m/z)

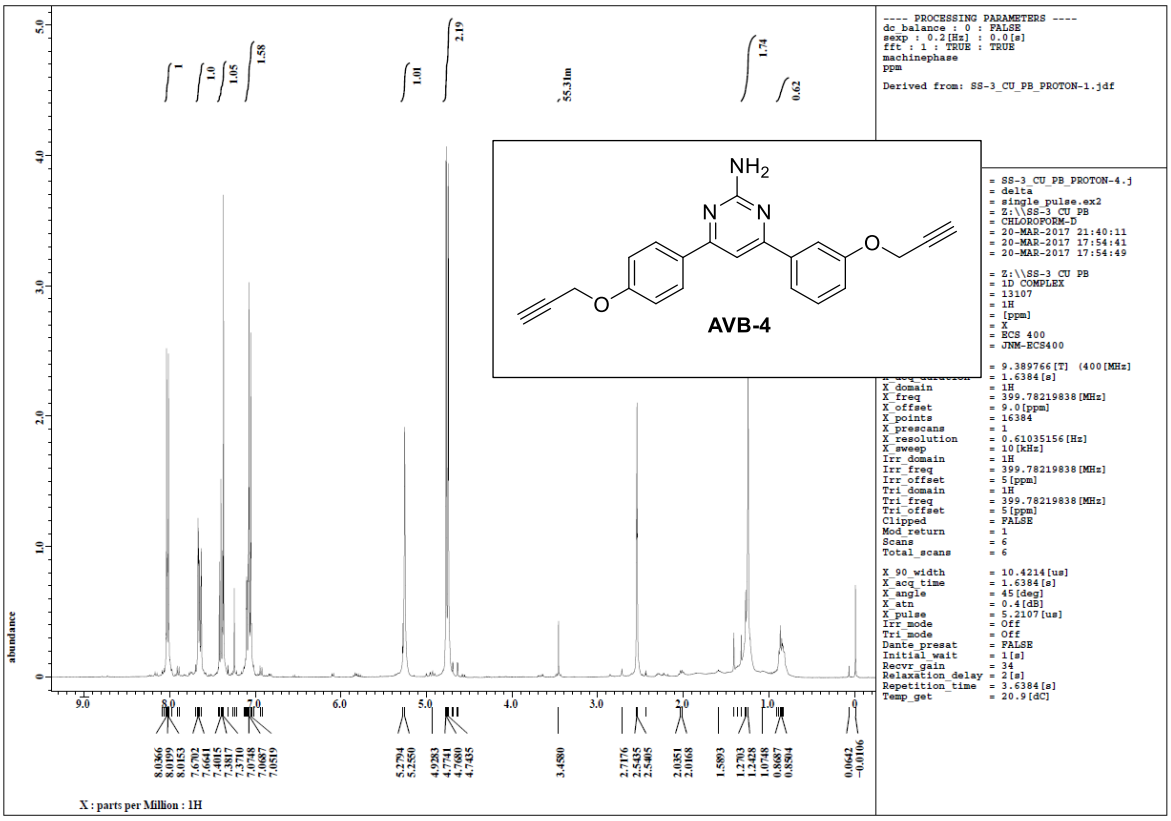
AVB-4
X : parts per Million : 1H

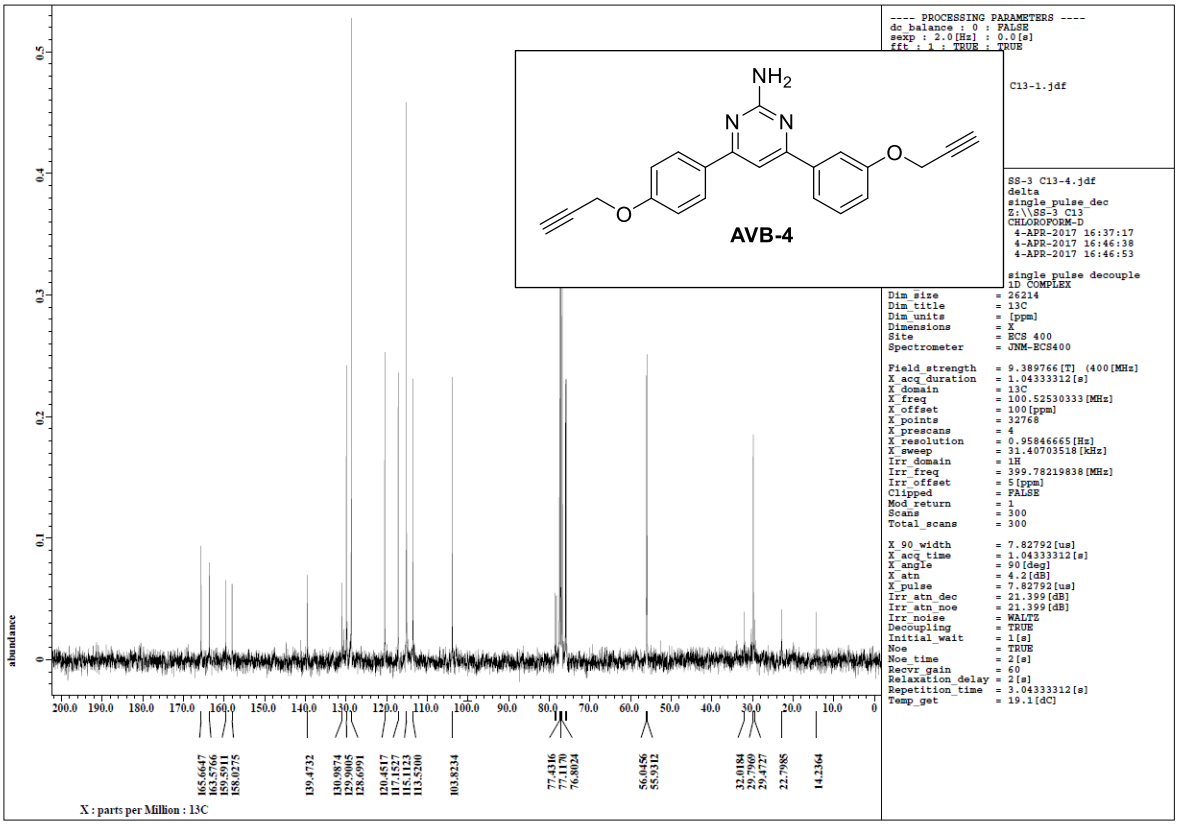
AVB-4
X : parts per Million : 13C

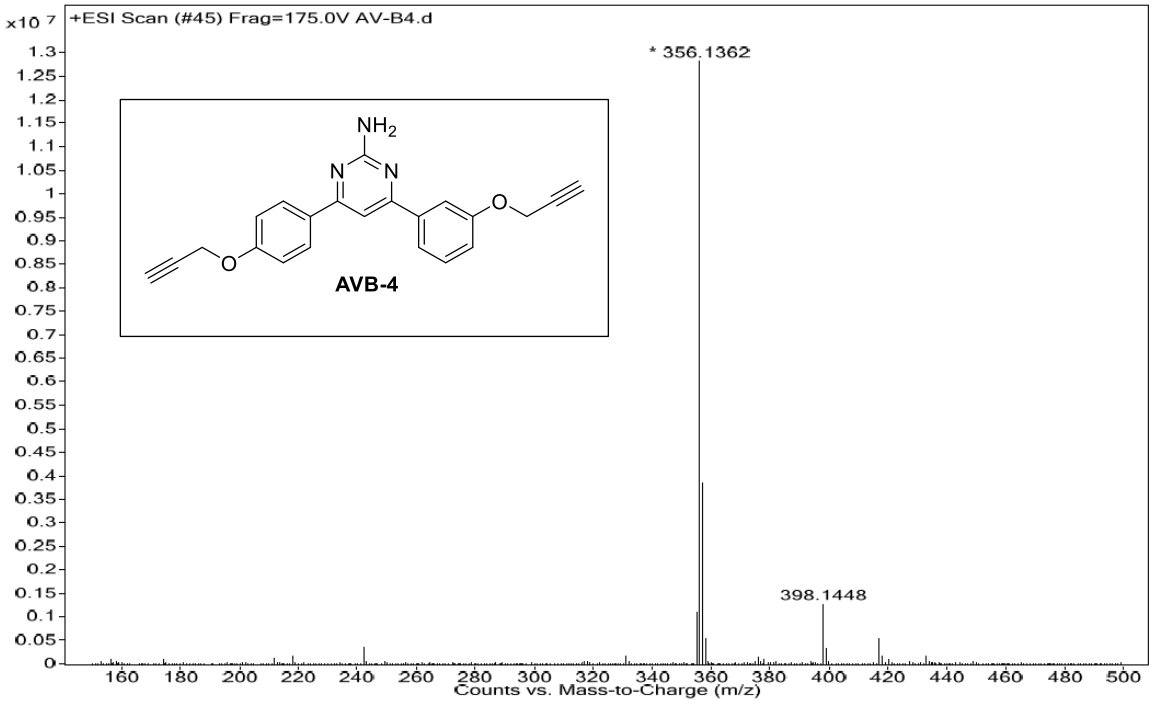
+ESI Scan (#45) Frag=175.0V AV-B4.d
x10 7
* 356.1362
398.1448
NH2
N
N
O
O
AVB-4
Counts vs. Mass-to-Charge (m/z)

INSTITUTIONAL ANIMAL ETHICS COMMITTEE
(IAEC), GNDU, Amritsar
(Registration No. 226/PO/Re/S/2000/CPCSEA)

No: 226/CPCSEA-2016/01
18/01/2017

CERTIFICATE

This is certified that the project title **Neural-glial-endothelial tripartite interactions: Unravel the basic cell-cell regulatory mechanisms involved in the central control of reproduction** has been approved by the IAEC in meeting held on 18/01/2017.

Prof. Gurcharan Kaur	Prof. Subheet Kumar Jain	Prof. Chander Shekhar Gautam
(Chairperson)	(Member Secretary)	(CPCSEA Nominee)

Reprints of Publications

ACS Chemical Neuroscience
Cite This: ACS Chem. Neurosci. 2019, 10, 252−265
Research Article
pubs.acs.org/chemneuro

4,6-Diphenylpyrimidine Derivatives as Dual Inhibitors of Monoamine Oxidase and Acetylcholinesterase for the Treatment of Alzheimer's Disease

Bhupinder Kumar,[†] Ashish Ranjan Dwivedi,[†] Bibekananda Sarkar,[‡] Sukesh Kumar Gupta,[§] Sairam Krishnamurthy,[§] Anil K. Mantha,[‡] Jyoti Parkash,[‡] and Vinod Kumar*[,†]

[†]Laboratory of Organic and Medicinal Chemistry, Department of Pharmaceutical Sciences and Natural Products, Central University of Punjab, Bathinda, Punjab 151001, India

[‡]Department of Animal Sciences, School of Basic and Applied Sciences, Central University of Punjab, Bathinda, Punjab 151001, India

[§]Department of Pharmaceutical Engineering and Technology, Indian Institute of Technology (Banaras Hindu University), Varanasi 221005, India

Supporting Information

ABSTRACT: Alzheimer's disease (AD) is a neurodegenerative disorder with multifactorial pathogenesis. Monoamine oxidase (MAO) and acetylcholinesterase enzymes (AChE) are potential targets for the treatment of AD. A total of 15 new propargyl containing 4,6-diphenylpyrimidine derivatives were synthesized and screened for the MAO and AChE inhibition activities along with ROS production inhibition and metal-chelation potential. All the synthesized compounds were found to be selective and potent inhibitors of MAO-A and AChE enzymes at nanomolar concentrations. **VB1** was found to be the most potent MAO-A and BuChE inhibitor with IC_{50} values of 18.34 ± 0.38 nM and 0.666 ± 0.03 μM, respectively. It also showed potent AChE inhibition with an IC_{50} value of 30.46 ± 0.23 nM. Compound **VB8** was found to be the most potent AChE inhibitor with an IC_{50} value of 9.54 ± 0.07 nM and displayed an IC_{50} value of 1010 ± 70.42 nM against the MAO-A isoform. In the cytotoxic studies, these compounds were found to be nontoxic to the human neuroblastoma SH-SY5Y cells even at 25 μM concentration. All the compounds were found to be reversible inhibitors of MAO-A and AChE enzymes. In addition, these compounds also showed good neuroprotective properties against 6-OHDA- and H_2O_2-induced neurotoxicity in SH-SY5Y cells. All the compounds accommodate nicely to the hydrophobic cavity of MAO-A and AChE enzymes. In the molecular dynamics simulation studies, both **VB1** and **VB8** were found to be stable in the respective cavities for 30 ns. Thus, 4,6-diphenylpyrimidine derivatives can act as promising leads in the development of dual-acting inhibitors targeting MAO-A and AChE enzymes for the treatment of Alzheimer's disease.

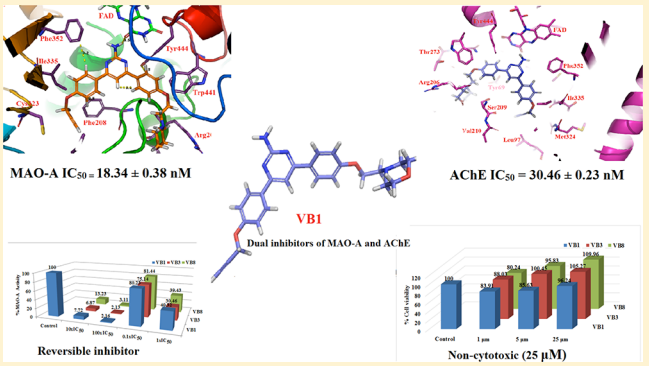

KEYWORDS: *Alzheimer's disease, MAO inhibitors, diphenylpyrimidine, acetylcholinesterase inhibitors, dual inhibitors, neuroprotective agents*

INTRODUCTION

Alzheimer's disease (AD) is a multifactorial neurodegenerative disorder characterized by the progressive memory loss, dementia, and other cognitive impairments.[1] It is estimated that 1 in every 3 senior persons dies with AD and 1 in 10 persons over 65 years of age has AD.[2] According to Alzheimer's association, in recent years' deaths due to stroke, heart disease, and HIV decreased 21%, 14%, and 54%, respectively, whereas deaths from AD increased 89%.[2] The exact molecular pathogenesis of AD is not clear; however, in most of the cases, the disease state is linked with the degeneration of neurons and glial cells or inclined metabolism of signaling neurotransmitters. Various biochemical and histopathological studies indicated that overexpressed monoamine oxidase (MAO) enzyme, low acetylcholine levels, amyloid-β (Aβ) deposits,[3] hyper-phosphorylated tau-protein aggregation, and oxidative stress play crucial roles in the pathophysiology of the disease. Depressive symptoms occur in patients suffering with AD and these may be associated with the decreased serotonergic and noradrenergic transmission in the limbic system,[4,5] Hyperactivation of MAO enzyme has been observed in patients suffering with AD that decreases the

Received: May 4, 2018
Accepted: October 8, 2018
Published: October 8, 2018

DOI: 10.1021/acschemneuro.8b00220
ACS Chem. Neurosci. 2019, 10, 252−265

Scheme 1. Reaction Scheme for the Synthesis of Target Molecules[a]

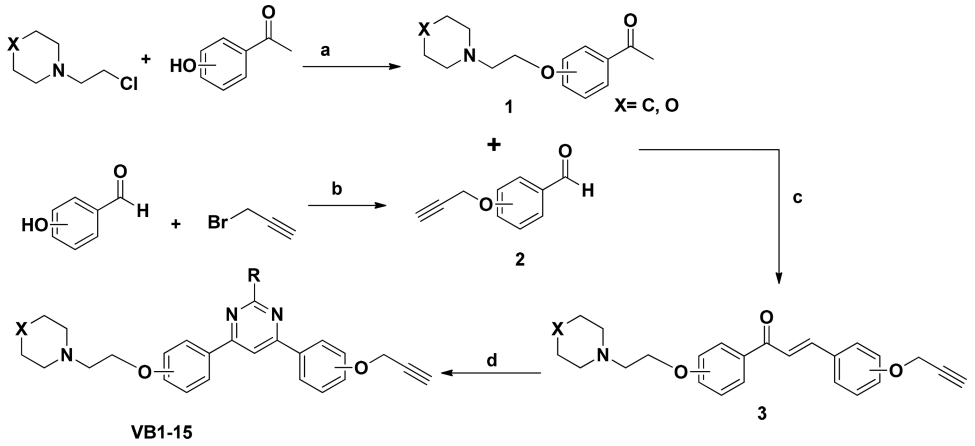

[a]Reagents and conditions: (a) K_2CO_3, KI, acetone, reflux, 6 h; (b) K_2CO_3, acetone, reflux, 6 h; (c) CH_3OH, 10% NaOH aq, rt, stirring, 3 h; and (d) Na_2CO_3, CH_3CN, amidine/guanidine/benzamidine, reflux, 24 h

concentration of dopaminergic and serotoninergic neurotransmitters. Some clinical trials have shown that deprenyl, a potential MAO-B inhibitor, alleviate the symptoms of AD.[6−8] Acetylcholine is an important neurotransmitter in the regulation of learning and memory processes. It is hydrolyzed by acetylcholinesterase (AChE) and cholinesterase inhibitors enhance the level of acetylcholine. Thus, cholinergic system has been explored as an important target for the treatment of AD. Currently, tacrine, donepezil,[9] galantamine,[10] and rivastigmine[11] are FDA (U.S. Food and Drug Administration) approved drugs that improve AD symptoms by inhibiting AChE.[11−13] Apart from the beneficial palliative properties of AChE inhibitors in AD,[14] cholinergic drugs have shown little efficacy to prevent the progression of the disease. Consequently, there is no efficient drug to cure, stop, or even slow the progression of the disease, and therefore, effective therapeutics are sought for the permanent treatment of AD.[15,16]

The pathogenesis of AD is complex, and targeting a single pathway may not be an effective strategy for the complete treatment of the disease. Multitargeted ligands design strategy involves the incorporation of two or more distinct pharmacophores of different drugs in the single structure to develop hybrid molecules.[17,18] Hence, the multitargeting ligands which can simultaneously inhibit MAO, AChE, and BuChE enzymes are being developed as drugs for the management/treatment of AD.[19,20] A number of multitargeting ligands have been reported as potential therapeutic agents for the treatment of AD.[21,22] Although many newly developed MAO, AChE, and BuChE inhibitors are under different phases of clinical trials, none of these has reached clinical use because of the number of adverse effects. Recently, we have reported various phenyl-/benzhydrylpiperazine derivatives[23] as selective ligands for MAO-A and MAO-B isoforms. In another study, we have synthesized and screened a number of pyrimidine bridged biaryls[24] for their MAO inhibition potential. Most of these compounds were found to be reversible and selective inhibitors of the MAO-B isoform. There is a high structural resemblance between the two isoforms of MAO enzyme. The volume of entrance cavity of MAO-B is smaller (~300 Å^3) as compared with the active cavity of MAO-A (~400 Å^3).[6,21] Thus, MAO-B accommodates smaller molecules, while bulkier ligands selectively bind to the MAO-A isoform. A small alteration in the structure of ligand can change its preference for either of the isoforms (MAO-A or MAO-B). Taking leads from these studies, we became interested in the design and synthesis of dual acting ligands that are equipotent to both MAO and AChE enzymes for the treatment of AD. From the literature search, we noted that the propargylamino group plays an important role in providing the neuronal and mitochondrial protective properties.[25,26] The propargyl group is also involved in the crucial covalent bond formation with FAD cofactor of MAO enzyme. Similarly, in the literature survey, it has been observed that most of the AChE inhibitors, such as donepezil, rivastigmine, pyridostigmine, phenserine galantamine, among others, contained a tertiary amino group in the scaffold as a part of ring or open chain.[9−13,27] Hence, we presumed that a tertiary nitrogen atom might be playing a crucial role for the AChE inhibition activity and introduced a piperidine/morpholine ring in the scaffold as potential pharmacophore for the AChE enzyme. The chain length between the propargyl and piperidine moieties is reported to control the dual interaction of these moieties with both the catalytic active site and peripheral anionic site of the AChE enzyme.[28] It is envisaged that incorporation of a piperidine/morpholine ring in the scaffold would make the molecules bulkier, and these compounds might show selectivity toward the MAO-A isoform.

Thus, on the basis of our previous experience and with the aim of developing dual inhibitors, a series of 4,6-diphenylpyrimidine derivatives (**VB1**-**VB15**) have been designed with a propargyl group and a piperidine/morpholine moiety as potential pharmacophores for the MAO and AChE enzymes. These compounds were found to be potent inhibitors of both MAO and AChE enzymes with IC_{50} values in nanomolar range. All the compounds were found to be reversible inhibitors of the MAO-A and AChE enzymes and displayed no toxicity to the human neuroblastoma SH-SY5Y cells. Most of these compounds were also found to be inhibitors of BuChE in the micro molar range. In the molecular dynamics simulation studies of 30 ns, the most potent MAO inhibitor (**VB1**) and most potent AChE inhibitor (**VB8**) were found quite stable in the active sites of the enzymes. These compounds also displayed neuroprotective potential against 6-OHDA and H_2O_2 induced neurotoxicity in SH-SY5Y cells.

DOI: 10.1021/acschemneuro.8b00220
ACS Chem. Neurosci. 2019, 10, 252−265

Table 1. Results of the MAO, AChE, and BuChE Inhibition Studies of Synthesized Compounds

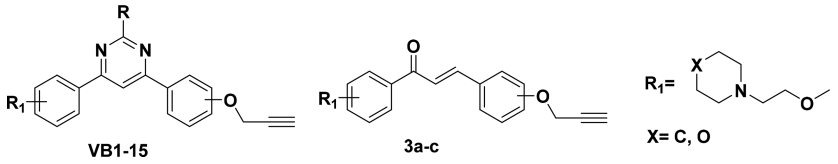

entry name	R_1	R	propargyl group position	X	IC_{50} values (mean ± SE nM) hMAO-A	hMAO-B	ee AChE	IC_{50} values (mean ± SE μM) eq BuChE	MAOSI
VB1	C4	NH_2	C4	O	18.34 ± 0.38	9910.14 ± 32.83	30.46 ± 0.23	0.666 ± 0.03	540
VB2	C4	C_6H_5	C4	O	86.35 ± 0.42	6915.62 ± 26.72	39.83 ± 0.39	14.84 ± 0.27	80
VB3	C4	CH_3	C4	O	28.33 ± 3.22	8409.53 ± 25.69	18.92 ± 0.29	14.98 ± 0.31	297
VB4	C4	C_6H_5	C4	C	103.42 ± 11.43	8376.28 ± 23.73	24.69 ± 0.76	19.72 ± 0.27	81
VB5	C4	CH_3	C4	C	752.63 ± 14.34	12140.12 ± 100.64	765.14 ± 3.51	54.46 ± 1.42	16
VB6	C4	C_6H_5	C3	O	2140.12 ± 50.43	14850.34 ± 80.62	1841.56 ± 27.67	8.216 ± 0.10	7
VB7	C4	NH_2	C3	O	230.12 ± 7.22	7313.76 ± 65.32	20.45. ± 0.17	16.65 ± 0.17	32
VB8	C4	CH_3	C3	O	1010 ± 70.42	12185.94 ± 190.86	9.54 ± 0.07	13.75 ± 0.23	12
VB9	C4	NH_2	C2	O	890.45 ± 8.32	8875.37 ± 110.52	2390.23 ± 20.72	161.6 ± 5.88	10
VB10	C4	C_6H_5	C2	O	690.34 ± 20.32	12305.63 ± 87.72	30105.12 ± 70.14	22.68 ± 0.36	18
VB11	C3	C_6H_5	C4	O	2430.23 ± 45.33	8974.73 ± 93.73	2269.82 ± 32.01	14.66 ± 0.20	4
VB12	C3	NH_2	C4	O	360.33 ± 2.34	8738.97 ± 51.73	1438.54 ± 27.67	23.48 ± 0.18	24
VB13	C3	CH_3	C4	O	450.44 ± 5.13	8469.63 ± 83.72	717.88 ± 7.54	15.27 ± 0.11	19
VB14	C4	C_6H_5	C3	C	1320.22 ± 30.22	9565.83 ± 120.53	2093.71 ± 15.69	15.95 ± 0.12	7
VB15	C4	NH_2	C3	C	1040.12 ± 40.12	7706.23 ± 95.73	1441.42 ± 20.33	34.79 ± 0.27	7
3a	C4	----	C4	O	260.12 ± 13.12	9320.12 ± 24.22	20427.18 ± 22.15	----	36
3b	C4	----	C2	O	313.23 ± 17.22	8110.11 ± 40.11	[a]	----	26
3c	C3	----	C4	O	532.42 ± 19.23	7809.02 ± 35.13	[a]	----	15
		clorgyline			4.39 ± 1.02	----	----	----	MAO-A
		pargyline			----	0.15 ± 0.02	----	----	MAO-B
		donepezil			----	----	11.32 ± 0.001	1.28 ± 0.04	----

[a]Inactive or showed less than 50% inhibitory activity at 50 μM concentration and precipitated at higher concentrations. IC_{50} values of BuChE are expressed in μM. MAO SI = IC_{50} of MAO-B/IC_{50} of MAO-A.

RESULTS AND DISCUSSION

Chemistry. All the compounds were synthesized as per the reaction procedures described in Scheme-1. Briefly, *O*-alkylated acetophenones (**1**) and benzaldehydes (**2**) were synthesized from corresponding hydroxy acetophenones or benzaldehydes by refluxing these with suitable alkyl halides in the presence of potassium carbonate and acetone as solvent. *O*-Alkylated acetophenones (**1**) and benzaldehydes (**2**) were reacted through aldol condensation to get the intermediate chalcones (**3**). In the final step, chalcones (**3**) were reacted with various amidines in the presence of sodium carbonate to obtain the target compounds 4,6-diphenylpyrimidine derivatives (**VB1-VB15**). All the final products were characterized by IR, ^{1}H NMR, ^{13}C NMR, ESI-MS, and HRMS.

MAO, AChE, and BuChE Enzyme Inhibition Studies. MAO inhibition potential of the synthesized 4,6-diphenylpyrimidine derivatives (**VB1−VB15**) was evaluated throughfluorimetric method using recombinant human MAO-A and MAO-B enzymes and Amplex Red assay kit.[29]Similarly, acetylcholinesterase inhibition activity was determined using Amplex Red Acetylcholine/Acetylcholinesterase assay kit (A12217) purchased from the Molecular Probes, Inc. /Invitrogen. The results of MAO inhibition studies are described in Table 1 in terms of IC_{50} values expressed in nanomolar concentrations. Morpholine or piperidine ethyl chains (R_1) were used as meta or para substituents at one of the phenyl rings. To develop structure activity relationship profile of 4,6-diphenylpyrimidines, three amidines were used with R as $-NH_2$, $-CH_3$ or $-C_6H_5$. Similarly, a second phenyl ring was substituted with a propargyl group at ortho/meta/para positions. MAO-A, MAO-B, and AChE inhibitory activities of some of the intermediate chalcones were also evaluated to compare them with the final products. Clorgyline, pargyline, and donepezil were used as standard inhibitors for MAO-A, MAO-B, and AChE enzymes, respectively. All the compounds were found to be selective toward the MAO-A isoform with IC_{50} values varying from 18 nM to 2430 nM. MAO-B inhibition activities of these compounds were found in the range of 7313 nM to 14850 nM. These compounds were also found to be potent inhibitors of AChE with IC_{50} values in nanomolar range. However, most of the compounds displayed BuChE inhibitory activity in the micro molar range (0.66 μM to 161.6 μM). **VB1** was found to be the most potent MAO-A inhibitor with IC_{50} value of 18.34 ± 0.38 nM and selectivity index (SI) of 540 over MAO-B. **VB1** was also found to be the most potent BuChE inhibitor in the series with IC_{50} value of 0.666 ± 0.03 μM. Similarly, **VB8** was found to be the most potentAChE inhibitor with IC_{50} value of 9.54 ± 0.07 nM. **VB3** was also found potent inhibitor of both AChE and MAO-A withIC_{50} values of 18.92 ± 0.29 nM and 28.33 ± 3.22 nM, respectively. All the chalcone intermediates were found less active as compared to the corresponding final products.

Reversibility Inhibition Studies. First generation MAO inhibitors were irreversible in nature and associated with severe side effects. Reversibility of the target compound is frequently

DOI: 10.1021/acschemneuro.8b00220
ACS Chem. Neurosci. 2019, 10, 252−265

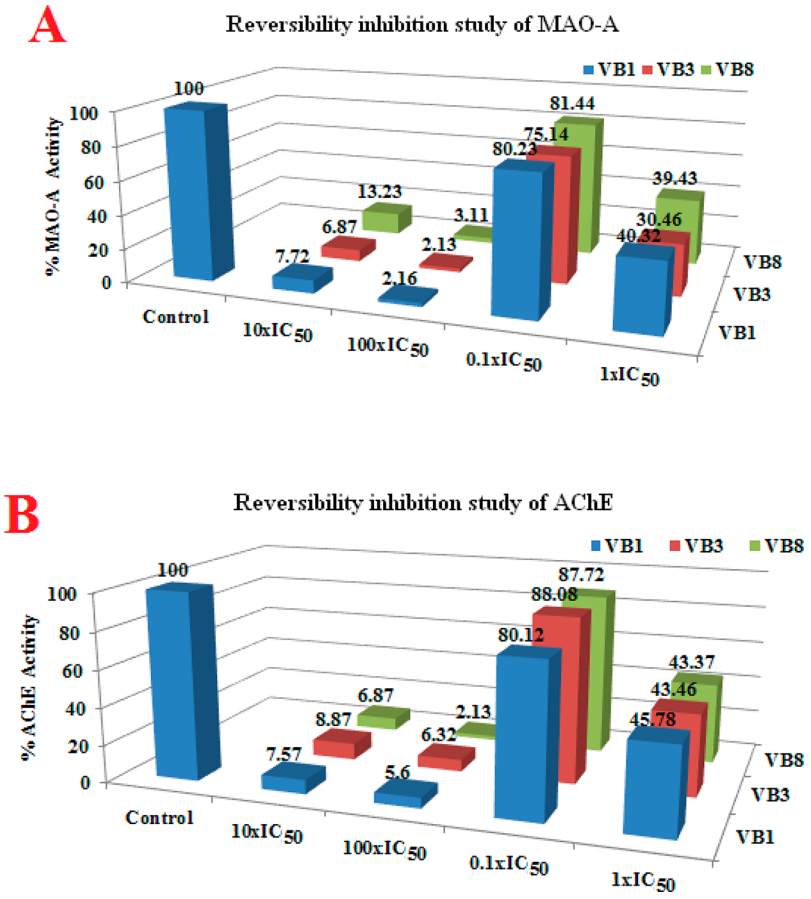

Figure 1. (A) Reversibility inhibition studies of the most potent and selective inhibitors with MAO-A enzyme; (B) Reversibility inhibition studies with AChE enzyme.

considered in designing and development of new class of inhibitors. Thus, to determine the reversible inhibition of the enzyme by the most active and selective compounds (i.e., **VB1**, **VB3** and **VB8**), reversibility inhibition studies were performed using earlier reported protocol by us and others.[23,30,31] All the tested compounds were found to be reversible inhibitors of both MAO-A and AChE enzymes. Upon treatment of MAO-A and AChE with the test compounds at concentrations of 10× IC_{50} and 100× IC_{50} activity was reduced to minimum. Upon 100 times dilution with the substrate solution, recovery of more than 75% enzymatic activity was achieved as shown in Figure 1A and Figure 1B for MAO-A and AChE respectively. Thus, it can be concluded that the tested compounds were found to be reversible inhibitors of MAO-A and AChE.

Intracellular ROS Determination. It is a well-known fact that monoamine-oxidase-mediated oxidative metabolism of monoamines leads to the production of H_2O_2 as a byproduct.[32,33] Subsequently, H_2O_2 is converted to the free radicals ($^{\bullet}OH$, $^{\bullet}O_2$) through Fenton's reaction, which contribute to the oxidative stress. An uncontrolled increase in the concentrations of the free radicals initiates free-radical-mediated chain reactions that causes oxidative damage to the cell membranes, lipid peroxidation, and DNA strand breakdown. Thus, prevention of ROS generation along with the MAO inhibition is an important strategy to reduce or eliminate neurotoxicity in neurodegenerative disorders.

Intracellular ROS level of SH-SY5Y cells was determined using nonfluorescent compound 2,7-dichlorofluorescein diacetate (DCF-DA). It is permeable and oxidized by ROS to a fluorescent compound 2,7-DCF. **VB1** was found to be the most potent ROS inhibitor and reduced the intracellular ROS level to 35.36% and 14.39% at 1 and 25 μM concentration, respectively (Figure 2). **VB3** and **VB8** also reduced the ROS levels to 42.25% and 65.25%, respectively, at 25 μM concentrations.

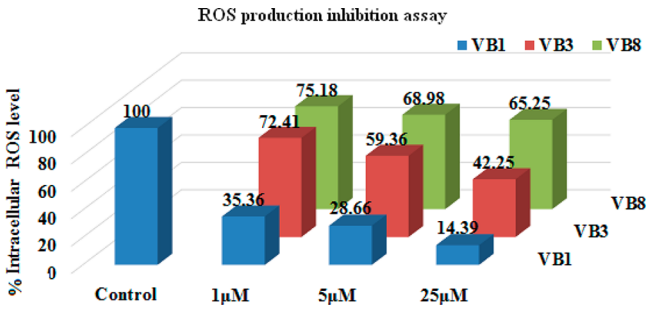

Figure 2. ROS production inhibition studies of **VB1**, **VB2**, and **VB3** against SH-SY5Y cells.

Neuroprotection Studies. The most potent compounds (**VB1**, **VB3**, and **VB8**) were evaluated for their neuroprotective potential against 6-hydroxydopamine (6-OHD) neurotoxin in the SH-SY5Y cells. However, none of the tested compounds showed promising neuroprotective potential at low concentrations (Figure 3). **VB8** was found to be the most potent among the tested compounds and displayed recovery of cells up to 61.77% at 25 μM concentration as compared with the 6-

DOI: 10.1021/acschemneuro.8b00220
ACS Chem. Neurosci. 2019, 10, 252−265

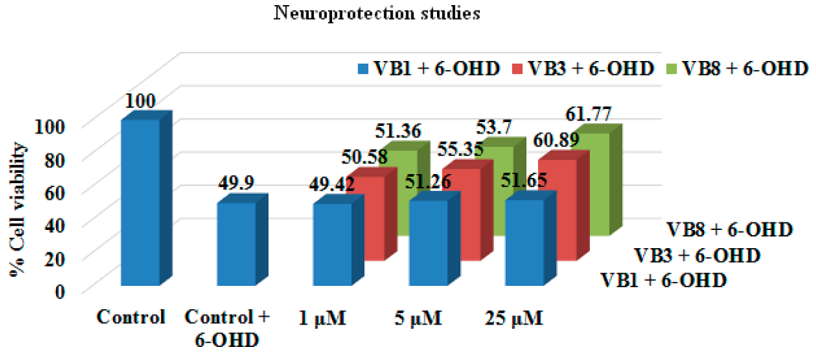

Figure 3. Neuroprotection studies of the most potent and selective MAO-A and AChE inhibitors.

OHD, which reduced the cell viability to less than 50% at 12.5 μM.

Cytotoxicity Studies. The cytotoxic effects of the most active compounds (**VB1**, **VB3**, and **VB8**) were evaluated against human neuroblastoma (SH-SY5Y) cells because of their similarity to the dopaminergic neurons.[34] The test compounds were incubated at 1, 5, and 25 μM concentrations and were analyzed after 24 h treatment time. The percentage cell viability was measured using MTT assay. As depicted in Figure 4, the compounds were found to be nontoxic against

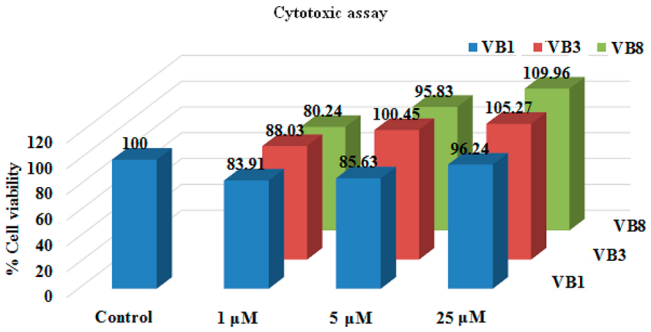

Figure 4. Cytotoxicity studies of **VB1**, **VB3**, and **VB8** against SH-SY5Y cell lines at 1, 5, and 25 μM.

the tested cells even at 25 μM concentrations. It has been observed that as concentration of the compounds increases, the percentage cell viability also increases. The least cell viability of 80% was observed with **VB8** at 1 μM concentration. Thus, keeping in view the nanomolar IC_{50} values obtained for enzyme inhibition, the current series of compounds were found to be nontoxic to the tissue cells.

Metal-Chelating Studies. Metal-chelating studies of the most potent compounds (i.e., **VB1**, **VB3**, and **VB8**) were performed with a UV−vis spectrophotometer. The absorption spectra of each compound (50 μM, final concentration) alone or in the presence of $CuSO_4$, $FeSO_4$, and $FeCl_3$ (50 μM, final concentration) was recorded. In metal-chelating studies, compounds were found to be ineffective against metals and do not form any chelates with the metal salts.

Kinetic Studies of AChE Inhibition. To determine the mechanism of inhibition of AChE, kinetic study was carried out with the most potent inhibitor of AChE (i.e., **VB8**) using eeAChE. The reciprocal Lineweaver−Burk plots (Figure 5) illustrate increased slope (decreased V_{max}) and higher intercepts (K_m) with the increasing concentration of **VB8.** The intersection point of the Lineweaver−Burk reciprocal plots was located in the second quadrant, which indicate that the inhibition mode of VB8 was mixed-type inhibition. Thus, it can be concluded that VB8 binds to both CAS and PAS of AChE simultaneously.

Molecular Docking Studies. The most potent compounds (**VB1**, **VB3**, and **VB8**) were subjected to molecular docking studies to find the interaction pattern of the molecules with the amino acid lining and their orientation at the active

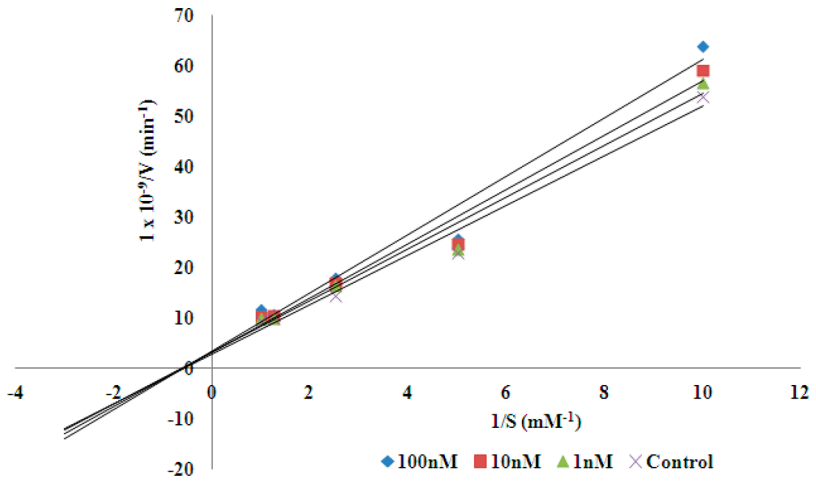

Figure 5. Kinetic study on the mechanism of ee AChE inhibition by **VB8**. Overlaid Lineweaver−Burk reciprocal plots of AChE initial velocity at increasing substrate concentration (0.1−1 mM) in the absence or presence of **VB8** are shown.

DOI: 10.1021/acschemneuro.8b00220
ACS Chem. Neurosci. 2019, 10, 252−265

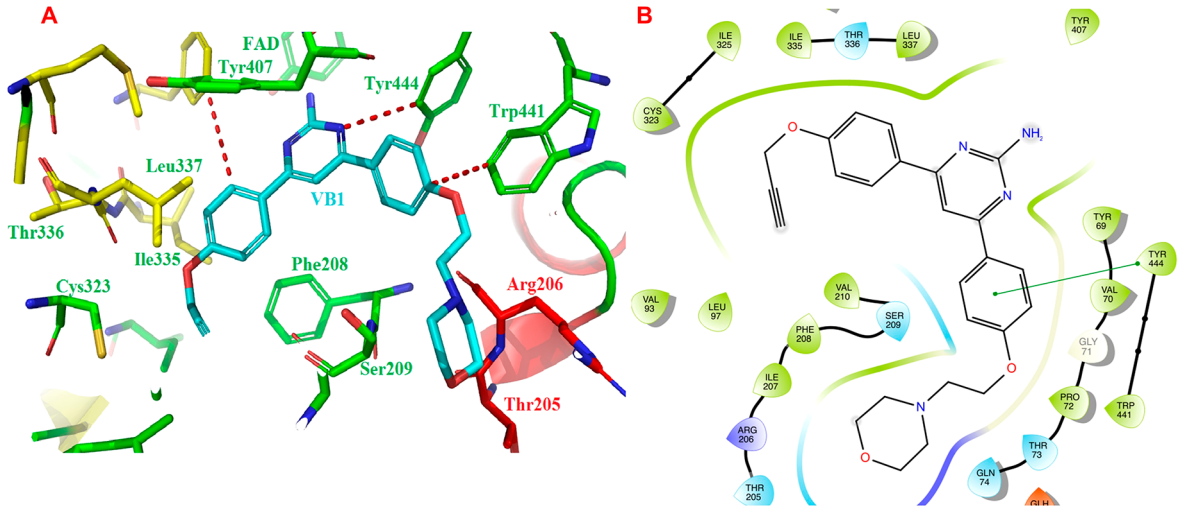

Figure 6. (A) Binding pattern (3D) of **VB1** with the amino acid residues at the active site of MAO-A (2BXR) and (B) binding interactions (2D) of **VB1** with various amino acids of MAO-A active cavity.

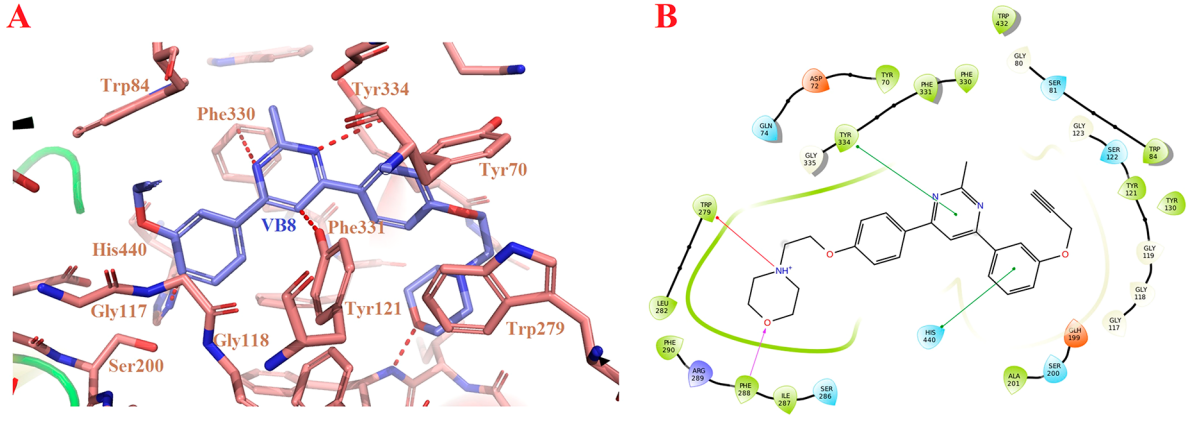

Figure 7. (A) Binding pattern (3D) of **VB8** with the amino acid residues at the active site of AChE (PDB ID 1EVE) and (B) binding interactions (2D) of **VB8** with various amino acids of AChE active cavity.

site of the receptors. Compounds were docked at the active site of hMAO-A (PDB IDs 2BXR and 2Z5X)[35,36] and AChE (PDB ID 1EVE).[37] The X-ray crystal structures were imported from the protein data bank using Maestro 11.1 (Schrödinger LLC). The docking procedure employed was first validated by redocking the cocrystallized ligands into the MAO and AChE models and the process was found suitable for the current study. Three most potent compounds (**VB1**, **VB3**, and **VB8**) were docked at the structure of MAO-A (2BXR and 2Z5X) enzymes cocrystallized with clorgyline and harmine.

All the compounds were found to accommodate nicely to the active site of MAO-A delineated by hydrophobic residues Tyr69, Phe208, Arg296, Ile335, Leu337, Phe352, Tyr407, Trp441, Tyr444, and FAD. Most of the interactions observed were hydrophobic and $\pi-\pi$ aromatic stacking which showed hydrophobic nature of the MAO-A active site. Pyrimidine moiety was aligned toward the FAD cofactor while 4-(2-phenoxyethyl)morpholine fragment was exposed to the outer part of the active site cavity lined by the polar amino acid residues Thr205 and Arg206. The (prop-2-yn-1-yloxy)benzene fragment of **VB1** showed $\pi-\pi$ aromatic interaction with Phe352, while the pyrimidine ring showed $\pi-\pi$ aromatic interaction with Tyr444. 4-(2-Phenoxyethyl)morpholine showed $\pi-\pi$ aromatic interaction with Trp441. **VB3** and **VB8** also showed interactions with the same set of amino acids at the active cavity of the enzyme (Figure S1). The only difference observed in the conformation of **VB8** was the orientation of propargyl group. In both **VB1** and **VB3**, the propargyl group was oriented toward the rest of the molecule to the inner side of the cavity, whereas in **VB8**, it was directed away from the rest of the molecule toward outer side of the cavity (Figure 6 and Figure S1). This difference in the conformation of **VB8** might be responsible for its lower activity toward MAO-A (Figures 6 and S1). The propargylamino group of clorgyline is reported to interact with FAD cofactor and form a strong covalent bond. These strong interactions might be responsible for the irreversible nature of clorgyline. As evident from Figure 6 and Figure S1, in **VB1**, **VB3** and **VB8** pyrimidine ring is aligned close to the FAD, whereas the propargyl group is oriented away from the FAD cofactor. These conformations of the ligands at the active site negate any possibility of covalent bond formation between the propargyl group and FAD. Thus, these ligands may not form strong covalent bond with the enzyme and hence display reversible inhibition activity. Son et al.[36] reported a very high-resolution structure of human MAO-A cocrystallized with a reversible MAO-A inhibitor harmine which was different from the structure reported by Colibus et al.[35] On the advice of one

DOI: 10.1021/acschemneuro.8b00220
ACS Chem. Neurosci. 2019, 10, 252−265

reviewer of this manuscript, we have also performed docking studies of reversible MAO-A inhibitor VB1 with PDB-2Z5X (Figure S2). In this case too, it has been observed that the pyrimidine ring was aligned toward the FAD cofactor, and the propargyl group was directed toward the outer part of the cavity aligned with amino acid resides Val484 and Thr487 (Figure S2). These observations further strengthen our claim that the propargyl group may not be able to form a strong covalent bond with the FAD and hence current series of compounds behave as reversible inhibitors.

Similarly, the most potent compounds (**VB1**, **VB3**, and **VB8**) were docked in the crystal structure of AChE (PDB ID 1EVE) enzyme cocrystallized with donepezil (Figures 7 and S3). All the compounds were accommodating nicely to the active site as well as the peripheral anionic site (PAS) of AChE as done by the standard inhibitor donepezil. The AChE anionic site, composed of Trp84, Tyr130, Phe330, and Phe331 residues, whereas the peripheral anionic site (PAS) consists of five amino acids-Tyr70, Asp72, Tyr121, Trp279, and Tyr334. The increased chain length between the phenyl and morpholine ring, as compared with the N-benzylpiperidine moiety of donepezil, pushed the 4-(2-phenoxyethyl)morpholine fragment of **VB1** and **VB3** inside the CAS of AChE. The morpholine moiety was aligned toward the narrowest part of the active site cavity. However, for **VB8**, the binding alignment was inverted and 4-(2-phenoxyethyl)morpholine fragment was aligned toward the 2,3-dihydroinden-1-one fragment of the donepezil (Figure 8). Thus, the (prop-2-yn-1-yloxy)benzene fragment of **VB8** was oriented toward CAS of AChE.

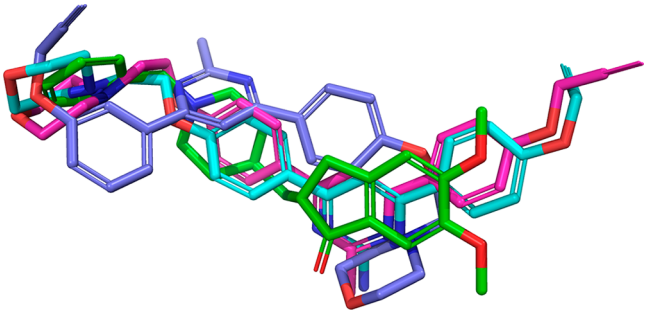

Figure 8. Superimposed poses of **VB1** (cyan), **VB3** (pink), and **VB8** (violet) with donepezil (green) at the active site of AChE (1EVE).

Comparison of the binding patterns (predicted) of donepezil and **VB8** reveals the plausible reason of its high potency for AChE. Donepezil showed $\pi-\pi$ aromatic interactions of N-benzylpiperidine fragment with Trp84 residue and cation$-\pi$ interactions with Phe331 and Tyr334 residues. The 2,3-dihydroinden-1-one fragment of the donepezil showed $\pi-\pi$ stacking with Trp279. **VB1** and **VB3** preserved most of the interactions of the donepezil with the same set of amino acid residues. These compounds showed cation$-\pi$ interactions with Trp84 and $\pi-\pi$ stacking with Trp279, Phe331, and Tyr334 residues. Similarly, pyrimidine fragment of **VB8** showed $\pi-\pi$ aromatic stacking with Phe331 and Tyr334. However, 4-(2-phenoxyethyl)morpholine fragment was aligned in the opposite direction as compared with the benzylpiperidine moiety of donepezil and displayed cation$-\pi$ interactions with the Trp279 residue and hydrogen bonding interactions with the Phe288 residue through oxygen atom of the morpholine ring (Figures 7 and S3). Furthermore, the (prop-2-yn-1-yloxy)benzene fragment of **VB8** showed additional aromatic $\pi-\pi$ stacking with His440 residue, which is not observed for **VB1**, **VB3**, and donepezil.

VB1, **VB3**, and **VB8** were superimposed with donepezil at the active site of AChE (Figure 8). The (prop-2-yn-1-yloxy)benzene fragments of **VB1** and **VB3** were oriented toward 2,3-dihydroinden-1-one fragment of the donepezil in PAS of AChE, whereas the 4-(2-phenoxyethyl)morpholine fragment overlaps with the N-benzylpiperidine moiety of donepezil and is oriented toward CAS. Pyrimidine rings of **VB1** and **VB3** showed good overlap with the dihydroindenone part of donepezil. Surprisingly, **VB8** showed reverse orientation and its (prop-2-yn-1-yloxy)benzene fragment overlapped with the benzylpiperidine moiety of the donepezil aligned toward CAS of AChE. The 4-(2-phenoxyethyl)-morpholine moiety of **VB8** oriented toward 2,3-dihydroinden-1-one fragment of donepezil and accommodate in the PAS of AChE. The pyrimidine ring of **VB8** overlapped with the piperidine ring of donepezil, whereas the (prop-2-yn-1-yloxy)benzene fragment overlapped with the benzylic ring. Thus, altered orientation and additional interactions at the active site might be responsible for the high potency of **VB8** toward AChE enzyme.

Molecular Dynamics Simulation Studies. Molecular dynamics simulation (MD) were performed to study the protein$-$ligand interactions and to determine the thermodynamic stability of the docked compounds at the active pocket of the enzymes. The protein$-$ligand docked complexes of the most active compounds **VB1** with MAO-A and **VB8** with AChE were used for MD simulations. The MD simulation studies were conducted for 30 ns, and the interaction pattern of the test compound with different amino acids was analyzed. MD simulations yielded stable trajectories for **VB1** with MAO-Ain the first 20 ns, as noted by the time evolution of the potential energy and the root-mean-square deviation (RMSD) of the protein backbone, which ranged from 0.6 to 1.0 Å (Figure 9). There were no major structural alterations, and the pyrimidine moiety adopted similar orientation in the active site of MAO-A (Figure 9) as obtained during the docking studies. In particular, the 4-(2-phenoxyethyl)morpholine fragment of **VB1** was stacked against Tyr444 and Arg206. After the time

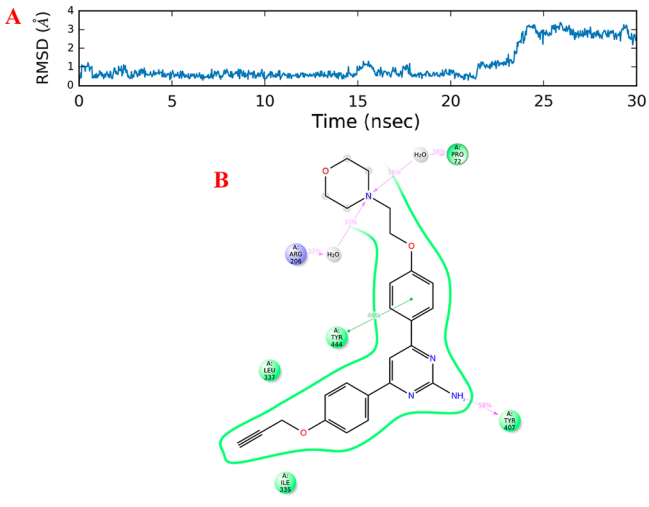

Figure 9. (A) RMSD graph of MD studies of **VB1** with MAO-A for 30 ns and (B) interactions of **VB1** with the active site residues of MAO-A after 30 ns MD simulation studies.

DOI: 10.1021/acschemneuro.8b00220
ACS Chem. Neurosci. 2019, 10, 252−265

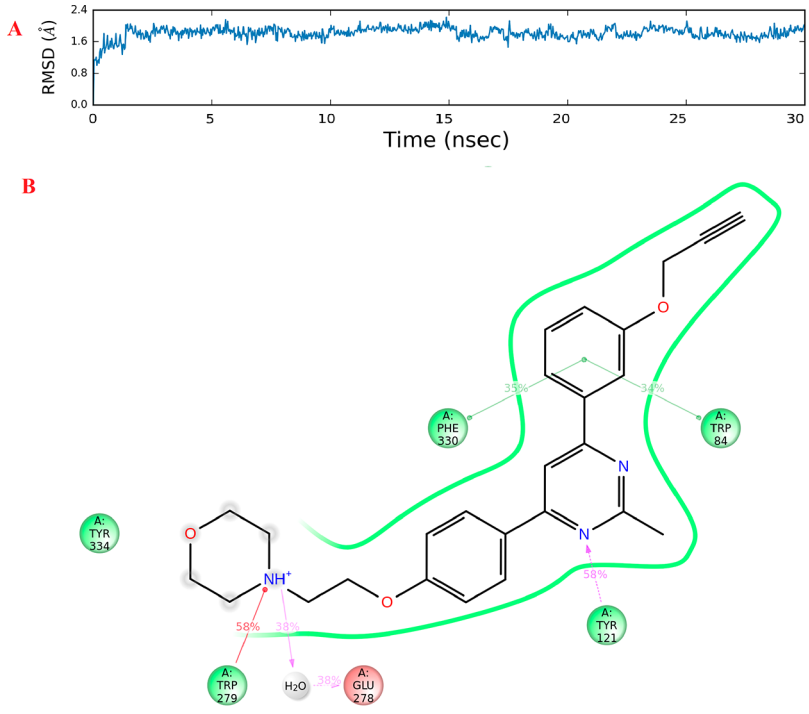

Figure 10. (A) RMSD graph of MD simulations studies of **VB8** with AChE for 30 ns and (B) interactions of **VB8** with the active site residues of AChE during 30 ns MD simulation studies.

Table 2. Physiochemical Properties of the Most Potent and Selective MAO-A and AChE Inhibitors[a]

name	mol. wt.	Log P	HB donor	HB acceptor	% human oral absorption	QPlogBB (optimum range −3.0−1.2)	BBB permeability predicted
VB1	430.505	3.94	3	8	96	−0.65	+ve
VB3	429.518	5.06	1	7	100	0.22	+ve
VB8	429.518	5.09	1	7	100	0.28	+ve

[a]+ve = high blood-brain barrier permeability, HB = hydrogen bond, QPlogBB = qualitatively predicted logarithmic ratio between the concentration of a compound in the brain and blood, LogP = partition coefficient of a molecule between an aqueous and lipophilic phase (octanol and water).

interval of 22 ns, there was a sudden hike in the RMSD, and thereafter, it showed stable trajectory up to 30 ns. RMSD oscillates in the range of 2 Å to 3 Å in this time interval. In the MD simulations studies it has been observed that **VB1** preserved most of the interactions observed during the docking studies. In addition, some new interactions with various amino acid residues were also observed (Figure 9). In the MD simulations, $\pi-\pi$ aromatic interaction with Tyr444 was retained. The NH_2 group present on the pyrimidine fragment move more toward Tyr407 and formed a hydrogen bond with it. The nitrogen atom of the morpholine ring formed hydrogen bonds with Pro72 and Arg206 through water bridge formation. It demonstrates the structural integrity of the MAO-A-VB1complex, and displayed similar binding features as done by clorgyline.

The MD simulations of AChE−**VB8** complex was performed to determine the binding stability of **VB8** at CAS and PAS of AChE. The complex yielded stable trajectories from 2 to 30 ns, as noted by the time evolution of the potential energy and the root-mean-square deviation (RMSD) of the protein backbone. The RMSD values for AChE−**VB8** complex ranged from 1.6 to 2.0 Å (Figure 10). For the initial 2 s, the RMSD value increase from 0.8 to 1.6, and thereafter it remained stable up to 30 ns. Analyzing the MD trajectory of AChE−**VB8** complex, it can be concluded that **VB8** showed strong tendency to be localized in the binding region of AChE. Nitrogen atom of the pyrimidine ring form hydrogen-bond with Tyr121. In the PAS of AChE, the protonated nitrogen atom of morpholine moiety maintained the initial cation−π interaction (from comparison of Figure 7 and Figure 10) throughout the MD simulations interval, indicating stable binding of **VB8** with AChE. In addition, the morpholine ring formed hydrogen bonding with the Glu278 residue through water bridge formation. The (prop-2-yn-1-yloxy)benzene fragment aligned toward CAS of AChE and showed aromatic $\pi-\pi$ interaction of **VB8** with Tyr330 and Trp84. The MD simulations of **VB8** does not indicate any abrupt local force that could potentially break up the inhibitor or can even delocalize it from the binding site of AChE. Thus, from the MD simulations studies of AChE-VB8complex, it can be concluded that the complex is stable and this stability might be responsible for the high *in vitro* potency of **VB8** for AChE.

ADME Properties. To determine the drug-like characteristics of the synthesized compounds, ADME parameters of these compounds were determined using Qikprop application of Schrodinger. **VB1** displayed very good drug-like profile with LogP value less than 5 and QPlogBB value as −0.65. In addition, **VB1** showed optimum oral absorption and blood-brain barrier permeability. **VB3** and **VB8** also showed 100% oral absorption and QPlogBB in the optimum range to cross the blood brain barrier (Table 2).

DOI: 10.1021/acschemneuro.8b00220
ACS Chem. Neurosci. 2019, 10, 252−265

SAR Studies. In the current studies, three different amidines have been used with R as $-NH_2$, $-CH_3$, or $-C_6H_5$ (Table 1). One ring of diphenylpyrimidines is optionally substituted with the morpholine or piperidine ethyl chain while other phenyl ring is functionalized with a propargyl group at ortho, meta, or para positions. The effect of different substituents on the activity is analyzed as reported in the Table 1. The compounds were evaluated for MAO-A, MAO-B, ee AChE, and eq BuChE inhibitory activities using enzymatic assays. All the compounds were found to be selective for MAO-A isoform with IC_{50} values in the nanomolar range and with moderate to very high selectivity index. It has been observed that the compounds with morpholine ethyl chain and propargyl group at para positions of both the phenyl rings showed high potency for MAO-A isoform and eeAChE. **VB1** with R as $-NH_2$ was found to be the most potent MAO-A inhibitor with an IC_{50} value of 18.34 nM, and it also showed potent ee AChE inhibitory activity with an IC_{50} value of 30.46 nM. **VB1** was also found to be the most potent BuChE inhibitor in the series with IC_{50} value of 0.666 ± 0.03 μM. **VB3** with R as −CH3 also showed strong inhibition potential against MAO-A and ee AChE with IC_{50} values of 28.33 and 18.92 nM, respectively. Replacement of -NH_2 with C_6H_5 in **VB2** reduces MAO-A activity by 5-fold. Shifting of propargyl group from para position to meta position (**VB7**) reduces MAO-A inhibitory activity by more than 12-fold, but there was no effect on the ee AChE inhibitory activity. Similarly, in **VB8**, meta propargyl group reduces MAO-A inhibitory activity by 35-fold when compared with **VB3**. However, **VB8** was found to be the most potent ee AChE inhibitor in the series with an IC_{50} value of 9.54 nM. In general, replacement of morpholine ring with the piperidine ring reduces MAO-A inhibitory activity (**VB4** and **VB5**). Shifting of morpholine substituent from para (**VB1**) to meta position (**VB12**) decreases MAO-A activity by 19-fold and ee AChE activity by 47-fold. It has been found that compounds with a propargyl substitution at the ortho and meta positions were less active toward MAO-A as compared with the para substituents. The current series of compounds displayed high selectivity index toward AChE as compared to BuChE (Table 1). **VB1** was found to be the most potent BuChE inhibitor, however, it showed SI of 22-fold for AChE. In the current series of compounds, VB8 displayed the highest SI of about 10^3 for AChE. Replacement of the amino group with methyl or phenyl groups (**VB2** and **VB3**) decreases BuChE inhibitory activity by about 22-fold. Shifting the propargyl group from para (**VB1**) to ortho (**VB9**) position drastically reduced the activity by about 240-fold. Similarly, shifting of morpholine ring from para (**VB1**) to meta position (**VB12**) decreases BuChE activity by 35-fold.Thus, **VB1**, **VB3**, and **VB8** were found to be the most promising compounds among the reported series of compounds.

CONCLUSIONS

AD is multifactorial in nature, and different enzymes including MAO, AChE, and amyloid beta are implicated in its pathogenesis. The pathomechanism of AD is complex in nature and single target drugs proved to be ineffective for the treatment of the disease. Thus, a multitarget directed approach is being explored for the development of effective drug candidates for the treatment of AD. A drug active on multiple targets may be characterized by an improved efficacy when compared with a highly selective pharmacological agent. Multitarget activities may potentiate efficacy either additively or synergistically and be less prone to the drug resistance. In the current study, a series of 4,6-diphenylpyrimidines has been rationally designed that can simultaneously target MAO enzymes and acetylcholinesterases for the treatment of AD. The phenyl rings were optionally substituted with a morpholine or piperidine ethyl chain and *O*-propargylated groups at ortho, meta, and para positions, and structure−activity relationship profile has been generated. Most of the compounds were found to be potent dual inhibitors of MAO-A isoform and AChE with IC_{50} values in nanomolar range. In the current series, **VB1** was found to be the most potent MAO-A and BuChE inhibitor with IC_{50} values of 18.34 ± 0.38 nM and 0.66 ± 0.03 μM. It also displayed potent AChE inhibitory activity with IC_{50} value of 30.46 ± 0.23 nM. **VB3** was another promising compound in the series with IC_{50} values of 28.33 ± 3.22 nM and 18.92 ± 0.29 nM against MAO-A and AChE, respectively. **VB8** was found to be the most potent AChE inhibitor with an IC_{50} value of 9.54 ± 0.07 nM and displayed very high SI (10^3) for AChE over BuChE. In the reversibility inhibition studies, **VB1**, **VB3**, and **VB8** were found to be reversible inhibitors of MAO-A and AChE. These compounds also displayed neuroprotective potential against 6-OHDA and H_2O_2 induced neurotoxicity in SH-SY5Y cells. Cytotoxicity studies were also performed with the three lead compounds using SH-SY5Y cell lines, and the compounds were found to be nontoxic even at 25 μM concentration. In the MD simulation studies of 30 ns, **VB1** and **VB8** were found to be stable in the active site of MAO-A and AChE, respectively. In the physicochemical evaluation studies, the most active compounds were found to possess drug-like characteristics with optimum oral absorption and good permeability to blood brain barrier. Thus, some of these dual acting compounds have the potential to be developed as drug candidates for the treatment of AD.[30]

EXPERIMENTAL SECTION

General Procedure for the Synthesis of 1 and 2. To hydroxy substituted acetophenone (0.5 g) or benzaldehydes (0.5 g), morpholine or piperidine ethyl chloride (1.2eq) was added in the presence of potassium carbonate as base (2.4eq) and acetone (30 mL) as solvent. The reaction mixture was refluxed for 12 h at 60 °C. The progress of reaction was monitored via TLC. After completion of the reaction, excess solvent was evaporated from the mixture using vacuum rotary evaporator. Then water (10 mL) was added, and the aqueous phase was extracted with ethyl acetate (10 mL × 3) washed with brine, dried over anhydrous Na_2SO_4, and the organic solvent was concentrated under vacuum using rotary evaporator.

General Procedure for the Synthesis of 3. To a mixture of **1** (1 equiv) and **2** (1 equiv) in methanol (20 mL), aqueous sodium hydroxide (20%) was added slowly with continuous stirring. The reaction mixture was stirred for 3 h at room temperature. The completion of the reaction was monitored via TLC. After completion of the reaction, excess solvent was evaporated from the mixture using a rotary evaporator. Chilled water was poured into the reaction mixture, and precipitates of **3** were filtered and dried.

General Procedure for the Synthesis of VB1−VB15. To a mixture of **3** (500 mg) and amidine (1.2 equiv), anhydrous sodium carbonate (2.4 equiv) was added in acetonitrile (5 mL) as solvent. The reaction mixture was refluxed for 24 h at 85 °C. The progress of the reaction was monitored via TLC. After completion of the reaction, excess solvent was evaporated under vacuum using rotary evaporator. Then water (10 mL) was added, and the aqueous phase was extracted with ethyl acetate (3 × 10 mL), washed with brine, dried over anhydrous Na_2SO_4, and the organic solvent was concentrated under vacuum using rotary evaporator and purified via column chromatog-

DOI: 10.1021/acschemneuro.8b00220
ACS Chem. Neurosci. 2019, 10, 252−265

raphy (EtOAc:Pet ether). The final products were characterized by NMR spectroscopy and HRMS.

Spectral Analysis. *4-(4-(2-Morpholinoethoxy)phenyl)-6-(4-(prop-2-yn-1-yloxy)phenyl)pyrimidin-2-amine (**VB1**).* Yield 59%, ^{1}H NMR ($CDCl_3$, 400 MH_Z, δ with TMS = 0): 8.05−8.00 (4H, m), 7.35 (1H, s), 7.07 (2H, d, J = 8 Hz), 6.99 (2H, d, J = 8 Hz), 5.16 (2H, s), 4.76 (2H, d, J = 2.4 Hz), 4.18 (2H, t, J = 4 Hz), 3.75 (4H, t, J = 4 Hz), 2.83 (2H, t, J = 4 Hz), 2.60 (4H, t, J = 4 Hz), 2.55 (1H, t, J = 2.4 Hz), ^{13}C NMR ($CDCl_3$, 100 MH_Z, δ with TMS = 0)δ: 165.40, 165.28, 163.49, 160.71, 159.41, 131.13, 130.36, 128.36, 128.58, 115.00, 114.70, 102.86, 78.19, 75.89, 66.93, 65.89, 57.58, 55.85, 54.13 **HRMS**: for $C_{25}H_{26}N_4O_3$, calculated $[M + H]^+$: 431.2083; observed $[M + H]^+$: 431.2060

*4-(2-(4-(2-Phenyl-6-(4-(prop-2-yn-1-yloxy)phenyl)pyrimidin-4-yl)phenoxy)ethyl)morpholine (**VB2**).* Yield 63%, ^{1}H NMR ($CDCl_3$, 400 MH_Z, δ with TMS = 0): 8.68 (2H, d, J = 8 Hz), 8.24 (4H, t, J = 8 Hz), 7.86 (1H, s), 7.53−7.49 (3H, m), 7.12 (2H, d, J = 8 Hz), 7.04 (2H, d, J = 8 Hz), 4.77 (2H, d, J = 2.4 Hz), 4.19 (2H, t, J = 4 Hz), 3.75 (4H, t, J = 4 Hz), 2.84 (2H, t, J = 4 Hz), 2.60 (4H, t, J = 4 Hz), 2.56 (1H, t, J = 2.4 Hz), ^{13}C NMR ($CDCl_3$, 100 MH_Z, δ with TMS = 0)δ: 164.01, 163.89, 161.02, 159.73, 138.40, 130.59, 130.28, 128.83, 128.48, 115.20, 114.89, 108.75, 78.19, 75.89, 66.99, 65.93, 57.66, 55.95, 54.20 **HRMS**: for $C_{31}H_{29}N_3O_3$, calculated $[M + H]^+$: 492.2287; observed $[M + H]^+$: 492.2271

*4-(2-(4-(2-Methyl-6-(4-(prop-2-yn-1-yloxy)phenyl)pyrimidin-4-yl)phenoxy)ethyl)morpholine (**VB3**).* Yield 58%, ^{1}H NMR ($CDCl_3$, 400 MH_Z, δ with TMS = 0): 8.11−8.07 (4H, m), 7.76 (1H, s), 7.10 (2H, d, J = 8 Hz), 7.02 (2H, d, J = 8 Hz), 4.77 (2H, d, J = 2.4 Hz), 4.19 (2H, t, J = 4 Hz), 3.75 (4H, t, J = 4 Hz), 2.84 (2H, t, J = 4 Hz), 2.81 (3H, s), 2.61 (2H, t, J = 4 Hz), 2.56 (1H, t, J = 2.4 Hz), ($CDCl_3$, 100 MH_Z, δ with TMS = 0)δ: 168.32, 164.07, 163.96, 160.85, 159.55, 130.94, 130.17, 128.72, 115.18, 114.87, 108.49, 78.13, 75.93, 66.91, 65.90, 57.57, 55.87, 54.13, 26.53 **HRMS**: for $C_{26}H_{27}N_3O_3$, calculated $[M + H]^+$: 430.2131; observed $[M + H]^+$: 430.2079

*2-Phenyl-4-(4-(2-(piperidin-1-yl)ethoxy)phenyl)-6-(4-(prop-2-yn-1-yloxy)phenyl)pyrimidine (**VB4**).* Yield 61%, ^{1}H NMR ($CDCl_3$, 400 MH_Z, δ with TMS = 0): 8.69 (2H, dd, J_1 = 8 Hz, J_2 = 4 Hz), 8.23 (4H, t, J = 8 Hz), 7.84 (1H, s), 7.52−7.42 (3H, m) 7.11 (2H, d, J = 8 Hz), 7.03 (2H, d, J = 8 Hz), 4.76 (2H, d, J = 2.4 Hz), 4.19 (2H, t, J = 4 Hz), 2.82 (2H, t, J = 4 Hz), 2.57−2.55 (5H, m), 1.66−1.60 (4H,m) 1.46 (2H, bd), ($CDCl_3$, 100 MH_Z, δ with TMS = 0)δ: 164.26, 164.04, 163.82, 161.12, 159.70, 138.43, 131.04, 130.56, 130.11, 128.80, 128.71, 128.48, 115.18, 114.89, 108.71, 78.26, 76.04, 66.02, 57.83, 55.94, 55.14, 29.81, 25.88, 24.19 **HRMS**: for $C_{32}H_{31}N_3O_2$, calculated $[M + H]^+$: 490.2495; observed $[M + H]^+$: 490.2470

*2-Methyl-4-(4-(2-(piperidin-1-yl)ethoxy)phenyl)-6-(4-(prop-2-yn-1-yloxy)phenyl)pyrimidine (**VB5**).* Yield 67%,^{1}H NMR ($CDCl_3$, 400 MH_Z, δ with TMS = 0): 8.07 (4H, t, J = 8 Hz), 7.74 (1H, s), 7.08 (2H, d, J = 8 Hz), 7.00 (2H, d, J = 8 Hz), 4.75 (2H, d, J = 4 Hz), 4.17 (2H, t, J = 4 Hz), 2.82−2.79 (5H, m), 2.53 (4H, b), 1.61 (4H, b), 1.44 (2H, b), 1.23 (1H, b), ($CDCl_3$, 100 MH_Z, δ with TMS = 0)δ: 168.35, 164.18, 163.98, 161.03, 159.59, 131.01, 130.79, 130.35, 130.11, 130.06, 129.47, 128.77, 115.33, 115.23, 114.95, 108.53, 78.21, 76.01, 66.07, 57.85, 55.92, 55.13, 29.79, 25.89, 24.17, **HRMS**: for $C_{27}H_{29}N_3O_2$, calculated $[M + H]^+$: 428.2338; observed $[M + H]^+$: 428.2293

*4-(2-(4-(2-Phenyl-6-(3-(prop-2-yn-1-yloxy)phenyl)pyrimidin-4-yl)phenoxy)ethyl)morpholine (**VB6**).* Yield 62%,^{1}H NMR ($CDCl_3$, 400 MH_Z, δ with TMS = 0): 8.70 (2H, dd, J_1 = 8 Hz, J_2 = 4 Hz), 8.25 (2H, d, J = 8 Hz), 7.97 (1H,s), 7.91 (1H,s), 7.86, (1H, d, J = 8 Hz), 7.54−7.56 (4H, m), 7.15 (1H, dd, J_1 = 8 Hz, J_2 = 4 Hz), 7.06 (2H, d, J = 8 Hz), 4.82 (2H, d, J = 4 Hz), 4.20 (2H, t, J = 4 Hz), 3.76 (4H, t, J = 4 Hz), 2.85 (2H, t, J = 4 Hz), 2.60 (5H, m), ($CDCl_3$, 100 MH_Z, δ with TMS = 0)δ: 164.37, 164.27, 164.06, 161.13, 158.17, 139.32, 138.25, 130.70, 130.10, 130.01, 128.88, 128.51, 120.50, 117.11, 114.93, 113.99, 109.61, 78.50, 75.94, 67.01, 65.98, 57.65, 56.13, 54.21, **HRMS**: for $C_{31}H_{29}N_3O_3$, calculated $[M + H]^+$: 492.2287; observed $[M + H]^+$: 492.2256

*4-(4-(2-Morpholinoethoxy)phenyl)-6-(3-(prop-2-yn-1-yloxy)-phenyl)pyrimidin-2-amine (**VB7**).* Yield 59%,^{1}H NMR ($CDCl_3$, 400 MH_Z, δ with TMS = 0): 8.00 (2H, d, J = 8 Hz), 7.90 (1H, dd, J_1 = 8 Hz, J_2 = 4 Hz), 7.65 (1H, m), 7.39 (1H, t, J = 8 Hz), 7.36 (1H, s), 7.08 (1H, dd, J_1 = 8 Hz, J_2 = 4 Hz), 6.98 (2H, d, J = 8 Hz), 6.90 (1H, t, J = 8 Hz), 5.22 (2H, s), 4.77 (2H, d, J = 4 Hz), 4.16 (4H, t, J = 4 Hz), 3.73 (2H, t, J = 4 Hz), 2.82 (4H, t, J = 4 Hz), 2.53 (2H, b), ($CDCl_3$, 100 MH_Z, δ with TMS = 0)δ: 165.71, 163.56, 160.86, 158.01, 139.49, 130.69, 129.89, 128.70, 120.44, 117.08, 114.79, 114.48, 114.29, 113.53, 103.73, 78.49, 75.82, 66.97, 65.93, 57.63, 56.04, 54.18, **HRMS**: for $C_{25}H_{26}N_4O_3$, calculated $[M + H]^+$: 431.2083; observed $[M + H]^+$: 431.2060

*4-(2-(4-(2-Methyl-6-(3-(prop-2-yn-1-yloxy)phenyl)pyrimidin-4-yl)phenoxy)ethyl)morpholine (**VB8**).* Yield 59%,^{1}H NMR ($CDCl_3$, 400 MH_Z, δ with TMS = 0): 8.08 (2H, d, J = 8 Hz), 7.78 (1H, m), 7.72−7.69 (2H, m), 7.43 (1H, t, J = 8 Hz), 7.10 (1H, d, J = 8 Hz), 7.01 (2H, t, J = 8 Hz), 4.78 (2H, d, J = 4 Hz), 4.18 (2H, t, J = 4 Hz), 3.74 (4H, t, J = 4 Hz), 2.83 (2H, t, J = 4 Hz), 2.83 (3H, s), 2.59 (4H, t, J = 4 Hz), 2.54 (1H, t, J = 4 Hz), ($CDCl_3$, 100 MH_Z, δ with TMS = 0)δ: 168.50, 164.37, 164.29, 161.01, 158.14, 139.31, 131.03, 130.07, 128.83, 120.56, 117.13, 114.97, 113.77, 109.45, 78.44, 75.84, 66.98, 65.97, 57.64, 56.08, 54.20, 29.79, **HRMS**: for $C_{26}H_{27}N_3O_3$, calculated $[M + H]^+$: 430.2131; observed $[M + H]^+$: 430.2086

*4-(4-(2-Morpholinoethoxy)phenyl)-6-(2-(prop-2-yn-1-yloxy)-phenyl)pyrimidin-2-amine (**VB9**).* Yield 55%,^{1}H NMR ($CDCl_3$, 400 MH_Z, δ with TMS = 0): 8.00 (2H, d, J = 8 Hz), 7.85 (1H, dd, J_1 = 8 Hz, J_2 = 4 Hz), 7.60 (1H, m), 7.40 (1H, dd, J_1 = 8 Hz, J_2 = 4 Hz), 7.12 (2H, t, J = 8 Hz), 6.97 (2H, d, J = 8 Hz), 5.12 (2H, s), 4.75 (2H, d, J = 4 Hz), 4.16 (2H, t, J = 4 Hz), 3.73 (4H, t, J = 4 Hz), 2.82 (2H, t, J = 4 Hz), 2.59 (4H, b), 2.52 (1H, t, J = 4 Hz), ($CDCl_3$, 100 MH_Z, δ with TMS = 0)δ: 164.69, 164.30, 163.39, 160.70, 155.69, 130.94, 128.81, 122.22, 114.70, 114.16, 113.54, 109.19, 108.56, 78.53, 75.92, 66.99, 65.92, 57.66, 56.69, 54.18, **HRMS**: for $C_{25}H_{26}N_4O_3$, calculated $[M + H]^+$: 431.2083; observed $[M + H]^+$: 431.2036

*4-(2-(4-(2-Phenyl-6-(2-(prop-2-yn-1-yloxy)phenyl)pyrimidin-4-yl)phenoxy)ethyl)morpholine (**VB10**).* Yield 63%,^{1}H NMR ($CDCl_3$, 400 MH_Z, δ with TMS = 0): 8.67 (1H, dd, J_1 = 8 Hz, J_2 = 4 Hz), 8.27 (1H, s), 8.26 (2H, d, J = 8 Hz), 7.53−7.44 (4H, m), 7.21 (1H, t, J = 8 Hz), 7.13 (1H, d, J = 8 Hz), 7.04 (2H, d, J = 8 Hz), 4.80 (2H, d, J = 4 Hz), 4.19 (2H, t, J = 4 Hz), 3.75 (4H, t, J = 4 Hz), 2.84 (2H, t, J = 4 Hz), 2.60 (4H, b), 2.56 (1H, t, J = 4 Hz), ($CDCl_3$, 100 MH_Z, δ with TMS = 0)δ: 164.19, 163.29, 162.79, 160.97, 156.23, 138.60, 131.59, 131.33, 130.56, 130.40, 128.97, 128.44, 128.41, 126.56, 122.35, 114.86, 114.72, 113.53, 78.50, 76.00, 67.02, 66.05, 57.68, 56.82, 54.22, **HRMS**: for $C_{31}H_{29}N_3O_3$, calculated $[M + H]^+$: 492.2287; observed $[M + H]^+$: 492.2256

*4-(2-(3-(2-Phenyl-6-(4-(prop-2-yn-1-yloxy)phenyl)pyrimidin-4-yl)phenoxy)ethyl)morpholine (**VB11**).* Yield 62%,^{1}H NMR ($CDCl_3$, 400 MH_Z, δ with TMS = 0): 8.68 (2H, dd, J_1 = 8 Hz, J_2 = 4 Hz), 8.26 (2H, dd, J_1 = 8 Hz, J_2 = 4 Hz), 7.90 (1H, d, J = 8 Hz), 7.85 (1H, s), 7.81 (1H, d, J = 8 Hz), 7.54−7.50 (3H, m), 7.44 (1H, d, J = 8 Hz), 7.13 (2H, dd, J_1 = 8 Hz, J_2 = 4 Hz), 7.01 (1H, dd, J_1 = 8 Hz, J_2 = 4 Hz), 4.78 (2H, d, J = 4 Hz), 4.26 (2H, t, J = 4 Hz), 3.77 (4H, t, J = 4 Hz), 2.90 (2H, t, J = 4 Hz), 2.67 (4H, b), 2.56 (1H, t, J = 4 Hz), ($CDCl_3$, 100 MH_Z, δ with TMS = 0)δ: 166.67, 163.80, 161.95, 160.94, 147.89, 138.06, 130.75, 129.60, 128.88, 128.62, 128.42, 119.49, 116.86, 114.91, 114.58, 112.04, 110.66, 80.96, 76.80, 71.58, 66.75, 65.72, 57.56, 54.09, **HRMS**: for $C_{31}H_{29}N_3O_3$, calculated $[M + H]^+$: 492.2287; observed $[M + H]^+$: 492.2256

*4-(3-(2-Morpholinoethoxy)phenyl)-6-(4-(prop-2-yn-1-yloxy)-phenyl)pyrimidin-2-amine (**VB12**).* Yield 72%, ^{1}H NMR ($CDCl_3$, 400 MH_Z, δ with TMS = 0): 8.01 (2H, d, J = 8 Hz), 7.60 (1H, s), 7.57 (1H, d, J = 8 Hz), 7.36 (2H, t, J = 8 Hz), 7.04 (2H, d, J = 12 Hz), 7.00 (1H, d, J = 8 Hz), 5.35 (2H, s), 4.73 (2H, d, J = 2.4 Hz), 4.18 (2H, t, J = 4 Hz), 3.73 (4H, t, J = 4 Hz), 2.82 (2H, t, J = 4 Hz), 2.59 (4H, t, J = 4 Hz), 2.54 (1H, t, J = 2.4 Hz), ($CDCl_3$, 100 MH_Z, δ with TMS = 0)δ: 165.71, 163.56, 160.86, 158.01, 139.49, 130.69, 129.89, 128.70, 120.44, 117.08, 114.79, 114.48, 114.29, 113.53, 103.73, 78.49, 75.82, 66.97, 65.93, 57.63, 56.04, 54.18, **HRMS**: for $C_{25}H_{26}N_4O_3$, calculated $[M + H]^+$: 431.2083; observed $[M + H]^+$: 431.2018

DOI: 10.1021/acschemneuro.8b00220
ACS Chem. Neurosci. 2019, 10, 252−265

*4-(2-(3-(2-Methyl-6-(4-(prop-2-yn-1-yloxy)phenyl)pyrimidin-4-yl)phenoxy)ethyl)morpholine (**VB13**).* Yield 54%, ^{1}H NMR ($CDCl_3$, 400 MH_Z, δ with TMS = 0): 8.09 (2H, d, J = 8 Hz), 7.78 (1H, s), 7.64 (1H, d, J = 8 Hz), 7.51−7.47 (1H, m), 7.38 (1H, t, J = 8 Hz), 7.07 (2H, d, J = 12 Hz), 7.02 (1H, dd, J_1 = 8 Hz, J_2 = 4 Hz), 4.74 (2H, d, J = 4 Hz), 4.28 (2H, t, J = 4 Hz), 4.19 (2H, t, J = 4 Hz), 3.72 (4H, t, J = 4 Hz), 2.81 (3H, s), 2.59 (4H, t, J = 4 Hz), 2.54 (1H, t, J = 2.4 Hz), ($CDCl_3$, 100 MH_Z, δ with TMS = 0)δ: 168.47, 164.44, 164.25, 159.72, 159.33, 139.14, 131.02, 130.02, 128.91, 128.83, 118.83, 116.96, 115.27, 113.29, 109.49, 78.18, 76.07, 66.98, 65.88, 65.66, 57.75, 55.92, 54.17, **HRMS**: for $C_{26}H_{27}N_3O_3$, calculated $[M + H]^+$: 430.2131; observed $[M + H]^+$: 430.2101

*2-Phenyl-4-(4-(2-(piperidin-1-yl)ethoxy)phenyl)-6-(3-(prop-2-yn-1-yloxy)phenyl)pyrimidine (**VB14**).* Yield 53%, ^{1}H NMR ($CDCl_3$, 400 MH_Z, δ with TMS = 0): 8.70 (2H, dd, J_1 = 8 Hz, J_2 = 4 Hz), 8.24 (2H, d, J = 8 Hz), 7.96 (1H, t, J = 8 Hz), 7.91 (1H, s), 7.85 (1H, dd, J_1 = 8 Hz, J_2 = 4 Hz), 7.53−7.45 (4H, m), 7.13 (1H, dd, J_1 = 8 Hz, J_2 = 4 Hz), 7.05 (2H, d, J = 8 Hz), 4.81 (2H, d, J = 8 Hz), 4.20 (2H, t, J = 4 Hz), 2.83 (2H, t, J = 4 Hz), 2.58 (4H, t, J = 4 Hz), 1.66−1.60 (4H, m), 1.47−1.40 (3H, m), ($CDCl_3$, 100 MH_Z, δ with TMS = 0)δ: 164.35, 164.37, 164.05, 161.16, 158.17, 139.36, 138.29, 130.70, 130.01, 128.85, 128.51, 120.52, 117.11, 114.56, 113.96, 109.61, 78.39, 75.83, 57.92, 56.16, 75.83, 29.72, 25.86, 24.13, **HRMS**: for $C_{32}H_{31}N_3O_2$, calculated $[M + H]^+$: 490.2495; observed $[M + H]^+$: 490.2480

*4-(4-(2-(Piperidin-1-yl)ethoxy)phenyl)-6-(3-(prop-2-yn-1-yloxy)-phenyl)pyrimidin-2-amine (**VB15**).* Yield 58%, ^{1}H NMR ($CDCl_3$, 400 MH_Z, δ with TMS = 0): 7.99 (2H, d, J = 8 Hz), 7.65−7.62 (2H, m), 7.39 (1H, t, J = 8 Hz), 7.35 (1H, s), 7.08 (1H, dd, J_1 = 8 Hz, J_2 = 4 Hz), 6.97 (2H, d, J = 8 Hz), 5.26 (2H, s), 4.75 (2H, d, J = 4 Hz), 4.16 (2H, t, J = 4 Hz), 2.80 (2H, t, J = 4 Hz), 2.53 (5H, b), 1.62−1.58 (4H, m), 0.97−0.92 (2H, m), ($CDCl_3$, 100 MH_Z, δ with TMS = 0)δ: 165.75, 165.55, 163.60, 160.96, 158.07, 139.53, 131.02, 129.87, 128.67, 120.45, 117.08, 114.79, 113.50, 103.68, 78.51, 75.83, 66.01, 57.85, 56.03, 55.11, 25.87, 34.17, **HRMS**: for $C_{26}H_{28}N_4O_2$, calculated $[M + H]^+$: 429.2291; observed $[M + H]^+$: 429.2238

*(E)-1-(4-(2-Morpholinoethoxy)phenyl)-3-(4-(prop-2-yn-1-yloxy)-phenyl)prop-2-en-1-one (**3a**).* Yield 85%, ^{1}H NMR ($CDCl_3$, 400 MH_Z, δ with TMS = 0):8.01 (2H, d, J = 8 Hz), 7.66 (1H, d, J = 16 Hz), 7.60 (2H, d, J = 8 Hz), 7.43 (1H, d, J = 16 Hz), 7.02−6.95 (4H, m), 4.73 (2H, d, J = 4 Hz), 4.18 (2H, t, J = 4 Hz), 3.73 (4H, t, J = 4 Hz), 2.83 (2H, t, J = 4 Hz), 2.58 (2H, t, J = 4 Hz), 2.55 (1H, t, J = 4 Hz), ^{13}C NMR ($CDCl_3$, 100 MH_Z, δ with TMS = 0): 188.72, 162.50, 159.37, 143.68, 131.45, 130.80, 130.12, 128.68, 120.01, 115.34, 114.42, 77.46, 76.12, 66.99, 66.09, 57.55, 55.90, 54.19 **MS**: for $C_{24}H_{25}NO_4$, calculated $[M]^+$: 391.17; observed $[M]^+$: 391

*(E)-1-(4-(2-Morpholinoethoxy)phenyl)-3-(2-(prop-2-yn-1-yloxy)-phenyl)prop-2-en-1-one (**3b**).* Yield 83%, ^{1}H NMR ($CDCl_3$, 400 MH_Z, δ with TMS = 0): 8.02−8.09 (3H, m), 7.63−7.69 (2H, m), 7.34 (1H, t, J = 8H_Z), 7.03 (2H, t, J = 8H_Z), 6.96 (2H, d, J = 8H_Z), 4.79 (2H, d, J = 2.4 H_Z), 4.18 (2H, t, J = 4H_Z), 3.73 (4H, t, J = 4H_Z), 2.82 (2H, t, J = 4H_Z), 2.56 (4H, t, J = 4H_Z), 2.55 (1H, t, J = 4H_Z), ^{13}C NMR ($CDCl_3$, 100 MH_Z, δ with TMS = 0)δ: 189.25, 162.48, 156.72, 139.33, 131.39, 130.93, 129.57, 124.76, 123.17, 121.77, 114.38, 112.80, 78.14, 76.07, 66.99, 66.06, 57.55, 56.26, 54.18 **MS**: for $C_{24}H_{25}NO_4$, calculated $[M]^+$: 391.17; observed $[M]^+$: 391

*(E)-1-(3-(2-Morpholinoethoxy)phenyl)-3-(4-(prop-2-yn-1-yloxy)-phenyl)prop-2-en-1-one (**3c**).* Yield 87%, ^{1}H NMR ($CDCl_3$, 400 MH_Z, δ with TMS = 0): 7.76 (1H, d, J = 16 Hz), 7.58 (3H, t, J = 8 Hz), 7.52 (1H, s), 7.40−7.36 (2H, m), 7.11 (1H, d, J = 8 Hz), 7.00 (2H, dd, J_1 = 8 Hz, J_2 = 4 Hz), 4.72 (2H, t, J = 4 Hz), 3.72 (4H, t, J = 4 Hz), 2.81 (2H, t, J = 4 Hz), 2.57 (4H, b), 2.54 (1H, t, J = 4 Hz), ^{13}C NMR ($CDCl_3$, 100 MH_Z, δ with TMS = 0)δ: 190.25, 159.57, 159.07, 144.61, 139.86, 130.27, 129.66, 128.47, 121.23, 120.23, 119.70, 115.39, 113.67, 78.06, 76.15, 66.97, 65.95, 57.67, 55.91, 54.15 **MS**: for $C_{24}H_{25}NO_4$, calculated $[M]^+$: 391.17; observed $[M]^+$: 391

BIOLOGICAL STUDIES

Determination of hMAO Inhibition Activity. The synthesized compounds were evaluated against MAO-A and MAO-B isoforms for their inhibitory potential using Amplex Red assay kit through fluorimetric method described by us and others.[23]

Briefly, 100 μL of sodium phosphate buffer (0.05 M, pH 7.4) containing the test drug and reference inhibitors, in various concentrations along with adequate amounts of recombinant hMAO (hMAO-A: 1.1 μg protein; specific activity: 150 nmol of p-tyramine oxidized to p-hydroxyphenylacetaldehyde/min/mg protein; hMAO-B: 7.5 μg of protein; specific activity: 22 nmol of p-tyramine transformed/min/mg protein) enzyme, were incubated for 15 min at 37 °C in a flat-black-bottom 96-well plates (Tarsons) in a incubator. After the incubation period, the reaction was started by adding (final concentrations) 200 μM Amplex Red reagent, 1 U/mL horseradish peroxidase and 1 mM p-tyramine. After 30 min of incubation in the dark, the production of H_2O_2 was quantified at 37 °C in a multidetection microplate fluorescence reader (Synergy^{HI}, Bio-Tek Instruments) based on the fluorescence generated at excitation wavelength of 545 nm and emission wavelength of 590 nm. Control experiments were carried out simultaneously by replacing the test drug with the vehicle. A direct reaction of test drug with the Amplex Red reagent in a sodium phosphate buffer was performed to minimize the possibility of the test drugs to influence the fluorescence generated in the reaction mixture due to nonenzymatic inhibition. However, no significant modulation in the fluorescence was observed. The specific final fluorescence emission was calculated after subtraction of the background activity determined from vials containing all the components except the hMAO enzymes replaced by a sodium phosphate buffer solution.

Acetylcholinesterase Inhibition Assay. Acetylcholinesterase inhibition activity was determined using Amplex Red Acetylcholine/Acetylcholinesterase assay kit (A12217) purchased from the Molecular Probes, Inc./Invitrogen.[38] Briefly, 100 μL of Tris-HCl buffer (0.05 M, pH 8.0) containing the synthesized test drugs and reference inhibitors, in various concentrations along with adequate amounts of recombinant AChE (0.2U/mL) enzyme, were incubated for 15 min at 37 °C in a flat-black-bottom 96-well plates (Tarsons). Reaction was started by adding 100 μL of working solution of 400 μM Amplex Red reagent containing 2 U/mL horseradish peroxidase, 0.2 U/mL choline oxidase, and 100 μM acetylcholine. After 30 min of incubation in the dark, the production of H_2O_2 and subsequent formation of resorufin from Amplex red dye was quantified at 37 °C in a multidetection microplate fluorescence reader (Synergy^{HI}, Bio-Tek Instruments) based on the fluorescence generated at excitation wavelength of 545 nm and emission wavelength of 590 nm. A positive control experiment was carried out simultaneously by replacing the test drugs with the vehicle. A second positive control was carried out by using 20 mM H_2O_2. A 1× reaction buffer without acetylcholinesterase was used as negative control. The specific final fluorescence emission was calculated after subtraction of the background activity, determined from wells containing all components except the AChE replaced by a 1× buffer solution. Each experiment was performed in triplicate (n = 3).

BuChE Inhibition Assay. The procedure described by Ellman et al. was used for BuChE inhibition assays with minor modifications.[39] BuChE was purchased from sigma Aldrich (CAS No. 9001-80-5). Butyrylthiocholine iodide (BTCI), 5.5′-dithiobis (2-nitrobenzoic acid) (DTNB − Ellman's reagent) were purchased from Himedia. The assays were performed in

DOI: 10.1021/acschemneuro.8b00220
ACS Chem. Neurosci. 2019, 10, 252−265

tris-HCl buffer (pH-8) and donepezil was used as standard compound. Six different concentrations of 20, 10, 1, 0.1, 0.01, and 0.001 μM of test compound were used to determine the IC_{50} values. Both 50 μL (0.6 Uml^{-1}) and 20 μL of test or standard compounds were incubated in 96-well plates for 30 min. Next, 100 μL (1.5 mM) of DTNB was added in the above solution. The substrate, that is, BTCI (30 mM, 10 μL), was added into it, and the absorbance was recorded immediately at 415 nm for 20 at 1 min interval using Biotek well plate reader. The IC_{50} values were calculated using absorbance obtained from the test and standard compounds. The assays were performed in triplicate and in three independent runs.

Reversibility Inhibition Studies. For reversibility inhibition studies, the protocol was adopted from the literature.[30,31] Briefly, the test inhibitors were incubated with the MAO enzymes at concentrations of 10 × IC_{50} and 100 × IC_{50} at 37 °C for 30 min (negative control performed in the absence of inhibitor), and 4% DMSO was added as cosolvent to all incubations. After a 30 min incubation period, the samples were subsequently diluted to 100-fold with the addition of tyramine substrate to achieve final inhibitor concentrations of 0.1 × IC_{50} and 1 × IC_{50} value, respectively. As positive controls, MAO-A and MAO-B were incubated with the irreversible inhibitors, clorgyline and pargyline, respectively, at 10 × IC_{50} concentrations and then diluted 100-fold to achieve final inhibitor concentrations of 0.1 × IC_{50}. The residual MAO activities after dilutions were measured (n = 3), and the residual enzyme activities were expressed as mean ± SD.

ROS Production Inhibition Studies. Intracellular levels of ROS were determined using protocol described elsewhere,[40] using nonfluorescent compound 2′,7′-dichlorofluorescein diacetate (DCF-DA). It is permeable to the cell membrane, where it is hydrolyzed by intracellular esterases and further oxidized by ROS to a fluorescent compound 2′,7′-DCF. Cells (SH-SY5Y) were seeded in 96-well plates (1×10^4 cells/well) and left for 24 h in complete media at 37 °C. Then media was removed, washed with PBS, and cells were treated with the test compounds (without FBS) for 24 h at different concentrations (1, 5, and 25 μM). After completion of the experiment, cells were rinsed with PBS thrice and then treated with H_2DCF-DA (50 μM) and incubated for 30 min at 37 °C. Following incubation, cells were rinsed with PBS, and fluorescence was detected at wavelength of 478 nm excitation and 518 nm emission.

Neuroprotective Studies. The neuroprotective potential of compounds was determined against 6-OHDA neurotoxin using MTT assay.[41] For this assay, SH-SY5Y cells were plated in 96 wells, at 10^6 cells/well density. The cells were cultured for 24 h in DMEM/F-12 media containing 10% FBS and horse serum supplemented 1% penicillin and streptomycin antibiotic solution. Then cells were treated with the target compounds (at concentrations of 1−25 μM), 4 h before 6-OHDA (12.5 μM). After 24 h of incubation in the oven, at 37 °C and a 5% CO_2, 95% O_2 atmosphere, the tested compounds were replaced with 80 mL of medium and 20 mL of MTT in PBS (0.5 mg/mL, final concentration). The cells were incubated for another 4 h. After the removal of MTT, the formazan crystals were dissolved in DMSO. The amount of formazan was measured using a microculture plate reader with a test wavelength of 570 nm. Results were expressed as the mean ± SD of three independent experiments.

Cytotoxicity Studies. With an aim to test the cytotoxicity of the synthesized compounds on neuronal cells, MTT assays were carried out with human neuroblastoma SH-SY5Y cells.[23] Approximately 10 000 cells were seeded per well of a 96-well plate in DMEM/F-12 media containing 10% FBS and horse serum supplemented 1% penicillin and streptomycin antibiotic solution for 24 h and treated as indicated in the experimental design. Cells were treated with synthesized compounds at concentrations of 1, 5, and 25 μM for 24 h in a humidified CO_2 incubator, maintained at 37 °C with 5% CO_2 and 95% humidity under serum-free conditions.

Metal-Chelating Study. Metal-chelating studies were performed with a UV−vis spectrophotometer. The absorption spectra of each compound (50 μM, final concentration) alone or in the presence of $CuSO_4$, $FeSO_4$, and $FeCl_3$ (50 μM, final concentration) for 30 min in 20% (v/v) methanol/buffer (20 mM HEPES, 150 mM NaCl, pH = 7.4) were recorded at room temperature.[42]

Kinetic Studies of AChE Inhibition. To determine the mechanism of action of the most potent inhibitor of AChE, **VB8**, kinetic study was performed using ee AChE with the help of earlier reported protocols.[25,43] A Lineweaver−Burk double reciprocal graph was plotted at different concentrations of substrate ACh (0.1 mM−1 mM) by using the same methodology reported for the *in vitro* inhibition study of AChE. Progress curves were analyzed by steady state turnover of substrate, and values of linear regression were fitted according to Lineweaver−Burk replots using excel software (2016). Three concentrations of VB8 (1, 10, and 100 nM) were used for kinetic study. The plots were assessed by weighted least-squares analysis that assumed the variance of ν to be constant for whole data set. Slopes of the reciprocal of ν were then plotted against the reciprocal of the substrate concentration.

Molecular Docking Studies. Docking studies can provide some valuable information on the ligand's orientation and its interactions at the receptor site. To determine the mode of interaction of the synthesized ligands at the active site of hMAO-A and AChE enzymes, molecular docking studies were performed using Maestro 11.1 (Schrödinger LLC).[44] X-ray crystal structures of hMAO-A (PDB IDs 2BXR and 2Z5X)[35,36] and AChE (PDB ID 1EVE)[37] enzymes were imported from the protein data bank (www.rscb.org). Protein was prepared using "protein preparation wizard" application of Schrödinger suite 2017. Energy was minimized using OPLS2005 force field. Ligands were drawn in ChemBio Draw Ultra-12 and prepared using ligand preparation application in Schrödinger suite 2017. For each compound, the top-score docking poses were chosen for final ligand-target interaction analysis employing XP interaction visualizer of Maestro 11.1 software. Validation of the docking procedure was done by redocking the cocrystallized ligand into the active site of the enzymes. The Qikprop application of Schrodinger suit was used to determine the drug like and ADME properties of the compounds.[45]

Molecular Dynamics Simulation Studies. In order to investigate the behavior and stability of the potent inhibitors into the active site of the MAO and AChE, molecular dynamic (MD) simulation was utilized. For this investigation, docking complexes of **VB1** with MAO-A and **VB8** with AChE were used. MD simulations were performed using the Desmond standard protocol.[46] Complex was solvated by TIP3P water model and then naturalized by adding 0.15 M Na^+ and Cl^- ions. The thickness of the water layer was set to 10 Å. Before

DOI: 10.1021/acschemneuro.8b00220
ACS Chem. Neurosci. 2019, 10, 252−265

the MD simulations, the systems were minimized with a maximum iteration of 2000 steps. Then, the systems were submitted to 30 ns MD simulation for equilibration and production MD run. Temperature and pressure were assigned on 300 K and 1.01325 bar, respectively, using the isothermal−isobaric (NPT) ensemble. A cutoff 9 Å was used for Coulomb interactions.

■ ASSOCIATED CONTENT

Supporting Information

The Supporting Information is available free of charge on the ACS Publications website at DOI: 10.1021/acschemneuro.8b00220.

NMR spectral data and HRMS graphs of the final compounds (PDF)

■ AUTHOR INFORMATION

Corresponding Author

*E-mails for V.K.: vinod.kumar@cup.edu.in; vpathania18@gmail.com. Tel.: +911642864214.

ORCID

Vinod Kumar: 0000-0002-1438-9438

Author Contributions

B.K. was involved in the design and synthesis of most of the compounds. He also performed hMAO and ee AChE inhibitory assays, performed *in silico* studies, and drafted the manuscript. A.R.D. was also involved in the synthesis of some of the compounds, column purification, and spectral analysis of the compounds. He also assisted in the molecular modeling studies and drafting of the manuscript. B.S. under the supervision of A.K.M., performed other *in vitro* biological studies like cytotoxic studies, ROS production inhibition potential, and neuroprotective studies. S.K.G. and S.K. conducted BuChE inhibition studies of the compounds. J.P. helped in the evaluation of hMAO and ee AChE inhibition activities and reversibility inhibition studies. V.K. conceptualized, supervised, and coordinated all the studies and prepared the final draft of the manuscript. All authors read and approved the final manuscript.

Notes

The authors declare the following competing financial interest(s): A patent application has been filed containing these compounds (Indian patent application number 201811008301).

■ ACKNOWLEDGMENTS

V.K. is thankful to the DST-SERB (EMR/2015/002339) and Central University of Punjab, Bathinda, (RSM GP25) for providing the financial assistance. B.K. is thankful to CUP, Bathinda and CSIR for the Senior Research Fellowship. J.P. is thankful to DST-SERB for the Research Grant (ECR/2015/000240).

■ ABBREVIATIONS

QPlogBB, qualitatively predicted logarithmic ratio between the concentration of a compound in brain and blood; LogP, partition coefficient of a molecule between an aqueous and lipophilic phase (octanol and water); CAS, Catalytic active site; PAS, Peripheral active site; MTT, 3-(4,5-dimethylthiazol-2-yl)-2,5-diphenyltetrazolium; 6-OHDA, 6-hydroxydopamine; DMEM, Dulbecco's Modified Eagle's medium; HEPES, (4-(2-hydroxyethyl)-1-piperazineethanesulfonic acid)

■ REFERENCES

(1) Goedert, M., and Spillantini, M. G. (2006) A century of Alzheimer's disease. *Science 314*, 777−781.

(2) Alzheimer's Association (2017) Alzheimer's disease facts and figures. *Alzheimer's Dementia 13*, 325−373.

(3) Kung, H. F. (2012) The β-amyloid hypothesis in Alzheimer's disease: seeing is believing. *ACS Med. Chem. Lett. 3*, 265−267.

(4) Garcia-Alloza, M., Gil-Bea, F., Diez-Ariza, M., Chen, C.-H., Francis, P. T., Lasheras, B., and Ramirez, M. (2005) Cholinergic−serotonergic imbalance contributes to cognitive and behavioral symptoms in Alzheimer's disease. *Neuropsychologia 43*, 442−449.

(5) Cummings, J. L., Ross, W., Absher, J., Gornbein, J., and Hadjiaghai, L. (1995) Depressive symptoms in Alzheimer disease: assessment and determinants. *Alzheimer Dis. Assoc. Disord. 9*, 87−93.

(6) Kumar, B., Gupta, V., and Kumar, V. (2016) A Perspective on Monoamine Oxidase Enzyme as Drug Target: Challenges and Opportunities. *Curr. Drug Targets 18*, 87−97.

(7) Sano, M., Ernesto, C., Thomas, R. G., Klauber, M. R., Schafer, K., Grundman, M., Woodbury, P., Growdon, J., Cotman, C. W., Pfeiffer, E., et al. (1997) A controlled trial of selegiline, alpha-tocopherol, or both as treatment for Alzheimer's disease. *N. Engl. J. Med. 336*, 1216−1222.

(8) Müller, T. J., Braun, R., and Ansorge, M. (2000) A Novel Three-Component One-Pot Pyrimidine Synthesis Based upon a Coupling−Isomerization Sequence. *Org. Lett. 2*, 1967−1970.

(9) Sugimoto, H., Yamanish, Y., Iimura, Y., and Kawakami, Y. (2000) Donepezil hydrochloride (E2020) and other acetylcholinesterase inhibitors. *Curr. Med. Chem. 7*, 303−339.

(10) Marco-Contelles, J., do Carmo Carreiras, M., Rodríguez, C., Villarroya, M., and Garcia, A. G. (2006) Synthesis and pharmacology of galantamine. *Chem. Rev. 106*, 116−133.

(11) Anand, P., and Singh, B. (2013) A review on cholinesterase inhibitors for Alzheimer's disease. *Arch. Pharmacal Res. 36*, 375−399.

(12) Racchi, M., Mazzucchelli, M., Porrello, E., Lanni, C., and Govoni, S. (2004) Acetylcholinesterase inhibitors: novel activities of old molecules. *Pharmacol. Res. 50*, 441−451.

(13) Gura, T. (2008) Hope in Alzheimer's fight emerges from unexpected places. *Nat. Med. 14*, 894−894.

(14) Munoz-Torrero, D. (2008) Acetylcholinesterase inhibitors as disease-modifying therapies for Alzheimer's disease. *Curr. Med. Chem. 15*, 2433−2455.

(15) Yiannopoulou, K. G., and Papageorgiou, S. G. (2013) Current and future treatments for Alzheimer's disease. *Ther. Adv. Neurol. Disord. 6*, 19−33.

(16) Small, G. W., and Greenfield, S. (2015) Current and future treatments for Alzheimer disease. *Am. J. Geriatric Psychiatry 23*, 1101−1105.

(17) Oset-Gasque, M. J. S., and Marco-Contelles, J. (2018) Alzheimer's Disease, the "One-Molecule, One-Target" Paradigm, and the Multitarget Directed Ligand Approach. *ACS Chem. Neurosci. 9*, 401−403.

(18) Oliveira Pedrosa, M. D., Duarte da Cruz, R., Oliveira Viana, J., de Moura, R. O., Ishiki, H. M., Barbosa Filho, F., Diniz, M. F., Scotti, M., Scotti, L., and Bezerra Mendonca, F. (2017) Hybrid Compounds as Direct Multitarget Ligands: A Review. *Curr. Top. Med. Chem. 17*, 1044−1079.

(19) Pisani, L., Farina, R., Soto-Otero, R., Denora, N., Mangiatordi, G. F., Nicolotti, O., Mendez-Alvarez, E., Altomare, C. D., Catto, M., and Carotti, A. (2016) Searching for multi-targeting neurotherapeutics against Alzheimer's: Discovery of potent AChE-MAO B inhibitors through the decoration of the 2H-chromen-2-one structural motif. *Molecules 21*, 362.

(20) Yanez, M., and Vina, D. (2013) Dual inhibitors of monoamine oxidase and cholinesterase for the treatment of Alzheimer disease. *Curr. Top. Med. Chem. 13*, 1692−1706.

DOI: 10.1021/acschemneuro.8b00220
ACS Chem. Neurosci. 2019, 10, 252−265

(21) Kumar, B., Sheetal, Mantha, A. K., and Kumar, V. (2016) Recent developments on the structure−activity relationship studies of MAO inhibitors and their role in different neurological disorders. *RSC Adv. 6*, 42660−42683.
(22) Agis-Torres, A., Sollhuber, M., Fernandez, M., and Sanchez-Montero, J. (2014) Multi-target-directed ligands and other therapeutic strategies in the search of a real solution for Alzheimer's disease. *Curr. Neuropharmacol. 12*, 2−36.
(23) Kumar, B., Sheetal, Mantha, A. K., and Kumar, V. (2018) Synthesis, Biological Evaluation and Molecular Modeling Studies of Phenyl-/Benzhydrylpiperazine Derivatives as Potential MAO Inhibitors. *Bioorg. Chem. 77*, 252−262.
(24) Kumar, B., Kumar, M., Dwivedi, A. R., and Kumar, V. (2018) Synthesis, Biological Evaluation and Molecular Modeling Studies of Propargyl-Containing 2, 4, 6-Trisubstituted Pyrimidine Derivatives as Potential Anti-Parkinson Agents. *ChemMedChem 13*, 705−712.
(25) Bolea, I., Juárez-Jiménez, J., de los Rıos, C. B., Chioua, M., Pouplana, R. N., Luque, F. J., Unzeta, M., Marco-Contelles, J., and Samadi, A. (2011) Synthesis, biological evaluation, and molecular modeling of donepezil and N-[(5-(benzyloxy)-1-methyl-1 H-indol-2-yl) methyl]-N-methylprop-2-yn-1-amine hybrids as new multipotent cholinesterase/monoamine oxidase inhibitors for the treatment of Alzheimer's disease. *J. Med. Chem. 54*, 8251−8270.
(26) Weinreb, O., Amit, T., Bar-Am, O., and Youdim, M. B. (2010) Rasagiline: a novel anti-Parkinsonian monoamine oxidase-B inhibitor with neuroprotective activity. *Prog. Neurobiol. 92*, 330−344.
(27) Hughes, R. E., Nikolic, K., and Ramsay, R. R. (2016) One for All? Hitting Multiple Alzheimer's Disease Targets with One Drug. *Front. Neurosci. 10*, Article No. 177.
(28) Samadi, A., Chioua, M., Bolea, I., de los Rios, C., Iriepa, I., Moraleda, I., Bastida, A., Esteban, G., Unzeta, M., Galvez, E., and Marco-Contelles, J. (2011) Synthesis, biological assessment and molecular modeling of new multipotent MAO and cholinesterase inhibitors as potential drugs for the treatment of Alzheimer's disease. *Eur. J. Med. Chem. 46*, 4665−4668.
(29) Chimenti, F., Carradori, S., Secci, D., Bolasco, A., Bizzarri, B., Chimenti, P., Granese, A., Yanez, M., and Orallo, F. (2010) Synthesis and inhibitory activity against human monoamine oxidase of N1-thiocarbamoyl-3, 5-di (hetero) aryl-4, 5-dihydro-(1H)-pyrazole derivatives. *Eur. J. Med. Chem. 45*, 800−804.
(30) Mostert, S., Mentz, W., Petzer, A., Bergh, J. J., and Petzer, J. P. (2012) Inhibition of monoamine oxidase by 8-[(phenylethyl) sulfanyl] caffeine analogues. *Bioorg. Med. Chem. 20*, 7040−7050.
(31) Minders, C., Petzer, J. P., Petzer, A., and Lourens, A. C. (2015) Monoamine oxidase inhibitory activities of heterocyclic chalcones. *Bioorg. Med. Chem. Lett. 25*, 5270−5276.
(32) Pizzinat, N., Copin, N., Vindis, C., Parini, A., and Cambon, C. (1999) Reactive oxygen species production by monoamine oxidases in intact cells. *Naunyn-Schmiedeberg's Arch. Pharmacol. 359*, 428−431.
(33) Sturza, A., Noveanu, L., Duicu, O., Angoulvant, D., and Muntean, D. M. (2014) 0209: Monoamine oxidases as novel sources of reactive oxygen species in experimental diabetes. *Arch. Cardiovasc. Dis. 6*, 15.
(34) Xie, H.-R., Hu, L.-S., and Li, G.-Y. (2010) SH-SY5Y human neuroblastoma cell line: in vitro cell model of dopaminergic neurons in Parkinson's disease. *J. Vis. Exp. 123*, 1086−1092.
(35) De Colibus, L., Li, M., Binda, C., Lustig, A., Edmondson, D. E., and Mattevi, A. (2005) Three-dimensional structure of human monoamine oxidase A (MAO A): relation to the structures of rat MAO A and human MAO B. *Proc. Natl. Acad. Sci. U. S. A. 102*, 12684−12689.
(36) Son, S.-Y., Ma, J., Kondou, Y., Yoshimura, M., Yamashita, E., and Tsukihara, T. (2008) Structure of human monoamine oxidase A at 2.2-Å resolution: the control of opening the entry for substrates/inhibitors. *Proc. Natl. Acad. Sci. U. S. A. 105*, 5739−5744.
(37) Cheung, J., Rudolph, M. J., Burshteyn, F., Cassidy, M. S., Gary, E. N., Love, J., Franklin, M. C., and Height, J. J. (2012) Structures of human acetylcholinesterase in complex with pharmacologically important ligands. *J. Med. Chem. 55*, 10282−10286.
(38) Kalb, A., von Haefen, C., Sifringer, M., Tegethoff, A., Paeschke, N., Kostova, M., Feldheiser, A., and Spies, C. D. (2013) Acetylcholinesterase inhibitors reduce neuroinflammation and-degeneration in the cortex and hippocampus of a surgery stress rat model. *PLoS One 8*, e62679.
(39) Kumar, D., Gupta, S. K., Ganeshpurkar, A., Gutti, G., Krishnamurthy, S., Modi, G., and Singh, S. K. (2018) Development of Piperazinediones as dual inhibitor for treatment of Alzheimer's disease. *Eur. J. Med. Chem. 150*, 87−101.
(40) Kaur, N., Dhiman, M., Perez-Polo, J. R., and Mantha, A. K. (2015) Ginkgolide B revamps neuroprotective role of apurinic/apyrimidinic endonuclease 1 and mitochondrial oxidative phosphorylation against Aβ25−35-induced neurotoxicity in human neuroblastoma cells. *J. Neurosci. Res. 93*, 938−947.
(41) Liang, Z., Shi, F., Wang, Y., Lu, L., Zhang, Z., Wang, X., and Wang, X. (2011) Neuroprotective effects of tenuigenin in a SH-SY5Y cell model with 6-OHDA-induced injury. *Neurosci. Lett. 497*, 104−109.
(42) Cai, P., Fang, S.-Q., Yang, X.-L., Wu, J.-J., Liu, Q.-H., Hong, H., Wang, X.-B., and Kong, L.-Y. (2017) Rational Design and Multibiological Profiling of Novel Donepezil−Trolox Hybrids against Alzheimer's Disease, with Cholinergic, Antioxidant, Neuroprotective, and Cognition Enhancing Properties. *ACS Chem. Neurosci. 8*, 2496−2511.
(43) Yan, J., Hu, J., Liu, A., He, L., Li, X., and Wei, H. (2017) Design, synthesis, and evaluation of multitarget-directed ligands against Alzheimer's disease based on the fusion of donepezil and curcumin. *Bioorg. Med. Chem. 25*, 2946−2955.
(44) Friesner, R. A., Murphy, R. B., Repasky, M. P., Frye, L. L., Greenwood, J. R., Halgren, T. A., Sanschagrin, P. C., and Mainz, D. T. (2006) Extra precision glide: Docking and scoring incorporating a model of hydrophobic enclosure for protein− ligand complexes. *J. Med. Chem. 49*, 6177−6196.
(45) Release, Q. S. (2017) *QikProp*, Schrödinger, LLC, New York, NY.
(46) Release, S. (2014) *Desmond Molecular Dynamics System, version 3.7* and *Maestro−Desmond Interoperability Tools, version 3*, DE Shaw Research, New York, NY.

DOI: 10.1021/acschemneuro.8b00220
ACS Chem. Neurosci. 2019, 10, 252−265

European Journal of Medicinal Chemistry 177 (2019) 221–234

Contents lists available at ScienceDirect

European Journal of Medicinal Chemistry

journal homepage: http://www.elsevier.com/locate/ejmech

Research paper

Dipropargyl substituted diphenylpyrimidines as dual inhibitors of monoamine oxidase and acetylcholinesterase

Bhupinder Kumar [a], Vijay Kumar [a], Vikash Prashar [b], Suresh Saini [a], Ashish Ranjan Dwivedi [a], Beenu Bajaj [a], Devashish Mehta [a], Jyoti Parkash [b, **], Vinod Kumar [a, *]

[a] Laboratory of Organic and Medicinal Chemistry, Department of Pharmaceutical Sciences and Natural Products, Central University of Punjab, Bathinda, Punjab, 151001, India
[b] Department of Animal Sciences, School of Basic and Applied Sciences, Central University of Punjab, Bathinda, Punjab, India

ARTICLE INFO

Article history:
Received 5 February 2019
Received in revised form
24 April 2019
Accepted 13 May 2019
Available online 16 May 2019

Keywords:
Alzheimer's disease
MAO inhibitors
Acetylcholinesterase inhibitors
Diphenylpyrimidine
Dual inhibitors
Neurological disorders

ABSTRACT

Alzheimer's disease (AD) is a multifactorial neurological disorder involving complex pathogenesis. Single target directed drugs proved ineffective and since last few years' different pharmacological strategies including multi-targeting agents are being explored for the effective drug development for AD. A total of 19 dipropargyl substituted diphenylpyrimidines have been synthesized and evaluated for the monoamine oxidase (MAO) and acetylcholinesterase (AChE) inhibition potential. All the compounds were found to be selective and reversible inhibitors of MAO-B isoform. These compounds also displayed good AChE inhibition potential with IC_{50} values in low micromolar range. **AVB4** was found to be the most potent MAO-B inhibitor with IC_{50} value of 1.49 ± 0.09 μM and **AVB1** was found to be the most potent AChE inhibitor with IC_{50} value of 1.35 ± 0.03 μM. In the ROS protection inhibition studies, **AVB1** and **AVB4** displayed weak but interesting activity in SH-SY5Y cells. In the cytotoxicity studies involving SH-SY5Y cells, both **AVB1** and **AVB4** were found to be non-toxic to the tissue cells. In the molecular dynamic simulation studies of **30 ns,** the potent compounds were found to be quite stable in the active site of MAO-B and AChE. The results suggested that **AVB1** and **AVB4** are promising dual inhibitors and have the potential to be developed as anti-Alzheimer's drug.

1. Introduction

Alzheimer's disease (AD) [1] is a multifactorial neurological disorder characterized by memory loss and cognitive impairment. Pathophysiology of AD is highly complex and the disease state is associated with number of factors such as over expressed monoamine oxidase enzyme, declined levels of acetylcholine (ACh), hyperphosphorylation of tau proteins, amyloid-β aggregation and oxidative stress [2]. Neurodegeneration in AD causes neuronal and synaptic impairment which alters the concentration of various neurotransmitter systems in the brain that include cholinergic systems [3,4], dopamine, serotonin [5] and glutamate [2]. Thus, multi targeting agents (MTA) that can simultaneously modulate different cellular pathways are being explored as drug candidates to achieve better therapeutic efficacy for AD.

Monoamine oxidase (MAO) enzyme is considered as an important target for the treatment of AD [6]. It is involved in the oxidation of xenobiotic and endogenous monoamines including monoamine neurotransmitters such as serotonin, adrenaline, noradrenaline and dopamine. The oxidation reaction results in the formation of neurotoxic aldehydes and reactive oxygen species (ROS) as end products [7]. MAO enzyme exists in two different isoforms, MAO-A and MAO-B which differ in substrate and inhibitor specificity. MAO inhibitors have the potential to attenuate the oxidative metabolism of monoamine neurotransmitters and improve their concentration in the brain. MAO-A selective inhibitors are found to be effective

Abbreviations: QPlogBB, qualitatively predicted logarithmic ratio between the concentration of a compound in brain and blood; LogP, partition coefficient of a molecule between an aqueous and lipophilic phase (octanol and water); CAS, Catalytic active site; PAS, Peripheral active site; MTT, 3-(4,5-dimethylthiazol-2-yl)-2,5-diphenyltetrazolium; 6-OHDA, 6-hydroxydopamine; DMEM, Dulbecco's Modified Eagle's medium; HEPES, (4-(2-hydroxyethyl)-1-piperazineethanesulfonic acid).

* Corresponding author.
** Corresponding author.
E-mail addresses: Jyoti.parkash@cup.edu.in (J. Parkash), vpathania18@gmail.com, vinod.kumar@cup.ac.in (V. Kumar).

https://doi.org/10.1016/j.ejmech.2019.05.039
0223-5234/

against depression [8] while MAO-B selective inhibitors are being explored for the treatment of Parkinson's disease [9] and AD [10]. Recent studies have demonstrated that MAO-B inhibitors possess broader therapeutic effects such as neuroprotection [11], neurorescue [12] and cognitive improvement [7] which are useful for the treatment of AD.

Acetylcholine (ACh) is a neurotransmitter associated with cognitive functions and physical awareness [13]. ACh is hydrolyzed by acetylcholine esterase (AChE) or butyrylcholinesterase (BuChE) enzymes and imbalance in the dynamics is linked to the pathology of AD. The concentration of ACh is found to be drastically low in the AD patients as compared to the healthy persons. The peripheral anionic site (PAS) of AChE catalyzes amyloid-β aggregation which leads to the formation of senile plaques in the brain causing neurodegeneration [14]. Thus, AChE inhibitors can increase the cholinergic transmission in the synaptic cleft by inhibiting the degradation of ACh. At present donepezil, galantamine, and rivastigmine are three AChE inhibitors (Fig. 1) in the clinical practice for the treatment of AD [15]. These cholinergic drugs are able to provide symptomatic relief but could not prevent the progression of disease. Hence, using a single drug that act on a specific target may not be an efficient therapeutic strategy for AD due to its complex etiology. Now the attention of many research groups is focused on the multi-targeting agents (MTAs) to develop effective drug candidates for the treatment of AD. MTAs have the ability to bind to two or more targets and intervene in the pathological events underlying the etiology of the disease. The design strategy for MTA involves incorporation of pharmacophoric groups of different drugs in the same scaffold. Thus, a ligand with MAO inhibitory potential can exhibit more efficient therapeutic effect in AD when it can show additional AChE inhibitory activity. Consequently, many MTAs have been developed and some of them are in various stages of clinical development. Ladostigil (Fig. 1), a dual inhibitor of acetylcholinesterase and MAO-B, has completed phase II trial for AD (NCT01354691). Rasagiline (Fig. 1), is under phase-II clinical trials to determine its effect in the regional brain metabolism in case of AD (NCT02359552, NCT00104273).

In our previous studies [15], we have developed novel pyrimidine derivatives as selective inhibitors of MAO-B isoform. Most of these compounds were found to be reversible MAO-B inhibitors and taking leads from this study, we have developed another series of 4,6-diphenylpyrimidines as dual inhibitors of monoamine oxidase and acetylcholinesterase enzymes. In both of the studies, propargyl group was incorporated in the main scaffold as potential pharmacophore for MAO enzyme. Propargyl group is present in number of potent MAO inhibitors [10,16] such as clorgyline, selegiline, pargyline, rasagiline etc. and other multitargeting agents [17–25]. It forms a crucial covalent bond with the FAD cofactor of MAO enzyme [26]. Recently, Zindo et al. thoroughly reviewed the role of propargyl group as functional moiety in the design and development of multifunctional drugs for various neurological disorders [25]. Weinreb et al. [27] investigated the role of propargyl group in rasagiline as a neuroprotective moiety. It has been concluded that neuroprotective effect of rasagiline is associated with the propargyl moiety, which promotes mitochondrial viability and stabilizes permeability transition by regulating Bcl-2 family proteins. Similarly, other research groups [28,29] also demonstrated that rasagiline and other propargyl containing ligands may rescue degenerating dopamine neurons by inhibiting death signal transduction initiated by mitochondrial permeability transition. Keeping in view the significance of propargyl moiety and following our previous work, in the current study we have incorporated two propargyl groups in the diphenylpyrimidine scaffold and investigated their MAO and AChE inhibition potential. To the best of our knowledge this is first report on the screening of compounds containing two propargyl groups on a scaffold. The synthesized compounds were screened against MAO-A and MAO-B isoforms and all the compounds were found to be selective and reversible inhibitors of MAO-B isoform. These compounds also displayed good AChE inhibition potential with IC_{50} values in low micro molar range. In the series, **AVB4** was found to be the most potent MAO-B inhibitor with IC_{50} value of 1.49 ± 0.09 μM and **AVB1** was found to be the most potent AChE inhibitor with IC_{50} value of 1.35 ± 0.03 μM. In the ROS protection inhibition studies, **AVB1** and **AVB4** displayed weak but interesting activity in SH-SY5Y human neuroblastoma cells. The most active compounds were also tested for neuroprotective potential in SH-SY5Y cells and showed moderate activity. In the cytotoxicity studies involving SH-SY5Y cells, both **AVB1** and **AVB4** were found to be non-toxic to the tissue cells.

2. Results and discussions

2.1. Chemistry

All the compounds were synthesized by following the reaction procedures described in Scheme 1. All the final products were characterized by ^{1}H NMR, ^{13}C NMR, ESI-MS and HRMS.

2.2. Biological results

2.2.1. hMAO and AChE inhibition studies

MAO and AChE inhibition potential of the synthesized

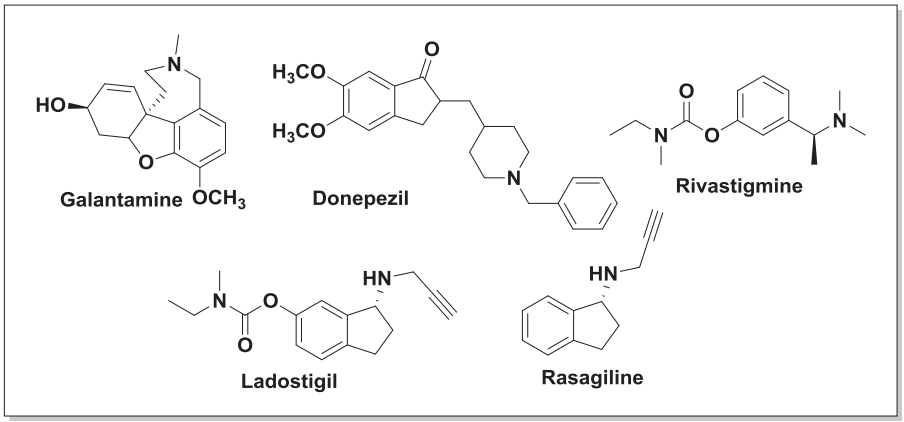

Fig. 1. Drugs in market and under clinical trials for Alzheimer's disease.

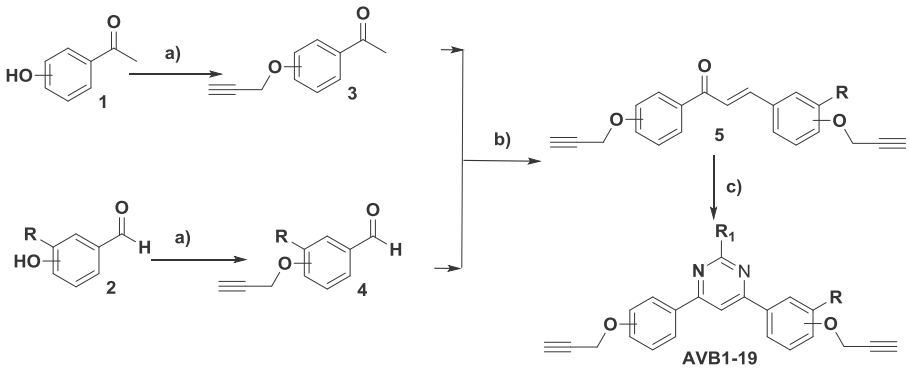

Scheme 1. Reagents and conditions: a) Propargyl bromide (1.2 eq), K_2CO_3 (2.4 eq), acetone, reflux, 12h; **b)** CH_3OH as solvent, 20% NaOH aq., rt, stirring 1h; **c)** Amidines (1.2 eq), Na_2CO_3 (2.4 eq), CH_3CN as solvent, reflux, 24h.

compounds (**AVB1**−**AVB19**) was evaluated through fluorimetric method using Amplex Red assay kits purchased from the Molecular Probes, Inc./Invitrogen. The results of MAO and AChE inhibition studies are expressed in the form of IC_{50} values (μM) described in Table 1. Both the phenyl rings of synthesized diphenylpyrimidine derivatives were substituted with propargyl groups at ortho/meta/para positions. Different amidines were used with R_1 as $-NH_2$, or $-CH_3$ or $-C_6H_5$ so as to develop structure activity relationship profile of this series of compounds. Clorgyline, pargyline, and donepezil were used as standard inhibitors for MAO-A, MAO-B, and AChE enzymes, respectively. All of the synthesized compounds were found to be potent inhibitors of MAO-B isoform (Selective over MAO-A) and AChE with IC_{50} values in low micromolar range. Compound **AVB4** was found to be the most potent MAO-B inhibitor with IC_{50} value of 1.49 ± 0.09 μM exhibiting 17-folds selectivity over MAO-A. It also showed potent inhibition of AChE with IC_{50} value of 1.74 ± 0.07 μM. In the reported series, **AVB1** was found to be the most potent AChE inhibitor with an IC_{50} value of 1.35 ± 0.03 μM and displayed MAO-B inhibitory activity with an IC_{50} value of 3.30 ± 1.17 μM. Unfortunately, as evident from Table 1, all the compounds were found to be unselective or weakly selective for MAO-B isoform.

2.2.2. Reversibility inhibition studies

To determine whether the synthesized compounds are reversible or irreversible inhibitors of the target enzymes, the most active

Table 1
Results of MAO-A, MAO-B and AChE inhibition studies of the synthesized compounds..

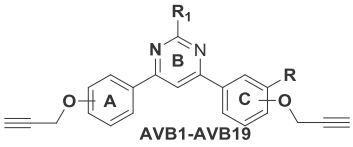

Entry Name	Propargyl at ring A	Propargyl at ring C	R	R_1	IC_{50} values (mean ± S.E. μM)			MAO Selectivity (SI)
					hMAO-A	hMAO-B	eeAChE	
AVB1	C4	C4	H	NH_2	32.06 ± 1.19	3.30 ± 1.17	1.35 ± 0.03	9.7
AVB2	C4	C4	H	CH_3	34.15 ± 2.03	7.83 ± 0.57	1.76 ± 0.06	4.4
AVB3	C4	C4	H	C_6H_5	25.57 ± 1.18	12.26 ± 0.99	7.53 ± 0.23	2.1
AVB4	C4	C3	H	NH_2	24.06 ± 0.71	1.49 ± 0.09	1.74 ± 0.07	16.1
AVB5	C4	C3	H	CH_3	21.14 ± 1.40	8.09 ± 0.54	5.88 ± 0.07	2.6
AVB6	C4	C3	H	C_6H_5	25.83 ± 1.92	17.69 ± 1.13	4.39 ± 0.16	1.5
AVB7	C4	C2	H	NH_2	28.55 ± 0.77	22.12 ± 1.68	1.81 ± 0.02	1.3
AVB8	C4	C2	H	CH_3	23.19 ± 1.87	18.07 ± 1.75	2.56 ± 0.13	1.3
AVB9	C4	C2	H	C_6H_5	22.02 ± 1.03	14.44 ± 0.78	7.25 ± 0.16	1.5
AVB10	C3	C3	H	NH_2	***	22.09 ± 0.94	6.99 ± 0.09	≥3
AVB11	C3	C3	H	C_6H_5	***	23.44 ± 1.17	6.73 ± 0.18	≥3
AVB12	C2	C2	H	NH_2	***	11.13 ± 0.16	5.19 ± 0.21	≥5
AVB13	C2	C2	H	C_6H_5	***	13.78 ± 0.22	8.12 ± 0.19	≥4
AVB14	C4	C4	OCH_3	NH_2	***	20.03 ± 1.18	4.58 ± 0.08	≥3
AVB15	C4	C4	OCH_3	CH_3	24.99 ± 2.13	21.08 ± 1.83	5.92 ± 0.18	1.2
AVB16	C4	C4	OCH_3	C_6H_5	24.93 ± 1.17	15.71 ± 0.95	6.99 ± 0.16	1.6
AVB17	C4	C4	OCH_2CH_3	NH_2	***	14.01 ± 1.07	7.05 ± 0.14	≥4
AVB18	C4	C4	OCH_2CH_3	CH_3	***	10.97 ± 0.82	6.38 ± 0.09	≥5
AVB19	C4	C4	OCH_2CH_3	C_6H_5	***	29.03 ± 1.33	6.94 ± 0.16	≥2
Clorgyline					4.39 ± 1.02 nM	nd	nd	
Pargyline					nd	0.15 ± 0.02	nd	
Donepezil					nd	nd	0.03 ± 0.001	

***Inactive or showed less than 50% inhibitory activity at 50 μM concentration and precipitated at higher concentrations. [nd]not determined, SI for MAO-B: IC_{50} MAO-A/IC_{50} MAO-B.

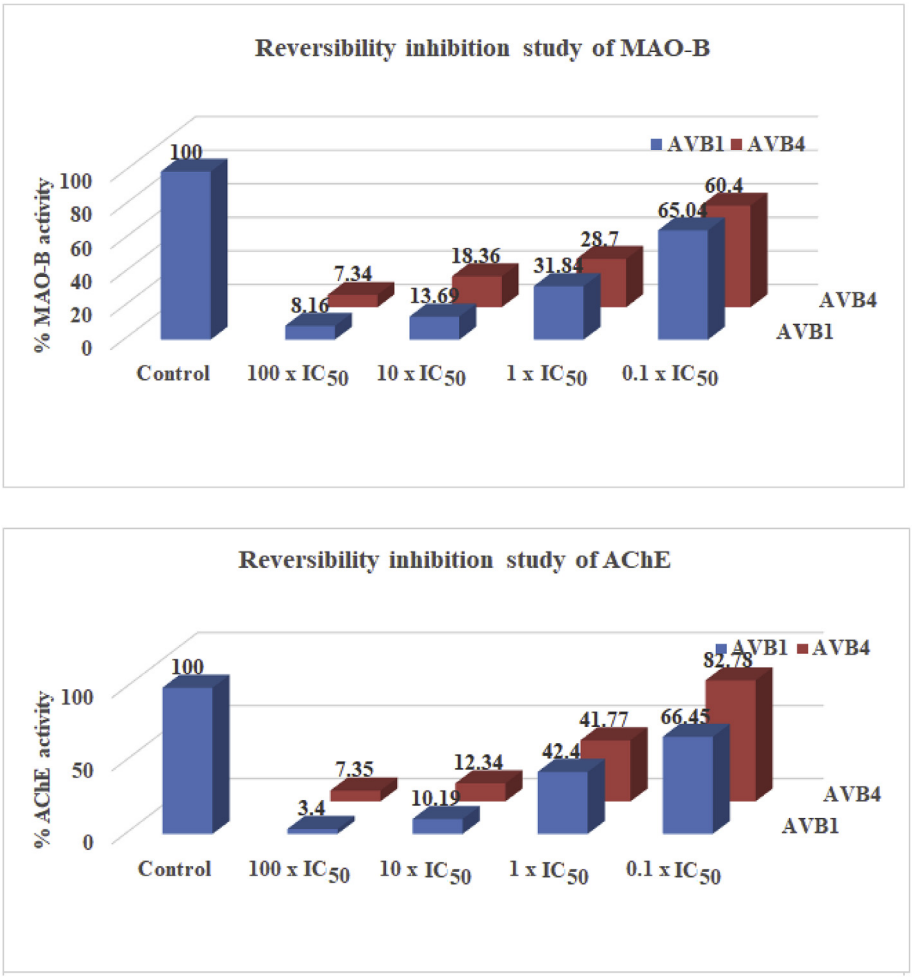

Fig. 2. Reversibility inhibition studies of **AVB1** and **AVB4** with **A)** MAO-B enzyme and **B)** AChE enzyme.

compounds i.e. **AVB1** and **AVB4** were subjected to reversibility inhibition studies [15]. Both the compounds were found to be reversible inhibitors of MAO-B and AChE enzymes. At the IC_{50} concentration **AVB1** showed 31.8% and 42.4% residual activity for MAO-B and AChE respectively. Similarly, **AVB4** displayed 28.7% and 41.7% residual activity for MAO-B and AChE respectively. Compound **AVB1** showed recovery in the enzyme activity by up to 65.04% and 66.45% for MAO-B and AChE respectively at 0.1 X IC_{50} concentration, while compound **AVB4** showed recovery in the enzyme activity up to 60.4% and 82.78% for MAO-B and AChE respectively at 0.1 X IC_{50} concentration (Fig. 2). At 1 X IC_{50} concentration of compound **AVB1**, enzymatic activity upto 31.84% and 42.4% was recovered for MAO-B and AChE respectively, while for **AVB4**, enzymatic activity upto 28.7% and 41.7% was recovered for MAO-B and AChE respectively. Thus, it can be concluded that the synthesized compounds are weak reversible inhibitors of both MAO-B and AChE enzymes at 1 X IC_{50} concentration of these inhibitors.

2.2.3. Kinetic studies of AChE inhibition

To determine the mechanism of inhibition of AChE, kinetic study was carried out with the most potent inhibitor of AChE (**AVB4**) using eeAChE. The reciprocal Lineweaver-Burk plots (Fig. 3) illustrates the increased slope (decreased V_{max}) and higher intercepts (K_m) with the increasing concentration of **AVB4.** The intersection point of the Lineweaver-Burk reciprocal plots was located in the third quadrant, which indicate that **AVB4** is mixed type inhibitor. **AVB4** might be binding to PAS and CAS of AChE simultaneously and inhibit the binding of substrate to active site. Binding of **AVB4** with the PAS and CAS is further supported by docking and molecular dynamics simulation studies.

2.2.4. ROS inhibition studies

From literature survey, it is clear that MAO mediated metabolism of various monoamines leads to the production of H_2O_2 which further get converted into free radicals through Fenton's reaction and induces oxidative stress. Increased levels of these free radicals, initiate free radical-mediated chain reactions that may cause oxidative damage to the cell membranes, DNA strand breakdown and neuronal cell death. Thus, prevention of ROS generation along with MAO inhibition is considered as an added advantage to prevent neurotoxicity in neurodegenerative diseases. The most potent compounds in the series i.e. **AVB1** and **AVB4** were evaluated for their ROS production inhibition potential against human neuroblastoma cells (SH-SY5Y) after 24h interval treatment. For activity evaluation, 2,7-dichlorofluorescein diacetate (DCF-DA), a non-fluorescent compound was used. DCF-DA in the presence of reactive oxygen species is oxidized to 2,7-DCF which is a fluorescence emitting agent. Compound **AVB1** reduced the ROS levels to 89.83% and 30.04% at 1 μM and 5 μM concentrations, respectively in the SH-SY5Y cells (Fig. 4). Similarly, compound **AVB4** reduced the ROS levels up to 68.3% and 47.25% at 1 μM and 5 μM concentrations,

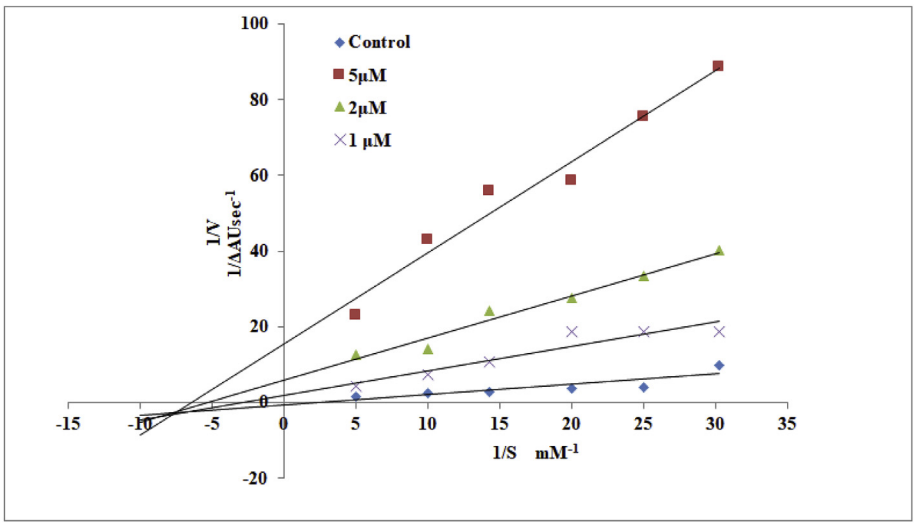

Fig. 3. Kinetic study on the mechanism of *ee*AChE inhibition by **AVB4**. Overlaid Lineweaver–Burk reciprocal plots of AChE initial velocity at increasing substrate concentration (0.1–1 mM) in the absence or presence of **AVB4** are shown.

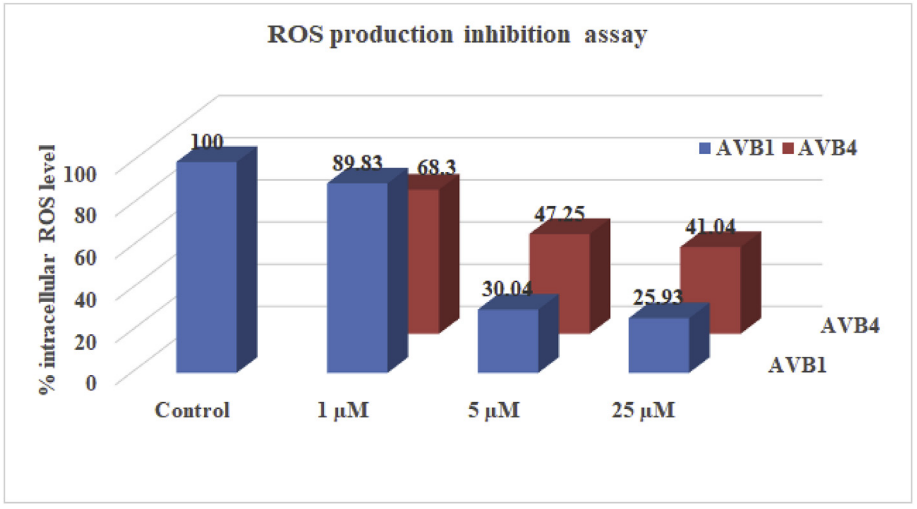

Fig. 4. ROS inhibition studies of compound **AVB1** and **AVB4** on SH-SY5Y cells after treatment for 24h.

respectively in the SH-SY5Y cells. Thus, from these results, it is apparent that this series of compounds with two propargyl moieties may weakly protect the neuronal cells from ROS.

2.2.5. Neuroprotective effects

The most potent AChE and MAO-B inhibitors i.e **AVB1** and **AVB4** were evaluated for their neuroprotective potential against 6-hydroxydopamine (6-OHDA) neurotoxin in SH-SY5Y cells. These compounds showed mild neuroprotective potential against 6-OHDA. Maximum cell viability of 66.6% was observed for compound **AVB1** as compared to the 6-OHDA treated cells (48.52%). As the concentration of the compounds increased from 5 μM to 25 μM, the cell viability was further reduced as shown in Fig. 5.

2.2.6. Metal chelation studies

Metal-chelating studies of **AVB1** and **AVB4** were performed with a UV–vis spectrophotometer. The absorption spectra of both compounds (50 μM, final concentration) alone or in the presence of $CuSO_4$, $FeSO_4$, and $FeCl_3$ (50 μM, final concentration) were recorded. In metal chelating studies, none of the compounds formed any metal chelate with any of the above metal salts. Thus, these compounds are ineffective against metal salts and did not show any metal chelating properties.

2.2.7. Cytotoxicity studies

Cytotoxicity of the most potent inhibitors (**AVB1 and AVB4**) was determined against SH-SY5Y cells using MTT assay. The test compounds at 1 μM, 5 μM and 25 μM concentrations were incubated with SH-SY5Y cells and cell viability was determined after 24h time interval using MTT assay. As depicted in Fig. 6, the compounds were found non-toxic at the lower concentrations. As the concentration of the compounds increased, there was a slight decrease in the cell viability. Minimum cell viability of 69.17% was observed for **AVB4** at 25 μM concentration. At lower concentration of 1 μM, cell viability of 87.34% was observed as compared to the control. Thus, keeping in view the IC_{50} values of the compounds which are in low

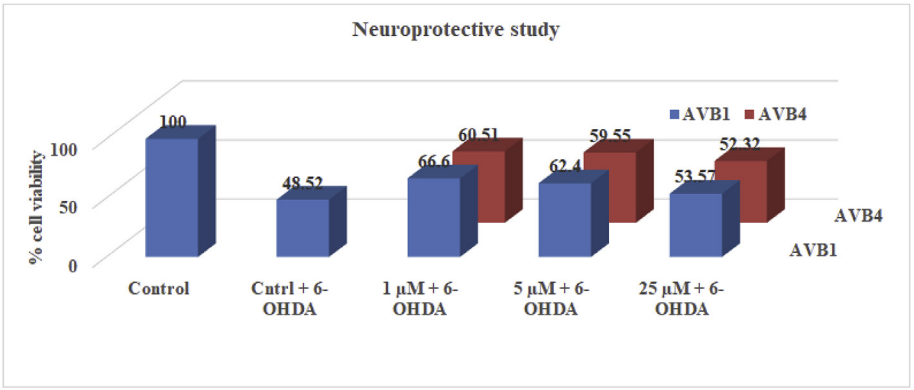

Fig. 5. Neuroprotective studies of **AVB1** and **AVB4** on SH-SY5Y cells.

micromolar range, the current series of compounds were found to be nontoxic to the tissue cells (Fig. 6).

2.2.8. *Molecular docking and simulation studies*

Docking of the ligands and molecular dynamics simulations in the active site of the receptors may provide crucial information about the orientations of the ligands and their interactions with various amino acid residues at the receptor site. Most active compounds obtained in the series were docked at the respective active sites of the receptor isoforms. Maestro 11.1 (Schrödinger LLC) software was used for carrying out the docking studies and compounds **AVB1** and **AVB4** were docked at the hMAO-B (PDB ID-2BYB) [30] and AChE (PDB ID-1EVE) [31] and their crystal structures were imported from the protein data bank. The docking procedures were first validated by accurately redocking the co-crystallized ligands into the MAO models. The active site of MAO-B is divided into two different compartments, an entrance cavity and a substrate cavity separated by the side chain of Ile199 which serves as a "gate" between the two cavities. The docking orientations of the compound **AVB1** and **AVB4** showed that the pyrimidine moiety in both the compounds interact with the Ile199 and kept this residue in open gate conformation. Phenyl ring with propargyl group at meta position in **AVB4** is oriented towards FAD cofactor and accommodated in the substrate cavity while the phenyl ring with para propargyl group is aligned in the entrance cavity. In the enzyme-AVB1 complex, both the phenyl rings contain propargyl groups at the para positions and one of the propargyl group is oriented towards the FAD cofactor. The NH_2 group of **AVB1** showed hydrogen bonding with Phe168 and Cys172. In the enzyme-AVB4 complex**,** pyrimidine ring remains close to the entrance cavity and NH_2 group formed hydrogen bonds with Cys172 and Tyr188. The pyrimidine ring in **AVB1** form π-π stacking with Tyr326 while in **AVB4** propargyl containing phenyl ring interacts with Tyr326 as shown in Fig. 7. The inner phenyl ring of **AVB4** in the substrate displayed π-π interactions with Phe343. The increased MAO-B activity of **AVB4** as compared to **AVB1** might be due to the additional π-π stacking of **AVB4** with Tyr326 and Phe343.

Similarly, both of these compounds i.e. **AVB1** and **AVB4** were docked against AChE (PDB ID- 1EVE co-crystallized with donepezil) to determine their binding alignment at the active site of the enzyme. The active site of AChE is divided into two compartments; i) catalytic active site (CAS) composed of Trp84, Tyr130, Phe330, Phe331 residues and, ii) peripheral anionic site (PAS) which consists of amino acids-Tyr70, Asp72, Tyr121, Trp279, and Tyr334. The compounds were found to interact both with CAS as well as with PAS of AChE. Pyrimidine ring in **AVB1** and **AVB4** accommodated in PAS and NH_2 group formed hydrogen bonds with Asp72 (Fig. 8). In case of **AVB1,** one of the phenyl rings with a propargyl group is accommodated in the CAS and showed π-π interactions with Trp84. In **AVB4,** phenyl ring with para propargyl group is oriented towards PAS and displayed π-π stacking with Tyr334. An additional hydrogen bond interaction of *O*-propargylated group with Phe288 in PAS was observed in **AVB1** (Fig. 8). Thus, interactions of these compounds at CAS, as well as PAS, make them more effective against AD.

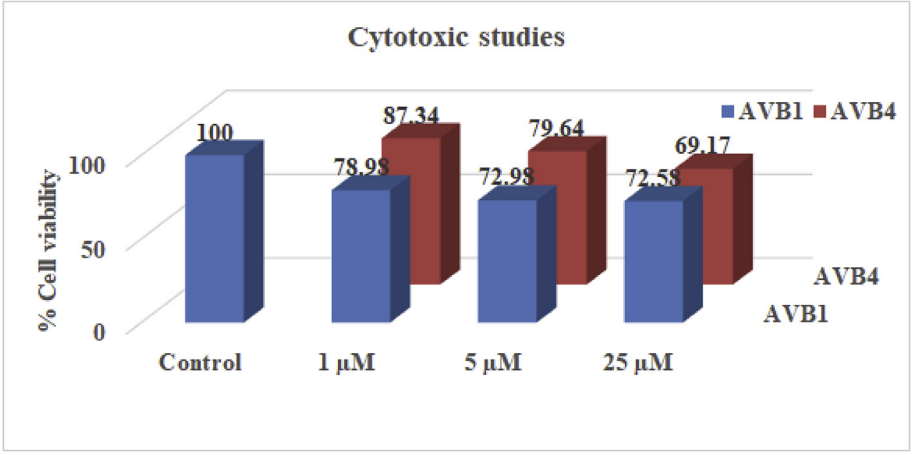

Fig. 6. Cytotoxicity studies of **AVB1** and **AVB4** on the SH-SY5Y cells after treatment for 24h.

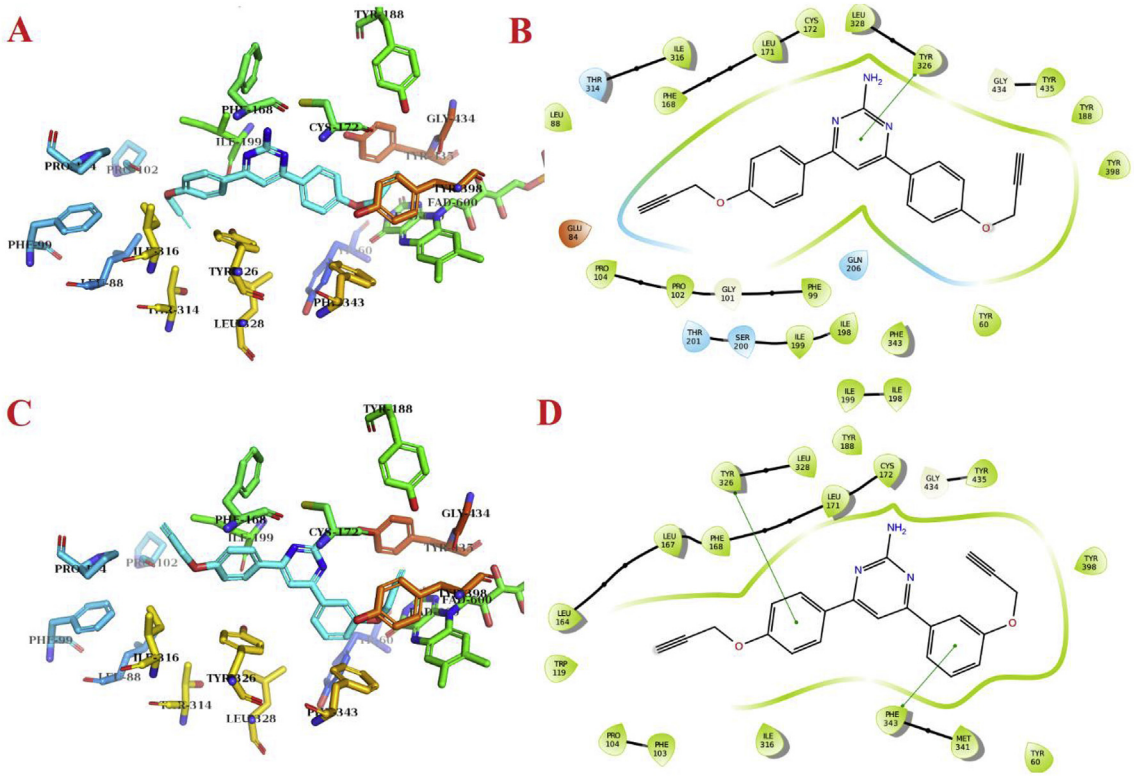

Fig. 7. A) Binding pattern (3D) of **AVB1** with the amino acid residues at the active site of MAO-B (2BYB), **B)** binding interactions (2D) of **AVB1** with various amino acids of MAO-B active cavity, **C**) Binding pattern (3D) of **AVB4** with the amino acid residues at the active site of MAO-B (2BYB), and **D)** binding interactions (2D) of **AVB4** with various amino acids of MAO-B active cavity.

2.2.9. Molecular dynamic simulation studies

In order to investigate the binding stability of the potent inhibitors into the active site of the MAO-B and AChE, molecular dynamic (MD) simulations studies were performed. For this docking complexes of **AVB1** and **AVB4** with MAO-B and AChE were used. The MD simulations studies were conducted for 30 ns and the interaction pattern of the test compounds with different amino acids was analyzed. MD simulations studies of **AVB4** with MAO-B yielded the stable trajectory from 3 ns to 30 ns, oscillating in between 0.8 Å to 1.2 Å. For the initial 2 ns time interval, a sharp hike was observed in RMSD from 0.4 Å to 1.6 Å, which stabilized to 1.2 Å after 3 ns interval. The pyrimidine ring of AVB4 maintained its initial ð-ð interaction with Tyr326 throughout MD time interval (Fig. 9).

Similarly, docking complexes of **AVB1** and **AVB4** with AChE were used for MD simulations to determine their binding stability at the active site of the enzyme. In case of **AVB4,** a stable trajectory was observed after the initial 3 ns interval which was determined through root-mean-square-deviation (RMSD) of the protein backbone ranging from 0.8 Å to 1.2 Å (Fig. 10). For the first 3 ns time interval, a hike in RMSD trajectory was observed from 0.4 Å to 0.8 Å. In case of **AVB1,** RMSD kept oscillating from 0.4 Å to 1.2 Å throughout the MD simulations studies of 30 ns. Analyzing these MD trajectories of AChE-AVB1 and AChE-AVB4 complexes, it can be concluded that these compounds (**AVB1** and **AVB4**) had a strong tendency to be localized in the binding region of AChE. One of the propargyl substituted ring of **AVB1** maintained its initial π-π interaction with Trp84. Similarly, for **AVB4** the initial interactions such as hydrogen bond formation of pyrimidine ring with Tyr121 and π-π interactions of pyrimidine ring with Trp84 were maintained throughout the MD simulations time interval (Fig. 10). Thus from these studies, it can be concluded that MD simulations of **AVB1** and **AVB4** do not indicate any abrupt local force that could potentially break up the inhibitors or can even delocalize these from the binding site of AChE.

2.2.9. Physicochemical properties

In order to assess the drug-like characteristics of the most active compounds (**AVB1** and **AVB4**), various physicochemical parameters of these compounds have been evaluated. Both the compounds showed good drug-like properties and follow Lipinski's rule of five (see Table 2). The logP value of both the compounds is less than five and hydrogen bond donor and acceptor atoms are also less than five. Both the compounds showed 100% human oral absorption in Qikprop studies. The QPlogBB values were also in the optimum range and hence these compounds are expected to cross the blood-brain barrier. Thus, it can be concluded that both of these compounds have an optimum chemical skeleton that can be developed as potential drug molecule.

2.2.10. SAR studies

In the current studies, diphenylpyrimidines containing two propargyl groups were designed and synthesized. A total of 19 compounds were synthesized and evaluated against MAO-A, MAO-B and AChE enzymes. Most of the compounds of this series were found to be selective inhibitors of MAO-B isoform and also displayed potent AChE inhibitory activities. As evident from Table 1, **AVB1** with propargyl groups at the para positions of the phenyl rings and a NH_2 group on the pyrimidine ring displayed IC_{50} values of 1.74 ± 0.07 μM and 1.35 ± 0.03 μM for MAO-B and AChE respectively. **AVB1** was found to be the most potent AChE inhibitor in the reported series of compounds. Replacement of NH_2 with CH_3 in **AVB2** reduced MAO-B inhibitory activity by more than 2-folds but

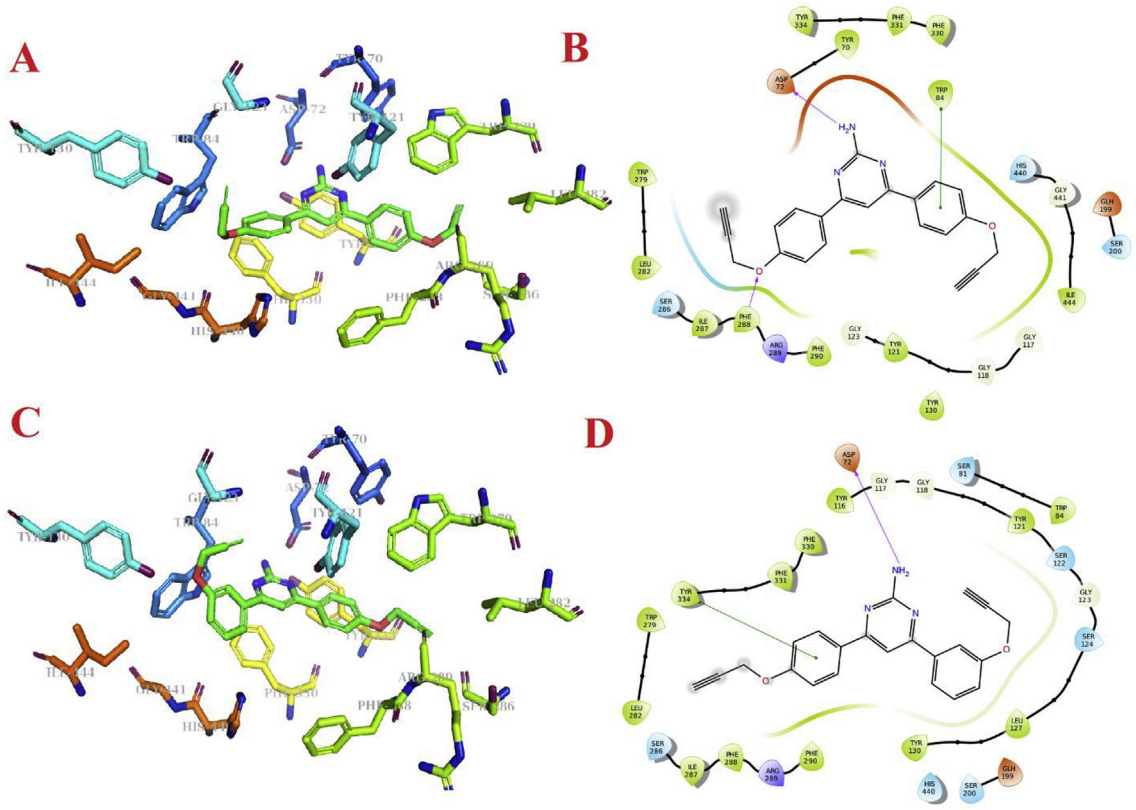

Fig. 8. A) Binding pattern (3D) of **AVB1** with the amino acid residues at the active site of AChE (1EVE)**, B)** binding interactions (2D) of **AVB1** with various amino acids of AChE active cavity, **C**) Binding pattern (3D) of **AVB4** with the amino acid residues at the active site of AChE (1EVE)**,** and **D)** binding interactions (2D) of **AVB4** with various amino acids of AChE active cavity.

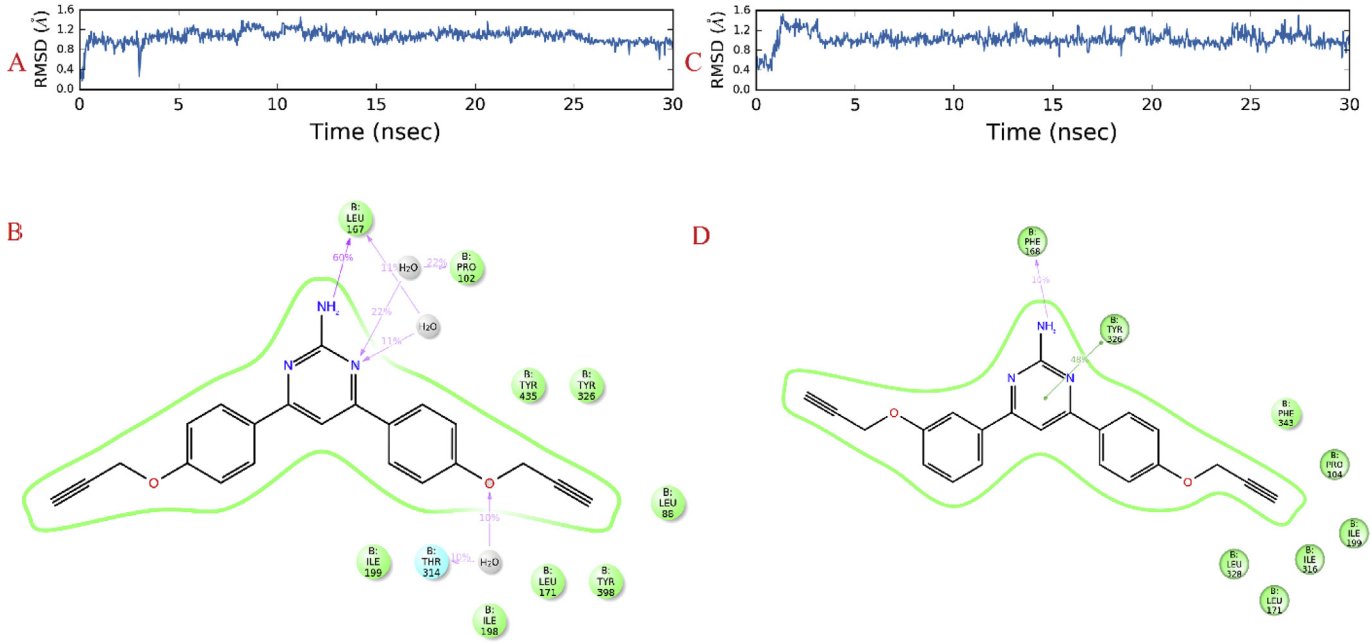

Fig. 9. A) RMSD graph of MD simulations studies of **AVB1** with MAO-B for 30 ns, **B**) interactions of **AVB1** with the active site residues of MAO-B during 30 ns MD simulations studies, **C)** RMSD graph of MD simulations studies of **AVB4** with MAO-B for 30 ns, and **D**) interactions of **AVB4** with the active site residues of MAO-B during 30 ns MD simulation studies.

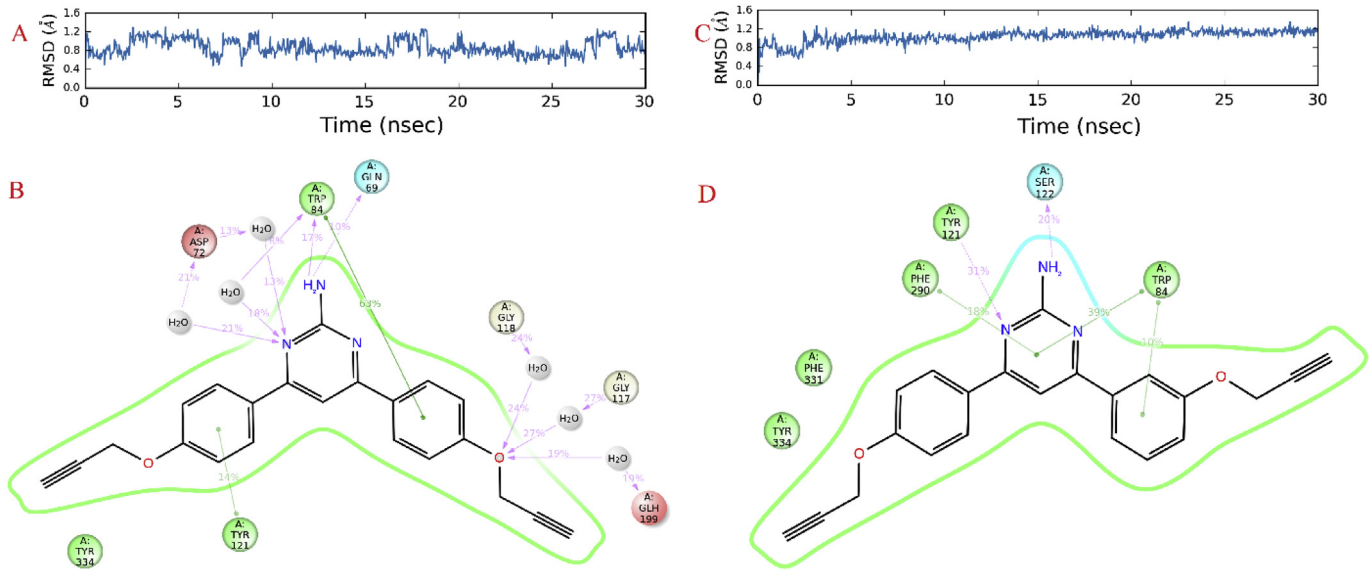

Fig. 10. A) RMSD graph of MD simulations studies of **AVB1** with AChE for 30 ns, **B**) interactions of **AVB1** with the active site residues of AChE during 30 ns MD simulation studies, **C)** RMSD graph of MD simulations studies of **AVB4** with AChE for 30 ns, and **D**) interactions of **AVB4** with the active site residues of AChE during 30 ns MD simulation studies.

Table 2
Physicochemical properties of some of the potent and selective MAO inhibitors.

Compound number	Mol. Wt.	Log P	HB donor	HB acceptor	% human oral absorption	QPlogBB (Optimum range −3.0 to 1.2)	BBB permeability predicted
AVB1	355.39	4.52	3	4	100	−0.934	+ve
AVB4	355.39	4.51	3	4	100	−0.93	+ve

+ ve = blood-brain barrier permeable; - ve = no permeability to the blood-brain barrier.

retained AChE inhibition activity. Replacing NH_2 with phenyl ring in **AVB3** further reduced the MAO-B inhibitory activity by almost 4-folds and AChE inhibition activity by more than 5-folds. Shifting of one of the propargyl group from para (**AVB1**) to meta position (**AVB4**) significantly increased MAO-B inhibitory activity by more than 2-folds and retained AChE inhibition activity. **AVB4** was found to be the most potent MAO-B inhibitor in the series with an IC_{50} value of 1.49 ± 0.09 μM. Replacement of NH_2 group of **AVB4** by CH_3 (**AVB5**) and phenyl (**AVB6**) groups reduced the MAO-B inhibitory activity by more than 5-folds and 12-folds respectively and AChE inhibitory activity was reduced by about 3-folds. Shifting of propargyl group from meta (**AVB4**) to ortho position (**AVB7** to **AVB9**) of the phenyl ring proved detrimental and the MAO-B inhibitory activity was found to be reduced by more than 14-folds. Similarly, reduced MAO-B inhibitory activity was observed when both the phenyl rings were substituted by propargyl groups at the meta positions (**AVB10** and **AVB11**) and at ortho positions (**AVB12** and **AVB13**). Presence of additional substituents at the phenyl ring (**AVB14** to **AVB19**) was also found unfavorable for the MAO-B and AChE inhibitory activities.

3. Conclusion

Multi-targeting agents can be an effective strategy for the treatment of multifactorial diseases like AD. Multi-targeting ligands which can simultaneously target MAO and AChE enzymes are being developed for the treatment of AD. In the current research work, a series of dipropargyl substituted diphenylpyrimidines, have been synthesized and evaluated for MAO and AChE inhibition activities. Most of the compounds were found to be selective inhibitors of MAO-B isoform and potent AChE inhibitors. In the series, **AVB1** and **AVB4** were found to be the most potent inhibitors of AChE and MAO-B with IC_{50} values of 1.35 ± 0.03 μM and 1.49 ± 0.09 μM respectively. In the reversible inhibition studies, the lead compounds were found to be reversible inhibitors of MAO-B and AChE enzymes. In the ROS protection inhibition studies, **AVB1** and **AVB4** displayed weak but interesting activity in SH-SY5Y cells and **AVB1** reduced the ROS levels up to 30% at 5 μM. In the cytotoxicity studies involving SH-SY5Y cells, both **AVB1** and **AVB4** were found to be non-toxic to the tissue cells. In the molecular dynamic simulation studies, the lead compounds were found to be stable in the active site of MAO-B and AChE for the time interval of 30 ns. The results suggested that **AVB1** and **AVB4** are promising dual inhibitors and have the potential to be developed as anti-Alzheimer's drug.

4. Experimental

4.1. Material and methods

All the reagents or chemicals used for the synthesis of intermediates or target compounds were purchased from Avra synthesis, Sigma-Aldrich, Loba-Chemie Pvt. Ltd. and S.D. Fine Chemicals and are used without further purification. Thin layer chromatography was done on glass silica plates with silica gel GF254 as the adsorbent. Ethyl acetate: petroleum ether (1:1, 1:2 and 1:3) mixtures were used as a solvent system for the chromatographic purification of compounds using column chromatography. Mass spectra were recorded on GC-MS (ESI), Central Instruments Laboratory (CIL), Central University of Punjab, Bathinda. The ^{1}H and ^{13}C NMR of the compounds were recorded on JEOL or Bruker Advance II instrument at 400 MHz frequency, in $CDCl_3$ or DMSO and TMS ($\delta = 0$) as an internal standard at IIT Ropar, and GJUS&T, Hisar. The chemical shifts are reported in parts per million (δ) downfield from the signal of tetramethylsilane added to the

deuterated solvent. Melting points were recorded with Stuart SMP30 melting point apparatus and are uncorrected. For MAO inhibition studies and acetylcholinesterase inhibition studies, Amplex® Red MAO kit was purchased from Molecular Probes (Invitrogen), Life technologies, India. Recombinant hMAO-A and hMAO-B enzymes were purchased from Sigma-Aldrich. For absorption studies, UV-VIS spectrophotometer of Shimadzu was used. Fluorescence studies were recorded using Biotek Microplate reader. Molecular modelling studies were carried out using Maestro 11.1 (Schrödinger LLC) and ChemBio Draw Ultra-12 installed on operating system centos 6.5 at HP-2800 workstation with configuration of Intel (R) Xenon (R) X5660 @2.80 GHz, 2.789 GHz (2 processors).

4.2. Chemistry

4.2.1. General procedure for the synthesis of O-propargylated derivatives 3 and 4

To hydroxy substituted acetophenones (0.5g) or benzaldehydes (0.5g), Propargyl bromide (1.2eq) was added in the presence of potassium carbonate as a base (2.4eq.) and acetone (30 ml) as solvent. The reaction mixture was refluxed overnight at 60 °C. Progress of the reaction was monitored via TLC. After completion of the reaction, excess of solvent was evaporated from the mixture using vacuum rotary evaporator, water (10 mL) was added and aqueous phase was extracted with ethyl acetate (10 mL × 3), and washed with brine, dried over anhydrous Na_2SO_4 and the organic solvent was concentrated under vacuum using rotary evaporator to obtain **3** and **4**.

4.2.2. General procedure for the synthesis of 5

To a mixture of **3** (1 eq.) and **4** (1 eq.) in methanol (20 ml), aqueous sodium hydroxide (20%) was added slowly with continuous stirring. The reaction mixture was stirred for 3 h at room temperature. The completion of reaction was monitored via TLC. After completion of reaction, excess of solvent was evaporated from the mixture using rotary evaporator. Chilled water was poured into the reaction mixture and precipitates of **5** were filtered and dried. Further crude product was recrystallized from ethanol or purified using column chromatography as per requirement.

4.2.3. General procedure for the synthesis of AVB1-19

To a mixture of **5** (500 mg), and amidine (1.2 eq.), anhydrous sodium carbonate (2.4 eq.) was added in acetonitrile (10 mL) as solvent. The reaction mixture was refluxed for 24 h at 85 °C. The progress of the reaction was monitored via TLC. After completion of the reaction, excess of solvent was evaporated under vacuum using rotary evaporator, and water (10 mL) was added which was extracted with ethyl acetate (3 × 10 mL), washed with brine, dried over anhydrous Na_2SO_4, and the organic solvent was concentrated under vacuum using rotary evaporator and purified via column chromatography (EtOAc:Pet ether). The final products were characterized by NMR spectroscopy and HRMS.

4,6-bis(4-(prop-2-yn-1-yloxy)phenyl)pyrimidin-2-amine (AVB1): Yield: 55%; yellow solid, mp 139–141 °C; ^{1}H NMR ($CDCl_3$, 400 MHz, δ with TMS = 0): 8.02 (4H, d, J = 8Hz), 7.34 (1H, s), 7.06 (4H, d, J = 8Hz), 5.17 (2H, s), 4.76 (4H, d, J = 4Hz), 2.54 (2H, t, J = 4Hz), ^{13}C NMR ($CDCl_3$, 100 MHz, δ with TMS = 0) δ: 165.40, 163.57, 159.49, 131.16, 128.66, 115.25, 103.02, 76.81, 75.98, 55.92, **HRMS**: for $C_{22}H_{17}N_3O_2$, calculated $[M+H]^+$: 356.1399; observed $[M+H]^+$: 356.1368.

2-methyl-4,6-bis(4-(prop-2-yn-1-yloxy)phenyl)pyrimidine (AVB2): Yield: 60%; blue solid, mp 158–160 °C; ^{1}H NMR ($CDCl_3$, 400 MHz, δ with TMS = 0): 8.10 (4H, d, J = 8Hz), 7.76 (1H, s), 7.10 (4H, d, J = 8Hz), 4.76 (4H, d, J = 4Hz), 2.81 (3H, s), 2.55 (2H, t, J = 4Hz), ^{13}C NMR ($CDCl_3$, 100 MHz, δ with TMS = 0) δ: 168.34, 164.00, 159.59, 130.92, 128.71, 115.21, 108.55, 78.15, 75.90, 55.89, 26.49, **HRMS**: for $C_{23}H_{18}N_2O_2$, calculated $[M+H]^+$: 355.1447; observed $[M+H]^+$: 355.1402.

2-phenyl-4,6-bis(4-(prop-2-yn-1-yloxy)phenyl)pyrimidine (AVB3): Yield: 65%; greenish solid, mp 148–150 °C; ^{1}H NMR ($CDCl_3$, 400 MHz, δ with TMS = 0) 8.73 (2H, d, J = 8Hz), 8.30 (4H, d, J = 8Hz), 7.92 (1H, s), 7.55 (3H, m), 7.18 (4H, d, J = 8Hz), 4.82 (4H, d, J = 4Hz), 2.59 (2H, t, J = 4Hz), ^{13}C NMR ($CDCl_3$, 100 MHz, δ with TMS = 0): 163.90, 159.70, 138.32, 130.98, 130.51, 128.75, 128.40, 115.17, 108.78, 78.17, 75.92, 55.90, **HRMS**: for $C_{28}H_{20}N_2O_2$, calculated $[M+H]^+$: 417.1603; observed $[M+H]^+$: 417.1549.

4-(3-(prop-2-yn-1-yloxy)phenyl)-6-(4-(prop-2-yn-1-yloxy) phenyl)pyrimidin-2-amine (AVB4): Yield: 65%; white solid, mp 139–141 °C; ^{1}H NMR ($CDCl_3$, 400 MHz, δ with TMS = 0): 8.02 (2H, d, J = 8Hz), 7.69-7.63 (2H, m), 7.42 (1H, d, J = 8Hz),7.37 (1H, s), 7.11 - 7.04 (3H, m), 5.25 (2H, s), 4.75 (4H, d, J = 4 Hz), 2.54 (2H, t, J = 4 Hz), ^{13}C NMR ($CDCl_3$, 100 MHz, δ with TMS = 0) δ: 165.66, 163.57, 159.59, 158.02, 139.47, 130.98, 129.90, 128.69, 120.45, 117.15, 115.11, 113.52 103.82, 78.49, 75.81, 56.04, 55.93, **HRMS**: for $C_{22}H_{17}N_3O_2$, calculated $[M+H]^+$: 356.1399; observed $[M+H]^+$: 356.1350.

2-methyl-4-(3-(prop-2-yn-1-yloxy)phenyl)-6-(4-(prop-2-yn-1-yloxy)phenyl)pyrimidine (AVB5): Yield: 63%; white solid, mp 116–118 °C; ^{1}H NMR ($CDCl_3$, 400 MHz, δ with TMS = 0) 8.15 (2H, d, J = 8Hz), 7.83 (1H, s), 7.78 (2H, d, J = 8Hz), 7.47 (1H, t, J = 8Hz), 7.15 (3H, m), 4.83 (4H, d, J = 4Hz), 2.86(3H, s), 2.58 (2H, t, J = 4Hz), ^{13}C NMR (CDCl3, 100 MHz, δ with TMS = 0): 164.27, 158.10, 139.22, 129.98, 128.75, 120.49, 117.14, 115.24, 113.73, 109.44, 78.37, 78.19, 75.92, 75.72, 56.04, 55.88, 26.48, **HRMS**: for $C_{23}H_{18}N_2O_2$, calculated $[M+H]^+$: 355.1447; observed $[M+H]^+$: 355.1390.

2-phenyl-4-(3-(prop-2-yn-1-yloxy)phenyl)-6-(4-(prop-2-yn-1-yloxy)phenyl)pyrimidine (AVB6): Yield: 60%; white solid, mp 147–148 °C; ^{1}H NMR ($CDCl_3$, 400 MHz, δ with TMS = 0): 8.72-8.70 (2H, m), 8.2 (2H, d, J = 8 Hz), 7.97-7.85 (3H, m), 7.54-7.48 (4H, m), 7.15 (3H, d, J = 8Hz), 4.83 (4H, d, J = 2.4 Hz), 2.59 (2H, m); ^{13}C NMR ($CDCl_3$, 100 MHz, δ with TMS = 0) δ: 164.38, 164.18, 164.11, 159.84, 158.18, 139.28, 138.20, 130.82, 130.72, 130.02, 128.87, 128.52, 120.50, 117.18, 115.24, 113.96, 109.70, 78.50, 76.06, 56.13, 55.95, **HRMS**: for $C_{28}H_{20}N_2O_2$, calculated $[M+H]^+$: 417.1603; observed $[M+H]^+$: 417.1553.

4-(2-(prop-2-yn-1-yloxy)phenyl)-6-(4-(prop-2-yn-1-yloxy) phenyl)pyrimidin-2-amine (AVB7): Yield: 64%; green solid, mp 134–136 °C; ^{1}H NMR ($CDCl_3$, 400 MHz, δ with TMS = 0) 8.07 (2H, d, J = 8Hz), 7.90 (1H, d, J = 8Hz), 7.66 (1H, s), 7.45 (1H, t, J = 8Hz), 7.18 (2H, d, J = 8Hz), 7.09 (2H, d, J = 8Hz), 5.15 (2H, bs), 4.79 (4H, t, J = 4Hz), 2.57 (2H, t, J = 4Hz), ^{13}C NMR ($CDCl_3$, 100 MHz, δ with TMS = 0): 164.54, 164.29, 163.34, 159.39, 155.67, 131.21, 130.87, 128.72, 128.21, 122.15, 114.95, 113.54, 108.57, 78.46, 78.23, 76.70, 75.83, 56.66, 55.85, 29.70, **HRMS**: for $C_{22}H_{17}N_3O_2$, calculated $[M+H]^+$: 356.1399; observed $[M+H]^+$: 356.1372.

2-methyl-4-(2-(prop-2-yn-1-yloxy)phenyl)-6-(4-(prop-2-yn-1-yloxy)phenyl)pyrimidine (AVB8): Yield: 58%; green solid, mp 132–134 °C; ^{1}H NMR ($CDCl_3$, 400 MHz, δ with TMS = 0) 8.13 (3H, t, J = 8Hz), 7.99 (1H, d, J = 8Hz), 7.47 (1H, t, J = 8Hz),7.17 (4H, m), 4.80 (4H, d, J = 4Hz), 2.86 (3H, s), 2.58 (2H, t, J = 4Hz), ^{13}C NMR (CDCl3, 100 MHz, δ with TMS = 0): 168.04, 163.14, 162.88, 159.49, 155.73, 131.22, 131.12, 131.08, 130.77, 128.85, 127.88, 122.30, 115.12, 114.64, 114.25, 113.34, 78.37, 78.19, 75.91, 75.86, 56.62, 55.86, 26.53, **HRMS**: for $C_{23}H_{18}N_2O_2$, calculated $[M+H]^+$: 355.1447; observed $[M+H]^+$: 355.1405.

2-phenyl-4-(2-(prop-2-yn-1-yloxy)phenyl)-6-(4-(prop-2-yn-1-yloxy)phenyl)pyrimidine (AVB9): Yield: 65%; cream solid, mp 89–91 °C; ^{1}H NMR ($CDCl_3$, 400 MHz, δ with TMS = 0): 8.67 (2H, dd, J_{13} = 8 Hz; J_{12} = 4 Hz), 8.29-8.25 (4H, m), 7.52 - 7.46 (4H, m), 7.24 - 7.19 (1H, m), 7.15-7.11 (3H, m); 4.77 (4H, d, J = 4 Hz), 2.54 (2H, t, J = 4Hz), ^{13}C NMR ($CDCl_3$, 100 MHz, δ with TMS = 0) δ: 164.18,

163.16, 162.83, 159.66, 156.18, 138.51, 131.61, 131.22, 130.47, 128.98, 128.48, 127.86 122.34, 115.14, 114.86, 113.49, 78.48, 76.82, 56.73, 55.94, **HRMS**: for $C_{28}H_{20}N_2O_2$, calculated $[M+H]^+$: 417.1603; observed $[M+H]^+$: 417.1555.

4,6-bis(3-(prop-2-yn-1-yloxy)phenyl)pyrimidin-2-amine (AVB10): Yield: 57%; yellowish brown, mp 146–148 °C; ^{1}H NMR ($CDCl_3$, 400 MHz, δ with TMS = 0): 7.72 (2H, s), 7.69 (2H, d, J = 8Hz), 7.45 (3H, t, J = 8Hz), 7.14 (2H, d, J = 8Hz), 5.21 (2H, bs), 4.81 (4H, d, J = 4 Hz), 2.58 (2H, bs), ^{13}C NMR ($CDCl_3$, 100 MHz, δ with TMS = 0) δ: 165.84, 163.50, 157.98, 139.23, 129.86, 120.39, 117.22, 113.46, 104.53, 78.40, 75.74, 55.99, 29.86, **HRMS**: for $C_{22}H_{17}N_3O_2$, calculated $[M+H]^+$: 356.1399; observed $[M+H]^+$: 356.1358.

2-phenyl-4,6-bis(3-(prop-2-yn-1-yloxy)phenyl)pyrimidine (AVB11): Yield: 59%; greenish yellow solid, mp 118–120 °C; ^{1}H NMR ($CDCl_3$, 400 MHz, δ with TMS = 0) 8.75 (2H, d, J = 8Hz), 8.45 (1H, s) 8.01 (2H, d, J = 8Hz), 7.59 (1H, s), 7.57 (2H, d, J = 8Hz), 7.50–7.59 (4H, m), 7.20 (2H, d, J = 8Hz), 4.86 (4H, d, J = 4Hz), 2.62 (2H, t, J = 4Hz), ^{13}C NMR (CDCl3, 100 MHz, δ with TMS = 0): 164.43, 164.35, 158.15, 139.05, 137.98, 130.74, 129.98, 128.48, 120.48, 117.28, 113.94, 110.51, 78.40, 75.86, 56.08, 29.71, **HRMS**: for $C_{28}H_{20}N_2O_2$, calculated $[M+H]^+$: 417.1603; observed $[M+H]^+$: 417.1602.

4,6-bis(2-(prop-2-yn-1-yloxy)phenyl)pyrimidin-2-amine (AVB12): Yield: 64%; semi-solid; ^{1}H NMR ($CDCl_3$, 400 MHz, δ with TMS = 0) 7.83 (2H, d, J = 8Hz), 7.68 (1H, s), 7.44 (2H, t, J = 8Hz), 7.13–7.19 (4H, m), 5.47 (2H, bs), 4.80 (4H, d, J = 4Hz), 2.53 (2H, bs), ^{13}C NMR (CDCl3, 100 MHz, δ with TMS = 0): 163.79, 163.19, 155.55, 131.04, 130.80, 128.25, 122.00, 113.73, 113.56, 78.58, 75.86, 56.47, 29.72, **HRMS**: for $C_{22}H_{17}N_3O_2$, calculated $[M+H]^+$: 356.1399; observed $[M+H]^+$: 356.1368.

2-phenyl-4,6-bis(2-(prop-2-yn-1-yloxy)phenyl)pyrimidine (AVB13): Yield: 68%; semi-solid; ^{1}H NMR ($CDCl_3$, 400 MHz, δ with TMS = 0) 8.69 (2H, d, J = 8Hz), 8.49 (1H, s), 8.24 (2H, d, J = 8Hz), 7.49–7.54 (5H, m), 7.22–7.27 (4H, m), 4.87 (4H, d, J = 4Hz), 2.55 (2H, bs), ^{13}C NMR (CDCl3, 100 MHz, δ with TMS = 0): 164.08, 162.32, 156.01, 138.53, 131.70, 131.10, 130.27, 128.38, 128.29, 128.22, 122.15, 120.46, 113.56, 78.57, 75.95, 56.48, 29.74, **HRMS**: for $C_{28}H_{20}N_2O_2$, calculated $[M+H]^+$: 417.1603; observed $[M+H]^+$: 417.1552.

4-(3-methoxy-4-(prop-2-yn-1-yloxy)phenyl)-6-(4-(prop-2-yn-1-yloxy)phenyl)pyrimidin-2-amine (AVB14): Yield: 60%; light brown solid, mp 118–120 °C; ^{1}H NMR ($CDCl_3$, 400 MHz, δ with TMS = 0): 8.04 (2H, d, J = 8Hz), 7.69 (1H, d, J = 8Hz), 7.60-7.58 (1H, m), 7.35 (1H, s), 7.12-7.06 (3H, m), 5.29 (2H, S), 4.83 (2H, d, J = 4Hz), 4.76 (2H, d, J = 4Hz), 3.99 (3H, s), 2.55 (2H, t, J = 4Hz), ^{13}C NMR ($CDCl_3$, 100 MHz, δ with TMS = 0) δ: 165.41, 163.47, 159.49, 149.78, 148.82, 131.73, 131.01, 128.63, 119.84, 115.04, 113.65, 110.48, 103.17, 78.19, 76.73, 75.09, 56.68, 56.06, 55.87, **HRMS**: for $C_{23}H_{19}N_3O_3$, calculated $[M+H]^+$: 386.1505; observed $[M+H]^+$: 386.1508.

4-(3-methoxy-4-(prop-2-yn-1-yloxy)phenyl)-2-methyl-6-(4-(prop-2-yn-1-yloxy)phenyl)pyrimidine (AVB15): Yield: 60%; white solid, mp 132–134 °C; ^{1}H NMR ($CDCl_3$, 400 MHz, δ with TMS = 0): 8.10 (2H, d, J = 8H), 7.77 (2H, s), 7.66 (1H, dd, J_{13} = 8Hz, J_{12} = 4Hz), 7.15–7.09 (3H, m), 4.84 (2H, d, J = 4Hz), 4.77 (2H, d, J = 4Hz), 4.01 (3H, s), 2.82 (3H, s), 2.56-2.53 (2H, t, J = 4Hz), ^{13}C NMR ($CDCl_3$, 100 MHz, δ with TMS = 0) δ: 168.34, 164.05, 164.03, 157.60, 149.97, 148.97, 131.62, 130.88, 128.72, 119.93, 115.22, 113.83, 110.56, 108.74, 78.16 78.14, 76.18, 75.92, 56.71, 56.12, 55.80, 26.50, **HRMS**: for $C_{24}H_{20}N_2O_3$, calculated $[M+H]^+$: 385.1552; observed $[M+H]^+$: 386.1555.

4-(3-methoxy-4-(prop-2-yn-1-yloxy)phenyl)-2-phenyl-6-(4-(prop-2-yn-1-yloxy)phenyl)pyrimidine (AVB16): Yield: 70%; greenish white solid, mp 160–162 °C; ^{1}H NMR ($CDCl_3$ and DMSO, 400 MHz, δ with TMS = 0): 8.64 (2H, d, J = 8Hz), 8.45 (2H, d, J = 8 Hz), 8.29 (1H, s), 8.05 - 8.01 (2H, m), 7.58 - 7.52 (3H, m), 7.18 (3H, m), 4.88 (4H, d, J = 4 Hz), 4.00 (3H, s), 3.36 (2H, t, J = 4Hz), ^{13}C NMR ($CDCl_3$ and DMSO, 100 MHz, δ with TMS = 0) δ: 163.39, 163.31, 163.03, 159.47, 149.32, 148.96, 137.74, 130.39, 130.37, 129.81, 128.76, 128.36, 127.86, 120.19, 114.85, 113.59, 110.62, 108.89, 79.88, 78.67, 78.58, 77.84, 56.11, 55.72, 55.55, **HRMS**: for $C_{29}H_{22}N_2O_3$, calculated $[M+H]^+$: 447.1709; observed $[M+H]^+$: 447.1709.

4-(3-ethoxy-4-(prop-2-yn-1-yloxy)phenyl)-6-(4-(prop-2-yn-1-yloxy)phenyl)pyrimidin-2-amine (AVB17): Yield: 65%; pale yellow solid, mp 162–164 °C; ^{1}H NMR ($CDCl_3$, 400 MHz, δ with TMS = 0) 8.05 (2H, d, J = 8Hz), 7.71 (1H, s), 7.62 (1H, d, J = 8Hz), 7.38 (1H, s), 7.16 (1H, d, J = 8Hz), 7.13 (2H, d, J = 8Hz), 5.21 (2H, bs), 4.87 (2H, d, J = 4Hz), 4.80 (2H, d, J = 4Hz), 4.26 (2H, q, J = 8Hz), 2.57 (2H, m), 1.53 (3H, t, J = 4Hz), ^{13}C NMR (CDCl3, 100 MHz, δ with TMS = 0): 165.51, 165.36, 163.42, 159.47, 149.27, 149.12, 131.83, 131.05, 128.60, 119.83, 115.03, 114.42, 112.00, 103.20, 78.43, 78.17, 75.99, 75.66, 64.64, 56.85, 55.87, 30.27, 29.67, 14.86, **HRMS**: for $C_{24}H_{21}N_3O_3$, calculatSed $[M+H]^+$: 400.1661; observed $[M+H]^+$: 400.1665.

4-(3-ethoxy-4-(prop-2-yn-1-yloxy)phenyl)-2-methyl-6-(4-(prop-2-yn-1-yloxy)phenyl)pyrimidine (AVB18): Yield: 60%; greenish yellow solid, mp 108–110 °C; ^{1}H NMR ($CDCl_3$, 400 MHz, δ with TMS = 0) 8.13 (2H, d, J = 8Hz), 7.79 (2H, s), 7.67 (1H, d, J = 4Hz), 7.17 (1H, d, J = 4Hz), 7.13 (2H, d, J = 8Hz), 4.87 (2H, d, J = 4Hz), 4.80 (2H, d, J = 4Hz), 4.28 (2H, q, J = 4Hz), 2.85 (3H, s), 2.57 (2H, m), 1.56 (3H, t, J = 4Hz), ^{13}C NMR (CDCl3, 100 MHz, δ with TMS = 0): 168.33, 164.13, 164.01, 159.59, 149.45, 149.27, 131.68, 130.91, 128.72, 119.94, 115.22, 114.56, 112.09, 108.78, 78.39, 78.14, 76.05, 75.91, 64.71, 56.85, 55.89, 26.50, 14.86, **HRMS**: for $C_{25}H_{22}N_2O_3$, calculated $[M+H]^+$: 399.1709; observed $[M+H]^+$: 399.1709.

4-(3-ethoxy-4-(prop-2-yn-1-yloxy)phenyl)-2-phenyl-6-(4-(prop-2-yn-1-yloxy)phenyl)pyrimidine (AVB19): Yield: 67%; greenish yellow solid, mp 138–140 °C; ^{1}H NMR ($CDCl_3$, 400 MHz, δ with TMS = 0) 8.72 (2H, d, J = 8Hz), 8.30 (2H, d, J = 8Hz), 7.97 (1H, d, J = 4Hz), 7.91 (1H, s), 7.82 (1H, d, J = 8Hz), 7.57 (3H, m), 7.21 (1H, d, J = 8Hz), 7.19 (2H, d, J = 8Hz), 4.90 (2H, d, J = 4Hz), 4.83 (2H, d, J = 4Hz), 4.32 (2H, q, J = 12Hz), 2.65 (2H, dd, J = 4Hz), 1.65 (3H, m) ^{13}C NMR (CDCl3, 100 MHz, δ with TMS = 0): 164.06, 159.72, 149.44, 149.41, 138.29, 131.75, 130.94, 130.54, 128.76, 128.42, 128.39, 120.03, 115.18, 114.52, 112.27, 109.02, 78.40, 78.16, 76.07, 75.93, 64.79, 56.86, 55.90, 14.88, **HRMS**: for $C_{30}H_{24}N_2O_3$, calculated $[M+H]^+$: 461.1865; observed $[M+H]^+$: 461.1866.

4.3. Biological studies

4.3.1. Determination of hMAO inhibition activity

The effects of the test compounds on hMAO-A and hMAO-B enzymes were evaluated by using Amplex® Red assay kit based on detection of fluorescence [32,33].

Briefly, 100 μL of sodium phosphate buffer (0.05 M, pH 7.4) containing the test drugs or reference inhibitors, in various concentrations along with adequate amounts of recombinant hMAO (hMAO-A: 1.1 μg protein; specific activity: 150 nmol of p-tyramine oxidized to p-hydroxyphenylacetaldehyde/min/mg protein; hMAO-B: 7.5 μg protein; specific activity: 22 nmol of p-tyramine transformed/min/mg protein) enzyme, were incubated for 30 min at 37 °C in a flat-black-bottom 96-well plate (Tarsons) in incubator. After this incubation period, the reaction was started by adding (final concentrations) 200 μM Amplex® Red reagent, 1 U/mL horseradish peroxidase and 1 mM p-tyramine. After 30 min incubation in the dark, the production of H_2O_2 was quantified at 37 °C in a multi-detection microplate fluorescence reader (Synergy^{HI}, Bio-Tek® Instruments) based on the fluorescence generated at the excitation wavelength of 545 nm, and emission wavelength of 590 nm. Control experiments were carried out simultaneously by replacing the test drugs with the vehicle. To minimize the possibility of any interference of test drugs to the non-enzymatic fluorescence generated through drug and Amplex® Red reagent

interactions blank reading was taken with drug and Amplex® Red reagent without adding MAO enzyme in a sodium phosphate buffer. No fluorescence could be observed in the absence of MAO enzyme thus eliminating the possibility of any false reading. The specific final fluorescence emission was calculated after subtraction of the background activity, determined from vials containing all components except the hMAO enzyme replaced by a sodium phosphate buffer solution.

4.3.2. Acetylcholinesterase inhibition assay

Acetylcholinesterase inhibition activity was determined using Amplex Red Acetylcholine/Acetylcholinesterase assay kit (A12217) purchased from the Molecular Probes Inc. Invitrogen [15,34]. Briefly, 100 μl of Tris-HCl buffer (0.05 M, pH 8.0) containing the synthesized test drugs and reference inhibitors, in various concentrations along with adequate amounts of recombinant AChE (0.2U/mL) enzyme, were incubated for 15 min at 37 °C in a flat bottom 96-well plates (Tarsons). Reaction was started by adding 100 μl of working solution of 400 μM Amplex Red reagent containing 2 U/mL horseradish peroxidase, 0.2 U/mL choline oxidase and 100 μM acetylcholine. After 30 min incubation in dark, the production of H_2O_2 and subsequent formation of resorufin from Amplex red dye was quantified at 37 °C in a multi-detection microplate fluorescence reader (Synergy^{HI}, Bio-Tek® Instruments) based on the fluorescence generated at excitation wavelength of 545 nm, and emission wavelength of 590 nm. Positive control experiment was carried out simultaneously by replacing the test drugs with the vehicle. Second positive control was carried out by using 20 mM H_2O_2. 1X reaction buffer without acetylcholinesterase was used as negative control. The specific final fluorescence emission was calculated after subtraction of the background activity, determined from wells containing all components except the AChE replaced by a 1X buffer solution. Each experiment was performed in triplicate (n = 3).

4.3.3. Reversibility studies

For reversibility studies, dilution protocol was adopted as reported in the literature [35,36]. Briefly, the test inhibitors were incubated with the MAO enzyme at concentrations of 10 × IC_{50} and 100 × IC_{50} at 37 °C for of 30 min (negative control performed in the absence of inhibitor), and 4% DMSO was added as co-solvent to all incubations. After 30 min incubation period, the samples were subsequently diluted to 100−fold with the addition of tyramine substrate to achieve final inhibitor concentrations of 0.1 × IC_{50} and 1 x IC_{50} value, respectively. As positive control MAO-B was incubated with the irreversible inhibitor pargyline at 10 × IC_{50} concentrations and then diluted 100-fold to achieve final inhibitor concentrations of 0.1 × IC_{50}. The residual MAO-B activity was measured (n = 3) after dilutions and enzyme activities were expressed as mean ± SD.

4.3.4. Kinetic studies

To determine the mechanism of action of the most potent inhibitor of AChE i.e. **AVB4,** kinetic study was performed using *ee*AChE with the help of earlier reported protocols [18,37]. Lineweaver-Burk double reciprocal graph was plotted at different concentrations of substrate ACh (0.1 mM- 1 mM) by using same methodology reported for the *in vitro* inhibition study of AChE. Progress curves were analyzed by steady-state turnover of substrate and values of linear regression were fitted according to Lineweaver-Burk replots using excel software (2016). Three concentrations of **AVB4** (1 μM, 2 μM and 5 μM) were used for the kinetic study. The plots were assessed by weighted least-square analysis that assumed the variance of ν to be constant for whole data set. Slopes of the reciprocal of ν were then plotted against the reciprocal of the substrate concentration.

4.3.5. Cell culture and treatment

The human neuroblastoma (SH-SY5Y) cells were obtained from National Centre for Cell Science (Pune, India). The cells were routinely grown in DMEM supplemented with 10% FBS (Biological Industries) and 1XxPSN mix (Invitrogen) at 37 °C in a humidified atmosphere containing 5% CO_2. Cells were subcultured by trypsinization and seeded in 96 and 24 well plates according to the requirement of the experiments.

4.3.6. ROS inhibition studies

Intracellular levels of ROS were determined by using the protocol described elsewhere [15], using non-fluorescent compound 2,7-dichlorofluorescein diacetate (DCF-DA) that is permeable to the cell membrane where it is hydrolyzed by intracellular esterases and oxidized by ROS to a fluorescent compound 2,7-DCF. The human neuroblastoma (SH-SY5Y) cells (approximately 10,000 cells/well) were seeded of 96 well plate in DMEM/F-12 media containing 10% FBS and horse serum supplemented 1% penicillin antibiotic solution for 24h in a humidified atmosphere containing 5% CO_2. The media was removed, washed with PBS and cells were treated with test compounds (without FBS) for 24 h at different concentrations (1 μM, 5 μM and 25 μM). Thereafter, cells were rinsed with PBS three times and treated with H_2DCF-DA (50 μM) and incubated for 30 min at 37 °C. Following incubation, cells were rinsed with PBS and fluorescence was detected at a wavelength of 478 nm excitation and 518 nm emission.

4.3.7. Neuroprotective studies

The neuroprotective potential of compounds was determined against 6-OHDA neurotoxin using MTT assay [38]. For this SH-SY5Y cells were plated in 96 wells, at 10^4 cells/well density. The cells were cultured for 24h in DMEM/F-12 media containing 10% FBS and horse serum supplemented 1% penicillin antibiotic solution. Then cells were treated with the target compounds (at concentrations of 1−25 μM), 4h before 6-OHDA (10 μM). After 24 h incubation in the oven, at 37 °C and a 5% CO_2, 95% O_2 atmosphere, the tested compounds were replaced with 100 μL of MTT in media (5 mg/mL, final concentration). The cells were incubated for another 3h. After the removal of MTT, the formazan crystals were dissolved in DMSO. The amount of formazan was measured using a microculture plate reader with a test wavelength of 594 nm. Results were expressed as the mean ± SD of three independent experiments.

4.3.8. Cytotoxicity studies

With an aim to test the cytotoxicity of the synthesized compounds, studies were carried out with human neuroblastoma SH-SY5Y cells, using the 3-(4, 5-dimethylthiazol-2-yl)-2, 5-diphenyltetrazolium bromide (MTT) test [38]. This method is based on the formation of blue formazan product by the cellular oxidoreductase. The amount of formazan produced is considered as a reliable representation of viable cell number. Approximately 10,000 cells were seeded per well of 96 well plate in DMEM/F-12 media containing 10% FBS and horse serum supplemented 1% penicillin antibiotic solution for 24h and treated as indicated in the experimental design. Cells were treated with synthesized compounds at concentration of 1 μM, 5 μM and 25 μM for 24h in humidified CO_2 incubator, maintained at 37 °C with 5% CO_2 and 95% humidity under serum-free conditions. After 4 h incubation at 37 °C, this solution was removed, and the resulting blue formazan was solubilized in 100 ml of DMSO and the optical density was recorded at 595 nm using microplate reader.

4.4. Computational studies

4.4.1. Molecular docking studies

To determine the mode of interaction between synthesized ligands and the active site of hMAO-A and hMAO-B enzymes, molecular docking studies were performed using Glide [39] module of Maestro 11.1 (Schrödinger LLC). X-ray crystal structures of hMAO-B (PDB ID- 2BYB) [30] and AChE (PDB ID- 1EVE) [31] enzymes were imported from the protein data bank (www.rscb.org). Protein was prepared using "protein preparation wizard" application of Schrödinger suite 2017. The energy was minimized using an OPLS2005 force field. The grid was generated (20 Å) around the co-crystallized ligand using receptor grid generation module of Maestro 11.1. Ligands were drawn in ChemBio Draw Ultra-12 (2D SDF) and prepared (3D Maestro input files) using ligand preparation application in Schrödinger suite 2017. In this module, hydrogens were attached, possible ionization states were generated at pH 7.4, possible tautomer for each structure were generated and lowest energy conformation for each possible structural conformation was generated using OPLS2005 force field. For each compound, the top-score docking poses were chosen for final ligand-target interaction analysis employing XP interaction visualizer of Maestro 11.1 software. Validation of docking procedure was first evaluated by re-docking of the co-crystalized ligand into the active site of MAO enzyme. Qikprop [40] application of Schrodinger suit was used to determine the drug like and ADME properties of the compounds.

4.4.2. Molecular dynamics simulation studies

In order to investigate the behavior and stability of the potent inhibitors into the active site of the MAO and AChE, molecular dynamic (MD) simulation was utilized. For this docking complexes of **AVB1** and **AVB4** with MAO-B and AChE were used. MD simulations were performed using Desmond standard protocol [41]. Complex was solvated by TIP3P water model and then naturalized by adding 0.15M Na^+ and Cl^- ions. The thickness of water layer was set to 10 Å. Before the MD simulations the systems were minimized with a maximum iteration of 2000 steps. Then, the systems were submitted to 30 ns MD simulation for equilibration and production MD run. Temperature and pressure were assigned on 300 K and 1.01325 bar, respectively using Isothermal–isobaric (NPT) ensemble. Cut-off radios of 9 Å was used for Coulomb interactions.

Acknowledgement

V.K. is thankful to the DST-SERB (EMR/2015/002339) and Central University of Punjab, Bathinda, (RSM GP25) for providing the financial assistance. B.K. is thankful to CUP, Bathinda and CSIR for the Senior Research Fellowship. Vijay Kumar is thankful to UGC for NET-JRF. J.P. is thankful to DST-SERB for the Research Grant (ECR/2015/000240).

Appendix A. Supplementary data

Supplementary data to this article can be found online at https://doi.org/10.1016/j.ejmech.2019.05.039.

Conflicts of interest

A provisional patent application has been filed containing these compounds (Indian patent application number 201811008301).

References

[1] M. Goedert, M.G. Spillantini, A century of Alzheimer's disease, Science 314 (2006) 777–781.
[2] J.T. Coyle, P. Puttfarcken, Oxidative stress, glutamate, and neurodegenerative disorders, Science 262 (1993) 689–695.
[3] J. Rodda, J. Carter, Cholinesterase inhibitors and memantine for symptomatic treatment of dementia, BMJ 344 (2012), e2986.
[4] G. Reid, N. Chilukuri, S. Darvesh, Butyrylcholinesterase and the cholinergic system, Neuroscience 234 (2013) 53–68.
[5] A.V. Terry Jr., J.J. Buccafusco, C. Wilson, Cognitive dysfunction in neuropsychiatric disorders: selected serotonin receptor subtypes as therapeutic targets, Behav. Brain Res. 195 (2008) 30–38.
[6] Z. Cai, Monoamine oxidase inhibitors: promising therapeutic agents for Alzheimer's disease, Mol. Med. Rep. 9 (2014) 1533–1541.
[7] M. Bortolato, K. Chen, J.C. Shih, Monoamine oxidase inactivation: from pathophysiology to therapeutics, Adv. Drug Deliv. Rev. 60 (2008) 1527–1533.
[8] R.W. Fuller, Selectivity among monoamine oxidase inhibitors and its possible importance for development of antidepressant drugs, Prog. Neuro Psychopharmacol. 2 (1978) 303–311.
[9] P. Riederer, M.B. Youdim, Monoamine oxidase activity and monoamine metabolism in brains of parkinsonian patients treated with l-deprenyl, J. Neurochem. 46 (1986) 1359–1365.
[10] B. Kumar, A.K. Mantha, V. Kumar, Recent developments on the structure–activity relationship studies of MAO inhibitors and their role in different neurological disorders, RSC Adv. 6 (2016) 42660–42683.
[11] M. Naoi, W. Maruyama, Functional mechanism of neuroprotection by inhibitors of type B monoamine oxidase in Parkinson's disease, Expert Rev. Neurother. 9 (2009) 1233–1250.
[12] O. Bar-Am, T. Amit, M.B. Youdim, Aminoindan and hydroxyaminoindan, metabolites of rasagiline and ladostigil, respectively, exert neuroprotective properties in vitro, J. Neurochem. 103 (2007) 500–508.
[13] D.J. Selkoe, Alzheimer's disease: genes, proteins, and therapy, Physiol. Rev. 81 (2001) 741–766.
[14] J. Hardy, D.J. Selkoe, The amyloid hypothesis of Alzheimer's disease: progress and problems on the road to therapeutics, Science 297 (2002) 353–356.
[15] B. Kumar, A.R. Dwivedi, B. Sarkar, S.K. Gupta, S. Krishnamurthy, A.K. Mantha, J. Parkash, V. Kumar, 4, 6-diphenylpyrimidine derivatives as dual inhibitors of monoamine oxidase and acetylcholinesterase for the treatment of Alzheimer's disease, ACS Chem. Neurosci. 10 (2019) 252–265.
[16] B. Kumar, V. Prakash Gupta, V. Kumar, A perspective on monoamine oxidase enzyme as drug target: challenges and opportunities, Curr. Drug Targets 18 (2017) 87–97.
[17] A. Samadi, M. Chioua, I. Bolea, C. de los Ríos, I. Iriepa, I. Moraleda, A. Bastida, G. Esteban, M. Unzeta, E. Gálvez, Synthesis, biological assessment and molecular modeling of new multipotent MAO and cholinesterase inhibitors as potential drugs for the treatment of Alzheimer's disease, Eur. J. Med. Chem. 46 (2011) 4665–4668.
[18] I. Bolea, J. Juarez-Jiménez, C.b. de los Rıos, M. Chioua, R.n. Pouplana, F.J. Luque, M. Unzeta, J. Marco-Contelles, A. Samadi, Synthesis, biological evaluation, and molecular modeling of donepezil and N-[(5-(benzyloxy)-1-methyl-1 H-indol-2-yl) methyl]-N-methylprop-2-yn-1-amine hybrids as new multipotent cholinesterase/monoamine oxidase inhibitors for the treatment of Alzheimer's disease, J. Med. Chem. 54 (2011) 8251–8270.
[19] A. Samadi, C. de los Ríos, I. Bolea, M. Chioua, I. Iriepa, I. Moraleda, M. Bartolini, V. Andrisano, E. Gálvez, C. Valderas, Multipotent MAO and cholinesterase inhibitors for the treatment of Alzheimer's disease: synthesis, pharmacological analysis and molecular modeling of heterocyclic substituted alkyl and cycloalkyl propargyl amine, Eur. J. Med. Chem. 52 (2012) 251–262.
[20] O.M. Bautista-Aguilera, G. Esteban, I. Bolea, K. Nikolic, D. Agbaba, I. Moraleda, I. Iriepa, A. Samadi, E. Soriano, M. Unzeta, Design, synthesis, pharmacological evaluation, QSAR analysis, molecular modeling and ADMET of novel donepezil–indolyl hybrids as multipotent cholinesterase/monoamine oxidase inhibitors for the potential treatment of Alzheimer's disease, Eur. J. Med. Chem. 75 (2014) 82–95.
[21] O.M. Bautista-Aguilera, A. Samadi, M. Chioua, K. Nikolic, S. Filipic, D. Agbaba, E. Soriano, L. de Andres, M.I. Rodríguez-Franco, S. Alcaro, N-Methyl-N-((1-methyl-5-(3-(1-(2-methylbenzyl) piperidin-4-yl) propoxy)-1 H-indol-2-yl) methyl) prop-2-yn-1-amine, a new cholinesterase and monoamine oxidase dual inhibitor, J. Med. Chem. 57 (2014) 10455–10463.
[22] H. Zheng, M.B. Youdim, M. Fridkin, Site-activated chelators targeting acetylcholinesterase and monoamine oxidase for Alzheimer's therapy, ACS Chem. Biol. 5 (2010) 603–610.
[23] M.-Y. Wu, G. Esteban, S. Brogi, M. Shionoya, L. Wang, G. Campiani, M. Unzeta, T. Inokuchi, S. Butini, J. Marco-Contelles, Donepezil-like multifunctional agents: design, synthesis, molecular modeling and biological evaluation, Eur. J. Med. Chem. 121 (2016) 864–879.
[24] L. Wang, G. Esteban, M. Ojima, O.M. Bautista-Aguilera, T. Inokuchi, I. Moraleda, I. Iriepa, A. Samadi, M.B. Youdim, A. Romero, Donepezil+ propargylamine+ 8-hydroxyquinoline hybrids as new multifunctional metal-chelators, ChE and MAO inhibitors for the potential treatment of Alzheimer's disease, Eur. J. Med. Chem. 80 (2014) 543–561.
[25] F.T. Zindo, J. Joubert, S.F. Malan, Propargylamine as functional moiety in the design of multifunctional drugs for neurodegenerative disorders: MAO inhibition and beyond, Future Med. Chem. 7 (2015) 609–629.
[26] I. Bolea, A. Gella, M. Unzeta, Propargylamine-derived multitarget-directed ligands: fighting Alzheimer's disease with monoamine oxidase inhibitors, J. Neural Transm. 120 (2013) 893–902.

[27] O. Weinreb, T. Amit, O. Bar-Am, M.B. Youdim, Rasagiline: a novel anti-Parkinsonian monoamine oxidase-B inhibitor with neuroprotective activity, Prog. Neurobiol. 92 (2010) 330–344.
[28] M.B. Youdim, O. Bar Am, M. Yogev-Falach, O. Weinreb, W. Maruyama, M. Naoi, T. Amit, Rasagiline: neurodegeneration, neuroprotection, and mitochondrial permeability transition, J. Neurosci. Res. 79 (2005) 172–179.
[29] W. Maruyama, Y. Akao, M.C. Carrillo, K.-i. Kitani, M.B. Youdium, M. Naoi, Neuroprotection by propargylamines in Parkinson's disease: suppression of apoptosis and induction of prosurvival genes, Neurotoxicol. Teratol. 24 (2002) 675–682.
[30] L. De Colibus, M. Li, C. Binda, A. Lustig, D.E. Edmondson, A. Mattevi, Three-dimensional structure of human monoamine oxidase A (MAO A): relation to the structures of rat MAO A and human MAO B, Proc. Natl. Acad. Sci. U.S.A. 102 (2005) 12684–12689.
[31] J. Cheung, M.J. Rudolph, F. Burshteyn, M.S. Cassidy, E.N. Gary, J. Love, M.C. Franklin, J.J. Height, Structures of human acetylcholinesterase in complex with pharmacologically important ligands, J. Med. Chem. 55 (2012) 10282–10286.
[32] F. Chimenti, S. Carradori, D. Secci, A. Bolasco, B. Bizzarri, P. Chimenti, A. Granese, M. Yanez, F. Orallo, Synthesis and inhibitory activity against human monoamine oxidase of N1-thiocarbamoyl-3, 5-di (hetero) aryl-4, 5-dihydro-(1H)-pyrazole derivatives, Eur. J. Med. Chem. 45 (2010) 800–804.
[33] B. Kumar, Sheetal, A.K. Mantha, V. Kumar, Synthesis, biological evaluation and molecular modeling studies of phenyl-/benzhydrylpiperazine derivatives as potential MAO inhibitors, Bioorg. Chem. 77 (2018) 252–262.
[34] A. Kalb, C. von Haefen, M. Sifringer, A. Tegethoff, N. Paeschke, M. Kostova, A. Feldheiser, C.D. Spies, Acetylcholinesterase inhibitors reduce neuro-inflammation and-degeneration in the cortex and hippocampus of a surgery stress rat model, PLoS One 8 (2013), e62679.
[35] S. Mostert, W. Mentz, A. Petzer, J.J. Bergh, J.P. Petzer, Inhibition of monoamine oxidase by 8-[(phenylethyl) sulfanyl] caffeine analogues, Bioorg. Med. Chem. 20 (2012) 7040–7050.
[36] C. Minders, J.P. Petzer, A. Petzer, A.C. Lourens, Monoamine oxidase inhibitory activities of heterocyclic chalcones, Bioorg. Med. Chem. Lett 25 (2015) 5270–5276.
[37] J. Yan, J. Hu, A. Liu, L. He, X. Li, H. Wei, Design, synthesis, and evaluation of multitarget-directed ligands against Alzheimer's disease based on the fusion of donepezil and curcumin, Bioorg. Med. Chem. 25 (2017) 2946–2955.
[38] B. Kumar, P. Sharma, V.P. Gupta, M. Khullar, S. Singh, N. Dogra, V. Kumar, Synthesis and biological evaluation of pyrimidine bridged combretastatin derivatives as potential anticancer agents and mechanistic studies, Bioorg. Chem. 78 (2018) 130–140.
[39] R.A. Friesner, J.L. Banks, R.B. Murphy, T.A. Halgren, J.J. Klicic, D.T. Mainz, M.P. Repasky, E.H. Knoll, M. Shelley, J.K. Perry, Glide: a new approach for rapid, accurate docking and scoring. 1. Method and assessment of docking accuracy, J. Med. Chem. 47 (2004) 1739–1749.
[40] L. Schrödinger, QikProp, Version 3.5, New York, NY, 2012.
[41] S. Release, 1: Desmond Molecular Dynamics System, Version 3.7, DE Shaw Research, New York, NY, Maestro-Desmond Interoperability Tools, Version 3, 2014.

RSC Advances

REVIEW

Cite this: *RSC Adv.*, 2016, **6**, 42660

Recent developments on the structure–activity relationship studies of MAO inhibitors and their role in different neurological disorders

Bhupinder Kumar,[a] Sheetal,[a] Anil K. Mantha[bc] and Vinod Kumar*[a]

Monoamine oxidase (MAO) enzyme catalyzes the oxidative deamination of xenobiotic and endogenous amines including many neurotransmitters. The MAO enzyme exists in two isoforms; MAO-A and MAO-B and these isoforms display considerable sequence similarity but differ in tissue distribution, inhibitor selectivity and specificity towards ligands. The altered concentration of the neurotransmitters in the brain is linked with the biochemical pathology of various neurological disorders including depression, Alzheimer's disease and Parkinson's disease. MAO inhibitors were the first antidepressants discovered but their irreversible binding to the enzyme resulted in a number of side effects including fatal food–drug interactions. The new generation MAO inhibitors, especially reversible and selective inhibitors, were less toxic and found to be effective against various neurological disorders. Now the MAO enzyme has been recognised as an important drug target and MAO-A selective inhibitors are being developed as drug candidates for the management of depression and anxiety disorders, whereas MAO-B selective inhibitors are found to be effective for the treatment of Parkinson's disease and Alzheimer's disease with a better safety profile as compared to nonselective MAO inhibitors. The current review article describes recent developments on the design, synthesis and screening of MAO inhibitors, structure–activity relationship studies, and their role in the etiology and treatment of various neurological disorders.

Received 5th January 2016
Accepted 19th April 2016

DOI: 10.1039/c6ra00302h

www.rsc.org/advances

1. Introduction

Monoamine oxidases (MAO) belong to a family of flavin adenine dinucleotide (FAD) dependent enzymes present on the outer membrane of the mitochondria.[1] MAOs are responsible for the oxidative deamination of various xenobiotic and endogenous neurotransmitters and modulate their concentration in the

[a]*Laboratory of Organic and Medicinal Chemistry, Centre for Pharmaceutical Sciences and Natural Products, Central University of Punjab, Bathinda, Punjab, India-151001. E-mail: vpathania18@gmail.com; vinod.kumar@cup.ac.in; Tel: +911642864214*

[b]*Centre for Animal Sciences, School of Basic and Applied Sciences, Central University of Punjab, Bathinda, Punjab, India*

[c]*Department of Biochemistry and Molecular Biology, University of Texas Medical Branch, Galveston, TX-77555, USA*

Bhupinder Kumar is currently working as Ph.D research scholar at Centre for Pharmaceutical Sciences and Natural Products under the supervision of Dr Vinod Kumar. He received Master's degree in Pharmacy (Medicinal Chemistry) from Central University of Punjab, Bathinda, Punjab (India) in 2015. Mr Bhupinder was awarded with GPAT Fellowship from All India Council of Technical Education, New Delhi (India). He is currently working on the synthesis and biological evaluation of novel MAO inhibitors as antidepressants and anti-Parkinson's agents.

Sheetal is currently working as Technical Supervisor in Quality Assurance at Cadila Pharmaceuticals Ltd., Samba, Jammu and Kashmir. In 2015, she received Master's degree in Pharmacy (Medicinal Chemistry) from Central University of Punjab, Bathinda, Punjab (India). She was awarded GPAT Fellowship from All India Council of Technical Education, New Delhi (India). She completed her thesis on topic entitled "Synthesis of Some Piperazine Containing Scaffolds as Potential MAO Inhibitors" under the supervision of Dr Vinod Kumar.

ChemPubSoc Europe

DOI: 10.1002/cmdc.201700589

CHEMMEDCHEM Full Papers

Synthesis, Biological Evaluation and Molecular Modeling Studies of Propargyl-Containing 2,4,6-Trisubstituted Pyrimidine Derivatives as Potential Anti-Parkinson Agents

Bhupinder Kumar, Mohit Kumar, Ashish Ranjan Dwivedi, and Vinod Kumar*[a]

Monoamine oxidase B (MAO-B) inhibitors are potential drug candidates for the treatment of various neurological disorders including Parkinson's disease. A total of 20 new propargyl-containing 2,4,6-trisubstituted pyrimidine derivatives were synthesized and screened for MAO inhibition using Amplex Red assays. All the synthesized compounds were found to be reversible and selective inhibitors of the MAO-B isoform at sub-micromolar concentrations. **MVB3** was the most potent MAO-B inhibitor with an IC_{50} value of 0.38 ± 0.02 μM, whereas **MVB6** ($IC_{50} = 0.51 \pm 0.04$ μM) and **MVB16** ($IC_{50} = 0.48 \pm 0.06$ μM) were the most selective for MAO-B with a selectivity index of more than 100-fold. In cytotoxic studies, these compounds were found to be nontoxic to human neuroblastoma SH-SY5Y cells at concentrations of 25 μM. **MVB6** was found to decrease the intracellular level of reactive oxygen species to 68% at 10 μM concentration, whereas other compounds did not produce significant changes in reactive oxygen species levels. In molecular modeling studies, **MVB3** displayed strong binding affinity for the MAO-B isoform with a dock score of −10.45, in agreement with the observed activity. All the compounds fitted well in the hydrophobic cavity of MAO-B. Thus, propargyl-substituted pyrimidine derivatives can be promising leads in the development of potent, selective and reversible MAO-B inhibitors for the treatment of Parkinson's disease.

Introduction

Parkinson's disease (PD) is a progressive neurological disorder characterized by a myriad of symptoms that gradually affects the patient's daily activities and gradually decreases their quality of life.[1] The pathology of PD is linked with the affected basal ganglia region where the monoamine oxidase B (MAO-B) isoform seems to be mainly responsible for the metabolism of dopamine. MAO-B-mediated metabolism in the glial neurons increases the concentration of the catalytic reaction product H_2O_2 in the brain.[2] This build up promotes apoptotic signaling events in neuronal cells, resulting in decreased levels of dopamine-producing cells.[3] Strategies for the treatment of PD involve increasing the concentration of dopamine in the brain either by the release of dopamine from presynaptic neurons, or by inhibiting its metabolism and reuptake from the synaptic cleft.[4] Inhibitors of the MAO-B isoform have been proposed as potential therapeutic agents for the management or treatment of PD. Selective MAO-B inhibitors (e.g., L-deprenyl, rasagiline) are used alone or in combination with levodopa,[5] a metabolic precursor of dopamine,to maintain dopamine levels for the treatment of PD. However, due to their irreversible mechanism of inhibition, these MAO-B inhibitors are associated with number of side effects that limit their use.[6] However, recent reports on the potential of reversible MAO-B inhibitors in the treatment of PD and their neuroprotective and neurorescue[7] potential is a strong driving force for the discovery of novel potent, selective and reversible MAO-B inhibitors.[8]

Pyrimidine is an important six-membered heterocyclic structure, present in many bioactive compounds.[9] This scaffold was found to be a remarkable building block and around it a variety of novel heterocycles with excellent pharmaceutical profile can be designed.[10] Mathew et al. synthesized a series of novel MAO-A inhibitors based on 1*H*-benzimidazole-bearing pyrimidine-triones (Figure 1a) and screened in vitro for antidepressant activity.[11] Altomare et al. reported condensed pyrimidine derivatives (Figure 1b,c) for their MAO-B inhibitory activity and found potent MAO-B inhibitors with little or no affinity for the MAO-A isoform.[12] The same research group also reported on the synthesis of new pyridazine-, pyrimidine- and 1,2,4-triazine-containing tricyclic derivatives (Figure 1d,e) as potential MAO-B inhibitors.[13] Rasagiline [*N*-propargyl-1(*R*)-aminoindan], is a potent second-generation irreversible MAO-B inhibitor and it has been found that the propargyl group in the molecule

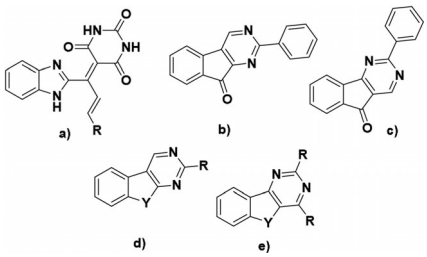

Figure 1. Examples of pyrimidine derivatives that are MAO inhibitors.

[a] *B. Kumar, M. Kumar, A. R. Dwivedi, Dr. V. Kumar*
Department of Pharmaceutical Sciences and Natural Products, Central University of Punjab, Mansa Road, Bathinda, Punjab 151001 (India)
E-mail: vinod.kumar@cup.edu.in

Supporting information and the ORCID identification number(s) for the author(s) of this article can be found under: https://doi.org/10.1002/cmdc.201700589.

Bioorganic Chemistry 77 (2018) 252–262

Contents lists available at ScienceDirect

Bioorganic Chemistry

journal homepage: www.elsevier.com/locate/bioorg

Synthesis, biological evaluation and molecular modeling studies of phenyl-/benzhydrylpiperazine derivatives as potential MAO inhibitors

Bhupinder Kumar [a], Sheetal [a], Anil K. Mantha [b], Vinod Kumar [a,*]

[a] Laboratory of Organic and Medicinal Chemistry, Department of Pharmaceutical Sciences and Natural Products, Central University of Punjab, Bathinda, Punjab 151001, India
[b] Department of Animal Sciences, School of Basic and Applied Sciences, Central University of Punjab, Bathinda, Punjab, India

ARTICLE INFO

Article history:
Received 12 October 2017
Revised 7 January 2018
Accepted 12 January 2018
Available online 16 January 2018

Keywords:
MAO inhibitor
Phenylpiperazine
1-Benzhydrylpiperazine
Cytotoxicity
Neurological disorders

ABSTRACT

Monoamine oxidase inhibitors (MAOIs) are potential drug candidates for the treatment of various neurological disorders like Parkinson's disease, Alzheimer's disease and depression. In the present study, two series of 4-substituted phenylpiperazine and 1-benzhydrylpiperazine (**1**–**21**) derivatives were synthesized and screened for their MAO-A and MAO-B inhibitory activity using Amplex Red assay. Most of the synthesized compounds were found selective for MAO-B isoform except compounds **3**, **7**, **8**, **9** and **13** (MAO-A selective) while compound **11** was non-selective. In the current series, compound **12** showed most potent MAO-B inhibitor activity with IC_{50} value of 80 nM and compound **7** was found to be most potent MAO-A inhibitor with IC_{50} value of 120 nM and both the compounds were found reversible inhibitors. Compound **8** was found most selective MAO-A inhibitor while compound **20** was found most selective inhibitor for MAO-B isoform. In the cytotoxicity evaluation, all the compounds were found non-toxic to SH-SY5Y and IMR-32 cells at 25 μM concentration. In the ROS studies, compound **8** (MAO-A inhibitor) reduced the ROS level by 51.2% while compound **13** reduced the ROS level by 61.81%. In the molecular dynamic simulation studies for 30 ns, compound **12** was found quite stable in the active cavity of MAO-B. Thus, it can be concluded that phenyl- and 1-benzhydrylpiperazine derivatives are promising MAO inhibitors and can act as a lead to design potent, and selective MAO inhibitors for the treatment of various neurological disorders.

1. Introduction

Monoamine oxidase (MAO, EC 1.4.3.4) is a flavin adenine dinucleotide (FAD)-containing outer mitochondrial membrane-bound enzyme found in the brain in neuronal, glial, and other cells [1] and also in periphery. FAD co-factor covalently bound to MAO at cysteine residue by an 8-alpha (s-cysteinyl) riboflavin linkage. MAO regulates the levels of biogenic and xenobiotic amines in the brain and in the peripheral tissues by catalyzing their oxidative deamination [2]. It acts as a catalytic agent in the oxidative deamination of various monoamines including serotonin, dopamine, histamine, adrenaline and noradrenaline. MAO enzyme exists in two isoforms, MAO-A and MAO-B [3] and these two isoforms have sequence similarity of around 73% but vary in their substrate specificity and inhibitor selectivity. MAO-A deaminates serotonin and is inhibited by clorgyline whereas MAO-B deaminates benzylamine and 2-phenylethylamine and is inhibited by (R)-deprenyl [4,5]. Iproniazid, an anti-tuberculosis drug showing mood elevation in depressed patients, was the first MAO inhibitor used in the treatment of depression [6]. It was followed by imipramine, isocarboxazid, phenelzine, tranylcypromine and propargylamines [7,8]. All of these drugs were non-selective and irreversible MAO inhibitors and were associated with number of side effects such as cheese effect, serotonin syndrome and lethal drug-drug interactions. Thus, new generations of MAO inhibitors were developed which were reversible and selective for one of the MAO isoform and devoid of many side effects [9,10]. Now, the MAO enzyme has been recognized as an important and attractive drug target for the treatment of various neurogenic disorders. Recent reports on the neuroprotective and neuro rescue potential [11,12] of MAO inhibitors have generated enormous interests for exploring their role in the treatment/management of various neurological disorders.

Piperazine is one the most promising heteroaromatic nucleus and integral part in most of the psychoactive compounds [13,14]. A number of phenylpiperazine derivatives have been synthesized and screened for their MAO inhibition potential and their role in the management of Parkinson's disease, Alzheimer's disease and depression. Pessoa-Mahana et al. [15] reported 4-arylpiperazine derivatives (A, Fig. 1) of moclobemide as new type of

* Corresponding author.
E-mail address: vinod.kumar@cup.edu.in (V. Kumar).

https://doi.org/10.1016/j.bioorg.2018.01.020
0045-2068/

Current Drug Targets, 2017, *18*, 87-97

REVIEW ARTICLE

A Perspective on Monoamine Oxidase Enzyme as Drug Target: Challenges and Opportunities

Bhupinder Kumar, Vivek Prakash Gupta and Vinod Kumar*

Laboratory of Organic and Medicinal Chemistry, Centre for Pharmaceutical Sciences and Natural Products, Central University of Punjab, Bathinda, Punjab, 151001-India

ARTICLE HISTORY

Received: September 08, 2015
Revised: November 17, 2015
Accepted: November 19, 2015

DOI:
10.2174/1389450117666151209123402

Abstract: The monoamine oxidase (MAO) enzyme is responsible for the deamination of monoamine neurotransmitters and regulates their concentration in the central and peripheral nervous systems. Imbalance in the concentration of neurotransmitters in the brain and central nervous system is linked with the biochemical pathology of various neurogenic disorders. Irreversible MAO inhibitors were the first line drugs developed for the management of severe depression but most of these were withdrawn from the clinical practice due to their fatal side effects including food-drug interactions. New generations of MAO inhibitors were developed which were reversible and selective for one of the enzyme isoform and showed improved pharmacological profile. The discovery of crystal structure of MAO-A & MAO-B isoforms helped in understanding the drug-receptor interactions at the molecular level and designing of ligands with selectivity for either of the isoforms. The current article provides an overview on the MAO enzyme as potential drug target for different disease states. The article describes catalytic mechanism of MAO enzyme, crystal structures of the two MAO isoforms, traditional MAO inhibitors and various problems associated with their use, new developments in the MAO inhibitors and their potential as therapeutic agents especially in neurological disorders.

Keywords: Monoamine oxidase, neurological disorders, parkinson's disease, alzheimer's disease, depression, food drug interactions.

1. INTRODUCTION

Monoamine oxidase (MAO, EC 1.4.3.4) is a flavin adenine dineucleotide dependent enzyme. It is responsible for the deamination of monoamine neurotransmitters, endogenous amines and xenobiotics in the central and peripheral nervous systems [1]. In most of the mammal tissues, MAO enzyme is localised in the outer membrane of the mitochondria. The MAO enzyme has two isoforms, MAO-A and MAO-B where in MAO-A isoform is predominant in liver, gut, skin and placenta while MAO-B is the major isoform in the brain. Human MAO-A and MAO-B isoforms contain amino acid sequences that are 70% identical, however, differ in tissue distribution, substrate specificity and inhibitor selectivity. MAO-A has substrate specificity for the bulkier endogenous amines like serotonin, epinephrine and norepinephrine whereas MAO-B has substrate specificity for the small exogenous amines such as benzylamine, β-phenyl ethylamine [2]. Dopamine and tyramine are common substrates for both the isoforms. MAO enzyme can modulate the concentration of monoamine neurotransmitters in the central nervous system (CNS) and is linked with the etiology of number of neurological disorders. MAO enzyme is one of the extensively studied targets for the neurological disorders with more than 21000 publications recorded in the PubMed database.

2. CRYSTAL STRUCTURES OF MAO-A & MAO-B

The MAO enzyme is bounded covalently to co-factor FAD at cysteine residue by an 8-alpha (s-cysteinyl) riboflavin linkage with highly conserved structure [3]. The X-ray crystal structure studies revealed the existence of human MAO-A as monomeric and human MAO-B as dimeric units. Most of the membrane proteins exist in dimeric form [4] however through molecular docking studies and species-dependent genetic analysis [5] it has been concluded that the monomeric structure of human MAO-A could be due to Glu151Lys mutation near the dimer interface. The MAO-A and MAO-B isoform have cavities with volumes of 400 A^{o3} and ~ 700 A^{o3} respectively. The MAO-B cavity is divided into two parts *i.e.* entrance cavity of volume 290 A^{o3} and substrate cavity of volume ~400A^{o3} [6, 7]. Ile199 and Tyr326 side chains separate the two cavities in MAO-B isoform. The difference in the structure of active site of human MAO-A and MAO-B isoforms is due to the change in 7 out of 20 amino acid residues that line the active site of the enzyme and a change in the cavity shaping loop 210-216 [8]. In general the cavities of both the isoforms are hydrophobic in nature however MAO-B isoform contains a small highly con-

*Address correspondence to this author at the Laboratory of Organic and Medicinal Chemistry, Centre for Pharmaceutical Sciences and Natural Products, Central University of Punjab, Bathinda, Punjab, 151001-India; Tel: 07696255588; Fax: 01642864106; E-mails: vpathania18@gmail.com; vinod.kumar@cup.ac.in

1873-5592/17 $58.00+.00

Tetrahedron Letters 59 (2018) 1986–1991

Contents lists available at ScienceDirect

Tetrahedron Letters

journal homepage: www.elsevier.com/locate/tetlet

Chitosan-supported copper as an efficient and recyclable heterogeneous catalyst for A^3/decarboxylative A^3-coupling reaction

Pavneet Kaur [a], Bhupinder Kumar [b], Vinod Kumar [b,*], Rakesh Kumar [a,*]

[a] Laboratory of Organic Chemistry, Department of Chemical Sciences, Central University of Punjab, Bathinda 151001, India
[b] Laboratory of Organic and Medicinal Chemistry, Department of Pharmaceutical Sciences and Natural Products, Central University of Punjab, Bathinda 151001, India

ARTICLE INFO

Article history:
Received 1 February 2018
Revised 14 March 2018
Accepted 19 March 2018
Available online 18 April 2018

Keywords:
Chitosan
Decarboxylative A^3-coupling
Propargylamines
Heterogeneous catalyst
Recyclability

ABSTRACT

Chitosan-supported copper (chit@copper) based heterogeneous catalysts have been explored for A^3-coupling and decarboxylative A^3-coupling. The developed protocol employs low catalyst loading, solventless condition and easy work-up for the synthesis of diversely substituted propargylamines. More importantly, the catalyst could be recovered and reused without any significant loss in the activity. This offer huge advantages as recyclability issues are rarely addressed in decarboxylative A^3-coupling. Leaching studies were carried out using AAS and ICPMS analysis. It is envisaged that chit@copper catalysts can have potential applications in terms of efficiency and recyclability in the emerging area of decarboxylative C—H bond activation/functionalization strategies.

Environmental degradation is one of the major concerns[1] of environmentalists and political discourse at the international level. The toxic waste generated by the chemical industries is one of the major threats to human, animals and plant lives on the earth. Novel reagents, solvent free synthesis[2] and recyclable catalytic systems[3] are being developed to minimize the waste in chemical synthesis. From the last few years, heterogeneous catalysis[4,5] has been proved to be an effective strategy to improve the efficiency and recyclability of the catalysts. In recent years, abundantly available and renewable biopolymers such as starch, cellulose, chitin, chitosan etc., have received a phenomenal attention for their use as a support for metals and their application in heterogeneous catalysis.[6–10]

Chitosan,[8] an amino-polysaccharide, is the second most abundant biopolymer after cellulose. This biodegradable polymer is insoluble in most of the organic solvents as well as in water and can act as a suitable material for the heterogeneous catalysis.[11,12] The presence of free amino and hydroxyl groups on chitosan enables it to coordinate with different metal atoms/ions and make it an attractive polymeric support for the immobilization of metal catalysts such as Pd,[13] Rh,[14] Cu,[15] Ti,[16] Ru,[17] etc. Furthermore, chitosan based catalysts exhibit high thermal stability and can be used in various organic transformations. Recently, Zhang and co-workers have reported chit@$Cu(OAc)_2$ as a highly active and recoverable heterogeneous catalyst for the C—S cross-coupling reaction which has led to the green synthesis of antiulcer drug zolimidine.[18] Similarly, chit@$CuSO_4$ as a heterogeneous catalyst has been employed for the azide-alkyne cycloaddition and for the synthesis of 1,2,3-triazoles using aryl boronic acids.[15]

The transition metal-catalyzed three-component coupling of an aldehyde, amine and alkyne (A^3-coupling) represents an important strategy for the synthesis of diversely substituted propargylamines in an atom economic way.[19–22] Similarly, decarboxylative A^3-coupling (coupling of aldehydes, amines and alkynyl carboxylic acids) is a useful and challenging transformation wherein alkynyl carboxylic acids act as economical and stable surrogate for polymerization prone alkynes *via* in situ decarboxylation.[23–26] There are only few protocols for decarboxylative A^3-coupling which mainly focus on substrate scope without addressing the recyclability aspect of the catalyst. Thus, development of efficient and recyclable heterogeneous catalytic system in such coupling is an important objective as generation of huge amount of metal waste is incongruous to the principles of Green Chemistry. This in particular is highly desired during synthesis of drug like molecules where even trapping of traces of metal impurity in the final product could be potentially harmful.

Following our research interest on the development of environmentally friendly methodologies,[27–29] we herein report chitosan-supported copper(I) as an efficient recyclable heterogeneous catalyst for A^3-coupling reaction. The versatility of developed

* Corresponding authors.
E-mail addresses: vinod.kumar@cup.edu.in (V. Kumar), rakesh.kumar@cup.edu.in (R. Kumar).

https://doi.org/10.1016/j.tetlet.2018.03.052
0040-4039/

Bioorganic Chemistry 78 (2018) 130–140

Contents lists available at ScienceDirect

Bioorganic Chemistry

journal homepage: www.elsevier.com/locate/bioorg

Synthesis and biological evaluation of pyrimidine bridged combretastatin derivatives as potential anticancer agents and mechanistic studies

Bhupinder Kumar [a], Praveen Sharma [b], Vivek Prakash Gupta [a], Madhu Khullar [c], Sandeep Singh [b], Nilambra Dogra [c,*], Vinod Kumar [a,*]

[a] Laboratory of Organic and Medicinal Chemistry, Department of Pharmaceutical Sciences and Natural Products, Central University of Punjab, Bathinda, Punjab 151001, India
[b] Laboratory of Molecular Medicine, Department of Human Genetics and Molecular Medicines, Central University of Punjab, Bathinda, Punjab 151001, India
[c] Department of Experimental Medicine and Biotechnology, PGIMER, Chandigarh 160012, India

ARTICLE INFO

Article history:
Received 23 January 2018
Revised 24 February 2018
Accepted 26 February 2018
Available online 28 February 2018

Keywords:
Pyrimidine
Combretastatin derivatives
Apoptosis
Tubulin inhibitors
Colchicine binding site
Anticancer

ABSTRACT

A number of pyrimidine bridged combretastatin derivatives were designed, synthesized and evaluated for anticancer activities against breast cancer (MCF-7) and lung cancer (A549) cell lines using MTT assays. Most of the synthesized compounds displayed good anticancer activity with IC_{50} values in low micromolar range. Compounds **4a** and **4p** were found most potent in the series with IC_{50} values of 4.67 μM & 3.38 μM and 4.63 μM & 3.71 μM against MCF7 and A549 cancer cell lines, respectively. Biological evaluation of these compounds showed that selective cancer cell toxicity (*in vitro* using human lung and breast cancer cell lines) might be due to the inhibition of antioxidant enzymes instigating elevated ROS levels which triggers intrinsic apoptotic pathways. These compounds were found nontoxic to the normal human primary cells. Compound **4a**, was found to be competitive inhibitor of colchicine and in the tubulin binding assay it showed tubulin polymerization inhibition potential comparable to colchicine. The molecular modeling studies also showed that the synthesized compounds fit well in the colchicine-binding pocket.

1. Introduction

Cancer is a multifactorial disease and considered as the most serious health problem all over the world. Despite recent advances in our understanding of the biological processes leading to the development of cancer, there is still need for the development of more potent and effective anticancer agents for the complete eradication of the disease [1]. Multi-drug resistance and acute toxicity are the two major issues with most of the currently available chemotherapeutic agents [2,3]. Therefore, novel anticancer agents need to be developed that are more potent, safe and selective. In a quest for the discovery of more effective anticancer drugs, a large number of structurally diverse synthetic and natural products have been screened for their anticancer potential [4,5]. Microtubules have been explored as an important target for the anticancer drug development. Microtubules play crucial role in the spindle formation during cell-division. A highly dynamic equilibrium exists between the microtubules and the free tubulin dimers [4]. Any disruption in the dynamic equilibrium of tubulin-microtubule blocks cell-division at the metaphase–anaphase transition that leads to the induction of the mitochondrial apoptosis [6].

Numerous structurally different natural as well as synthetic compounds have been identified that target microtubule polymerization [7]. Since last few years combretastatins have received special attention due to their simple structure and easy synthesis [8,9]. Combretastatin A-4 (CA-4) binds with the colchicine binding site and disrupts microtubule polymerization and induces rapid vascular disruption which leads to tumor cell death [10,11]. Fosbretabulin, a water-soluble phosphate prodrug of CA-4, is under phase II/III clinical trials alone and/or in combination with other chemotherapeutic agents. Although, numerous CA-4 analogs have been developed with improved antitubulin activities, but clinical application of these agents is not successful till now [12]. Thus, it is a challenge to synthesize CA-4 analogs with improved activity along with therapeutic potency.

* Corresponding authors at: Laboratory of Organic and Medicinal Chemistry, Department of Pharmaceutical Sciences and Natural Products, Central University of Punjab, Bathinda, Punjab 151001, India (V. Kumar). Department of Experimental Medicine and Biotechnology, PGIMER, Chandigarh 160012, India (N. Dogra).
E-mail addresses: nilambra@gmail.com (N. Dogra), vinod.kumar@cup.edu.in (V. Kumar).

https://doi.org/10.1016/j.bioorg.2018.02.027
0045-2068/

Ramandeep Kaur, Bhupinder Kumar, Ashish Ranjan Dwivedi and Vinod Kumar*

Regioselective alkylation of 1,2,4-triazole using ionic liquids under microwave conditions

DOI 10.1515/gps-2015-0138
Received January 4, 2016; accepted February 16, 2016; previously published online May 9, 2016

Abstract: 1-Substituted 1,2,4-triazole derivatives present in a large number of compounds and display a variety of bioactivities such as antibiotic, anti-inflammatory, anti-diabetic, antipsychotic, and anticancer. A regioselective protocol has been developed for the alkylation of 1,2,4-triazole using mild conditions. The 1-alkyl-1,2,4-triazole derivatives were synthesized under microwave conditions using potassium carbonate as a base and ionic liquid (hexylpyridinium bromide) as a solvent. The products were obtained in excellent yield, and the base-ionic liquid combination was recycled for a number of times.

Keywords: 1,2,4-triazole; green chemistry; ionic liquids; microwave; regioselective alkylation.

1 Introduction

1,2,4-Triazole is an important nucleus [1] present in a large number of compounds exhibiting a variety of bioactivities [2] including antibiotic, anti-inflammatory, anti-diabetic, antipsychotic, and anticancer activities. This nucleus is also a part of many herbicides, fungicides, and plant growth regulators [3]. The 1,2,4-triazole nucleus is stable to metabolism and act as an important pharmacophore by interacting at the active site of the receptor as hydrogen bond acceptor as well as donor. Owing to its polar nature, the triazole nucleus can increase the solubility of the ligands and may improve the pharmacokinetic and pharmacodynamic profile of the drugs [4].

Among the various 1,2,4-triazole derivatives, 1-substituted 1,2,4-triazole nucleus is of particular interest as it can be traced in many commercialized drugs [5] like rizatriptan, fluconazole, and terconazole. Two different methods are reported for the synthesis of anti-migraine drug rizatriptan, and the most obvious synthetic step for the introduction of 1,2,4-triazole is through alkylation reaction [6]. The triazole nucleus exists in two tautomeric forms, namely, 4*H*-1,2,4-triazoles and 1*H*-1,2,4-triazoles, and in general, the alkylation reaction results in the formation of an isomeric mixture of 1-substituted 1,2,4-triazole and 4-substituted 1,2,4-triazole. In addition to this, over-alkylation of the product may lead to salt formation [7]. The ratios of the isomers formed depend on the nature of the alkylating agents and reaction conditions. To obtain a single isomer, some regioselective protocols were also developed. For example, Astleford et al. [8] reported a regioselective alkylation of 1,2,4-triazoles from the corresponding 4-amino-1,2,4-triazoles. The products were obtained by subsequent deamination of the triazolium salt. Similarly, alkylation of 1,2,4-triazole was reported using NaOH as a base and DMF as a solvent. The products were obtained in a regioselective way; however, the isomer ratio of the crude mixtures of the synthesized compounds before the work up was only 90:10 [9]. In another report, the synthesis of 1-ethyl-1,2,4-triazole was performed under mild conditions using THF as a solvent and DBU as a base. The isomeric ratios of the product obtained vary from 94:6 to 86:14. The precipitation of DBU-HX from the reaction mixture and its separation by simple filtration was the advantage of this method [10]. Rezaei et al. [11] reported the regioselective formation of the N-1 isomer in higher yield using anhydrous potassium carbonate, sodium hydroxide, and tetra ethyl ammonium iodide. Mirzaei et al. [12] reported the regioselective alkylation of 1,2,4-triazoles wherein 1,2,4-triazole was dissolved in methanolic solution of sodium methoxide, and iodoalkane was added at -40°C. Thus, most of the methods reported for the regioselective alkylation of 1,2,4-triazole make use of strong bases like sodium hydride and sodium hydroxide and sub-zero temperatures (-40°C or -78°C). Therefore, we got interested in developing a milder protocol for the regioselective alkylation of 1,2,4-triazole. Different mild bases were explored using recyclable ionic liquids as solvent under microwave conditions. The reaction conditions were optimized with potassium carbonate as the base and 1-hexylpyridinum bromide as the solvent

***Corresponding author: Vinod Kumar,** Laboratory of Organic and Medicinal Chemistry, Centre for Pharmaceutical Sciences and Natural Products, Central University of Punjab, Bathinda, Punjab-151001, India, e-mail: vinod.kumar@cup.ac.in
Ramandeep Kaur, Bhupinder Kumar and Ashish Ranjan Dwivedi: Laboratory of Organic and Medicinal Chemistry, Centre for Pharmaceutical Sciences and Natural Products, Central University of Punjab, Bathinda, Punjab-151001, India

Current Cancer Drug Targets, 2017, *17*, 357-375

REVIEW ARTICLE

Mechanisms of Tubulin Binding Ligands to Target Cancer Cells: Updates on their Therapeutic Potential and Clinical Trials

Bhupinder Kumar[1], Rakesh Kumar[2], Ira Skvortsova[3,*] and Vinod Kumar[1,*]

[1]*Laboratory of Organic and Medicinal Chemistry, Centre for Pharmaceutical Sciences and Natural Products, Central University of Punjab, Bathinda, Punjab, India;* [2]*Laboratory of Organic Chemistry, Centre for Chemical Sciences, Central University of Punjab, Bathinda, Punjab, India;* [3]*Department of Therapeutic Radiology and Oncology, Innsbruck Medical University, Innsbruck, Austria*

ARTICLE HISTORY

Received: February 08, 2016
Revised: September 15, 2016
Accepted: September 16, 2016

DOI:
10.2174/1568009616666160928110818

Abstract: ***Background*:** A number of chemically diverse substances bind to the tubulin and inhibit cell proliferation by disrupting microtubule dynamics. There are four binding sites for the ligands binding to the tubulin; taxane/epothilone and laulimalide/peloruside binding ligands stabilize microtubule while vinca and colchicine binding site agents promote microtubule depolymerization. Most of the tubulin binding ligands disturb the tubulin-microtubule dynamic equilibrium but these may exhibit anticancer activities through different mechanisms. Taxanes and epothilones are widely used cytotoxic agents and are found effective against different types of human malignancies. However, taxanes are susceptible to pgp mediated multi-drug resistance, dose limiting hematopoietic toxicity and cumulative neurotoxicity. Vinca alkaloids are already in clinical practice, but ligands binding to the colchicine site are still in the different stages of clinical trials.

***Objective*:** In the current review article, plausible mechanistic details about the interactions of ligands at the binding pocket and subsequent changes in the tubulin structure are described. The review article also illustrated different formulations of the tubulin binding agents in combination with other chemotherapeutic agents and their therapeutic potential against various human malignancies.

***Conclusion*:** Tubulin targeting agents emerged as one of the most successful anticancer drugs and a number of structurally different chemical compounds are in advance stages of clinical development.

Keywords: Tubulin inhibitor, microtubule stabilizing agents, tubulin polymerization/depolymerization, anticancer, combination therapy, tubulin binding ligands.

1. INTRODUCTION

Microtubules are universal cytoskeletal structures formed by the association of α and β tubulin heterodimers. These play crucial role in the cell division, cell signalling, cellular movements and in the development and maintenance of cell shape [1]. The α and β hetero polypeptides of tubulin have about 36-42 % similarity to each other and each subunit consists of about 445 amino acid residues. Three-dimensional structure of the α,β-tubulin heterodimer has been determined by the electron crystallography [2]. Both α and β monomer units of tubulin encompass a GTP molecule. In the α-subunit of tubulin, GTP molecule is bound in an irreversible way at the dimer interface and is non-hydrolysable. However in the β-subunit of tubulin, GTP molecule binds in a reversible way and it can be exchanged with a GDP molecule. In the formation of polymeric microtubules, α,β-tubulin acts as a monomer unit and β polypeptide of one tubulin monomer unit get attached to the α-polypeptide of another tubulin monomer in head to tail manner and this arrangement results in the formation of protofilaments. Consequently, thirteen protofilaments arrange in the parallel fashion to give rise to a cylindrical microtubule wall. The two ends of microtubules structure are different as α-tubulin subunit is exposed at one end (minus end) while β-subunit is exposed at the other end (plus end).

Microtubules are dynamic polymers and equilibrium exists between the α,β-tubulin heterodimer and the microtubule through polymerization and depolymerization cycles (Fig. **1**). Dynamic behaviour of the microtubule is maintained through dynamic instability and treadmilling. In dynamic instability phase, each of the microtubule end shift between phases of growth (polymerization) and shortening (depolymerization) [3]. The growth phase of the microtubules is called 'rescue' while the shortening phase is called 'catastrophe'. The treadmilling involves a net growth at the plus end and a net shortening at the minus end of the microtubule. There are six α-tubulin and ten β-tubulin (βI, βIIa, βIIb, βIII, βIVa, βIVb, βV, βVI, βVII, and βVIII) isotypes that regulate different functions of the microtubules [4]. For the polymerization cycle of the microtubule, β-subunit of tubulin should be in a GTP-bound state. After attachment to

*Address correspondence to these authors at the Laboratory of Organic and Medicinal Chemistry, Centre for Pharmaceutical Sciences and Natural Product, Central University of Punjab, Bathinda, Punjab, India; Tel: +917696255588; E-mails: vpathania18@gmail.com; vinod.kumar@cup.ac.in
Laboratory for Experimental and Translational Research on Radiation Oncology (EXTRO-Lab), Department of Therapeutic Radiology and Oncology, Innsbruck Medical University, Anichstr. 35, A-6020 Innsbruck, Austria; Tel: ++43-512-504-27758; Fax: ++43-512-504-27756;
E-mail: Ira.Skvortsova@i-med.ac.at

1873-5576/17 $58.00+.00

Send Orders for Reprints to reprints@benthamscience.ae

Anti-Cancer Agents in Medicinal Chemistry, **2016**, *16,* 465-489

Recent Developments on 1,2,4-Triazole Nucleus in Anticancer Compounds: A Review

Ramandeep Kaur, Ashish Ranjan Dwivedi, Bhupinder Kumar and Vinod Kumar*

Laboratory of Organic and Medicinal Chemistry, Centre for Pharmaceutical Sciences and Natural Products, Central University of Punjab, Bathinda, Punjab, India-151001

V. Kumar

Abstract: 1,2,4-triazole is an important nucleus present in a large number of compounds. More than thirty-five compounds containing this nucleus are introduced into the market. 1,2,4-triazole nucleus is stable to metabolism and acts as an important pharmacophore by interacting at the active site of a receptor as hydrogen bond acceptor and as a donor. Due to its polar nature, the triazole nucleus can increase the solubility of the ligand and it can significantly improve the pharmacological profile of the drug. A large number of 1,2,4-triazole derivatives are reported to possess a wide range of bioactivities including anti-cancer activity. This review article describes the role of 1,2,4-triazole nucleus in different types of anti-cancer agents such as nucleoside based anti-cancer agents, kinase inhibitors, tubulin modulators, aromatase and steroid sulfatase inhibitors, methionine aminopeptidase inhibitors, tankyrase inhibitors and metal complex based anti-cancer agents. It is expected that the current review article will provide insight into various ligand-receptor interactions and help in the rational design and development of novel 1,2,4-triazole based anti-cancer drugs with improved selectivity for cancer cells.

Keywords: 1,2,4-triazoles, anticancer, kinase inhibitors, tubulin modulators, structure-activity relationship.

1. INTRODUCTION

Triazoles are an important class of heterocyclic compounds containing three nitrogen atoms in a five membered ring having molecular formula $C_2H_3N_3$. These exist in two isomeric forms depending upon the position of the nitrogen atom in the heterocyclic ring: 1,2,3-triazoles or 1,2,4-triazoles. Both the structural isomers of triazoles exhibit tautomerism and exist in two tautomeric forms. For example 1,2,3-triazoles can exist as 1,2,3-(1*H*)-triazole and 1,2,3-(2*H*)-triazole while 1,2,4-triazoles exhibit two tautomeric forms namely 1,2,4-(1*H*)-triazoles and 1,2,4-(4*H*)-triazoles (Fig. **1**). Out of the two isomeric forms of triazoles, 1,2,4-triazole derivatives are synthesized in the form of fused ring system or as heterocyclic or aromatic substitutions. 1,2,4-triazole nucleus has received the considerable attention of researchers owing to its wide range of applications in pharmaceuticals, agrochemicals and material sciences [1]. For example, various optionally substituted 1,2,4-triazole derivatives are reported to possess wide range of bioactivities including antifungal, antimicrobial [2], antibacterial [3], anti-inflammatory [4], anti-tubercular [5], hypoglycaemic [6], antidiabetic [7], antidepressant [8], anticonvulsant [9], anti-malarial [10], analgesic [11], anti-migraine [12], arthritis [13], antihypertensive [14, 15], antiviral [16], antileishmanial [17], potassium channel activators [18], antiplatelet [19] and antioxidant [20].

A number of 1,2,4-triazole derivatives are commercialized as important fungicides [21], (Fig. **2**) herbicides (Fig. **3**) and plant growth regulators [22]. The 1,2,4-triazole nucleus is stable to metabolic degradation and shows target specificity and wide spectrum of activities. The triazole ring contains three nitrogen atoms and can act as hydrogen bond acceptor or donor at the active site of the receptors and can modulate their activity accordingly. Being polar in nature, the triazole nucleus can increase the solubility of the ligands and contribute better pharmacokinetic and pharmacodynamic properties [23]. In most of the cases, triazole nucleus is found to behave as linker unit with which different functionalities are attached as pharmacophore and at the same time nucleus imparts required flexibility to the drug for effective ligand-receptor interactions. There are a number of reviews written on the chemistry of triazole derivatives describing its synthesis [24] and various bioactivities [25]. The mandate of this review article is to investigate various reports on the anti-cancer potential of compounds containing 1,2,4-trizole nucleus. To the best of our knowledge, there is no review article exclusively dealing with the anti-cancer potential of 1,2,4-triazole derivatives.

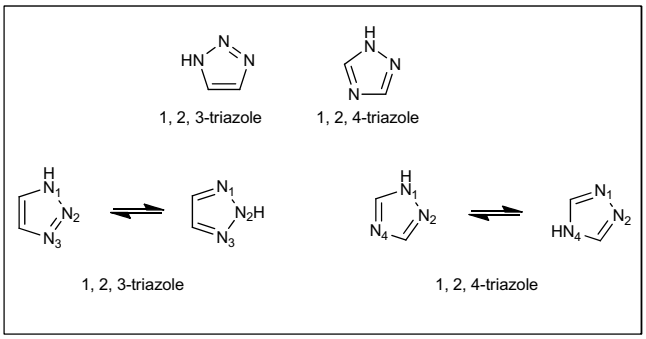

Fig. (1). Different isomeric and tautomeric forms of triazoles.

2. COMPOUNDS INTRODUCED IN THE MARKET CONTAINING 1,2,4-TRIAZOLENUCLEUS

1,2,4-triazole derivatives have been explored for various bioactivities, and a number of compounds containing this nucleus have been already developed as commercial products. A large number of triazoles have been developed as fungicides, herbicides, anti-depressant, anti-convulsant, anti-hypertensive, tranquilizer, sedative, anti-inflammatory, anti-migraine, anti-neoplastic etc. as described in Figs. **2** to **6**.

3. 1,2,4-TRIAZOLE NUCLEUS IN ANTI-CANCER COMPOUNDS

The 1,2,4-triazole nucleus is present in variety of structurally different anti-cancer compounds. This nucleus is explored extensively in nucleoside based anti-cancer agents, kinase inhibitors, tubulin modulators, aromatase and sulfatase inhibitors and metal complex based antitumor agents. The review article is divided into different

*Address correspondence to this author at the Laboratory of Organic and Medicinal Chemistry, Centre for Pharmaceutical Sciences and Natural Products, Central University of Punjab, Bathinda, Punjab, India-151001; Tel: 07696255588; Fax: 01642864106; E-mails: vpathania18@gmail.com; vinod.kumar@cup.ac.in; CUPB communication number: PA 64/14

1875-5992/16 $58.00+.00

Current Medicinal Chemistry, 2017, *24*, 4729-4752

REVIEW ARTICLE

Promising Targets in Anti-cancer Drug Development: Recent Updates

Bhupinder Kumar[1], Sandeep Singh[2], Ira Skvortsova[3,*] and Vinod Kumar[1,*]

[1]*Laboratory of Organic and Medicinal Chemistry, Centre for Pharmaceutical Sciences and Natural Products, Central University of Punjab, Bathinda, Punjab, India-151001;* [2]*Centre for Human Genetics and Molecular Medicines, Central University of Punjab, Bathinda, Punjab, India-151001;* [3]*Department of Therapeutic Radiology and Oncology, Innsbruck Medical University, Innsbruck, Austria*

ARTICLE HISTORY

Received: September 23, 2016
Revised: February 20, 2017
Accepted: March 03, 2017

DOI:
10.2174/0929867324666170331123648

Abstract: Cancer is a multifactorial disease and its genesis and progression are extremely complex. The biggest problem in the anticancer drug development is acquiring of multidrug resistance and relapse. Classical chemotherapeutics directly target the DNA of the cell, while the contemporary anticancer drugs involve molecular-targeted therapy such as targeting the proteins possessing abnormal expression inside the cancer cells. Conventional strategies for the complete eradication of the cancer cells proved ineffective. Targeted chemotherapy was successful in certain malignancies however, the effectiveness has often been limited by drug resistance and side effects on normal tissues and cells. Since last few years, many promising drug targets have been identified for the effective treatment of cancer. The current review article describes some of these promising anticancer targets that include kinases, tubulin, cancer stem cells, monoclonal antibodies and vascular targeting agents. In addition, promising drug candidates under various phases of clinical trials are also described. Multi-acting drugs that simultaneously target different cancer cell signaling pathways may facilitate the process of effective anti-cancer drug development.

Keywords: Anticancer, tubulin inhibitor, kinases, cancer stem cells, multi-drug resistance, multi-targeting agents.

1. INTRODUCTION

Cancer is caused by the uncontrolled growth of cells and is a major cause of death throughout the world. It has more than 200 distinct types affecting over 60 human body organs. The major challenge in the anticancer drug development is to design a drug that targets cancer cells with high selectivity and specificity. It is difficult to identify most of the tumors at the primary level and at later stages metastasis of tumor may lead to cancer-related deaths [1-5]. Various strategies employed for the treatment of cancer includes surgery, chemotherapy and radiation therapy used either alone or in combination. Classical chemotherapeutics directly target the DNA of the cell, while the contemporary anticancer drugs involve molecular-targeted therapy such as targeting the proteins possessing abnormal expression inside the cancer cells. These molecular-targeted drugs selectively kill the cancer cells with decreased toxicity towards the normal cells in comparison to the traditional anticancer drugs [6]. Targeted drugs inhibit specific cell signaling pathways that contribute to the malignant phenotype of cancer cells. Chemotherapy has gradually improved with the development of novel antitumor drugs. The treatment of some malignancies with the targeted chemotherapy was successful however, development of drug resistance and toxicity to the normal tissues and cells are the major limitations. Drug transporters are overexpressed in many of the cancer cells and these reduce intracellular drug concentrations. In addition, the evolution of point mutations may be responsible for stronger drug resistance. Multidrug resistance (MDR) is a major obstacle in the effective treatment and complete eradication of cancer.

*Address correspondence to these authors at the Laboratory of Organic and Medicinal Chemistry, Centre for Pharmaceutical Sciences and Natural Products, Central University of Punjab, Bathinda, Punjab, India-151001; Tel: +917696255588; E-mails: vpathania18@gmail.com; vinod.kumar@cup.ac.in; and Laboratory for Experimental and Translational Research on Radiation Oncology (EXTRO-Lab), Department of Therapeutic Radiology and Oncology, Innsbruck Medical University, Anichstr. 35, A-6020 Innsbruck, Austria; Tel: ++43-512-504-27758; Fax: ++43-512-504-27756; E-mail: Ira.Skvortsova@i-med.ac.at

